Charles University

Faculty of Science

Study programme: Biology

Branch of study: Ecology

Bc. Marie Bulínová

A comparison between paleo and recent freshwater diatom communities from Vega Island, Antarctica

Porovnání paleo a recentních společenstev sladkovodních rozsivek z ostrova Vega, Antarktida

Diploma thesis

Supervisor: Mgr. Kateřina Kopalová, Ph.D.

Consultant: Prof. Bart Van de Vijver, Ph.D.

Prague, 2019

"There is a difference between what we see and what we are aware of."

(Tristan Gooley)

Statement

I hereby state that I have completed this thesis by myself and that I have properly cited all literature and other information sources I have used. Neither this thesis nor its parts have been submitted to achieve any other academic title(s).

Prohlášení:

Prohlašuji, že jsem závěrečnou práci zpracoval/a samostatně a že jsem uvedl/a všechny použité informační zdroje a literaturu. Tato práce ani její podstatná část nebyla předložena k získání jiného nebo stejného akademického titulu.

In Prague / V Praze, 29.04.2019

Signature / Podpis

CONTENTS

ACKNOWLEDGEMENTS

I want to thank my parents and Dáda Hrabětová for such a great support during my studies, and my sisters Kristýna and Vendy who constantly kept my awareness of other disciplines. Also, Kristýna is the author of those beautiful drawings of the glacier and penguins.

Many thanks also belong to my supervisor Kateřina Kopalová for all the opportunities and help she gave me during my studies and to my co-supervisor Bart Van de Vijver, who led my internship in Belgium and was helpful anytime I needed; and especially for his personal decision to make me gain 5 kilos by bringing me desserts every morning and creating the best Friday playlists!

I am super grateful to Tyler Kohler for advices, great help, statistics lessons and emails coming usually way too early in the morning, and together with Jakub Žárský for introducing me the Arctic during the Svalbard fieldwork, and to everyone who I met there.

Further, I want to thank Jordan for the constant supply of chocolate, coffee, fun and moral support in the office.

I also want to thank to Vincent, because without him coming to this world, there might not be any Antarctic campaign for me last year. Talking about Antarctica, I send thanks to Juan and Silvia, my great Lagos team partners. And of course many thanks to Marek Stibal, Petra Vinšová, Guillaume Lamarche-Gagnon, Stefan Hofer and Jon Hawkings for Greenland fieldwork and my coffee education!

Many thanks belong to Mirek for his great support and patience with my 'creative' ideas.

And one big thanks goes to no wifi and mobile signal on Dundee Island, ferry between Helsinki and Travemunde and all those lonely days in Buenos Aires. Without them this thesis might have never existed.

ABSTRACT

In Antarctica, diatoms inhabit multiple limno-terrestrial habitat types, which may each individually offer unique ecological information for use in biomonitoring, paleoecology, and biogeography. However, we are still at the initial exploration stage of documenting the diversity among habitat types from different Antarctic regions, which is necessary to serve as baseline data for the aforementioned scientific disciplines, and ultimately inform conservation decisions.

To gain insight into the spatial and habitat controls on Antarctic diatom communities, the importance of habitat type and island aspect was investigated by studying diatoms living in ponds, mosses, streams, and seepage areas on two opposite sides Vega Island, Antarctic Peninsula. A diverse flora of 136 taxa belonging to 31 genera was revealed, which was dominated by the genus *Nitzschia*, and suggests that the flora of Vega Island is biogeographically influenced by both continental and Maritime Antarctic bioregions. Habitat type was found to be a crucial factor for diatom community composition, and was stronger than the influence of island aspect. In ordination analyses, moss samples were separated primarily by their abundances of the diatom *Chamaepinnularia krookiformis*, while pond samples were separated by *Nitzschia paleacea* and stream habitats by *Fistulifera pelliculosa*.

These 'recent' communities were then compared with paleo-assemblages characterized from sediment cores extracted from prominent lakes from both sides of the island. In both cores, diatom assemblages were relatively uniform throughout, suggesting stable lake communities and/or allochthonous inputs over time. However, sediment cores differed substantially from each other in their species richness and diversity, and reflected patterns described for modern communities between the two sides of the island, suggesting that the drivers of these differences in modern communities are probably operating over long timescales.

This thesis expands ongoing research of diatom diversity and distributions on Maritime Antarctic islands, and reveals that both habitat and spatial controls are prominent in structuring communities. Furthermore, this research provides a fresh, holistic approach to interpreting diatoms in sediment cores to reconstructing past ecological conditions. Lastly, as the human presence in Antarctica continues to increase, this knowledge can help to develop specially managed and protected areas throughout the region by helping to understand factors that promote high and endemic diversity.

Keywords: James Ross Archipelago; Vega Island; Bacillariophyta; Ecology; Paleolimnology; Taxonomy

ABSTRAKT

Rozsivky v Antarktické oblasti obývají různorodé limno-terestrické habitaty, z nichž každý má svůj jedinečný ekologický význam v biomonitoringu, paleoekologii a v biogeografii, avšak naše znalosti se stále zaměřují převážně na obsáhnutí a zaznamenávání diversity u daných habitatů v různých částech Antarktidy.

Abychom získali větší vhled do toho, co ovlivňuje strukturu společenstev antarktických rozsivek z prostorového a habitatového hlediska, popisuji jejich rozmanitost a ekologii. Zaměřuji se na čtyři různé habitaty (jezera, mechy, potoky a mělké mokřady) na dvou protilehlých stranách ostrova Vega, který se nachází v souostroví Jamese Rosse ve Weddellově moři.

Nalezla jsem různorodou flóru 136 taxonů patřících do 31 rodů, kterým dominoval rod *Nitzschia*. Dále naznačuje, že flóra ostrova Vega je biogeograficky ovlivněna jak kontinentálními, tak Maritimními antarktickými bioregiony. Bylo zjištěno, že typ stanoviště je rozhodujícím faktorem pro složení společenstva rozsivek, a že tento vliv je silnější, než vliv rozmístění v rámci ostrova. V ordinační analýze byly separovány vzorky mechů primárně druhem *Chamaepinnularia krookiformis*, zatímco vzorky jezer byly odděleny hlavně druhem *Nitzschia paleacea.* Potoky určuje především *Fistulifera pelliculosa.*

Tato recentní společenstva byla následně porovnána s paleo vzorky z jezerních sedimentových jader, které byly odebrány z dvou jezer na protilehlých stranách ostrova Vega. V obou jádrech byla nalezena relativně uniformní společenstva rozsivek, což naznačuje stabilní jezerní komunity a/nebo allochtonní přísun do jezera v průběhu jeho historie. Nicméně jádra sedimentů se jedno od druhého podstatně lišila druhovou bohatostí a diverzitou, a to se promítlo i do rozdílů v moderních vzorcích z obou studovaných lokalit. To naznačuje, že faktory ovlivňující tyto rozdíly v recentních společenstvech pravděpodobně operují v dlouhém časovém rámci.

Tato diplomová práce rozšiřuje probíhající výzkum diverzity a distribuce rozsivek na ostrovech v oblasti Maritimní Antarktidy a ukazuje, že podstatná jsou jak stanoviště, tak prostorová distribuce. Dále tato studie poskytuje nový, holistický přístup k interpretaci rozsivek v jádrech sedimentů za účelem rekonstrukce ekologických podmínek v minulosti.

Se zvyšujícím se množstvím lidí v Antarktidě mohou tyto znalosti napomoci k rozvoji speciálně řízených a chráněných oblastí napříč regiony tím, že dopomohou k pochopení faktorů, které podporují vysokou a endemickou druhovou rozmanitost.

Klíčová slova: souostroví Jamese Rosse; ostrov Vega; Bacillariophyta; Ekologie; Paleolimnologie; Taxonomie

CHAPTER 1

INTRODUCTION

Diatoms

Site description

Diatom research in the area

Paleolimnology

Aim and outline of this thesis
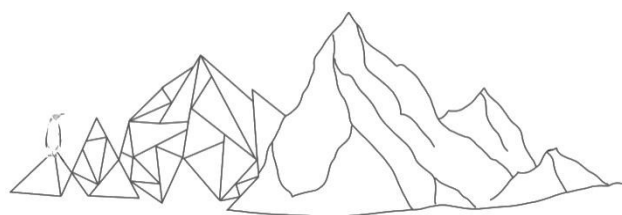
DIATOMS

Diatoms (Bacillariophyceae) are single-cell diploid eukaryotic organisms with the ability to photosynthesize. This (sub)division of heterokont algae is one of the most species-abundant globally, and rose to prominence during the Cretaceous period, with the first fossil records appearing in the early Jurassic. They occupy almost every known aquatic environment, including marine, freshwaters, and wetted soils (Round et al. 1990).

Diatom cell walls are made of silica (opal, SiO_2 x nH_2O). The capsule itself is composed of two valves (the 'epitheca' and 'hypotheca'), one of which is slightly smaller than the other. The two valve halves are connected with a siliceous girdle band (or 'cingulum'), and together make the capsule which is called the 'frustule'. This unique cellular structure is related to their reproductive strategy, which is mostly asexual vegetative (mitotic) cell division. When a diatom divides, the daughter cell receives one of the valves from the mother cell, and the smaller valve must be created itself. This process leads to a gradual decrease in the mean cell size of the population. After the critical size limit is reached, sexual reproduction is initiated (Round et al. 1990), though the actual trigger is not yet known.

Ornamentation on each frustule is species-specific, and allows for relatively straightforward morphological identification. Characters traditionally used to distinguish diatom taxa include size, shape, and symmetry of the frustule, together with "ornaments" such as the apices, striae, raphe, central raphe endings, the central area, puncta, stigma, and alveoli (Figure 1.1) (Smol et al. 2003). Scanning electron microscopy during the last half of the 20th century substantially increased the resolution of cells, providing more detailed and accurate study of their morphology (Round et al. 1990).
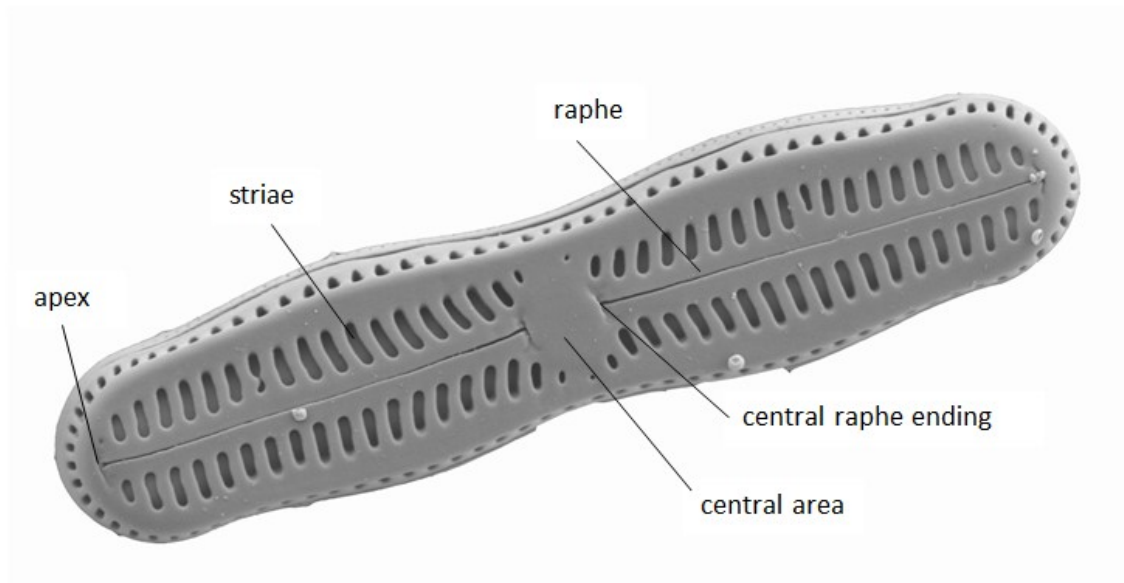
Figure 1.1 Selected valve elements shown on an image of *Humidophila nienta* from a scanning electron microscope.

Interestingly, diatoms exhibit species-specific responses to changes in the physical and chemical properties of their environment, and are therefore widely utilized as indicator taxa in environmental and biogeographical studies (Smol & Stoermer 2010). Diatoms have already proved their worth as being great ecological indicators in Antarctica, as they are present in almost all moist or semi-dry habitats, and their fossils preserve well in sediments (Spaulding et al. 2010). Their value as bioindicators, however, depends on the accurate taxonomic assignment of valves in samples (Jones 1996). As a recent taxonomical revision of the diatom flora from James Ross Island (JRI) has recently been performed (Kopalová et al. 2014; Zidarova et al. 2016), , this makes the JRI region an ideal location to study diatom ecology and conduct long-term ecological monitoring.

Aside from their utility as environmental indicators, diatoms play globally important roles in earth's biogeochemical cycles. Because of their silica cell walls, diatoms are a major player in the global silicon cycle (Hawkings et al. 2014). Furthermore, given their ability to photosynthesize, diatoms produce up to 20% of the world's O_2 and a substantial proportion of aquatic organic matter, making them major players in the global carbon cycle as well (Zidarova et al. 2016). At smaller scales, diatoms are important community members through their interactions with other groups, some of which predictably co-occurring with individual species (e.g. Stanish et al. 2013). For example, some taxa produce mucilage and extracellular polymeric substances ('EPS'), which can be utilized by heterotrophic bacteria growing within mosses, biofilms, or microbial mats, and can stimulate heterotrophic activity especially under low-nutrient conditions (Danger et al. 2013).

SITE DESCRIPTION

Locality of interest

Vega Island is part of the James Ross Archipelago (JRA) located in the north-eastern side of the Antarctic Peninsula (AP) (Figure 1), and was discovered in October of 1903 by the Swedish Antarctic Expedition led by Swedish geologist Otto Nordenskjöld and Carl Anton Larsen. Nordenskjöld named Vega Island after his uncle's Arctic ship, the *Vega,* which made the first voyage through the Northeast Passage in 1878-79 (Stewart 2011).

The climate of Vega Island is cold and semi-arid. The mean annual air temperature at J. G. Mendel Station on northern James Ross Island (~25 km to the west) was −7.0 °C in the period of 2006–2015, with summer daily maxima exceeding +10 °C and winter minima dropping below −30 °C (Hrbáček et al. 2017). The interannual temperature variability is strongly related to the extent and persistence of sea ice, which affects the air temperature above the low-lying and coastal areas (Ambrožová et al. 2019). The whole JRA lies in the precipitation shadow of the AP with annual precipitation estimates between 300 and 500 mm of water-equivalent (van Lipzig et al. 2004). However, the strong winds affect snow redistribution, and a significant proportion of the snow is blown away from flat and concave surfaces, thus limiting their moisture (Nývlt et al. 2016). The highest point of the island lies 630 m above sea level (a.s.l.).

The basement of Vega Island is made of Late Cretaceous sandstones, mudstones and conglomerates of the Santa Marta, Snow Hill Island, and López de Bertodano formations (Crame et al. 2004). The elevated volcanic mesas in the surrounding are formed by basaltic to trachybasaltic rocks (Košler et al. 2009) of the Miocene to Pleistocene James Ross Island Volcanic Group (Nelson 1966; Smellie et al. 2013). The mostly subglacial volcanic setting produced specific morphology including steeply-inclined hyaloclastite breccia foresets covered by flat topsets of subaerial basalt lavas (Smellie et al. 2008). Minor amount of subaquatic eruptions is represented on Vega Island by tuffs and lapilli tuffs (Smellie et al. 2008). The ice-free areas are covered by till and glaciofluvial sediments emplaced here after the retreat of local glaciers and by marine sediments in coastal areas (Zale & Karlén 1989).
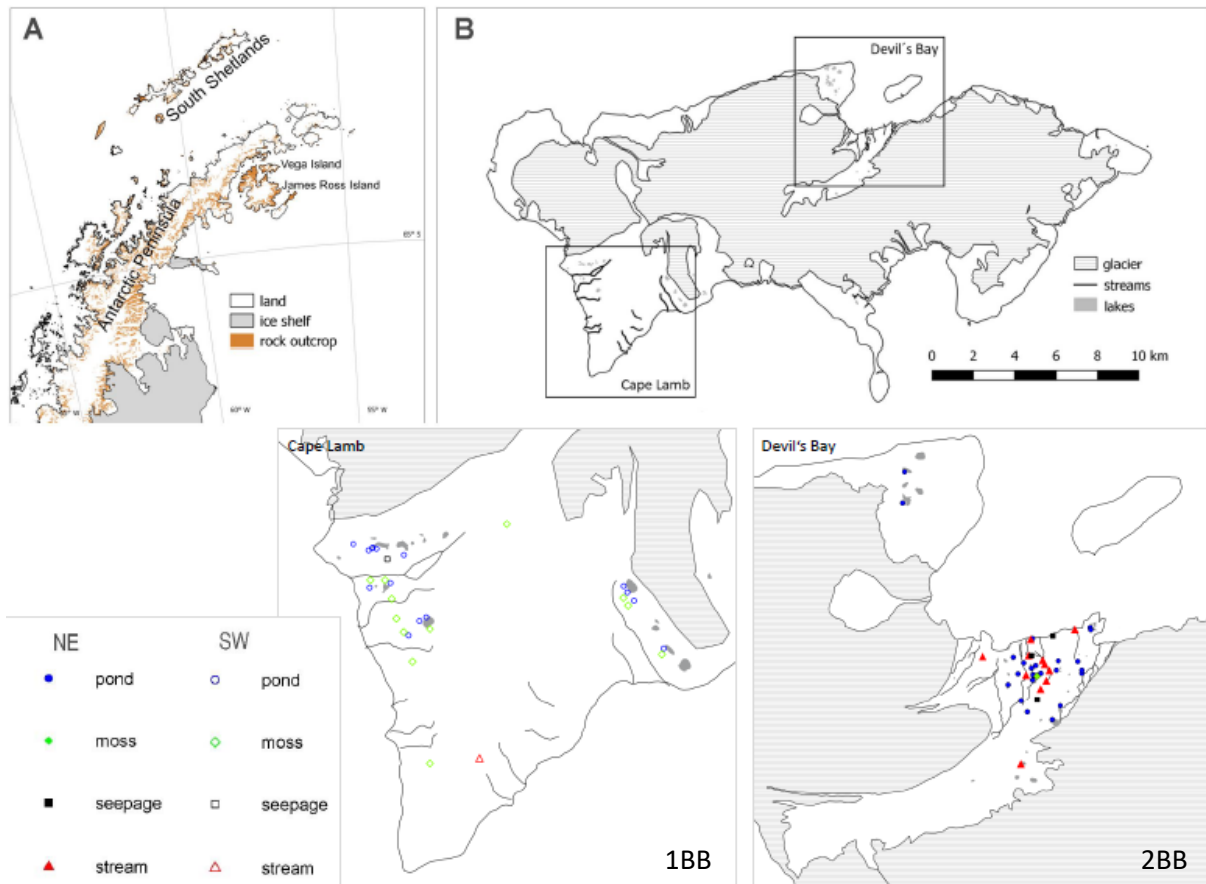
Figure 1.2 Map of Antarctica (A), with inset of James Ross Island and Vega Island. (B) detail of Vega Island indicating two study sides (NE Devils Bay and SW Cape Lamb). Pond habitats are indicated by blue circles, moss habitats by green diamonds, seepages by black squares, and streams by red triangles. Symbols for north sites are filled, and south sites are represented by outlines only.

Of these ice-free areas, Cape Lamb (63°54' S, 57°37' W, Figure 1B) forms the southwest (SW) tip of Vega Island. It was first mapped in 1903 by the Swedish Antarctic Expedition led by Otto Nordenskjöld and Carl Anton Larsen, and later was named after Ivan Mackenzie Lamb (Stewart 2011). It is the largest ice-free area on the island, with a maximum elevation of 482 m a.s.l. The outcrops consist of Cretaceous-Miocene sediments and volcanic rocks (Rinaldi 1982; Pirrie et al. 1991). Streams in this area are shallow, carrying clay and silt, and often change course and catchments because of fluvial erosion (Moreno et al. 2012).

Devil's Bay (Figure 2B) is representative of the north side of Vega Island, and is climatically influenced by the nearby AP. The ice-free area of Devil's Bay is surrounded by adjacent dome glaciers on volcanic mesas with some outlets, including the Glacier Bahía del Diablo (Marinsek & Ermolin 2015). Here, the snow accumulation is less than on the southern side of the island represented by Cape Lamb (Kopalová, pers. obs.). However, the higher average precipitation observed on Cape Lamb is expected to expand to the whole of Vega Island as the climate warms (Steig et al. 2009).

Flora & fauna

The harsh Antarctic climate and limited light conditions allow only sparse vegetation cover on Vega Island. The aboveground primary production is therefore mainly composed of lichens and mosses, as no vascular plants occur here (Peat et al. 2007). Furthermore, no permanent bird colony has been reported here, and human presence on the island is limited only to scientific campaigns in the summertime.

Photo 1.1 View around Lake Esmeralda, Cape Lamb. Photo credit: Kateřina Kopalová

DIATOM RESEARCH IN THE AREA

Previous work

Investigations of diatoms from the AP have been mainly conducted on the South Shetland Islands to the north of the peninsula (Zidarova et al. 2010, 2012; Van de Vijver et al. 2011; Kopalová et al. 2014), and from James Ross Island (JRI) to the south, which has been explored in part thanks to the construction of the Johann Gregor Mendel Czech Research Station on the northern tip of JRI in 2006. This infrastructure provides the possibility to conduct long-term monitoring of several locations in the vicinity. Accordingly, the most investigated region of JRI in terms of diatom research is the Ulu Peninsula, where several new taxa have been described (Zidarova et al. 2009, 2012; Kopalová et al. 2011; Kopalová et al. 2012; Van de Vijver et al. 2010a, 2010b, 2013; Van de Vijver & Zidarova 2011; Van de Vijver & Kopalová 2014), resulting in the establishment of a modern, fine-grained diatom taxonomy for use in this area, as well as ecological characterization

of the assemblages (Kopalová & Van De Vijver 2013a, Kopalová et al. 2013b). However, the neighboring Vega Island has only just started to be explored, and is still lacking a detailed evaluation of its diatom flora.

Diatom communities may significantly differ among habitat types, as has been shown on the sub-Antarctic islands (Van De Vijver & Beyens 1999; Van de Vijver et al. 2008) and in Maritime Antarctica (Kopalová et al. 2012; Kopalová et al. 2014). On Ulu Peninsula (JRI), significant differences were found among habitat types, not only in terms of diatom relative abundances, but also in diversity, as ponds were more diverse than seepage areas and streams (Kopalová et al. 2013). Stream diatom communities specifically may be strongly influenced by flow regime (Esposito et al. 2006; Stanish et al. 2011, 2012; Kohler et al. 2015), as well as water temperature, which may differ greatly between the glacier snout and in downstream reaches, and influence growth rates and survival strategies (Darling et al. 2017). Furthermore, research on the Antarctic Continent has previously linked differences in abundances stemming from stream 'harshness' to the biogeographical distributions of individual taxa (Esposito et al. 2006). For lakes and ponds, conductivity may be a dominant ecological control, and may indicate marine influence and proximity (Saunders et al. 2015), as well as hydrological connectivity through concentration and dilution (Sakaeva et al. 2016; Roman et al. *in press*). On the other hand, moss and seepage communities may be more adapted to 'harsher' conditions with frequent desiccation and greater exposure to the elements, and are often composed of heavily-silicified taxa commonly found in terrestrial habitats (Kopalová et al. 2014).

PALEOLIMNOLOGY

From the beginning of a lake's origin, sediment is continuously deposited (Kachlík & Chlupáč 2003), and chemical and physical characteristics of the environment, as well as information about the resident organisms and associated climate changes, can be studied from these resulting layers (Wetzel 2001). All of these different proxies can then be combined and calibrated to reconstruct the past environment of the given lake (Pokorný et al. 1992). Diatoms, with their ability to indicate different factors within the environment (Van Dam et al. 1994), together with the excellent preservation of their frustules (Hall & Smol 1999), are great model organisms for paleolimnology (Round et al. 1990; Smol et al. 2003). The fossil record, however, is usually incomplete, and does not capture the ecosystem in its entirety (Pokorný et al. 1992). For example, some hydrochemical processes can destroy the silica frustules of dead diatom cells, and as such the fossil community does not correspond to its living one, especially in terms of abundances (Cohen 2003; Smol et al. 2003). This is especially possible in hypersaline lakes with high pH, or under high temperatures or pressure (Barker et al. 1994). Distortion can also occur given that smaller valves dissolve faster (Smol et al. 2003), and that mechanical movement, whether caused by inflow, other organisms (bioturbulance), or sediment processes, can

cause valve breaks (Smol et al. 2003). Despite all these difficulties, it is possible to obtain a lot of information from the diatom lake fossil record.

Sediment cores from this area

Unlike East Antarctica, where most of the lake sediment cores with diatom analysis were performed (Fulford-Smirth & Sikes 1996; Roberts & McMinn 1998; Roberts et al. 1999, 2001, 2004; Cremer et al. 2004; Hodgson et al. 2005), not many have been done in the Antarctic Peninsula area. On Vega Island, paleolimnological work has been recently conducted (Pišková et al. 2019; Čejka et al. *in review*; Moreno et al. 2012; sinito 2011, Irurzun et al. 2013, 2017), though the diatoms recovered from the cores present some unclear patterns and mysteries, which will be discussed further in this thesis. One of the first studies from Vega Island provided a hydrological examination of the Cape Lamb area, including Lake Esmeralda (Moreno et al. 2012). Sinito et al. (2011) and Irurzun et al. (2013, 2017) studied the paleomagnetic properties of Lake Esmeralda sediments. On Beak Island, to the north-east of Vega Island, lake sediments were studied by Sterken et al. (2012). Elsewhere in the Antarctic Peninsula region, cores have been examined to reconstruct ice-sheet changes since the Last Glacial Maximum (Cofaigh et al. 2014). The study nearest to Vega Island is from the northern part of James Ross Island (Björck et al. 1996). Lake Terrapin, Monolith, and Keyhole were dated during that study; however a continuous paleoclimatic record was detected only on Keyhole Lake. Studies on James Ross Island ice cores were provided by Mulvaney et al. (2012) and Abram et al. (2013) on Mt. Haddington ice cap; however no diatom analysis were performed there. On a broader scale, diatom analyses on lake sediment cores have been conducted by Schmidt et al. (1990) on King George Island, and by Heroy et al. (2008) in the Bransfield Basin.

AIM AND OUTLINE OF THIS THESIS

This thesis focuses on the taxonomical, ecological, and paleoecological characterization of aquatic, semi-aquatic, and moss-inhabiting diatom communities from Vega Island, a Maritime Antarctic Island located in the Antarctic Peninsula region. More specifically, this thesis investigates the diversity and ecology of diatoms living in different habitat types such as ponds, mosses, streams, and seepage areas on two opposite sides of Vega Island with different climate conditions (**Chapter 2**), and compares these modern communities with those from sediment cores from two prominent lakes extracted from both sides of the island (**Chapter 7**). Further comparison of the two sediment cores is provided in **Chapter 6**. This paleoecological component of the thesis was part of bigger project (The past is the key to the future: Ecology and Holocene evolution of freshwater diatom communities in the northern Antarctic Peninsula region; GAČR 16-17346Y), where I was involved in the Lake Esmeralda sediment analysis and Lake Anonima sediment core preparation, and resulted in two publications where I am listed as a co-author (Píšková et al. 2019; Čejka et al. *in review*) (**Chapters 4,5**). Finally, a first author paper (Bulínová et al. 2018) (**Chapter 3**) with a description of a new diatom species is a result of the taxonomical revision of the modern diatom flora (see **Appendix 2**).

More specifically, the thesis focuses on three key subjects:

- Floristic and taxonomic analysis of the diatom flora of Vega Island: How cosmopolitan is the Vega Island diatom flora in the context of the Maritime Antarctic? Can all observed taxa be identified using the currently available literature? Must new species be described?

- Ecological analysis of the modern diatom communities of Vega Island: Do diatom communities differ by habitat type? Are there differences in the diatom flora between opposing sides of Vega Island with differing climatic characteristics?

- Comparative analysis of the diversity and composition of diatom assemblages from two lake sediment cores, each from a different side of Vega Island: Do diatom assemblages differ between cores? How are diatom assemblages from each core related to modern diatom communities from each side?

REFERENCES

Abram, N. J., Mulvaney, R., Wolff, E. W., Triest, J., Kipfstuhl, S., Trusel, L. D., Vimeux, F., Fleet, L. & Arrowsmith, C. (2013). Acceleration of snow melt in an Antarctic Peninsula ice core during the twentieth century. Nature Geoscience, 6(5), 404.

Ambrožová, K., Láska, K., Hrbáček, F., Kavan, J., & Ondruch, J. (2019). Air temperature and lapse rate variation in the ice-free and glaciated areas of northern James Ross Island, Antarctic Peninsula, during 2013–2016. International Journal of Climatology, 39(2), 643-657.

Barker, P., Fontes, J. C., & Gasse, F. (1994). Experimental dissolution of diatom silica in concentrated salt solutions and implications for paleoenvironmental reconstruction. *Limnology and Oceanography*, *39*(1), 99-110.

Björck, S., Olsson, S., Ellis-Evans, C., Håkansson, H., Humlum, O., & de Lirio, J. M. (1996). Late Holocene palaeoclimatic records from lake sediments on James Ross Island, Antarctica. Palaeogeography, Palaeoclimatology, Palaeoecology, 121(3-4), 195-220.

Bulínová, M., Kochman-Kędziora, N., Kopalová, K., & Van De Vijver, B. (2018). Three new Hantzschia species (Bacillariophyta) from the Maritime Antarctic Region. Phytotaxa, 371(3), 168-184.

Cofaigh, C. Ó., Davies, B. J., Livingstone, S. J., Smith, J. A., Johnson, J. S., Hocking, E. P., Hodgson, D. A., Anderson, J. B., Bentley, M. J., Canals, M., Domack, E., Dowdeswell, J. A., Evans, J., Glasser, N. F., Hillenbrand, C.-D., Larter, R. D., Roberts, S. J. & Simms, A. R. (2014). Reconstruction of ice-sheet changes in the Antarctic Peninsula since the Last Glacial Maximum. Quaternary Science Reviews, 100, 87-110.

Cohen, A. S. (2003). Paleolimnology: the history and evolution of lake systems. Oxford University Press.

Crame, J. A., Francis, J. E., Cantrill, D. J., & Pirrie, D. (2004). Maastrichtian stratigraphy of Antarctica. Cretaceous Research, 25(3), 411-423.

Cremer, H., Gore, D., Hultzsch, N., Melles, M., & Wagner, B. (2004). The diatom flora and limnology of lakes in the Amery Oasis, East Antarctica. Polar Biology, *27*(9), 513-531.

Čejka, T., Nývlt, D., Kopalová, K., Bulínová, M., Kavan, J., Lirio, J.M., Coria, S.H., Van de Vijver, B. (*in review*). Timing of the Neoglacial onset on the north-eastern Antarctic Peninsula based on lacustrine archive from Lake Anónima, Vega Island. Global and Planetary Change

Danger, M., Cornut, J., Chauvet, E., Chavez, P., Elger, A., & Lecerf, A. (2013). Benthic algae stimulate leaf litter decomposition in detritus-based headwater streams: a case of aquatic priming effect?. Ecology, 94(7), 1604-1613.

Darling, J. P., Garland, D. D., Stanish, L. F., Esposito, R. M., Sokol, E. R., & McKnight, D. M. (2017). Thermal autecology describes the occurrence patterns of four benthic diatoms in McMurdo Dry Valley streams. Polar Biology, 40(12), 2381-2396.

Ermolin, E., De Angelis, H., & Skvarca, P. (2002). Mapping of permafrost on Vega Island, Antarctic Peninsula, using satellite images and aerial photography. Annals of Glaciology, 34, 184-188.

Esposito, R. M. M., Horn, S. L., McKnight, D. M., Cox, M. J., Grant, M. C., Spaulding, S. A., Doran, P. T. & Cozzetto, K. D. (2006). Antarctic climate cooling and response of diatoms in glacial meltwater streams. Geophysical Research Letters, 33(7).

Fulford-Smith, S. P., & Sikes, E. L. (1996). The evolution of Ace Lake, Antarctica, determined from sedimentary diatom assemblages. Palaeogeography, Palaeoclimatology, Palaeoecology, *124*(1-2), 73-86.

Hall, R. I. & Smol, J. P. (1999). Diatoms as indicators of lake eutrophication. The diatoms: applications for the environmental and earth sciences, 128-168.

Hawkings, J. R., Wadham, J. L., Tranter, M., Raiswell, R., Benning, L. G., Statham, P. J., Tedstone, A., Nienow, P., Lee, K. & Telling, J. (2014). Ice sheets as a significant source of highly reactive nanoparticulate iron to the oceans. Nature communications, 5, 3929.

Heroy, D. C., Sjunneskog, C., & Anderson, J. B. (2008). Holocene climate change in the Bransfield Basin, Antarctic Peninsula: evidence from sediment and diatom analysis. Antarctic Science, 20(1), 69-87.

Hodgson, D. A., Verleyen, E., Sabbe, K., Squier, A. H., Keely, B. J., Leng, M. J., Saunders, K. M. & Vyverman, W. (2005). Late Quaternary climate-driven environmental change in the Larsemann Hills, East Antarctica, multi-proxy evidence from a lake sediment core. Quaternary Research, *64*(1), 83-99.

Hrbáček, F., Nývlt, D., & Láska, K. (2017). Active layer thermal dynamics at two lithologically different sites on James Ross Island, Eastern Antarctic Peninsula. *Catena*, *149*, 592-602.

Irurzun, M. A., Chaparro, M. A. E., Sinito, A. M., Gogorza, C. S. G., Lirio, J. M., Nuñez, H., Nowaczyk, N. R. & Böhnel, H. N. (2013). Preliminary relative palaeointensity record and chronology on sedimentary cores from Lake Esmeralda (Vega Island, Antarctica). Latimag Letters, 3(6).

Irurzun, M. A., Chaparro, M. A. E., Sinito, A. M., Gogorza, C. S. G., Nuñez, H., Nowaczyk, N. R., & Böhnel, H. N. (2017). Relative palaeointensity and reservoir effect on Lake Esmeralda, Antarctica. Antarctic Science, 29(4), 356-368.

Jones, J. (1996). The diversity, distribution and ecology of diatoms from Antarctic inland waters. Biodiversity & Conservation, 5(11), 1433-1449.

Kachlík, V., & Chlupáč, I. (2003). Základy geologie. Historická geologie. Karolinum.

Kohler, T. J., Stanish, L. F., Crisp, S. W., Koch, J. C., Liptzin, D., Baeseman, J. L., & McKnight, D. M. (2015). Life in the main channel: long-term hydrologic control of microbial mat abundance in McMurdo Dry Valley streams, Antarctica. Ecosystems, 18(2), 310-327.

Kopalová, K., Veselá, J., Elster, J., Nedbalová, L., Komárek, J., & Van de Vijver, B. (2012). Benthic diatoms (Bacillariophyta) from seepages and streams on James Ross Island (NW Weddell Sea, Antarctica). Plant Ecology and Evolution, 145(2), 190-208.

Kopalová, K., Nedbalová, L., De Haan, M., & Van de Vijver, B. (2011). Description of five new species of the diatom genus Luticola (Bacillariophyta, Diadesmidaceae) found in lakes of James Ross Island (Maritime Antarctic Region). Phytotaxa, 27(1), 44-60.

Kopalová, K., & Van de Vijver, B. (2013a). Structure and ecology of freshwater benthic diatom communities from Byers Peninsula, Livingston Island, South Shetland Islands. Antarctic science, 25(2), 239-253.

Kopalová, K., Nedbalová, L., Nývlt, D., Elster, J., & Van de Vijver, B. (2013b). Diversity, ecology and biogeography of the freshwater diatom communities from Ulu Peninsula (James Ross Island, NE Antarctic Peninsula). Polar Biology, 36(7), 933-948.

Kopalová, K., Ochyra, R., Nedbalová, L., & Van de Vijver, B. (2014). Moss-inhabiting diatoms from two contrasting Maritime Antarctic islands. Plant Ecology and Evolution, 147(1), 67-84.

Košler, J., Magna, T., Mlčoch, B., Mixa, P., Nývlt, D., & Holub, F. V. (2009). Combined Sr, Nd, Pb and Li isotope geochemistry of alkaline lavas from northern James Ross Island (Antarctic Peninsula) and implications for back-arc magma formation. Chemical Geology, 258(3-4), 207-218.

Marinsek, S., & Ermolin, E. (2015). 10 year mass balance by glaciological and geodetic methods of Glaciar Bahía del Diablo, Vega Island, Antarctic Peninsula. Annals of Glaciology, 56(70), 141-146.

Moreno, L., Silva-Busso, A., López-Martínez, J., Durán-Valsero, J. J., Martínez-Navarrete, C., Cuchí, J. A., & Ermolin, E. (2012). Hydrogeochemical characteristics at Cape Lamb, Vega Island, Antarctic Peninsula. Antarctic Science, 24(6), 591-607.

Mulvaney, R., Abram, N. J., Hindmarsh, R. C., Arrowsmith, C., Fleet, L., Triest, J., Sime, L. C., Alemany, O. & Foord, S. (2012). Recent Antarctic Peninsula warming relative to Holocene climate and ice-shelf history. Nature, 489(7414), 141.

Nelson, P. H. H. (1966). The James Ross Island Volcanic Group of north-east Graham Land (Vol. 54). British Antarctic Survey.

Nývlt, D., Fišáková, M. N., Barták, M., Stachoň, Z., Pavel, V., Mlčoch, B., & Láska, K. (2016). Death age, seasonality, taphonomy and colonization of seal carcasses from Ulu Peninsula, James Ross Island, Antarctic Peninsula. Antarctic Science, 28(1), 3-16.

Peat, H. J., Clarke, A., & Convey, P. (2007). Diversity and biogeography of the Antarctic flora. Journal of Biogeography, 34(1), 132-146.

Pirrie, D., Crame, J. A., & Riding, J. B. (1991). Late Cretaceous stratigraphy and sedimentology of Cape Lamb, Vega Island, Antarctica. Cretaceous Research, 12(3), 227-258.

Píšková, A., Roman, M., Bulínová, M., Pokorný, M., Sanderson, D., Cresswell, A., Lirio, J. M., Coria, S. H., Nedbalová, L., Lami, A., Musazzi, S., Van de Vijver, B., Nývlt, D. & Kopalová, K. (2019). Late-Holocene palaeoenvironmental changes at Lake Esmeralda (Vega Island, Antarctic Peninsula) based on a multi-proxy analysis of laminated lake sediment. The Holocene, 0959683619838033.

Pokorný, Vladimír. Všeobecná paleontologie. 1. vyd. Praha: Karolinum, 1992. 296 s. ISBN 80-7066-585-8.

Rinaldi, C. A. (1982). The upper cretaceous in the James Ross Island group. Antarctic geoscience, 281-286.

Roberts, D., & McMinn, A. (1998). A weighted-averaging regression and calibration model for inferring lakewater salinity from fossil diatom assemblages in saline lakes of the Vestfold Hills: a new tool for interpreting Holocene lake histories in Antarctica. Journal of Paleolimnology, 19(2), 99-113.

Roberts, D., & McMinn, A. (1999). A diatom-based palaeosalinity history of Ace Lake, Vestfold Hills, Antarctica. The Holocene, 9(4), 401-408.

Roberts, D., McMinn, A., Cremer, H., Gore, D. B., & Melles, M. (2004). The Holocene evolution and palaeosalinity history of Beall Lake, Windmill Islands (East Antarctica) using an expanded diatom-based weighted averaging model. Palaeogeography, Palaeoclimatology, Palaeoecology, 208(1-2), 121-140.

Roberts, D., van Ommen, T. D., McMinn, A., Morgan, V., & Roberts, J. L. (2001). Late-Holocene East Antarctic climate trends from ice-core and lake-sediment proxies. The Holocene, 11(1), 117-120.

Roman, M., Nedbalová, L., Kohler, T.J., Lirio, J.M., Coria, S.H., Kopáček, J., Vignoni, P.A., Kopalová, K., Lecomte, K.L., Elster, J., Nývlt, D. (in press). Lacustrine systems of Clearwater Mesa (James Ross Island, northeastern Antarctic Peninsula): geomorphological settings and limnological characterization. Antarctic Science.

Round, F. E., Crawford, R. M., & Mann, D. G. (1990). Diatoms: biology and morphology of the genera. Cambridge university press.

Sakaeva, A., Sokol, E. R., Kohler, T. J., Stanish, L. F., Spaulding, S. A., Howkins, A., Welch, K. A., Lyons, W. B., Barrett, J. E. & McKnight, D. M. (2016). Evidence for dispersal and habitat controls on pond diatom communities from the McMurdo Sound Region of Antarctica. Polar Biology, 39(12), 2441-2456.

Saunders, K. M., Hodgson, D. A., McMurtrie, S., & Grosjean, M. (2015). A diatom–conductivity transfer function for reconstructing past changes in the Southern Hemisphere westerly winds over the Southern Ocean. Journal of Quaternary Science, 30(5), 464-477.

Schmidt, R., Mäusbacher, R., & Müller, J. (1990). Holocene diatom flora and stratigraphy from sediment cores of two Antarctic lakes (King George Island). Journal of paleolimnology, *3*(1), 55-74.

Sinito, A. M., Chaparro, M. A., Irurzun, M. A., Lirio, J. M., Nowaczyk, N. R., Böhnel, H. N., & Nuñez, H. (2011) Preliminary palaeomagnetic and rock-magnetic studies on sediments from lake Esmeralda (Vega Island), Anatarctica, Conference paper 2ª Reunión Bienal de la Asociación Latinoamericana de Paleomagnetismo y Geomagnetismo. 23–26 November 2011, Buenos Aires.

Smellie, J. L., Johnson, J. S., & Nelson, A. E. (2013). Geological map of James Ross Island. I. James Ross Island volcanic group.

Smellie, J. L., Johnson, J. S., McIntosh, W. C., Esser, R., Gudmundsson, M. T., Hambrey, M. J., & De Vries, B. V. W. (2008). Six million years of glacial history recorded in volcanic lithofacies of the James Ross Island Volcanic Group, Antarctic Peninsula. Palaeogeography, Palaeoclimatology, Palaeoecology, 260(1-2), 122-148.

Smol, J. P., & Stoermer, E. F. (Eds.). (2010). The diatoms: applications for the environmental and earth sciences. Cambridge University Press.

Smol, J. P., Birks, H. J., & Last, W. M. (Eds.). (2002). Tracking environmental change using lake sediments: Volume 3: Terrestrial, algal, and siliceous indicators (Vol. 3). Springer Science & Business Media (Second edition-2003)

Spaulding, S. A., Lubinski, D. J., & Potapova, M. (2010). Diatoms of the United States. Diatom identification guide & ecological resource. US Geological Survey, Boulder CO, USA. Available from: http://westerndiatoms. colorado. edu/(accessed: 28 August 2013).

Stanish, L. F., Kohler, T. J., Esposito, R. M., Simmons, B. L., Nielsen, U. N., Wall, D. H., ... & McKnight, D. M. (2012). Extreme streams: flow intermittency as a control on diatom communities in meltwater streams in the McMurdo Dry Valleys, Antarctica. Canadian journal of fisheries and aquatic sciences, 69(8), 1405-1419.

Stanish, L. F., Nemergut, D. R., & McKnight, D. M. (2011). Hydrologic processes influence diatom community composition in Dry Valley streams. Journal of the North American Benthological Society, 30(4), 1057-1073.

Stanish, L. F., O'Neill, S. P., Gonzalez, A., Legg, T. M., Knelman, J., McKnight, D. M., ... & Nemergut, D. R. (2013). Bacteria and diatom co-occurrence patterns in microbial mats from polar desert streams. Environmental microbiology, 15(4), 1115-1131.

Steig, E. J., Schneider, D. P., Rutherford, S. D., Mann, M. E., Comiso, J. C., & Shindell, D. T. (2009). Warming of the Antarctic ice-sheet surface since the 1957 International Geophysical Year. Nature, 457(7228), 459.

Sterken, M., Roberts, S. J., Hodgson, D. A., Vyverman, W., Balbo, A. L., Sabbe, K., ... & Verleyen, E. (2012). Holocene glacial and climate history of Prince Gustav Channel, northeastern Antarctic Peninsula. Quaternary Science Reviews, 31, 93-111.

Stewart, J. (2011). Antarctica-An Encyclopedia. McFarland & Company. Inc., London.

Van Dam, H., Mertens, A., & Sinkeldam, J. (1994). A coded checklist and ecological indicator values of freshwater diatoms from the Netherlands. Netherland Journal of Aquatic Ecology, 28(1), 117-133.

Van de Vijver, B., Ector, L., de Haan, M., & Zidarova, R. (2010a). The genus Microcostatus in the Antarctic region. Diatom research, 25(2), 417-429.

Van de Vijver, B., Sterken, M., Vyverman, W., Mataloni, G., Nedbalová, L., Kopalová, K., Elster, J., Verleyen, E. & Sabbe, K. (2010b). Four new non-marine diatom taxa from the Subantarctic and Antarctic regions. Diatom research, 25(2), 431-443.

Van de Vijver, B., Kopalová, K., Zidarova, R., & Cox, E. J. (2013). New and interesting small-celled naviculoid diatoms (Bacillariophyta) from the Maritime Antarctic Region. Nova Hedwigia, 97(1-2), 189-208.Van de Vijver, B., & Beyens, L. (1999). Biogeography and ecology of freshwater diatoms in Subantarctica: a review. Journal of biogeography, 26(5), 993-1000.

Van de Vijver, B., & Kopalová, K. (2014). Four Achnanthidium species (Bacillariophyta) formerly identified as Achnanthidium minutissimum from the Antarctic Region. European Journal of Taxonomy, (79).

Van de Vijver, B., & Zidarova, R. (2011). Five new taxa in the genus Pinnularia sectio Distantes (Bacillariophyta) from Livingston Island (South Shetland Islands). Phytotaxa, 24(1), 39-50.

Van de Vijver, B., Gremmen, N., & Smith, V. (2008). Diatom communities from the sub-Antarctic Prince Edward Islands: diversity and distribution patterns. Polar biology, 31(7), 795-808.

Van Lipzig, N. P. M., King, J. C., Lachlan-Cope, T. A., & Van den Broeke, M. R. (2004). Precipitation, sublimation, and snow drift in the Antarctic Peninsula region from a regional atmospheric model. Journal of Geophysical Research: Atmospheres, 109(D24).

Wetzel, R. G. (2001). Limnology: lake and river ecosystems. Gulf professional publishing.

Zale, R., & Karlén, W. (1989). Lake sediment cores from the Antarctic Peninsula and surrounding islands. Geografiska Annaler: Series A, Physical Geography, 71(3-4), 211-220.

Zidarova, R., Kopalová, K., & Van de Vijver, B. (2012). The genus Pinnularia (Bacillariophyta) excluding the section Distantes on Livingston Island (South Shetland Islands) with the description of twelve new taxa. Phytotaxa, 44(1), 11-37.

Zidarova, R., Kopalová, K., Van de Vijver, B., & Lange-Bertalot, H. (2016). Diatoms from the Antarctic Region, Maritime Antarctica.

Zidarova, R., Van de Vijver, B., Mataloni, G., Kopalová, K., & Nedbalová, L. (2009). Four new freshwater diatom species (Bacillariophyceae) from Antarctica. Cryptogamie: algologie.-Paris, 30, 295-310.

Zidarova, R., Van de Vijver, B., Quesada, A., & de Haan, M. (2010). Revision of the genus Hantzschia (Bacillariophyceae) on Livingston Island (South Shetland Islands, Southern Atlantic Ocean). Plant Ecology and Evolution, 143(3), 318-333.

CHAPTER 2

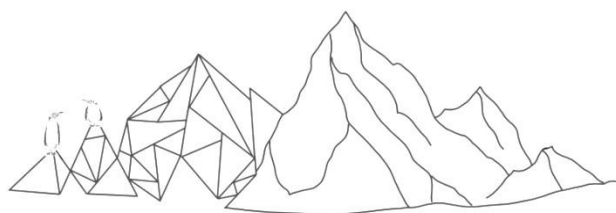**GENERAL OVERVIEW OF THE RECENT MATERIAL**

Materials and methods

Results from analysis of recent material

Species composition

Species diversity and accumulation curves

Comparison of community structure

MATERIALS AND METHODS

Sampling

A total set of 113 samples were collected from four different habitat types (ponds, moss, streams, seepages) on two different sides of Vega Island (GPS, Figure 1), during the austral summers of 2013 (Devil's Bay) and 2014 (Cape Lamb) (Table 1). From all habitat types, samples were collected by removing the upper layer of material (mosses/biofilms/microbial mat) from substrata, placing them in a clean plastic container, and immediately fixing them with 96% EtOH. Samples were then transported to the Department of Ecology at Charles University (Prague, Czech Republic).

When possible, basic ecological parameters such as pH, conductivity and temperature were measured with a Hanna Combo instrument (Hanna Instruments, USA, upper detection limit = 4,000 μS cm^{-1}). A detailed list of the collected samples with their ecological data is given in Appendix 1.

Slide preparation and sample analysis

Samples were prepared following the method described in Van der Werff (1955). First, samples were cleaned by adding 37% H_2O_2 and heated to 80 °C for 1 hour. Oxidation of organic material was followed by adding $KMnO_4$. After digestion samples were rinsed three times with deionised H_2O and centrifuged (3 × 10 minutes at 3700 × g). The material was diluted with distilled water so excessive concentrations of diatom valves were avoid, dried on microscope cover slips and permanently mounted with Naphrax® medium onto slides. Samples and slides as well are stored at the Department of Ecology at Charles University.

In each sample, 400 valves were enumerated on random transects at 1,000 x magnification under oil immersion using an Olympus BX43 microscope, equipped with Nomarski Contrast and Olympus DP27 camera using the cellSens Entry Imaging Software. Valve dimensions [length (L), width (W) and stria density (S)] were determined on every species to compare it with previously known minimum and maximum values for each of those dimensions to be certain of classification. For taxonomical identification Zidarova et al. (2016) was used as a main source of information. For several species, identification up to species level was not possible due to their unclear taxonomic situation. When the identity of a taxon could not be determined with 100% certainty, it was shown using 'cf.' or 'sp.' For Antarctic species, the geographic distribution was further subdivided in sub-Antarctic (SA), Maritime Antarctic (MA) and Continental Antarctic (CA) Region based on Chown & Convey (2007) and Zidarova et al. (2016).

Statistical analysis

To compare diatom community structure among different habitat types and sides of the island, diatom species counts were transformed to relative abundances (% of total diatom valves counted per sample), and species richness, Shannon diversity (Shannon & Weaver 1949), and evenness (Pielou 1966) were calculated. Tukey's Honest Significant Differences (HSD) was used to determine significant differences between categories (i.e. habitat types and NE/SW sides of the island).

The raw relative abundance data were visualized with a dot plot diagram organized by different habitat types and sides of the island. In order to better observe relationships between samples, a principal components analysis (PCA) was generated by first filtering out rare taxa (all those that did not appear in any sample at more than 8% relative abundance) to reduce the influence of rare species. Data were then square root transformed, and a PCA generated using the *vegan* package in R (Oksanen 2018).

To test the hypothesis that diatom communities significantly differ by habitat, we created a redundancy analysis (RDA) on this same dataset, but this time constraining the PCA analysis by habitat type. The variables were scaled to a zero mean and variance. To test if diatom communities were different by different sides of the island, we included only pond habitats, since other habitat types did not provide adequate replication between island sides for evaluation.

To test for statistical differences in community structure based on categorical variables, such as differences in habitat and island aspect, we used permutational multivariate analysis of variance PERMANOVA, (Anderson 2001). Significance was designated at $\alpha = 0.05$, and all analyses and figures were generated using R version 3.4.3 (R Core Team 2017).

RESULTS FROM ANALYSIS OF RECENT MATERIAL

The aim of this chapter is to study the diversity, ecology, and biogeography of modern diatoms between two sides of Vega Island (Maritime Antarctic Region) to evaluate any differences in diatom communities as a function of their habitat type and island aspect. Specifically, four different habitat types (ponds, streams, seepages, and mosses) were sampled on Vega Island from two different localities; Cape Lamb located on the south-west (SW) of the island, and Devil's Bay on the north-east (NE). Due to the naturally low abundances of diatoms in some samples, only 72 samples were analyzed in total, and in each sample a standard quantity of 400 diatom valves was counted. From Devil's Bay, 25 pond, 4 moss, 11 stream, and 3 seepage samples were successfully analyzed, while from Cape Lamb, 15 pond, 12 moss, 1 stream, and 1 seepage samples were examined. In total, 28,800 valves were counted from all analyzed recent samples. From this survey, a new species was furthermore described (Chapter 3).

The recent diatom flora of Vega Island revealed a total of 136 diatom taxa (including species, varieties, and forms) belonging to 31 genera, and a complete list of observed taxa is presented in Appendix 2. The identification and biogeographical distribution of diatom taxa was based on the recent *Iconographia Diatomologica* volume by Zidarova et al. (2016), which is specific to the Maritime Antarctic Region.

Our analyses revealed that 56 % of all observed taxa showed a restricted Antarctic distribution with a majority of 44 % confined only to the Maritime Antarctic Region, whereas only 19 % have a typical cosmopolitan distribution. The biogeographical distribution of the recent diatom flora observed on Vega Island is shown in Figure 2.1. The results also reveal that 7 % of the observed species are only in common with the Maritime and Continental Antarctic Region (MA/CA), 4 % only for the Maritime and Sub- Antarctic Region (MA/SA), and only 1 % of the species is present within the entire Antarctic Region (MA/CA/SA). For 28 valves out of 28,800, it was impossible to establish their correct taxonomical identity, and therefore their distribution was left unidentified (marked as 'U' in the Appendix 2).
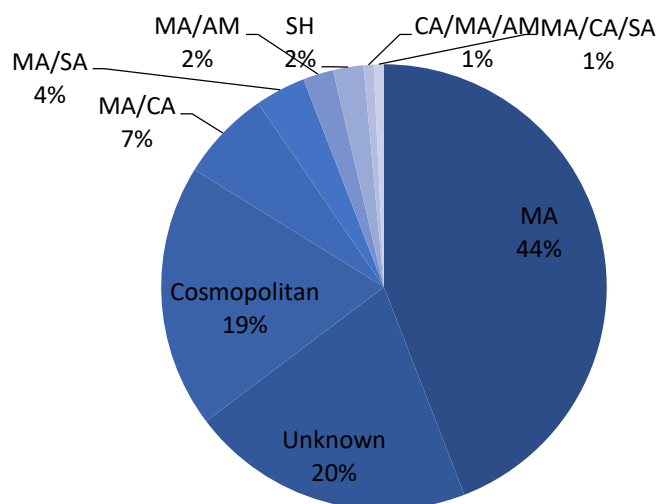
Figure 2.1 Biogeographical distribution of species recovered from modern samples of Vega Island. Legend: MA= Maritime Antarctic Region, MA/CA= Maritime and Continental Antarctic Region, MA/SA= Maritime and Sub- Antarctic Region, MA/AM= Maritime Antarctic and South America, SH= Southern Hemisphere, CA/MA/AM= Continental and Maritime Antarctic and South America, MA/CA/SA= entire Antarctic Region.

Between the two sides of Vega Island, biogeographic distribution was very similar, as shown in Figure 2.2. 53 % of all taxa observed from the north-east side of Vega Island, Devil's Bay (Figure 2.2, A), demonstrated a restricted Antarctic distribution with a majority of 41 % restricted only to the Maritime Antarctic Region. 21 % of species are cosmopolitan.

The results also reveal that 8 % of the observed species belong only to the Antarctic Continent (MA/CA) and only 4 % are connected with the sub-Antarctic islands (MA/SA).

Figure 2.2 (B) shows the biogeographic results from the south-west side of Vega Island, Cape Lamb. 54 % of all observed taxa show restricted Antarctic distribution with a majority of 43 % confined only to the Maritime Antarctic Region, whereas 18 % have a cosmopolitan distribution. The results also show that 6 % of the observed species are only in common with the Antarctic Continent (MA/CA), 4 % only with the sub-Antarctic islands (MA/SA) and 1 % of the species are present within the entire Antarctic Region. Therefore, Devil's Bay flora contains slightly more continental genera, whilst Cape Lamb includes more Maritime Antarctic genera.
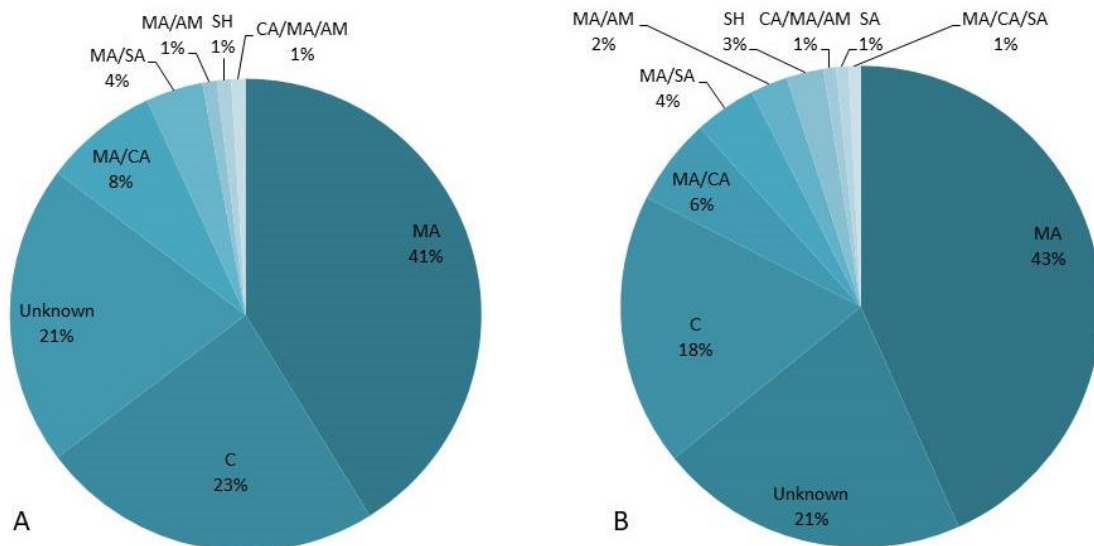
Figure 2.2 Biogeographical distribution of species recovered from modern samples of Devil's Bay (A) and Cape Lamb (B), Vega Island. Legend: MA= Maritime Antarctic Region, C= Cosmopolitan, MA/CA= Maritime and Continental Antarctic Region, MA/SA= Maritime and Sub- Antarctic Region, MA/AM= Maritime Antarctic and South America, SH=Southern Hemisphere, CA/MA/AM= Continental and Maritime Antarctic and South America, MA/CA/SA = entire Antarctic Region.

SPECIES COMPOSITION

Figure 2.3 presents the most important genera (based on the number of recorded taxa) observed in the recent samples from Vega Island. Even though there are differences in the composition between the two sides, taxa from *Luticola* dominate in both. This genus is common for Antarctic lakes and soils (Levkov et al. 2013). The genus *Psammothidium* and *Pinnularia* are more diverse on Cape Lamb than Devil's Bay, and are abundant mainly in semi-aquatic and moss habitats common for sub-Antantartic islands (Krammer 2000; Van de Vijver et al. 2002). On the other hand, *Psammothidium* and *Pinnularia* are sparser

on the Antarctic Continent as their preferred habitats are almost absent there (Sabbe et al. 2003). Therefore, the genera composition of Cape Lamb may indicate a greater Maritime Antarctic influence in comparison with Devil's Bay. However, it should be mentioned that more semi-aquatic samples were collected from Cape Lamb as stated above. Also, in contrast to their Maritime Antarctic position, *Psammothidium* and *Pinnularia* were previously found to be more diverse on Livingston Island than on James Ross Island (Kopalová 2013), which is closer to Vega Island, especially Cape Lamb.
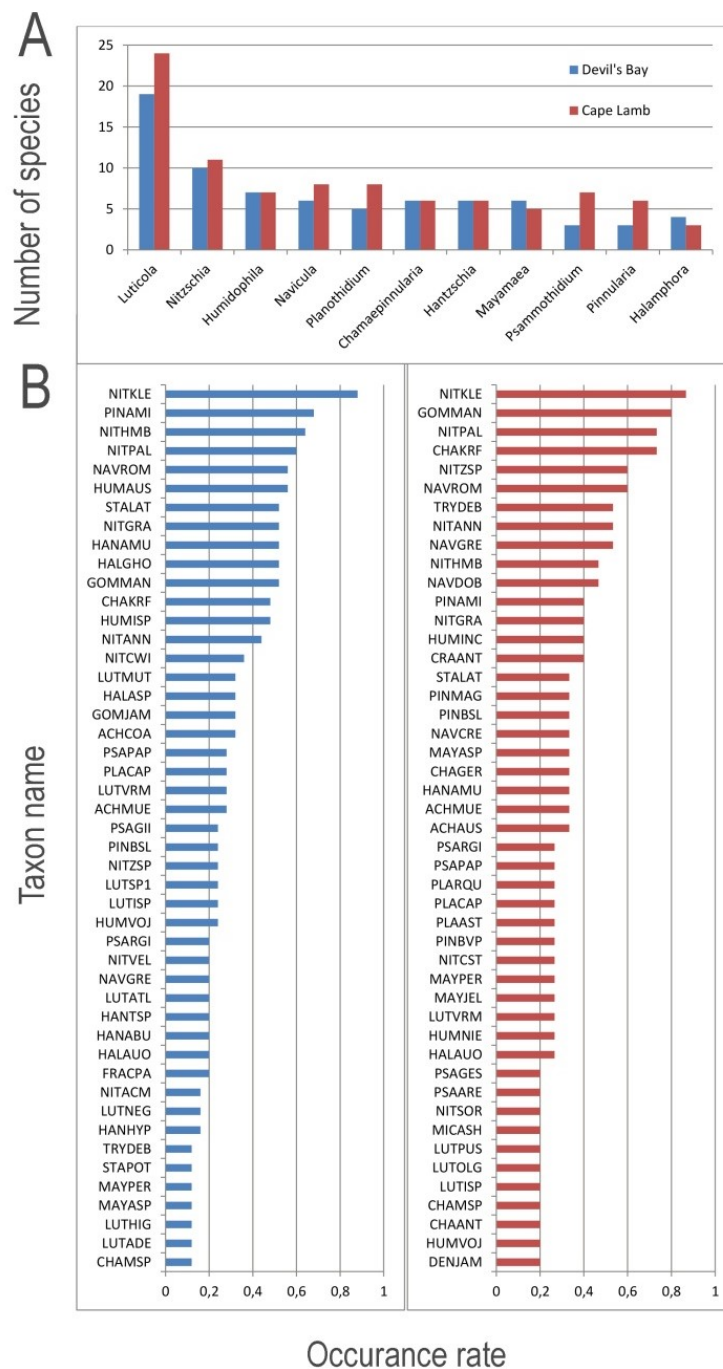

Figure 2.3 Rank abundance plot for genera (A) and rank occurrence plots of diatom taxa in 35 samples collected from ponds in Cape Lamb (15) and Devil's Bay (25) (B). Key for diatom species abbreviations can be found in Appendix 2.

Some important differences can be noted when more rare taxa are taken into account. Some species such as *Fistulifera pelliculosa* (Brébisson) Lange-Bertalot, *Nitzchia gracilis* Hantzsch and *Psammothidium germainii* (Manguin) Sabbe dominate the flora on Devil's Bay but do not appear among the ten most abundant taxa on Cape Lamb, whereas *Gomphonema maritimo-antarcticum* Van de Vijver, Kopalová, Zidarova & Kociolek, *Navicula dobrinatemniskovae* Zidarova & Van de Vijver and *Navicula gregaria* Donkin dominate the species composition on Cape Lamb. Table 2.1 shows the 10 most abundant diatom taxa encountered in all 72 samples, together with the total number of diatom valves per species and their corresponding relative abundances.

Diatom taxon	total number of diatoms counted	total relative abundance
Nitzschia kleinteichiana	5846	20.3%
Chamaepinnularia krookiformis	2555	8.9%
Nitzschia paleacea	2468	8.6%
Nitzschia homburgiensis	2236	7.8%
Nitzschia annewillemsiana	1186	4.1%
Fistulifera pelliculosa	1144	4.0%
Gomphonema maritimo-antarcticum	985	3.4%
Nitzschia gracilis	913	3.2%
Navicula romanedwardii	896	3.1%
Pinnularia australomicrostauron	842	2.9%

Table 2.1 Overview of the 10 most abundant diatom taxa based on whole dataset from Vega Island.

The most abundant species from our survey was *Nitzschia kleinteichiana,* representing 20.30 % of all valves counted, followed by *Chamaepinnularia krookiiformis* (8.87 %), *Nitzschia paleacea* (8.57 %) and *Nitzschia homburgiensis* (7.76 %).

Diatom taxon	Devil's Bay		Cape Lamb	
	total number of valves counted	total relative abundance	total number of valves counted	total relative abundance
Nitzschia kleinteichiana	**4591**	**26.7%**	**1255**	**10.8%**
Nitzschia homburgiensis	**1521**	**8.8%**	**715**	**6.2%**
Nitzschia paleacea	**1287**	**7.5%**	**1181**	**10.2%**
Fistulifera pelliculosa	**1144**	**6.7%**	0	0.0%
Chamaepinnularia krookiformis	**958**	**5.6%**	**1597**	**13.8%**
Nitzschia annewillemsiana	**651**	**3.8%**	**535**	**4.6%**
Nitzschia gracilis	**623**	**3.6%**	290	2.5%
Pinnularia australomicrostauron	**477**	**2.8%**	**365**	**3.1%**
Psammothidium germainii	**477**	**2.8%**	0	0.0%
Navicula romanedwardii	**422**	**2.5%**	**474**	**4.1%**
Gomphonema mar.-antarcticum	307	1.8%	**678**	**5.8%**
Navicula dobrinatemniskovae	0	0.0%	**452**	**3.9%**
Navicula gregaria	28	0.2%	**409**	**3.5%**

Table 2.2 Overview of the 10 most abundant diatom taxa for Devil's Bay and Cape Lamb (top 10 species are marked as bold for each locality).

Table 2.2 presents the same data but for each site separately. The ten most common species from Cape Lamb accounted for 65.3 % of all counted valves from Cape Lamb dataset, while ten most common taxa from Devil's Bay accounted for 68.8 % of all counted valves from Devil's Bay dataset. The most species-rich genus was *Luticola* with 23 species, followed by *Nitzschia* with 11 species.

SPECIES DIVERSITY AND ACCUMULATION CURVES

To evaluate the extent to which our sampling effort represented the diatom flora in the overall dataset and in the different habitats, species accumulation curves (sample-based rarefaction curves, using *vegan* R package (Oksanen et al. 2018) were calculated, and the results are presented in Figure 2.4.

Since species discovery will always continue with greater analytical effort, species accumulation curves will never be completely flat, and are used here to provide a basis of comparison in how thoroughly diversity has been assessed. When all samples were combined, the species accumulation curve begins to flatten, indicating that a large proportion of the diatom flora was collected. However, when this is broken into individual habitat types, it becomes apparent that some habitat types were sampled more completely than others. For example, for seepage and stream habitats, it is obvious that not enough samples were collected to make robust conclusions based on richness and diversity.
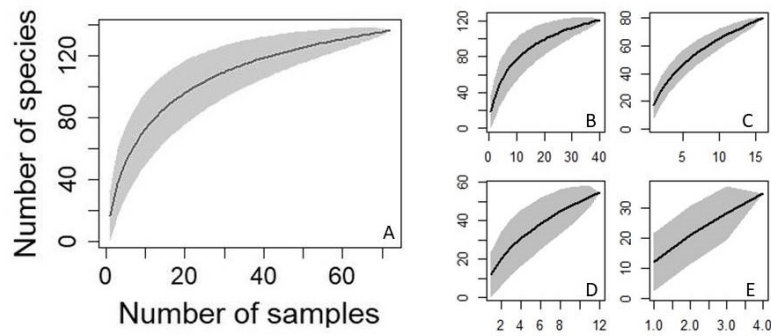
Figure 2.4 Expected species accumulation curves (sample based rarefaction curves) for: total sample set (A), ponds (B), mosses (C), streams (D), seepages (E). Shaded areas indicate the 95% confidence intervals.

With the results of the species accumulation curves in mind, diversity was variable between and amongst different habitat types on Vega Island. The number of genera ranged from 2 to 18, with a median value of 9. The highest genera richness was recorded in the sample L_NE_2 and lowest genera richness was found in the sample ST_NE_48. The ten most important genera accounted for 89.4 % of all counted valves.
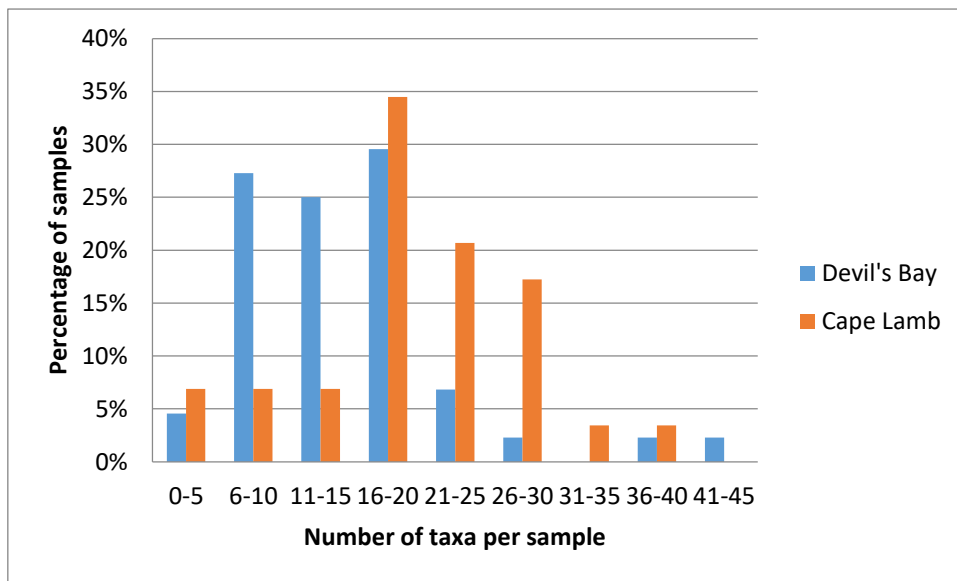
Figure 2.5 Distribution of species richness per sample.

Species richness per sample ranged from 4 to 45 (Figure. 2.5). The highest species richness was recorded in the sample L_NE_2 and lowest species richness was found in sample M_NE_55. The average number of diatom taxa encountered in a sample for both islands together was 17.8. The distribution of species richness per sample clearly differs between both islands. The average number of taxa per sample on Cape Lamb was 20.0, whereas on Devil's Bay it was 15.0. The highest numbers of taxa were observed in pond samples from Cape Lamb. In contrast, the lowest species richness was found in stream samples

on Cape Lamb and seepages from Devil's Bay, which can probably be explained by the unstable nature of these habitat types.

Comparing richness and Shannon diversity between the two sites across all the habitat types revealed significant differences (p = 0.007 and p = 0.003, respectively) when using Tukey HSD test. It is visually summarized in Figure 2.7. Devil's Bay exhibits lower species richness and diversity index. Evenness values follow the same trend and they are higher for Cape Lamb.

Photo 2.1 Lake Esmeralda, Cape Lamb. Photo credit: Kateřina Kopalová

COMPARISON OF COMMUNITY STRUCTURE

Raw relative abundance data were visualized with a dot plot diagram organized by different habitat types and sides of the island (Figure 2.6). From this, it is clear that some diatom species tolerate a broad range of habitat characteristics whereas others show more restricted habitat preferences.
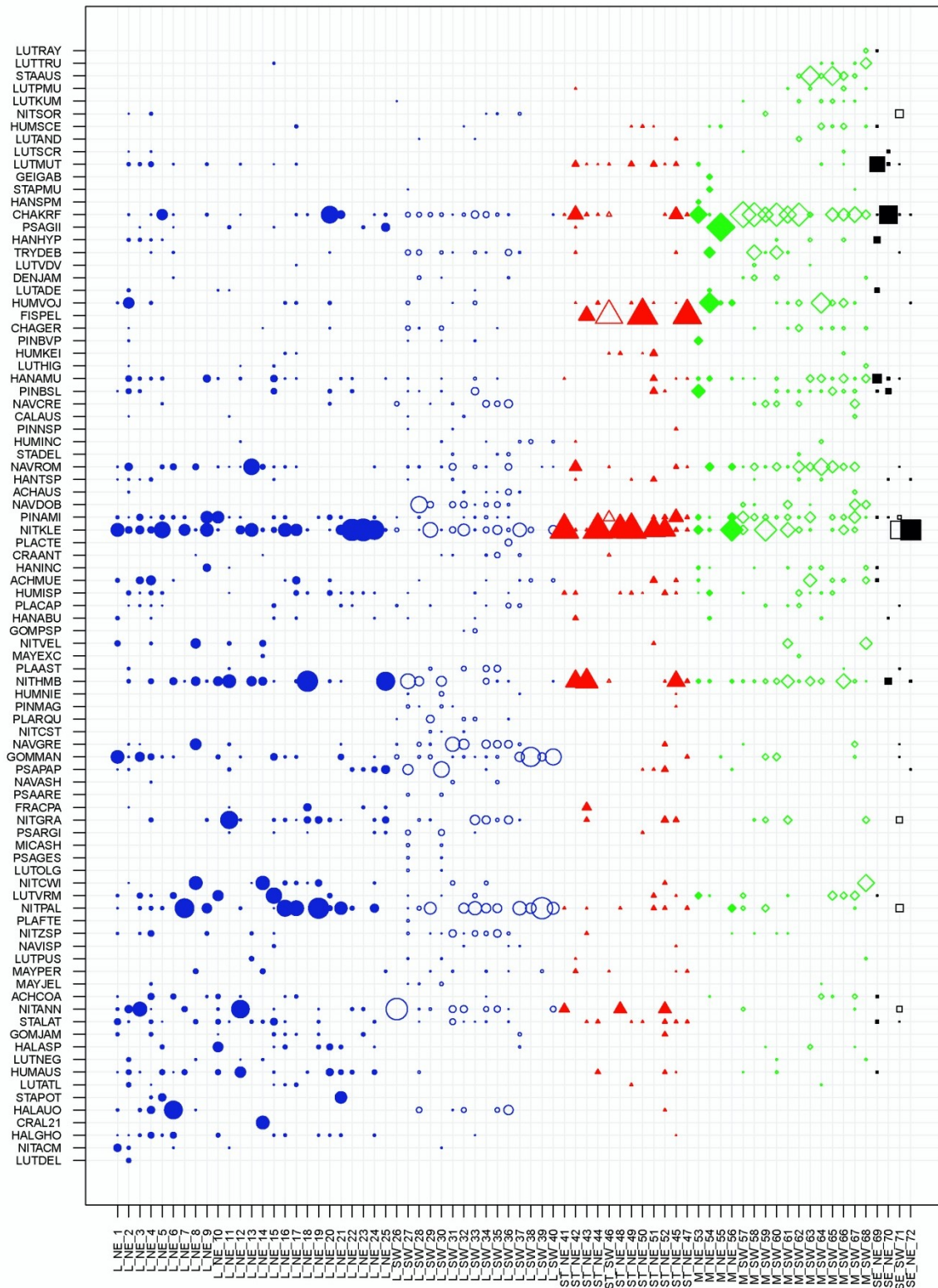
Figure 2.6 Dot plot representation of relative abundance counts averaged by sample. Site codes are on the x-axis, and species names are on the y-axis. The size of a dot is proportional to the average relative abundance of a particular species in a given sample. Only diatoms with relative abundances greater than 1 % are plotted. Pond habitats are indicated by blue circles, moss habitats by green diamonds, seepages by black squares, and streams by red triangles. Symbols for north sites are filled, and south sites are represented by outlines only. Key for species abbreviations are available in Appendix 2, and site names in Appendix 1.

Stream habitats are dominated by *Nitzschia kleinteichiana* (38.00 %), *Fistulifera pelliculosa* (23.83 %), and *Nitzschia* species in the Maritime Antarctic *Nitzschia homburgiensis* (11.10 %) and moss vegetation are characterized mainly *Chamaepinnularia krookiformis* (23.69 %), *Nitzschia kleinteichiana* (10.63 %), and *Humidophila vojtajarosikii* (7.11 %).

Pond habitats are dominated by *Nitzschia* species: *Nitzschia kleinteichiana* (17.83 %), *Nitzschia paleacea* (14.55 %) and *Nitzschia homburgiensis* (9.41 %). Given separately Cape Lamb ponds largely represent *Nitzschia paleacea* (18.43 %), *Gomphonema maritimo-antarcticum* (10.55 %), *Nitzschia kleinteichiana* (10.30 %), *Nitzschia annewillemsiana* (8.38 %) and another rather common Maritime Antarctic species *Psammothidium papilio* (7.38 %) whereas Devil's Bay ponds are dominated by *Nitzschia kleinteichiana* (20.99 %), *Nitzschia paleacea* (12.20 %) and *Nitzschia homburgiensis* (9.85 %). Differences in habitat type composition were significant when tested with PERMANOVA ($P > 0.001$) (Pseudo-F = 2.2754, 999 permutations).

Figure 2.7 Boxplots of species richness (A), Shannon diversity (B), and evenness (C) calculated by island aspect. Pond habitats are indicated by blue circles, moss habitats by green diamonds, seepages by black squares, and streams by red triangles. Symbols for north sites are filled, and south sites are represented by outlines only. Box bottoms and tops represent first and third quartiles and thick black lines represent median values.

For all recent samples taken together, Shannon diversity fluctuated between 3.09 and 0.21, with an average value of 1.60 and evenness ranged from 0.14 to 0.46 with an average of 0.28. Species richness in the samples varied between 5 and 45 (median = 18.5) for the pond samples, from 5 to 26 for the stream samples (median = 12), and from 4 to 27 for moss samples (median = 17.2).

When the NE side was analyzed alone, evenness values ranged from 0.17 to 0.43, with an average of 0.28. Species richness per sample ranged from 4 to 45, with an average of 14.65. Shannon diversity calculated for the NE ranged from 0.21 to 3.09, with an average of 1.41. When the SW side was considered alone, evenness values ranged from 0.14 to 0.46 with average 0.28, richness ranged from 5 to 38 with average 19.97 and Shannon ranged from 0.51 to 2.67 with average 1.89. Richness and evenness were not statistically different between sample types when using Tukey's Honest Significant Differences test. Shannon diversity index was statistically lower in streams compared with ponds (TukeyHSD, $p = 0.010$) and mosses ($p = 0.013$). Given separately for each habitat, ponds and mosses show the highest richness, diversity and evenness values (Figure 2.8)
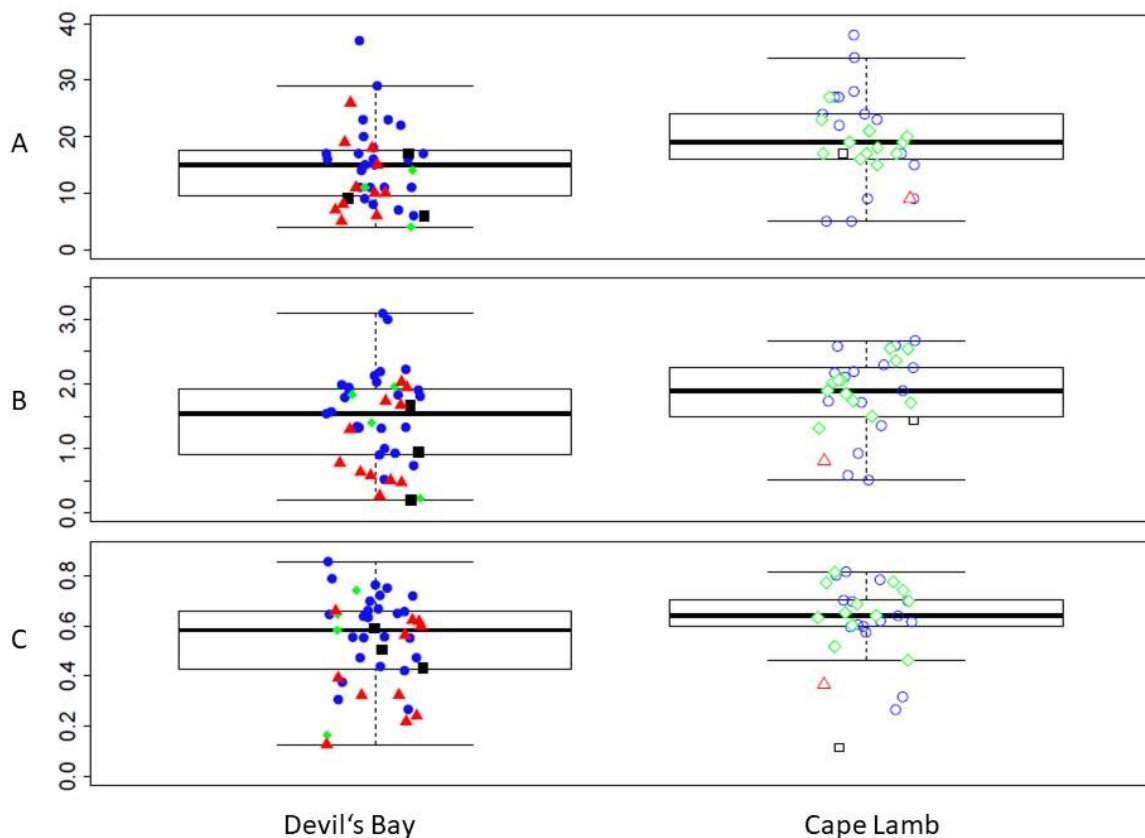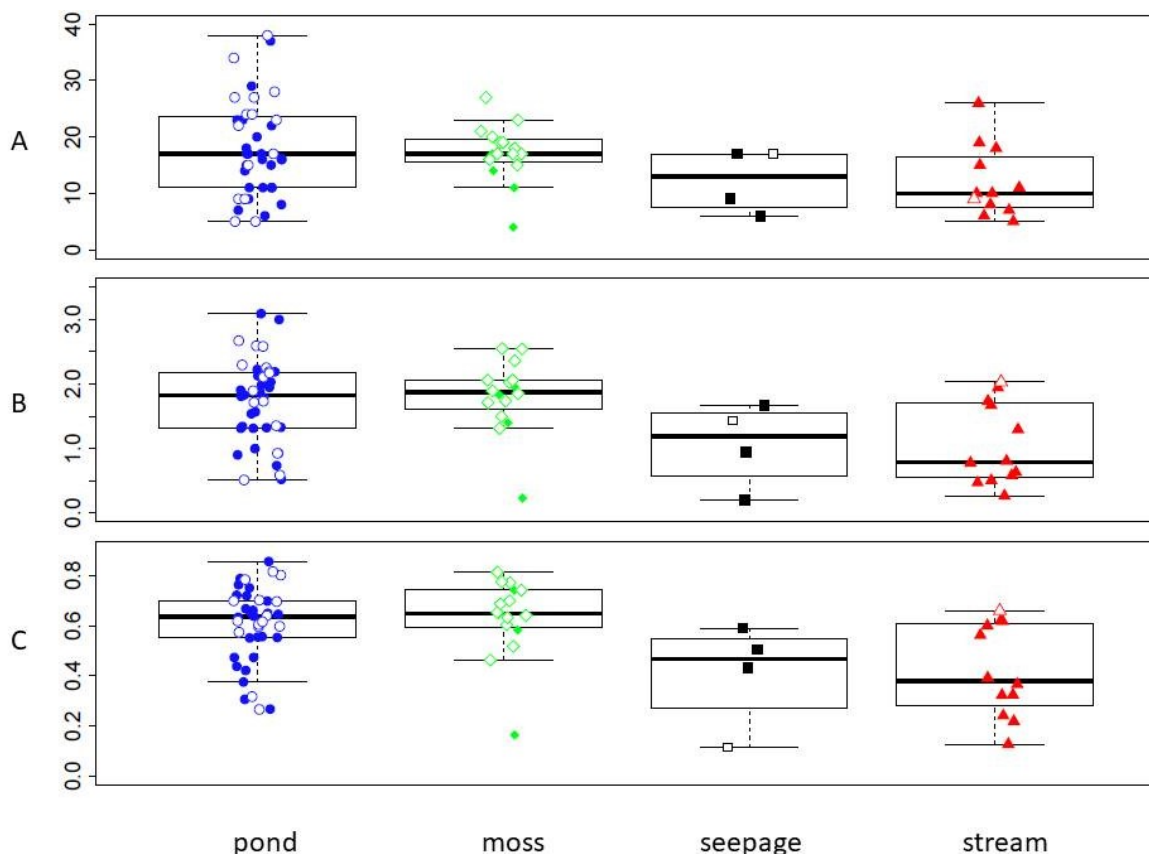

Figure 2.8 Boxplots of species richness (A), Shannon diversity (B), and evenness (C) calculated by habitat type. Pond habitats are indicated by blue circles, moss habitats by green diamonds, seepages by black squares, and streams by red triangles. Symbols for north sites are filled, and south sites are represented by outlines only. Box bottoms and tops represent first and third quartiles and thick black lines represent median values.

A Principal Component Analysis (PCA) based on species composition was performed to better observe relationships between habitat and sites, and the results are summarized in the ordination diagram in Figure 2.9. The first two axes explain 17.8 % of the total variation in community composition. The y-axis alone explained 10.1 %, and was driven by pond samples to the right and moss samples to the left. The x-axis alone explains 7.7 % and was primarily driven by the stream samples to the bottom. It is clear that the communities of both sides have large overlap. Nonetheless, when tested with PERMANOVA, the differences between sides are significant (P > 0.049) (Pseudo-F = 1.8454).

Nitzschia kleinteichiana seems to be influencing streams and ponds from Devil's Bay, whereas moss samples are influenced by *Navicula romanedwardii, Chamaepinnularia krookiformis* and *Hantzschia amphioxys f. muelleri.* South moss and ponds are separated more clearly than the rest of the habitats.
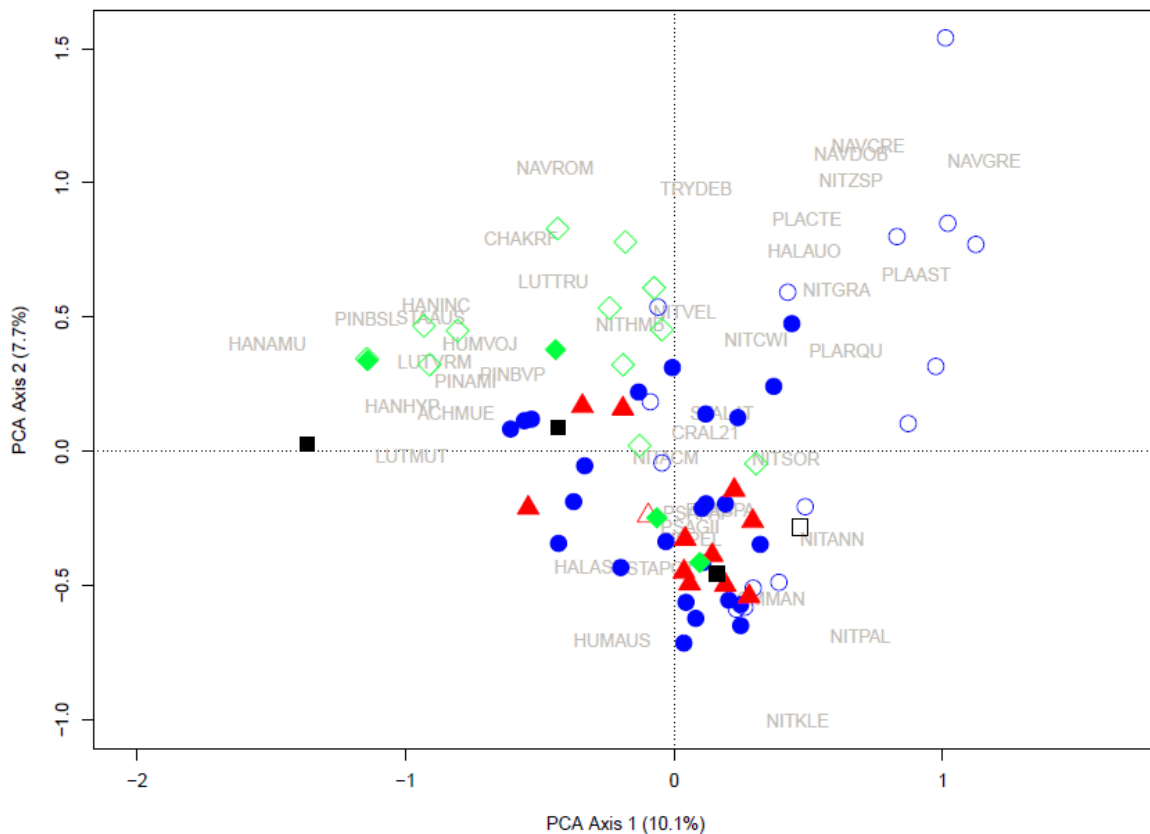
Figure 2.9 Principle components analysis (PCA) of the recent diatom community dataset from Vega Island. Diatoms with relative abundances greater than 8 % are plotted. Pond habitats are indicated by blue circles, moss habitats by green diamonds, seepages by black squares, and streams by red triangles. Symbols for north sites are filled, and south sites are represented by outlines only. Diatom codes are superimposed onto figure (key for species abbreviations are available in Appendix 2).

An RDA was also created to test the influence of north versus south sides of the island on pond communities alone (given that the differences in sampled habitats can skew the results, this makes the analyses more comparable). The results of RDA are summarized in the ordination diagram in Figure 2.10, and it explained 44.8 % of the total variation in community composition. *Nitzschia kleinteichiana* and *Nitzschia paleacea* are among the main factors pulling symbols to the bottom, whereas *Nitzschia homburgiensis* pulls symbols up. *Navicula gregaria*, *Navicula dobrinatemniskovae,* and *Gomphonema maritimo-antarcticum* seems to influence the SW side by pulling symbols to the right side of the graph. While tested with PERMANOVA, the differences of pond diatom communities between sides are significant (P > 0.005) (Pseudo-F = 2.8653).
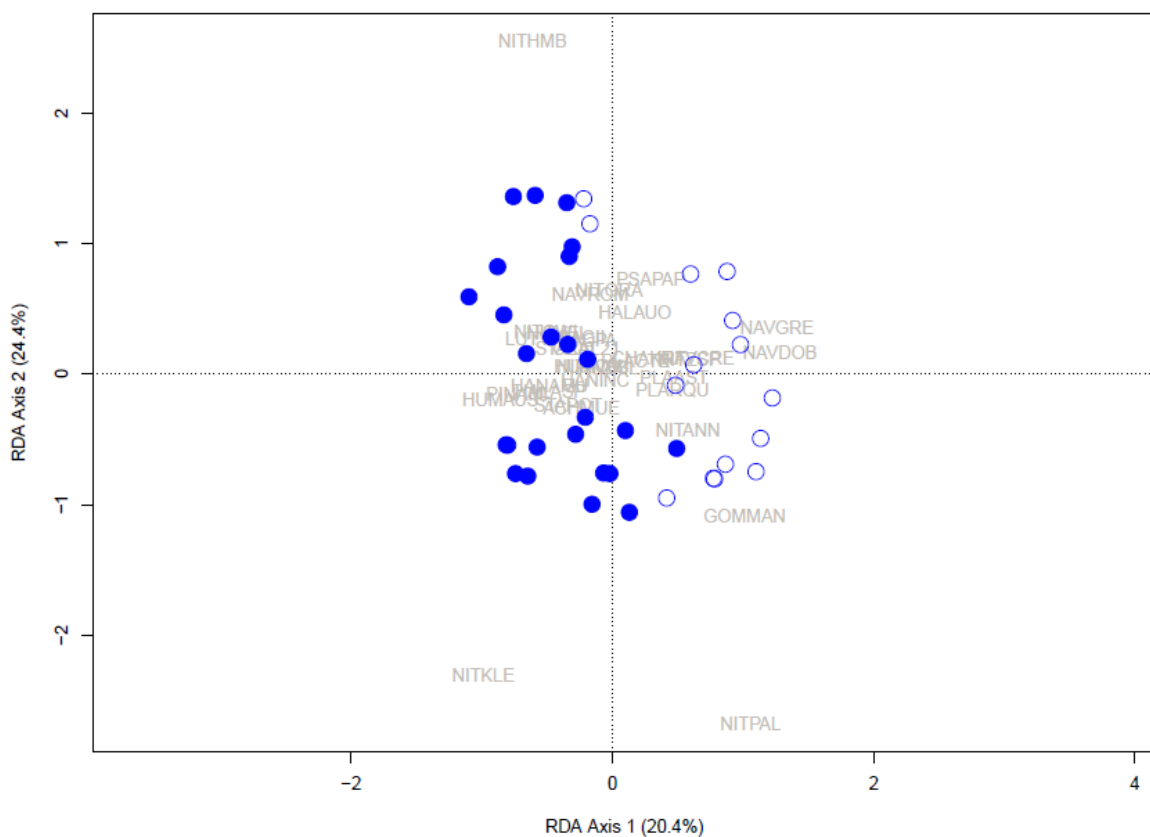
Figure 2.10 Redundancy analysis (RDA) of diatom communities from pond habitats only. Data are constrained by island aspect (SW/Cape Lamb versus NE/Devil's Bay). Symbols for north site ponds are filled blue circles and south ponds are represented by outlined blue circles. Diatom species names are superimposed, with a key for abbreviations found in Appendix 2. Only species with relative abundance < 8 % were taken to this analysis.

CONCLUSIONS

This chapter focused on the ecological characterization of ponds, streams, seepages, and mosses inhabiting diatom communities from two opposite sides of Vega Island (James Ross Islands) located in the Antarctic Peninsula Region.

Main results:
- In total, 72 samples were analyzed and 136 diatom species were identified.
- Unique diatom communities were found for each habitat type investigated on Vega Island (ponds, streams, mosses, and seepages), with important differences between the north and south sides.
    - Diatoms from moss and pond habitats showed the greatest richness and diversity.
    - Pond habitats were compared from the two sides of the island (Cape Lamb, Devil's Bay) and were found to be significantly different in structure.
    - The Cape Lamb diatom flora is more diverse and species rich than Devil's Bay, despite having less representation from streams and seepages compared to Devil's Bay.
- A new species was described from a Devil's Bay moss sample belonging to the genus *Hantzschia*.

REFERENCES

Anderson, M. J. (2001). A new method for non-parametric multivariate analysis of variance. Austral ecology, 26(1), 32-46.

Chown, S. L., & Convey, P. (2007). Spatial and temporal variability across life's hierarchies in the terrestrial Antarctic. Philosophical Transactions of the Royal Society B: Biological Sciences, 362(1488), 2307-2331.

Kopalová, K. (2013). Taxonomy, ecology and biogeography of aquatic and limno-terrestrial diatoms (Bacillariophyta) in the Maritime Antarctic Region. (Ph.D. Thesis). Charles Univesity and Universiteit Antwerpen. Prague. Czech Republic.

Krammer, K. (2000). Diatoms of Europe. Diatoms of the European Inland Waters and Comparable Habitats, Vol. 1. The genus Pinnularia.

Levkov, Z., Metzeltin, D., & Pavlov, A. (2013). Diatoms of Europe: Diatoms of the European Inland Waters and Comparable Habitats (Vol. 7. Luticola and Luticolopsis).

Sabbe, K., Verleyen, E., Hodgson, D. A., Vanhoutte, K., & Vyverman, W. (2003). Benthic diatom flora of freshwater and saline lakes in the Larsemann Hills and Rauer Islands, East Antarctica. Antarctic Science, 15(2), 227-248.

Shannon, C. E., & Weaver, W. (1949). The mathematical theory of information.

Van de Vijver, B., Ledeganck, P., & Beyens, L. (2002). Soil diatom communities from Ile de la Possession (Crozet, sub-Antarctica). Polar biology, 25(10), 721-729.

Van der Werff, A. (1955). A new method for cleaning and concentrating diatoms and other organisms. Verhandlungen der Internationalen Vereinigung für theoretische und angewandte. Limnologie, 12, 276– 277.

Zidarova, R., Kopalová, K. & Van der Vijver, B., 2016. Diatoms from the Antarctic Region: Maritime Antarctica. Iconographia Diatomologica, 24, pp.1–509.

Web and statistical resources

Oksanen, J., Blanchet, F. G., Friendly, M., Kindt, R., Legendre, P., McGlinn, D., ... & Stevens, M. H. H. vegan: Community Ecology Package. R package version 2.5-2. 2018.

Pielou, E. C. (1966). The measurement of diversity in different types of biological collections. Journal of theoretical biology, 13, 131-144.

R Core Team (2017). R: A language and environment for statistical computing. R Foundation for Statistical Computing, Vienna, Austria. URL https://www.R-project.org/.

CHAPTER 3

Three new Hantzschia species (Bacillariophyta) from the Maritime Antarctic Region

Phytotaxa
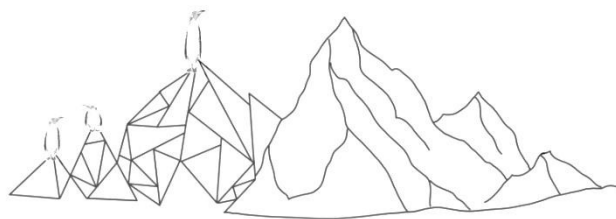
Three new *Hantzschia* species (Bacillariophyta) from the Maritime Antarctic Region

MARIE BULÍNOVÁ[1], NATALIA KOCHMAN-KĘDZIORA[3], KATEŘINA KOPALOVÁ[1,2] & BART VAN DE VIJVER[4,5*]

[1]*Department of Ecology, Faculty of Science, Charles University, Prague, Czech Republic*
[2]*Academy of Sciences of the Czech Republic, Institute of Botany, Section of Plant Ecology, Dukelská 135, CZ-37982 Třeboň, Czech Republic*
[3]*University of Rzeszow, Faculty of Biology and Agriculture, Podkarpackie Innovative Research Center of Environment, Zelwerowicza 8B, 35–601 Rzeszów, Poland*
[4]*Botanic Garden Meise, Research Department, Nieuwelaan 38, B–1860 Meise, Belgium*
*(*author for correspondence: bart.vandevijver@plantentuinmeise.be)*
[5]*University of Antwerp, Department of Biology, ECOBE, Universiteitsplein 1, B–2610 Wilrijk, Antwerpen, Belgium*

Abstract

Following an earlier revision of the genus *Hantzschia* (Bacillariophyta) in the Maritime Antarctic Region, several at present unidentified or poorly known taxa of this aerophilic genus have been investigated using both light and scanning electron microscopy. Based on the morphological analysis of the observations, three new species are currently described: *Hantzschia australabundans* sp. nov., *H. zidarovae* sp. nov. and *H. zikmundiana* sp. nov. The new species differ from comparable taxa in valve outline, structure of the internal proximal raphe endings and structure of the striae and areolae. Additional observations are presented on *Hantzschia amphioxys* and its forma *muelleri*, *H. abundans* and *H. incognita*, based on observations of Antarctic populations from the South Shetland Islands, Vega Island and James Ross Island. Brief notes on the ecology of all reported species are added.

Keywords: *Hantzschia*, diatoms, Maritime Antarctic Region, morphology, new species

Introduction

The genus *Hantzschia* (Grunow 1877: 174) was originally described by Grunow in 1877. It is a relatively small genus with less than hundred species known worldwide, occurring in a wide variety of habitats ranging from freshwater to terrestrial and even intertidal and marine environments (Round *et al.* 1990). The generitype of the genus, *Hantzschia amphioxys* (Ehrenberg 1843: 413) Grunow (in Cleve & Grunow 1880: 103) was restudied in 2014 and a lectotype was chosen (Jahn *et al.* 2014). In 2015, You *et al.* (2015) analysed the number of species within the genus, based on data from the Catalogue of diatom names (Fourtanier & Kociolek 2012) and Algaebase (Guiry & Guiry 2014), and only 76 accepted names were listed for the genus.

Morphologically, the genus is characterized by a typical dorsiventral valve outline showing a more convex dorsal side and a concave ventral side, the presence of uniseriate striae composed of small rounded areolae externally covered by hymenes, a raphe that is subtended by fibulae and a complex girdle structure (Round *et al.* 1990). There is only a relatively small number of discriminating features used to separate the different *Hantzschia* species such as valve width, stria density and number of areolae per stria, the position and shape of the fibulae, the shape of the external and internal proximal raphe endings and the shape of the valve apices.

The past 10 years, several new *Hantzschia* species have been described, usually following the adoption of a narrower species concept (Mallet 2007) and the exploration of remote, previously unstudied areas. New taxa were described from Sardinia (Lange-Bertalot *et al.* 2003), Uruguay (Metzeltin *et al.* 2005), Mongolia (Metzeltin *et al.* 2009), China (You *et al.* 2015), the sub-Antarctic Islands (Van de Vijver *et al.* 2002) and the Maritime Antarctic Region (Zidarova *et al.* 2010). Others, formerly known as infraspecific taxa within the *H. amphioxys*-complex were raised to species rank (Lange-Bertalot 1993). Most of these studies however are based on morphological research. Only in recent years, occasionally, molecular tools were adopted studying the diversity in the genus *Hantzschia* (a.o.

Zimmerman *et al.* 2011, Ruck & Theriot 2011, Jahn *et al.* 2014). Souffreau *et al.* (2013) analysed several *H. amphioxys* strains from several Antarctic localities and concluded that distinct lineages were present within this species-complex that could hardly be identified and separated based on morphological criteria only.

Zidarova *et al.* (2010) separated 7 different *Hantzschia* taxa from a Maritime Antarctic island, five of which were described as new to science. Two others were identified as *H. amphioxys* f. *muelleri* Ts.Kobayashi (1965: 14–15) and *H. abundans* Lange-Bertalot (1993: 75–76). The morphology of the latter differed however from the type population of *H. abundans* that was collected from a flooded meadow in Germany (Lange-Bertalot 1993) in having different morphometrics (length, width, stria density). The discovery of an unknown *Hantzschia* taxon on the Antarctic Vega Island sharing some morphological features with *H. abundans*, and the subsequent reanalysis of all *H. abundans* populations in the Maritime Antarctic Region, resulted in the separation of two taxa that could not be identified using the currently available literature. A third taxon was already reported by Zidarova *et al.* (2010) but due to the lack of sufficient specimens, no formal description was proposed and in the recently published monograph on the Maritime Antarctic diatoms (Zidarova *et al.* 2016), the taxon was enlisted as *Hantzschia* sp1. During the survey for *Hantzschia* taxa in the Maritime Antarctic region material, large populations of *H. abundans*, *H. amphioxys* f. *muelleri*, *H. amphioxys* and *H. incognita* Zidarova & Van de Vijver in Zidarova *et al.* (2010: 331) were observed allowing a good morphological analysis and characterization of the ultrastructure of all these taxa. In the present paper, three taxa will be described as new species: *H. australabundans* sp. nov., *H. zidarovae* sp. nov. and *H. zikmundiana* sp. nov. Morphological details of four other, comparable, *Hantzschia* taxa are added.

Material & Methods

Samples were collected from various terrestrial habitats on Vega Island, James Ross Island and the South Shetland Islands (Livingston Island and King George Island) during the austral summers of 2004, 2006, 2007, 2012 and 2013. The South Shetland Islands (63°00′ S/60°00′ W), situated just north of the Antarctic Peninsula, are composed of 11 larger and many smaller islands and islets, of which King George Island (1150 km²) and Livingston Island (972 km²) are the largest. They have a typically maritime oceanic climate with mean annual temperatures around −5 °C, high precipitation rates and strong westerly winds (Chipev & Veltchev 1996). Most of the land areas are covered by permanent ice and snow cover, leaving only small parts ice-free. The terrestrial vegetation is limited to lichens and mosses with only two flowering plants [*Colobanthus quitensis* (Kunth) Bartling and *Deschampsia antarctica* Desvaux]. Vega Island (63°50′S/57°25′W) and James Ross Island (64°10′S/57°45′W) are two neighbouring islands situated in the northern Weddell Sea, south of the Antarctic Peninsula. The islands belong to the transitory zone between the Maritime Antarctic and Continental Antarctic regions (Øvstedal & Lewis-Smith 2001). With more than 75% of the island permanently covered with ice, only a few areas remain ice-free. The temperature is comparable to the South Shetland Islands, but precipitation is limited to only 150 mm/y in the northern part (Aristarain *et al.* 1987), with high evaporation rates reducing the formation of large open waterbodies. The terrestrial vegetation is limited to non-vascular plants forming a bryophyte-and-lichen-tundra in places.

All samples were fixed with alcohol and stored in plastic vials. Sampling locations together with GPS coordinates are presented in table 1. Due to the restricted logistic possibilities of working in these extreme conditions, it was almost impossible to collect data on environmental parameters for every sample. Basic ecological parameters (pH, conductivity) were measured using a WTW multi 340i (WTW®, Weilheim, Germany) (Kopalová 2012, 2014).

Diatom samples were prepared following the method of van der Werff (1955). In total, 5 samples containing large *Hantzschia* populations were examined in this study, with all samples listed in Table 1. Subsamples of the original material were cleaned by adding 37% H_2O_2 and heating to 80 °C for about one hour, followed by addition of $KMnO_4$. After digestion and centrifugation (3 x 10 minutes at 3700g), the material was diluted with distilled water to avoid excessive concentrations of diatom valves. Cleaned diatom valves were mounted in Naphrax®. Samples and slides are stored at the BR-collection (Botanic Garden Meise, Belgium). The slides were analysed using an Olympus BX53 compound microscope, equipped with Differential Interference Contrast (Nomarski®) and the Olympus UC30 Imaging System. For scanning electron microscopy (SEM), aliquots of the oxidized suspensions were filtered through 5-μm pore size polycarbonate filters which were cut in small pieces, fixed on aluminium stubs after air-drying and sputter coated (Cressington 208HR, Watford, UK) with PtPd (10 nm). Observations and photomicrographs were performed with a Jeol® JSM-7100F SEM at 2 kV at the Botanic Garden Meise, Belgium. Terminology is based on Hendey (1964), Ross *et al.* (1979) and Round *et al.* (1990). For each new taxon, the number of specimens measured at random in the

type slide is indicated (n=X). The new species were compared with similar taxa from the Antarctic Region (Zidarova *et al.* 2010, 2016), Europe (Lange-Bertalot 1993, Lange-Bertalot *et al.* 2003), Siberia (Lange-Bertalot & Genkal 1999), South America (Rumrich *et al.* 2000, Metzeltin *et al.* 2005), Mongolia (Metzeltin *et al.* 2009).

The morphometric details of additional specimens from various parts in the world were determined based on published illustrations from Germany (type populations; Lange-Bertalot 1993), Sardinia (Lange-Bertalot *et al.* 2003), Uruguay (Metzeltin *et al.* 2005) and Mongolia (Metzeltin *et al.* 2009). Four morphometric parameters were measured on all specimens: length (µm), width (µm), stria density (in 10 µm) and fibula density (in 10 µm).

TABLE 1. List of the samples containing the newly described taxa.

sample	collection date	locality	GPS coordinates	short description
Π1a	31/01/2004	Livingston Island, Hurd Peninsula, close to the "Juan Carlos I" Spanish Antarctic Base	(62°39'46.9"W/60°22'41.2"W)	wet soil under moss vegetation near a small stream
LIV-BY16A	16/12/2006	Livingston Island, Byers Peninsula, close to the main plateau	(62°38'10.8"S/61°6'27.4"W)	biofilm in a flooded area between stones
S1E	22/02/2007	James Ross Island, Komarek's slopes below Berry Hill	(63°48.183"S/57°50.980"W)	seepage area
ANNA POOL	1/02/2012	James Ross Island	(63°57'54.3"S/57°54'37.8"W)	moss vegetation
VEGA-M2	17/01/2013	Vega Island	(63°48'55.4"S/57°18'35.6"W)	very dry moss vegetation around the stream going along the moraine

Results

Division **Bacillariophyta**
Class **Bacillariophyceae**
Subclass **Bacillariophycidae**
Order **Bacillariales**
Family **Bacillariaceae**
Genus *Hantzschia*

Hantzschia australabundans sp. nov. (Figs 1–10)

Synonym:—*Hantzschia abundans* sensu Zidarova *et al.* (2010, p. 322, Fig. 2) non sensu Lange-Bertalot (1993, p. 75, Fig. 85: 12–17)

LM (Figs 1–6): Valves clearly dorsiventral with a convex ventral side, occasionally flattened in the middle. Dorsal side distinctly concave in the middle but convex towards the apices. Valve apices clearly protracted, rostrate to sub-capitate in large valves, almost capitate in smaller valves. Valve dimensions (n=30): length 48–101 µm, 7.5–12.0 µm. Fibulae, 5–7 in 10 µm, with the median two clearly distant. Each fibula connected to 1–3 transapical costae. Striae radiate in the valve middle, parallel to slightly curved near the apices, equidistant 17–23 in 10 µm. Areolae not discernible in LM. SEM (Figs 7–10): Valves showing a narrow hyaline, weakly thickened ventral margin (Fig. 7). Striae uniseriate, composed of small, rounded areolae externally covered by individual hymenes (Figs 9, 10), ca. 45 in 10 µm. Striae never situated in deep grooves (Fig. 8). Externally, the central raphe endings weakly deflected to almost straight, clearly interrupted near the middle (Fig. 8). Internally, proximal raphe endings close together, straight, terminating on a thickened central nodule (Fig. 10). Internally, fibulae clearly unevenly distributed, connected to 1–4 transapical costae (Fig. 9). Transapical striae located in deep grooves (Figs 9, 10).

Type:–SOUTH SHETLAND ISLANDS, Livingston Island, sample LIV-BY16A (62°38'10.8"S/61°6'27.4"W), leg. M. Toro, coll. date 16 December 2006 (holotype, slide BR 4512; isotype, slide PLP–342, University of Antwerp, Belgium).

Ecology:—*Hantzschia australabundans* was found in several soil and moss samples on the South Shetland Islands. The largest population was found in sample LIV-BY16A, taken from a biofilm in an area flooded by freshwater between stones on Byers Peninsula close to the main plateau. The sample is dominated by various *Luticola, Hantzschia, Pinnularia* and *Humidophila* taxa. Due to confusion with *H. abundans*, the exact distribution and ecology of this species is not entirely known.
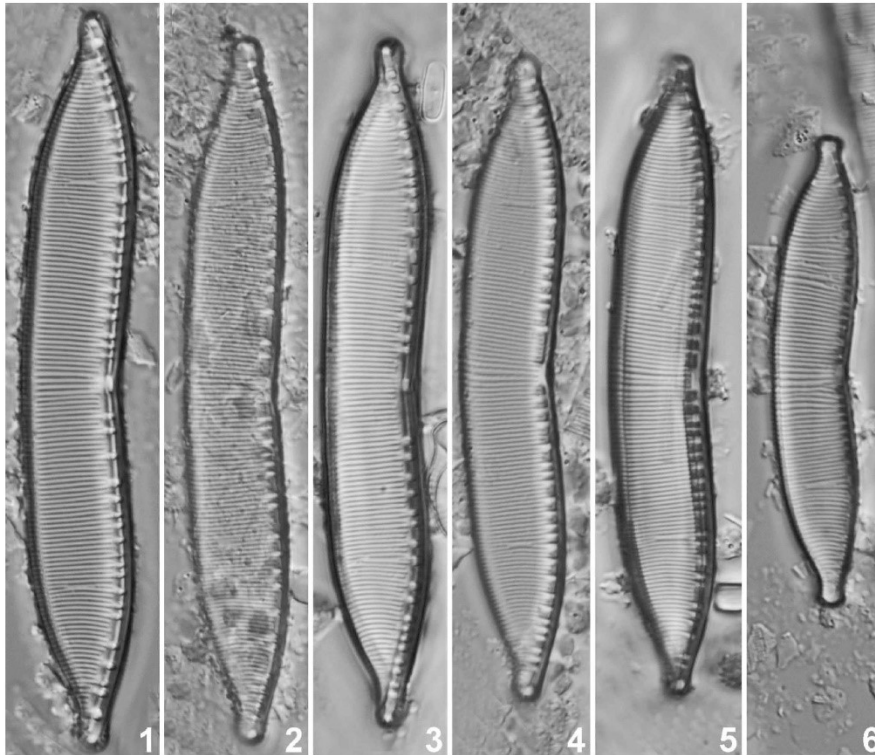
FIGURES 1–6. *Hantzschia australabundans*. Light micrographs (LM) of the type population (Livingston Island, Byers Peninsula, sample LIV-BY16A). Scale bar represents 10 μm.
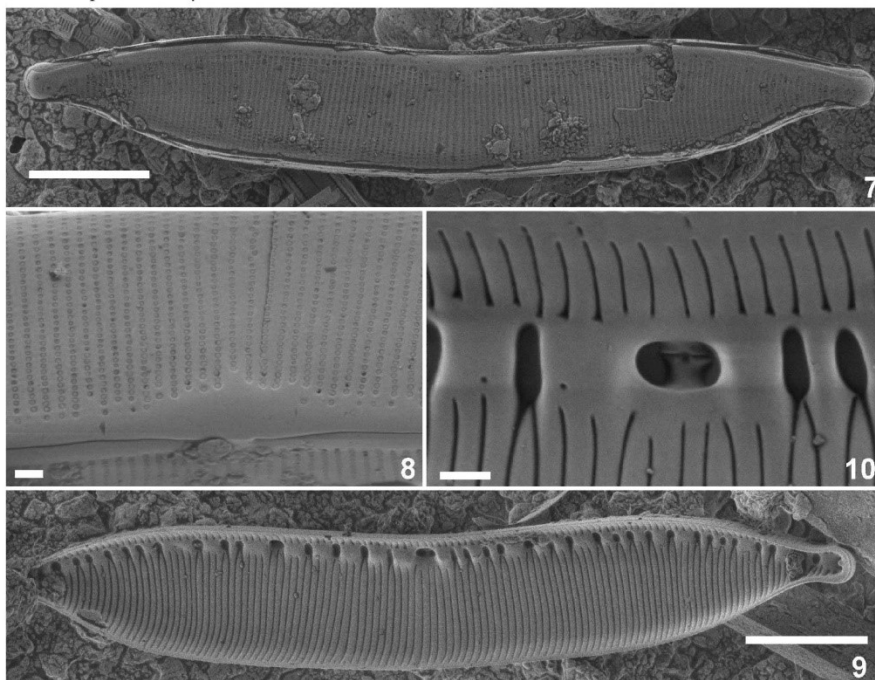
FIGURES 7–10. *Hantzschia australabundans*. Scanning electron micrographs (SEM) of the type population (Livingston Island, Byers Peninsula, sample LIV-BY16A). Fig. 7. External view of an entire valve showing the ventral hyaline border. Fig. 8. External detail of the central area with the interrupted proximal raphe endings and the shallow areolae. Fig. 9. Internal view of an entire valve showing the irregularly placed fibulae. Fig. 10. Internal detail of the central area with the interrupted proximal raphe endings located on a heavily silicified central nodule. Scale bar represents 10 μm except for figs 9 & 11 where scale bar = 1 μm.

Phytotaxa 371 (3) © 2018 Magnolia Press • **171**
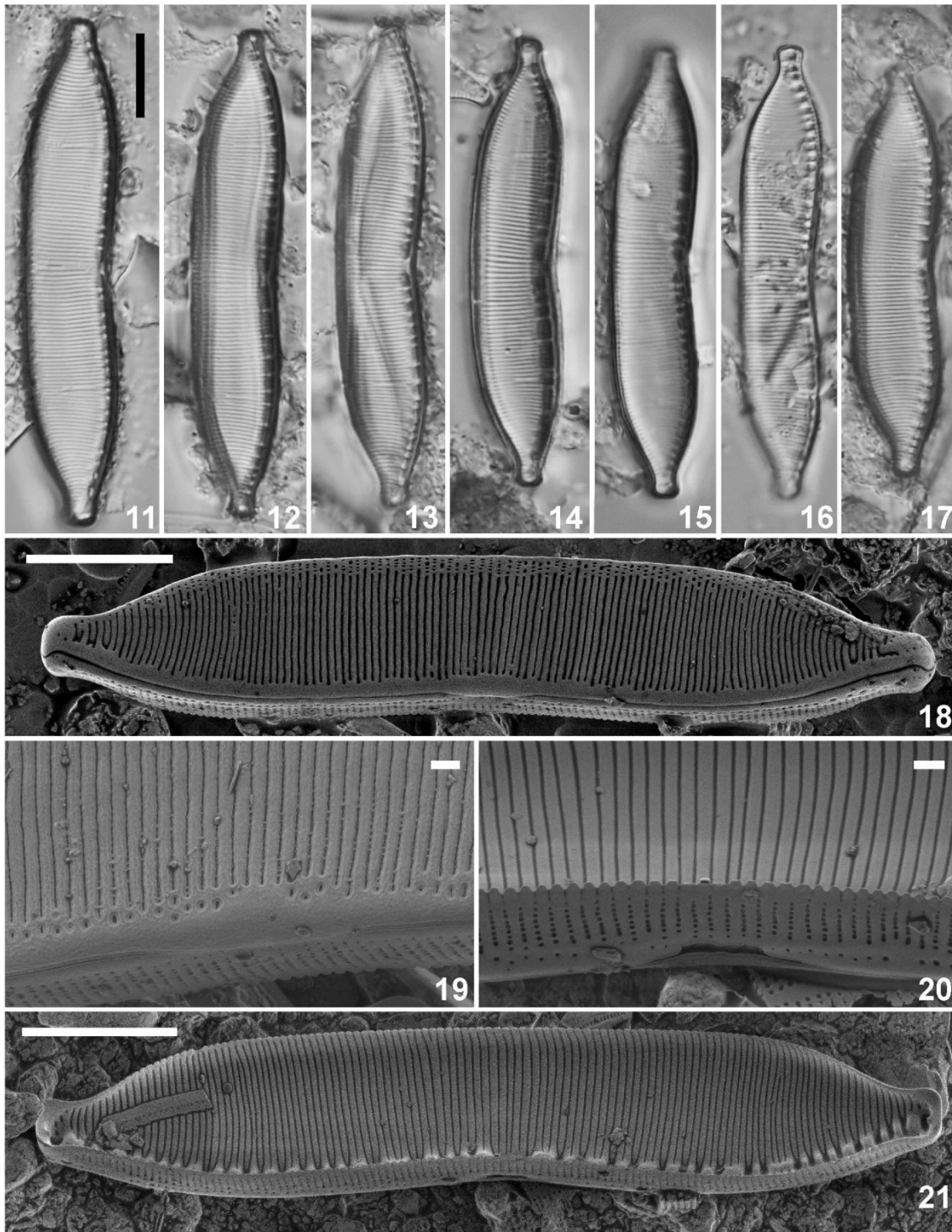
FIGURES 11–21. *Hantzschia zidarovae*. LM and SEM observations of the type population (Livingston Island, Byers Peninsula, sample LIV-BY16A). Figs 11–17. Light micrographs showing a reduction in valve length. Fig. 18. External view of an entire valve showing the thickened ventral hyaline border and the very deep grooves with the striae. Fig. 19. External detail of the central area with the deflected, interrupted, proximal raphe endings and the deep striae grooves. Fig. 20. Internal detail of the central area showing the external, interrupted proximal raphe endings. Note the groove under the raphe endings. Fig. 21. Internal view of an entire valve showing the irregularly placed fibulae. Scale bar represents 10 μm except for figs 19 & 20 where scale bar = 1 μm.

Hantzschia zidarovae **sp. nov.** (Figs 11–21)

LM (Figs 11–17):—Valves typically dorsiventral with a concave to almost straight ventral margin and a slightly convex dorsal margin, often more or less straight in the middle of the valve. Apices shortly protracted, subcapitate, never clearly elongated. Valve dimensions (n=10): length 45–60 μm, width 8.0–10.5 μm. Fibulae 5–6 in 10 μm, almost equidistantly spaced, the middle two fibulae more distant than the others. Each fibula connected to 2–3 transapical costae. Transapical striae slightly radiate in the middle, becoming parallel and even convergent near the apices, 19–20 in 10 μm. Areolae not discernible in LM. SEM (Figs 18–21): Valves showing a rather broad hyaline, weakly thickened margin. Dorsally, margin entirely covered with isolated areolae, arranged in transapical series (Fig. 18). Areolae on the valve face located in deep, transapically running grooves, externally covered by individual hymenes (Fig. 19). Mantle striae composed of a series of isolated, rounded areolae (Figs 19, 20). External proximal raphe endings clearly bent, unclear whether interrupted or not (Figs 19, 20). Occasionally, deep groove present below the proximal endings (Fig. 20). Internally, fibulae clearly unevenly distributed, connected to 1–4 transapical costae (Fig. 21). Transapical striae located in deep grooves (Fig. 21).

 Type:—SOUTH SHETLAND ISLANDS, Livingston Island, sample LIV-BY16A (62°38'10.8"S/61°6'27.4"W), leg. M. Toro, coll. date 16 December 2006 (holotype, slide BR 4513; isotype, slide PLP–343, University of Antwerp, Belgium).

 Ecology:—*Hantzschia zidarovae* was found with certainty in sample LIV-BY16A, taken from a biofilm in a flooded area between stones on Byers Peninsula close to the main plateau. The sample is dominated by various taxa of *Luticola, Hantzschia, Pinnularia* and *Humidophila*. On King George Island, another small population was found in a sample collected from soil on the Ecology Glacier Forefield area close to the Polish Arctowski station.

 Etymology:—The species is named after our colleague and friend Dr. Ralitsa Zidarova in honour of her work on the diatoms of the Maritime Antarctic Region.

Hantzschia zikmundiana **sp. nov.** (Figs 22–34)

LM (Figs 22–30):—Valves clearly dorsiventral with a very convex dorsal side. Ventral side deeply concave in the middle becoming more convex towards the apices. Valve apices protracted, capitate, distinctly deflected towards the dorsal side. Valve dimensions (n=25): length 37.5–45.0 μm, width 7.0–8.5 μm. Fibulae, 6–9 in 10 μm, the middle two fibulae visibly distant from each other. Each fibula connected to 1–3 transapical costae. Striae almost parallel throughout the entire valve, equidistant, 19–22 in 10 μm, towards the apices, becoming slightly curved. In the middle a few (2–4) striae slightly to clearly radiate, more distant than the other striae. Areolae not discernible in LM. SEM (Figs 31–34): Valves on the ventral side bordered by a slightly raised keel (Figs 31, 32). Striae located in shallow grooves bordered by raised costae (Fig. 32). Grooves irregularly interrupted near the ventral margin. Mantle striae located in similar grooves, one areola clearly being separated from the mantle striae (Fig. 32). External areola openings rounded occluded by individual hymenes (Fig. 32) External proximal raphe branches straight, clearly interrupted near the valve middle (Fig. 32). Fibulae not equidistant, the middle clearly more separated than the others (Fig. 34), each of them connected to 1–3 transapical costae. Internal proximal raphe endings weakly deflected, clearly interrupted by a raised central nodule (Fig. 33).

 Type:—VEGA ISLAND, sample VEG-M2 (63°48'55.4"S/57°18'35.6"W), leg. J. Kavan, coll. date 17 January 2013 (holotype, slide BR 4514; isotype, slide PLP–344, University of Antwerp, Belgium).

 Ecology:—So far *Hantzschia zikmundiana* was found in only one sample taken from a very dry moss vegetation around the stream going along the moraine. The sample was dominated by *Chamaepinnularia krookiformis* (Krammer 1992: 79–80) Lange-Bertalot & Krammer (in Lange-Bertalot & Genkal 1999: 37) and *Pinnularia borealis* Ehrenberg (1843: 420) sensu lato. Due to confusion with *H. abundans*, the exact distribution and ecology of this species is not entirely known.

 Etymology:—The species is named after Ing. Miroslav Zikmund (°1919), a famous Czech traveller, author, filmmaker and photographer.

Hantzschia amphioxys **(Ehrenberg) Grunow** (Figs 35–50)

LM (Figs 35–46):—Valves dorsiventral with a slightly convex to almost straight dorsal margin. Ventral margin weakly concave in the middle becoming straight near the apices. Apices abruptly protracted, shortly elongated, clearly capitate, almost straight to slightly deflected towards the dorsal side. Valve dimensions (n=25): length 34–52 μm, width is
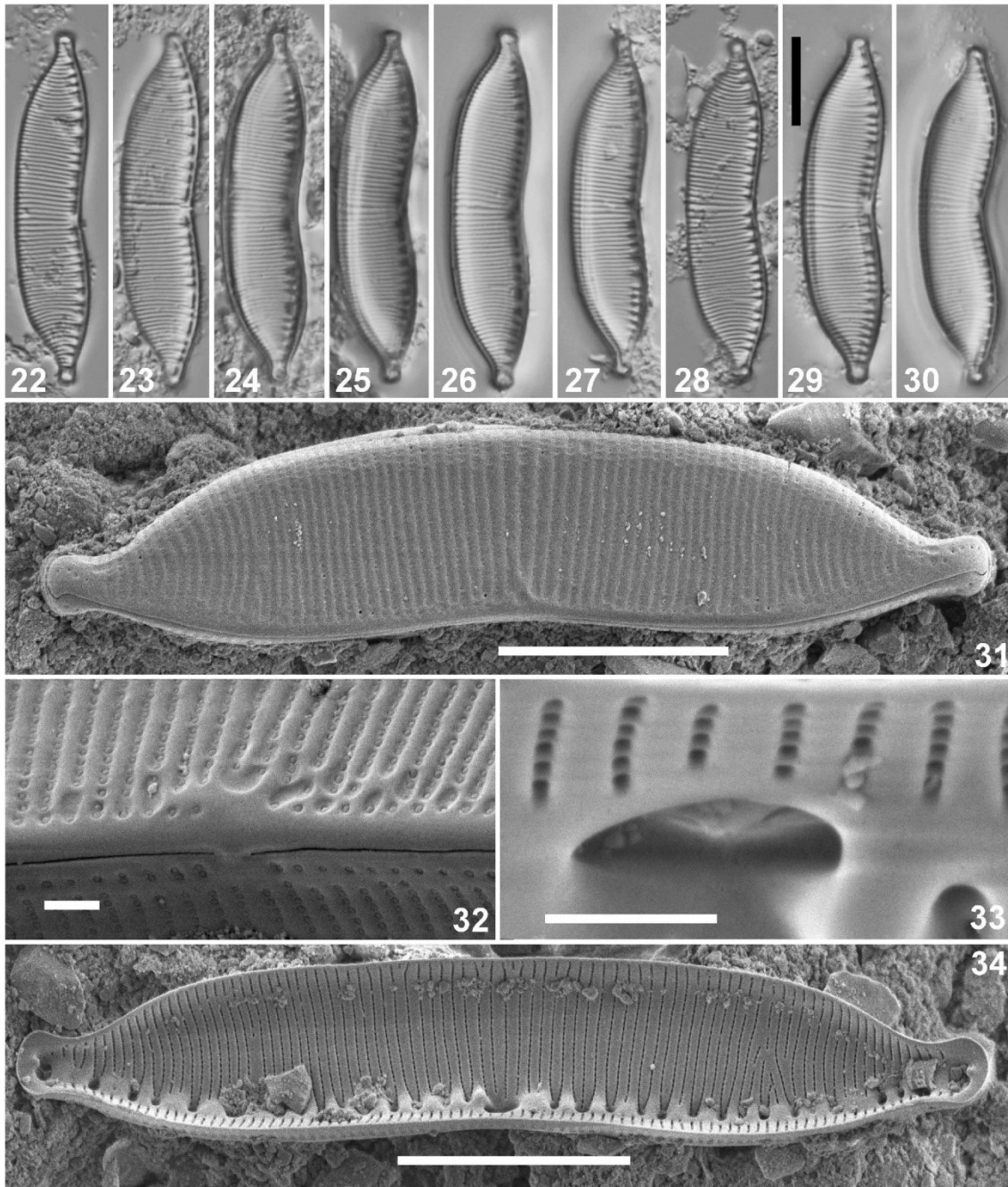
FIGURES 22–34. *Hantzschia zikmundiana*. LM and SEM observations of the type population (Vega Island, sample VEGA-M2). Figs 22–30. Light micrographs showing a reduction in valve length. Fig. 31. External view of an entire valve showing the narrow ventral hyaline border and the shallow grooves with the rounded areolae. Fig. 32. External detail of the central area with the straight, interrupted, proximal raphe endings. Fig. 33. Internal detail of the central area with the interrupted proximal raphe endings. Fig. 34. Internal view of an entire valve showing the irregularly placed fibulae. Scale bar represents 10 μm except for figs 32 & 33 where scale bar = 1 μm.
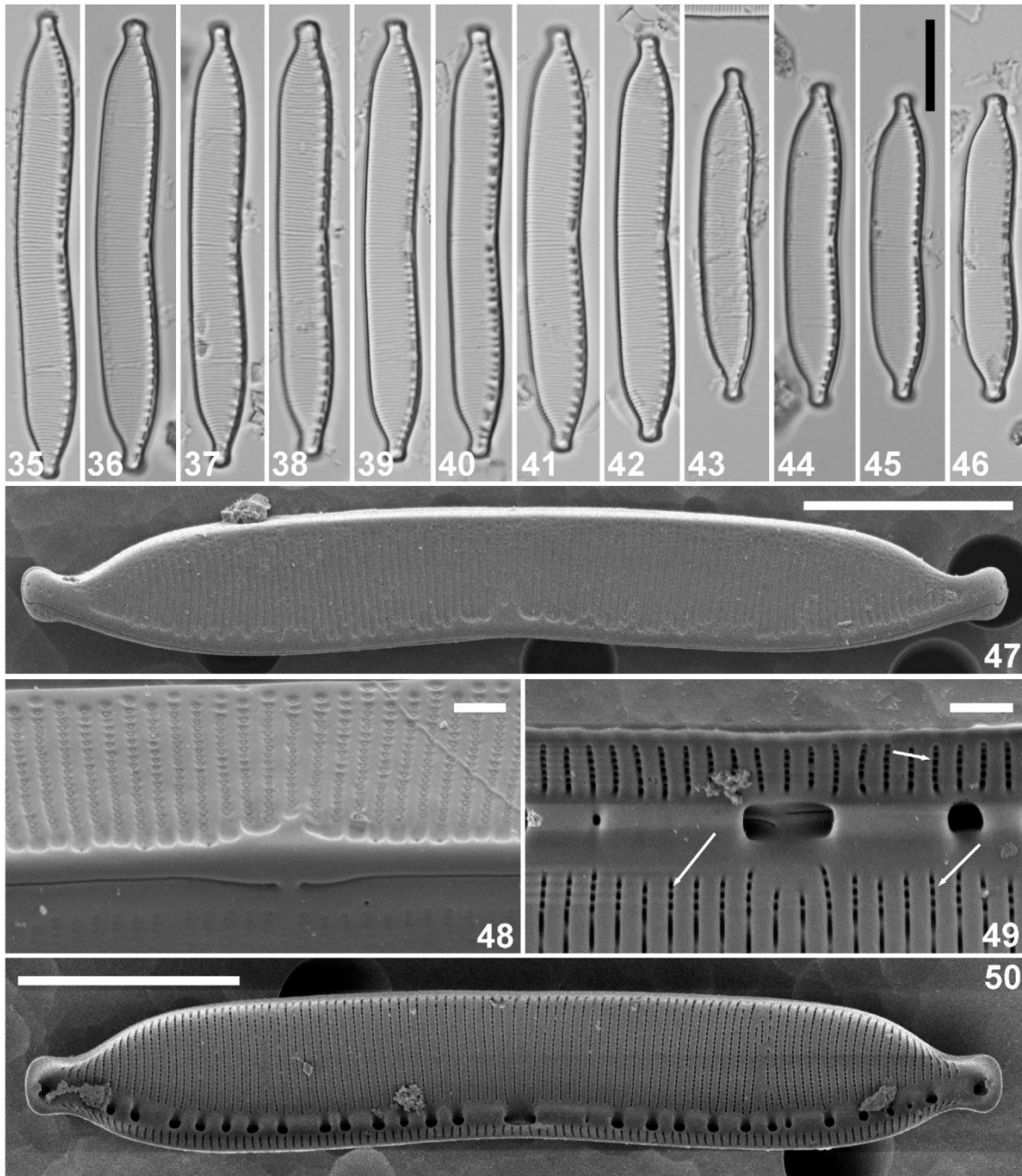
FIGURES 35–50. *Hantzschia amphioxys.* LM and SEM observations of a population from James Ross Island (sample Anna Pool). Figs 35–46. Light micrographs showing a reduction in valve length. Fig. 47. External view of an entire valve showing the irregular, narrow ventral hyaline border. Fig. 48. External detail of the central area with the deflected, interrupted proximal raphe endings. Fig. 49. Internal detail of the central area with the interrupted, deflected proximal raphe endings. The arrows indicate the small silica bars separating the areolae. Fig. 50. Internal view of an entire valve showing the irregularly placed fibulae. Scale bar represents 10 μm except for figs 48 & 49 where scale bar = 1 μm.

5.0–6.0 µm. Fibulae 6–9 in 10 µm, unequally spaced, the middle two fibulae clearly more distant. Each fibula connected to 1–3 transapical costae. Striae equidistant, weakly radiate in the middle becoming more parallel near the apices, 24–25 in 10 µm. Areolae not discernible in LM. SEM (Figs 47–50): Valves on the ventral side bordered by a narrow, clearly thickened hyaline keel (Fig. 47). Striae located in shallow individual depressions bordered by slightly raised costae (Fig. 48). External areola openings rounded occluded by individual hymenes (Fig. 48). External proximal raphe branches deflected, clearly interrupted near the valve middle (Fig. 48). Internally, fibulae clearly not equidistant (Fig. 50). Internal proximal raphe endings interrupted, one end being deflected and the other more or less straight (Fig. 49). Striae forming narrow, deep, parallel grooves (Fig. 50). Areolae separated by thin struts (Fig. 49, arrows).

Ecology:—So far, the species was only with certainty confirmed from the moss vegetation collected in a small pool on James Ross Island. Detailed analysis of the stria structure and the internal raphe endings is necessary to avoid confusion with *H. amphioxys* f. *muelleri*.

Hantzschia amphioxys (Ehrenberg) Grunow f. *muelleri* Ko-Bayashi (Figs 51–65)

LM (Figs 51–61):—Valves dorsiventral with a slightly convex to almost straight dorsal margin. Ventral margin weakly concave in the middle becoming slightly convex near the apices. Apices abruptly protracted, elongated and clearly capitate, slightly deflected towards the dorsal side. Valve dimensions (n=25): length 40–55 µm, width 5.0–6.0 µm. Fibulae 6–7 in 10 µm, unequally spaced, the middle two fibulae clearly more distant. Each fibula connected to 1–3 transapical costae. Striae equidistant, weakly radiate in the middle becoming more parallel and even convergent near the apices, 22–26 in 10 µm. Occasionally, middle striae slightly more spaced than the others. Areolae not discernible in LM. SEM (Figs 62–65): Valves on the ventral side bordered by a clearly thickened keel covered with irregularly scattered areolae (Fig. 62). Striae located in rather deep grooves bordered by raised costae (Figs 62, 63), more prominently deepened near the ventral margins (Fig. 63). External areola openings rounded occluded by individual hymenes (Fig. 63). External proximal raphe branches deflected, clearly interrupted near the valve middle (Fig. 63). Internally, fibulae clearly not equidistant (Fig. 65). Internal proximal raphe endings unclear, interrupted by a thickened central nodule (Fig. 64). Striae forming narrow, deep, parallel grooves (Fig. 64).

Ecology:—*Hantzschia amphioxys* f. *muelleri* is a very commonly reported species, often observed in terrestrial habitats such as seepage areas, wet moss vegetations and soils (Kellogg & Kellogg 2002 and references therein). The ecological separation from *H. amphioxys* is unclear. All populations will need further morphological research to determine their exact ecological preferences.

Hantzschia abundans Lange-Bertalot (Figs 66–76)

LM (Figs 66–73):—Valves dorsiventral with a convex dorsal and a concave ventral margin, typically ventrally constricted near the middle. Apices protracted, clearly elongated. Valve dimensions (n=20): length 55–65 µm, width is 7.0–8.0 µm. Fibulae 5–8 in 10 µm, unequally spaced, the middle two fibulae clearly more distant. Each fibula connected to 1–4 transapical costae. Striae equidistant, weakly radiate in the middle becoming more parallel near the apices, 19–21 in 10 µm. Central striae usually slightly more distant. Areolae not discernible in LM. SEM (Figs 74–76): Valves on the ventral side bordered by a narrow hyaline keel (Fig. 74). Striae composed of small, rounded areolae, towards the ventral margin located in rather broad, shallow grooves (Figs 74, 75). Isolated areolae bordering the ventral keel (Fig. 75). External proximal raphe branches straight, clearly interrupted near the valve middle (Fig. 75). Internal proximal raphe endings interrupted, straight (Fig. 76).

Ecology:—So far, the species was only with certainty confirmed from a seepage area on James Ross Island.

Hantzschia incognita Zidarova & Van de Vijver (Figs 77–89)

LM (Figs 77–85):—Valves clearly dorsiventral with a moderately convex but never straight dorsal side. Ventral side concave in the middle part becoming convex near the apices, never constricted in the middle. Valve apices weakly protracted, rostrate, never subcapitate to capitate. Valve dimensions (n=20): length 48–67 µm, 7.5–8.0 µm. Fibulae, more or less spaced, the middle ones usually not more distant than the others, 5–8 in 10 µm, connected to 1–3 transapical costae. Striae parallel, equidistant throughout, becoming convergent near the apices, 18–20 in 10 µm. Areolae not discernible in LM. SEM (Figs 86–89): Valves on the ventral side bordered by a narrow, irregularly shaped, hyaline keel (Fig. 86). Striae uniseriate, composed of small, rounded areolae, situated in a shallow, continuous groove, externally covered by small, individual hymenes, ca. 45 in 10 µm (Fig. 87). External (Fig. 87) and internal (Fig. 88) raphe branches continuous, lacking a central interruption. Fibulae irregularly shaped (Fig. 89).
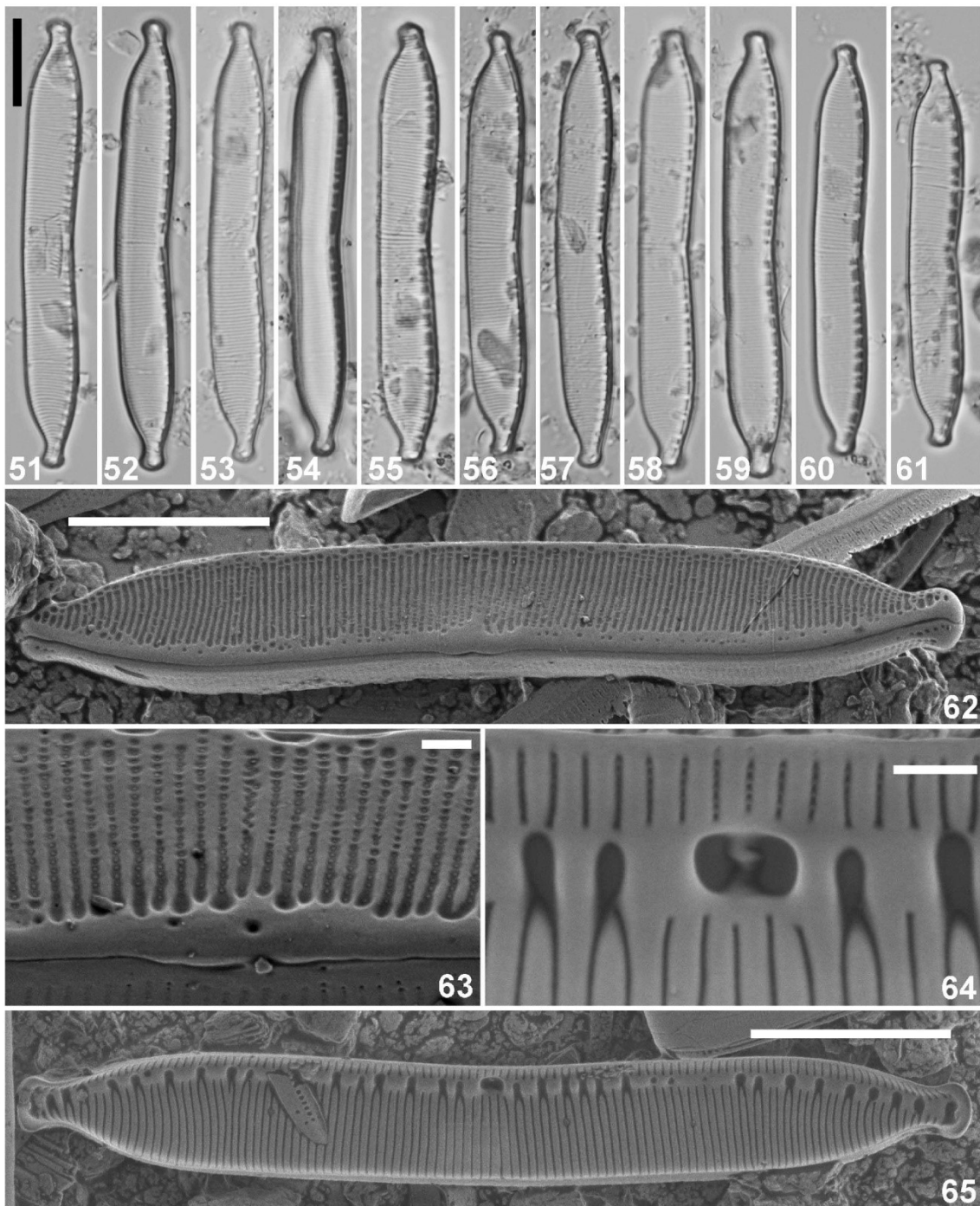
FIGURES 51–65. *Hantzschia amphioxys* f. *muelleri*. LM and SEM observations of a population from Livingston Island (sample LIV-16A). Figs 51–61. Light micrographs showing a reduction in valve length. Fig. 62. External view of an entire valve showing the thickened ventral hyaline border with scattered areolae. Fig. 63. External detail of the central area with the deflected, interrupted proximal raphe endings. Fig. 64. Internal detail of the central area with the thickened central nodule. Proximal raphe endings are not clearly discernible. Fig. 65. Internal view of an entire valve showing the irregularly placed fibulae. Scale bar represents 10 μm except for figs 63 & 64 where scale bar = 1 μm.
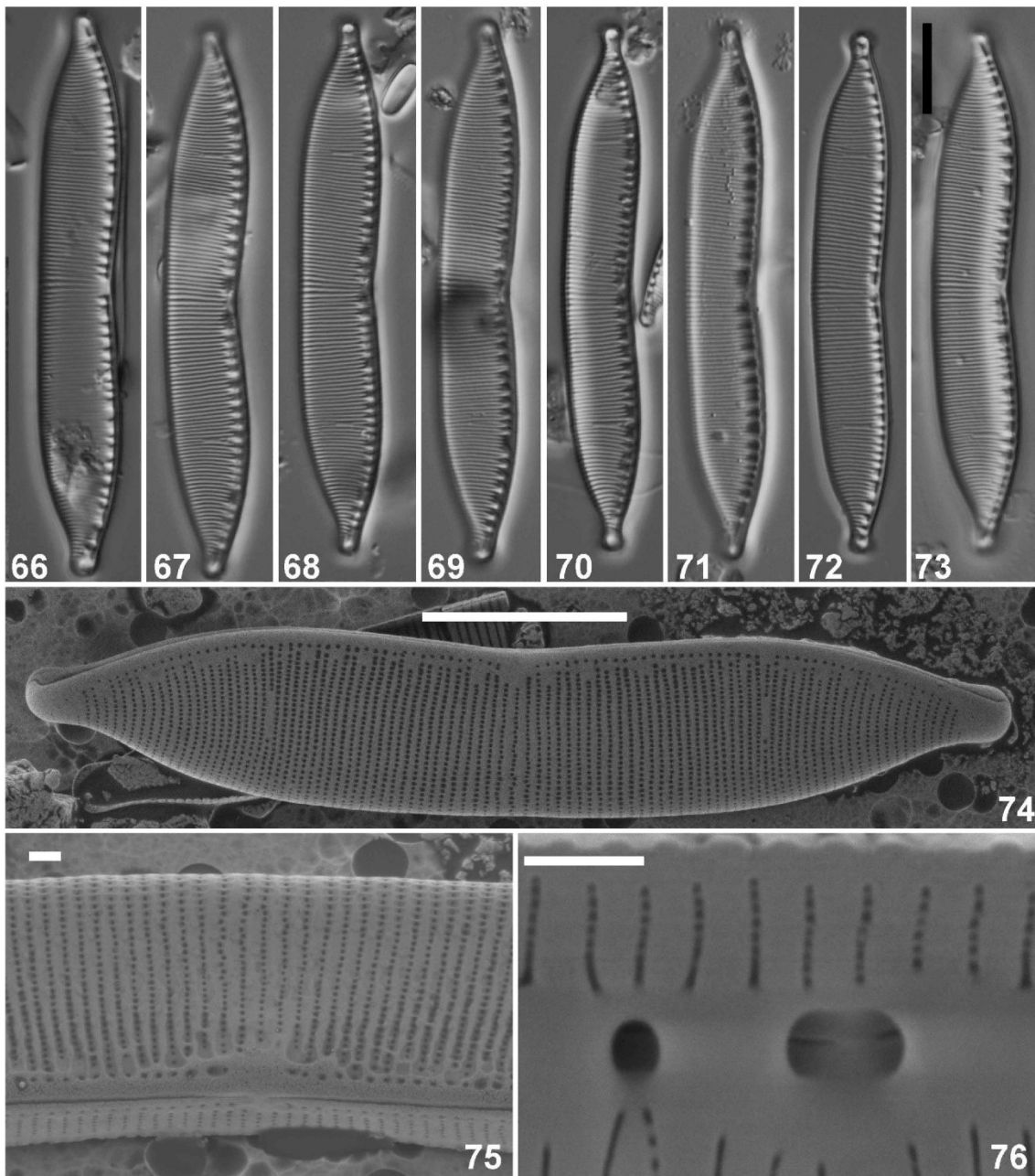
FIGURES 66–76. *Hantzschia abundans*. LM and SEM observations of a population from James Ross Island (sample S1E). Figs 66–73. Light micrographs showing a reduction in valve length. Fig. 74. External view of an entire valve showing the very narrow ventral hyaline border and striae composed of rounded areolae. Fig. 75. External detail of the central area with the straight, interrupted, proximal raphe endings. Note the striae that are weakly depressed near the ventral area. Fig. 76. Internal detail of the central area with the interrupted proximal raphe endings. Scale bar represents 10 μm except for figs 75 & 76 where scale bar = 1 μm.
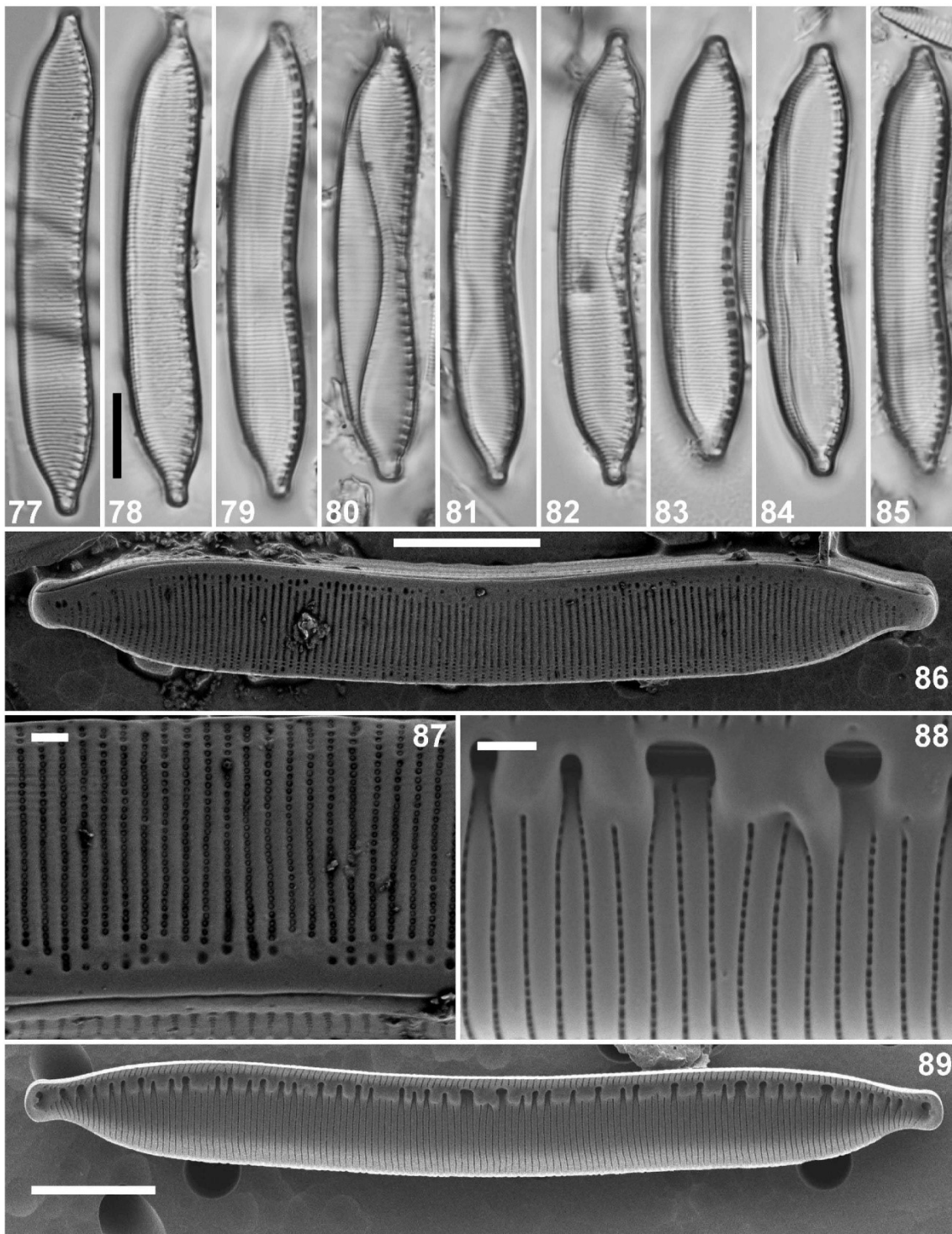
FIGURES 77–89. *Hantzschia incognita*. LM and SEM observations of the type population (Livingston Island, Hurd Peninsula, sample Π1a). Figs 77–85. Light micrographs showing a rather limited morphological variability. Fig. 86. External view of an entire valve showing the thickened ventral hyaline border and the grooves with the striae. Fig. 87. External detail of the central area with the continuous proximal raphe endings and the deep stria grooves. Fig. 88. Internal detail of the central area with the continuous proximal raphe endings. Fig. 89. Internal view of an entire valve showing the irregularly placed fibulae. Scale bar represents 10 μm except for figs 87 & 88 where scale bar = 1 μm.

Ecology:—*Hantzschia incognita* is a common species in soil and on mosses in the Maritime Antarctic Region. The type population was found in sample Π1a/04, taken from wet soil near a stream, close to the Spanish Juan Carlos I base (Zidarova *et al.* 2010).

Discussion

The limnoterrestrial diatom flora of the Maritime Antarctic Region is dominated by the genera *Muelleria* (Frenguelli 1924: 256) Frenguelli (1945: 172), *Luticola* D.G.Mann in Round *et al.* (1990: 670), *Humidophila* Lowe *et al.* (2014: 352), *Pinnularia* Ehrenberg (1843: 45) and *Hantzschia* (Zidarova *et al.* 2016 and references therein). The ongoing taxonomic revision of the past few years clearly indicated that a high endemism prevails in these genera. Kociolek *et al.* (2017) analysed the biogeographic distribution of all *Luticola* taxa in the Antarctic Region and concluded that the genus showed an incredible high endemism, far much larger than observed in any other organismal group. Recent molecular analysis proved that this endemism, despite being only based on morphological research, is confirmed by genetic studies (Souffreau *et al.* 2013, Pinseel *et al.* 2017). Nevertheless, the actual diversity within the terrestrial diatoms is still underestimated as shown by some of the conclusions in Souffreau *et al.* (2013) suggesting that "*many presumed cosmopolitan Antarctic diatom species are in fact species complexes, possibly containing Antarctic endemics*".

The results of the present paper confirm the latter statement with the description of three new *Hantzschia* species despite an earlier elaborate revision of the genus in 2010 describing 5 new taxa (Zidarova *et al.* 2010). Especially within the (cosmopolitan) *H. amphioxys* and *H. abundans* (-complexes), new species still needed to be split off. The description of three new species related to both cosmopolitan taxa should be seen in the light of a further refinement of our knowledge of this genus. Nevertheless, several taxonomic problems remain and will most likely only be solved by a thorough molecular phylogenetic analysis of the entire *amphioxys-abundans* complex as is currently being the case for the *Pinnularia borealis* complex (E. Pinseel, pers. comm.). Especially the separation of *H. amphioxys* and *H. amphioxys* f. *muelleri* remains questionable in the Antarctic Region. It is clear that using only light microscopy, observations will not allow a good distinction between both taxa. Originally, Müller (1909) separated *H. amphioxys* f. *muelleri* (as *H. amphioxys* f. *capitata* Müller (1909:34)) from the nominate variety by its more capitate apices. Unfortunately, earlier attempts to obtain the type material of the latter taxon in order to study its ultrastructure, failed (Zidarova *et al.* 2010). Both taxa are widely distributed in the entire Antarctic Region. Kellogg & Kellogg (2002) listed more than 100 records for *H. amphioxys* and almost 20 records for the f. *muelleri*. Jahn *et al.* (2014) doubted however that a taxonomical distinction based on the presence of capitate apices alone will not be sufficient. The analysis of several populations in the Maritime Antarctic Region based on SEM observations, however, showed that two different morphological groups can be separated, possibly reflecting the separation between *H. amphioxys* and its f. *muelleri*. Two important morphological features showed clear differences: the ultrastructure of the striae and the structure of the internal proximal raphe endings. *Hantzschia amphioxys* f. *muelleri* seems to have striae located in deep grooves (Fig. 63) whereas the striae in *H. amphioxys* are composed of a series of shallow areolae (Fig. 48). The internal raphe endings in the f. *muelleri* terminate on a raised, clearly thickened central nodule (Fig. 64), whereas this structure is absent in *H. amphioxys* (Fig. 49). A third taxon, often found in the Maritime Antarctic Region (Zidarova *et al.* 2016), *Hantzschia incognita*, and showing a comparable outline in LM, is clearly different from *H. amphioxys* and its *f. muelleri*, lacking the interrupted proximal raphe endings and the typical ventral constriction in the valve outline. In LM, the continuous raphe is recognisable in the lack of a gap between the middle fibulae, when observed normally indicating the presence of a raised central nodule.

In this study, three new taxa were described. Table 2 presents a morphological comparison between all the new species and several other *Hantzschia* taxa. These new taxa showed a clear resemblance with *H. abundans* and were most likely force-fitted in the latter in the past. Zidarova *et al.* (2010) erroneously combined several pictures supposedly representing *H. abundans* in one plate (see Fig. 2 A–I). Some of the pictures representing specimens with short, blunt apices, proved to belong to *H. zidarovae* (see for instance Fig. 2 E & F). The latter was earlier recognized as an independent taxon (Zidarova *et al.* 2010, as *Hantzschia* sp. 1), but due to a lack of sufficient specimens, the taxon was never described as a new species. Careful re-analysis of all observations and additional SEM analysis, added new specimens and made clear that the species has a very distinct morphology and should be described as a new species. The presence of the very deep, narrow grooves in which the striae are located, is a feature rarely seen in the genus *Hantzschia*. In LM, the apices are short, never elongated and bluntly rounded, a feature not observed in either *H. abundans* and *H. australabundans*.

TABLE 2. Comparison of the new *Hantzschia* taxa with similar *Hantzschia* taxa worldwide.

	H. australabundans	H. zidarovae	H. zikmundiana	H. amphioxys	H. amphioxys f. muelleri	H. abundans	H. incognita	H. considerata	H. compactoides	H. abruptirostrata
length (μm)	48.0–101.0	45.0–60.0	37.5–45.0	15.0–50.0	41.0–56.0	40.0–80.0	48–67	70.0–160.0	60.0–80.0	75.0–103.0
width (μm)	7.5–12.0	8.0–10.5	7.0–8.5	5.0–7.0	5.0–6.0	7.0–10.0	7.4–8.1	13.0–15.0	10.0–12.0	10.5–12.0
dorsal margin	convex, slightly flattened in the middle	almost straight	strongly convex	slightly convex to almost straight	slightly convex to almost straight	convex, flattened in the middle	moderately convex	convex	convex	straight to weakly convex
ventral margin	distinctly concave in the middle, convex towards the apices	slightly concave in the middle, slightly convex near the apices	deeply concave in the middle, more convex towards the apices	moderately concave in the middle, slightly convex near the apices	moderately concave in the middle, slightly convex near the apices	concave in the middle, convex towards the apices	concave in the middle, convex toward the apices	slightly concave in the middle and moderately convex near the apices	concave in the middle and convex near the apices	slightly concave in the middle and moderately convex near the apices
valve apices	clearly protracted, rostrate to subcapitate	shortly protracted, subcapitate	protracted, capitate, deflected towards the dorsal side	shortly protracted rostrate-capitate	abruptly protracted, capitate	slightly protracted, rostrate to subcapitate	rostrate	protracted, rostrate-capitate	slightly proctated, rostrate	protracted, rostrate-capitate to clearly capitate
striae	radiate in the middle, parallel to slightly curved near the apices	slightly radiate in the middle, parallel near the apices	radiate in the middle, almost parallel throughout the entire valve, slightly curved near the apices	parallel to slightly radiate in the middle, slightly curved near the apices	parallel to slightly radiate in the middle, slightly curved near the apices	parallel in the middle, slightly curved near the apices	parallel	parallel to slightly radiate in the middle, slightly curved near the apices	parallel to slightly radiate in the middle, slightly curved near the apices	parallel to slightly radiate in the middle, slightly curved near the apices
number of striae (in 10 μm)	17–23	19–20	19–22	20–29	22–26	15–20	18–20	13–15	14–16	15.5–16.5
number of areolae (in 10 μm)	c. 45	c. 45	c. 45	40–50	c. 50	c. 40	ca 45	27–30	c. 30	?
number of fibulae (in 10 μm)	5–7	5–6	6–9	variable	6–9	5–8	5/aug	4–6	5–6	6–7.5
middle fibulae	more distant	more distant	more distant	distant	more distant	more distant	not distant	distant	more distant	more distant
raphe structure	not continuous, proximal raphe endings straight to weakly deflected	not continuous, proximal raphe endings clearly deflected, often with deep groove	not continuous, proximal raphe endings straight	not continuous, proximal raphe endings externally unilaterally bent, internally bent to opposite directions	not continuous, proximal raphe endings unilaterally bent	slightly unilaterally bent in the middle	straight, continuous, lacking proximal pores	?	straight	?

The distinction between *H. australabundans*, *H. abundans* and *H. zikmundiana* is less obvious. Figure 90 shows length vs. width of several Antarctic populations (LIV: *H. australabundans*, M2: *H. zikmundiana*, JRI: *H. abundans*) and *H. abundans* populations worldwide. Table 3 compares the biometric data of several analysed populations of *Hantzschia abundans*. *Hantzschia abundans* was originally described in 1993 from a Phalaridetum-vegetation on the shore of a small river in the vicinity of Frankfurt a/M in Germany (Lange-Bertalot 1993). Although the original description mentions a valve width of 7–10 μm, the illustrated specimens never showed a valve width above 8.5 μm (Lange-Bertalot 1993, plate 85, Figs 12–17). Measured specimens, identified by Lange-Bertalot from Mongolia (Metzeltin *et al.* 2009, plate 234, Figs 1–12), Uruguay (Metzeltin *et al.* 2005, plate 212, Figs 1–3, 5–8) and Sardinia (Lange-Bertalot *et al.* 2003, Plate 102, Figs 6–16) likewise never showed a valve width above 9 μm. On the other hand, the populations from the South Shetland Islands (Livingston & King George Island) clearly are wider than the other populations. They also seem to be slightly longer resulting in a lower length/width ratio (Table 3). In the length/width diagram, both populations are separated in the upper half of the diagram. *Hantzschia australabundans* has a higher stria density than *H. abundans*. Valves showing a stria density above 21 are relatively common. The internal proximal raphe endings in *H. australabundans* terminate on a heavily silicified central nodule whereas the latter is less developed in *H. abundans*. Although being relatively small, these differences are sufficient to separate both taxa as independent species. Other *H. abundans* populations worldwide show differences with the European type populations. Further morphological and preferentially also molecular analysis, will be necessary to clarify their correct taxonomic position. *Hantzschia zikmundiana* from Vega Island was clearly different being much smaller in length and width. Moreover, the species shows a distinct dorsiventrality with a clear ventral constriction. Both *H. abundans* and *H. australabundans* never show this dorsiventrality and are much larger in their valve dimensions. Worldwide, only *Hantzschia compacta* (Hustedt 1922: 145) Lange-Bertalot in Lange-Bertalot & Genkal (1999: 62), *H. compactoides* Lange-Bertalot *et al.* (2003: 56) and *H. considerata* Lange-Bertalot *et al.* (2003: 57) show a similar valve outline (Lange-Bertalot *et al.* 2003). All three however, are much larger with a minimum valve width exceeding 10 μm (Table 2).
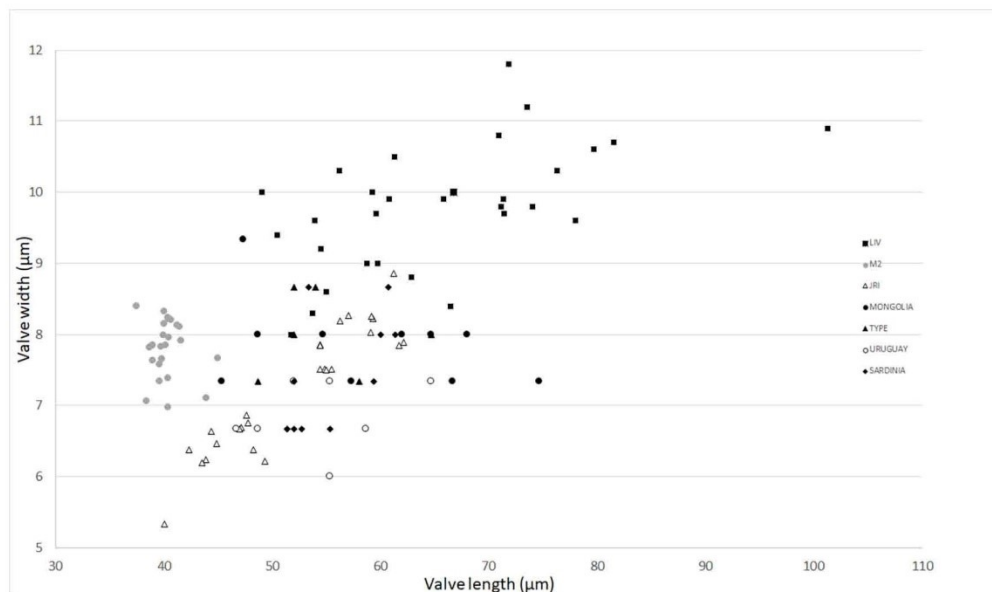
FIGURE 90. Diagram representing length vs. width for several *H. abundans* populations worldwide based on literature data for the populations from Mongolia, Uruguay, Sardinia and Germany (type population). (JRI=James Ross Island, M2=Vega Island, LIV=Livingston Island).

The addition of these three new *Hantzschia* species allows for a better understanding of the biogeography of the genus. Curiously, a large number of *Hantzschia* species described from the northern hemisphere seem to possess external proximal raphe endings, often well separated from each other while species described from the southern hemisphere usually lack separated proximal endings. Lange-Bertalot (1993), discussing several commonly reported *Hantzschia* taxa, clearly illustrates the proximal raphe endings in a.o. *H. amphioxys*, *H. abundans*, *H. subrupestris* or *H. hyperborea*, all possessing proximal raphe endings. Populations of these taxa from the southern hemisphere (e.g., *H. amphioxys* from Namibia, see plate 88, fig. 1) show no central interruption in the raphe course, probably

suggesting that these populations do not belong to the northern hemisphere species and may represent unknown (new) species. The southern hemisphere relatives such as *H. hyperaustralis* or *H. incognita* (Zidarova et al. 2010) have uninterrupted raphe branches. Unfortunately, this morphological difference does not seem to be the general rule since a few exceptions can be found. *Hantzschia giessiana* Lange-Bertalot & Rumrich (1993: 80) was described from Namibia and possesses clearly separated proximal raphe endings. On the other hand, taxa described from Sardinia, such *as H. sardiniensis* Lange-Bertalot et al. (2003: 66) lack proximal raphe endings (Lange-Bertalot et al. 2003). Nevertheless, in the Antarctic region, all so far described taxa lack the proximal endings, clearly separating them from their northern hemisphere relatives.

TABLE 3. Morphometric data of the *Hantzschia* cf. *abundans* populations in the Antarctic region and several published *H. abundans* populations worldwide.

locality	Source abbreviation	# measured specimens	length (μm)	width (μm)	striae (in μm)	fibulae (in μm)	ratio length/width
King George Island	KGI	5	67.5 ± 13.5	11.6 ± 1.2	19.0 ± 1.0	5.5 ± 0.7	6.2 ± 1.4
Livingston Island	LIV	30	65.5 ± 11.5	9.8 ± 0.9	19.4 ± 1.3	6.5 ± 1.0	6.7 ± 0.9
Vega Island	VEGA	25	38.1 ± 1.6	8.1 ± 0.4	20.5 ± 0.8	8.5 ± 1.2	4.7 ± 0.4
James Ross Island	JRI	26	44.6 ± 6.7	6.5 ± 0.9	22.0 ± 1.2	7.0 ± 0.7	6.8 ± 0.3
Mongolia	MON	10	46.3 ± 9.9	8.3 ± 0.6	19.5 ± 1.4	7.5 ± 1.3	5.6 ± 1.5
type (Germany)	TYPE	6	56.7 ± 5.7	7.7 ± 0.6	18.5 ± 1.3	7.0 ± 1.0	7.3 ± 0.9
Uruguay	URU	7	55.7 ± 6.1	7.0 ± 0.5	17.5 ± 1.2	6.0 ± 0.8	7.9 ± 0.9
Sardinia	SAR	11	54.3 ± 4.1	7.7 ± 0.8	17.5 ± 0.8	6.5 ± 0.8	7.2 ± 0.6

References

Aristarain, A.J., Pinglot, J.F. & Pourchet, M. (1987) Accumulation and temperature measurements on the James Ross Island, Antarctic Peninsula, Antarctica. *Journal of Glaciology* 33: 1–6.

Chipev, N. & Veltchev, K. (1996) Livingston Island: an environment for Antarctic life. *In: Bulgarian Antarctic Research, Life Sciences.* pp. 1–10.

Cleve, P.T. & Grunow, A. (1880) Beiträge zur Kenntnis der arktischen Diatomeen. *Kungliga Svenska vetenskapsakademiens handlingar* 17: 1–121.

Ehrenberg, C.G. (1843) Verbreitung und Einfluss des mikroskopischen Lebens in Süd-und Nord-Amerika. *Abhandlungen der Königlichen Akademie der Wissenschaften zu Berlin* 1841: 291–445.

Fourtanier, E. & Kociolek, J.P. (2012) *Catalogue of Diatom Names, updated 19.09.2011 [online].* California Academy of Sciences. Available from: http://research.calacademy.org/research/diatoms/names/index.asp (accessed 7 January 2017)

Grunow, A. (1877) New Diatoms from Honduras, with notes by F. Kitton. *Monthly Microscopical Journal* 18: 165–186.

Guiry, M.D. & Guiry, G.M. (2014) Algaebase. World-wide electronic publication, National University of Ireland, Galway. Available from: http://www.algaebase.org/ (accessed 1 October 2018)

Hendey, N.I. (1964) *An introductory account of the smaller algae of British coastal waters. Part V. Bacillariophyceae (Diatoms).* Her Majesty's Stationery Office, London.

Jahn, R., Kusber, W. & Lange-Bertalot, H. (2014) Typification and taxonomy of *Hantzschia amphioxys* (Ehrenberg) Grunow (Bacillariophyta): type of the genus name *Hantzschia* Grunow. *Nova Hedwigia* 143: 103–110.

https://doi.org/10.1127/1438-9134/2014/005

Kobayashi, T. (1965) IX. Variations in *Hantzschia amphioxys* (Ehren.) Grun. var. Recta O.Müller. *Japanese Antarctic Research Expedition 1956–1962. Scientific Reports, Series E. (Biology)* 24: 13–16.

Kopalová, K., Veselá, J., Elster, J., Nedbalová, L., Komárek, J. & Van de Vijver, B. (2012) Benthic diatoms (Bacillariophyta) from seepages and streams on James Ross Island (NW Weddell Sea, Antarctica). *Plant Ecology & Evolution* 145: 190–208.

Kopalová, K., Ochyra, R., Nedbalová, L. & Van de Vijver, B. (2014) Moss-inhabiting diatoms from two contrasting Maritime Antarctic islands. *Plant Ecology and Evolution* 147: 67–84.
https://doi.org/10.5091/plecevo.2014.896

Krammer, K. (1992) *Pinnularia, eine monographie der europaischen taxa. Bibliotheca Diatomologica* 26: 1–353.

Lange-Bertalot, H. (1993) 85 Neue Taxa und über 100 weitere neu definierte Taxa ergänzend zur Süßwasser flora von Mitteleuropa. *Bibliotheca Diatomologica* 27: 1–454.

Lange-Bertalot, H. & Genkal, S.I. (1999) Diatoms from Siberia I. Islands in the Arctic Ocean (Yugorsky-Shar Strait). *Iconographia Diatomologica* 6: 1–271.

Lange-Bertalot, H., Cavacini, P., Tagliaventi, N. & Alfinito, S. (2003) Rare a,d 76 new species in rock pools and other ephemeral waters. *Iconographia Diatomologica* 12: 1–438.

Mallet, J. (2007) Species. *In: Encyclopedia of Biodiversity.* Elsevier Inc

Metzeltin, D., Lange-Bertalot, H. & Garcia-Rodriguez, F. (2005) Diatoms of Uruguay. *Iconographia Diatomologica* 15: 1–736.

Metzeltin, D., Lange-Bertalot, H. & Nergui, S. (2009) Diatoms in Mongolia. *Iconographia Diatomologica* 20: 1–686.

Müller, O. (1909) Bacillariaceen aus Sudpatagonien. *(Engler's) Botanische Jahrbucher fur Systematik, Pflanzengeschichte, und Pflanzengeographie, Leipzig* 43 (Heft 4, Beiblatt Nr. 100): 1–40.

Øvstedal, D.O. & Lewis-Smith, R.L. (2001) *Lichens of Antarctica and South Georgia. A guide to their identification and ecology.* Cambridge University Press, Cambridge.

Ross, R., Cox, E.J., Karayeva, N.I., Mann, D.G., Paddock, T.B.B., Simonsen, R. & Sims, P.A. (1979) An amended terminology for the siliceous components of the diatom cell. *Nova Hedwigia* 64: 513–533.

Round, F.E., Crawford, R.M. & Mann, D.G. (1990) *The diatoms: biology and morphology of the genera.* Cambridge, Cambridge University Press.

Ruck, E.C. & Theriot, E.C. (2011) Origin and evolution of the canal raphe system in diatoms. *Protist* 162: 723–737.
https://doi.org/10.1016/j.protis.2011.02.003

Rumrich, U., Lange-Bertalot, H. & Rumrich, M. (2000) Diatoms of the Andes. From Venezuela to Patagonia/Tierra del Fuego and two additional contributions. *Iconographia Diatomologica* 9: 1–673.

Souffreau, C., Vanormelingen, P., Van de Vijver, B., Isheva, T., Verleyen, E., Sabbe, K. & Vyverman, W. (2013) Molecular evidence for distinct Antarctic lineages in the cosmopolitan terrestrial diatoms *Pinnularia borealis* and *Hantzschia amphioxys. Protist* 164: 101–115.
http://dx.doi.org/10.1016/j.protis.2012.04.001

Van de Vijver, B., Frenot, Y. & Beyens, L. (2002) Freshwater diatoms from Ile de la Possession (Crozet Archipelago, Subantarctica). *Bibliotheca Diatomologica* 46: 1–412.

van der Werff, A. (1955) A new method of concentrating and cleaning diatoms and other organisms. *Verhandlungen Internationalen Vereinigung für Theoretische und Angewandte Limnologie* 2: 276–277.

You, Q., Kociolek, J.J. & Wang, Q. (2015) The diatom genus *Hantzschia* (Bacillariophyta) in Xinjiang Province, China. *Phytotaxa* 197: 1–14.
https://doi.org/10.11646/phytotaxa.197.1.1

Zidarova, R., Kopalova, K. & Van de Vijver, B (2016) Diatoms from the Antarctic Region. I: Maritime Antarctica. *Iconographia Diatomologica* 24: 1–501.

Zidarova, R., Van de Vijver, B., Quesada, A. & de Haan, M. (2010) Revision of the genus *Hantzschia* (Bacillariophyceae) on Livingston Island (South Shetland Islands, Southern Atlantic Ocean). *Plant Ecology and Evolution* 143: 318–333.
https://doi.org/10.5091/plecevo.2010.402

Zimmermann, J., Jahn, R. & Gemeinholzer, B. (2011) Barcoding diatoms: evaluation of the V4 subregion on the 18S rRNA gene, including new primers and protocols. *Organisms Diversity & Evolotion* 11: 173–192.
https://doi.org/10.1007/s13127-011-0050-6

CHAPTER 4

Late-holocene palaeoenvironmental changes at Lake Esmeralda (Vega Island, Antarctic Peninsula) based on a multi-proxy analysis of laminated lake sediment

The Holocene

Research Paper
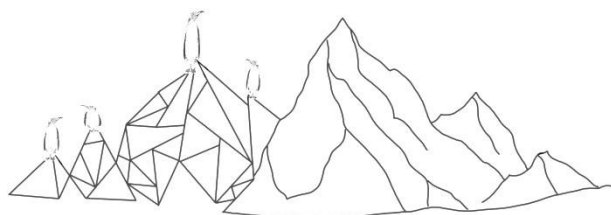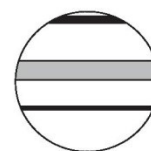
Late-Holocene palaeoenvironmental changes at Lake Esmeralda (Vega Island, Antarctic Peninsula) based on a multi-proxy analysis of laminated lake sediment

Anna Píšková,[1] iD **Matěj Roman,**[2,3] **Marie Bulínová,**[1] **Matěj Pokorný,**[1] iD
David Sanderson,[4] **Alan Cresswell,**[4] **Juan Manuel Lirio,**[5]
Silvia Herminda Coria,[5] **Linda Nedbalová,**[1] **Andrea Lami,**[6] iD
Simona Musazzi,[6] iD **Bart Van de Vijver,**[7] **Daniel Nývlt**[2]
and Kateřina Kopalová[1]

Abstract

We have studied laminated sediments from Lake Esmeralda, Vega Island, in order to reconstruct its history. We describe both inorganic and organic components of the sediment using a combination of the following analytical methods: x-ray fluorescence (XRF), x-ray diffraction (XRD), magnetic susceptibility measurement, chemical analysis for determination of cation exchange capacity, grain size determination, geochemical analyses (total inorganic carbon (TIC), total organic carbon (TOC), total sulphur (TS)), spectrophotometry, high-pressure liquid chromatography, and diatom assemblage and faunal remains characterization. The geochronology of the core was based on modelling optically stimulated luminescence ages and supported by laminae counting. The dating results imply a maximum age of ~400 years for the 177-cm long core and a period covered of ~200 years, suggesting (quasi-) annual laminae formation. Such a young age contradicts previous findings based on radiocarbon dating. Geomorphological evidence indicates that river capture isolated the lake catchment from upslope sediment delivery, effectively terminating accumulation ~230 years ago. Conversely, our short-term palaeoenvironmental record yields a subdecadal temporal resolution, which is unparalleled in comparison with other Antarctic palaeolimnological studies. Our interpretations of the geochemical and mineralogical proxy data give us insight into the past lake catchment and waterbody evolution, and lead us to recognize periods of enhanced weathering, bottom anoxia and to distinguish major lake level changes.

Introduction

Topographically and climatically, the environment of the Antarctic Peninsula (AP) differs from the rest of Continental Antarctica (Vaughan et al., 2003). The AP consists of an unbroken chain of rugged, alpine terrain (Schwerdtfeger, 1984), which forms a climatic barrier separating the warmer Bellingshausen Sea on the west from the cooler Weddell Sea on the east. Because of this topography, the western side of the AP is ca. 7°C warmer than similar latitudes and elevations on the eastern side (Morris and Vaughan, 1994; Reynolds, 1981; Vaughan et al., 2003). In the second half of the 20th century, the AP has experienced one of the greatest near-surface air temperature increases on Earth as a response to ongoing global warming (Turner et al., 2005). Although the past decade was colder, and a significant decrease in air temperature was detected in the north-eastern part of the AP (Oliva et al., 2017; Turner et al., 2016), the warming is expected to continue in the 21st century (Bracegirdle et al., 2008). The extreme sensitivity of the region to climate changes and large latitudinal and longitudinal climatic gradients contribute to an exceptional potential for palaeoclimatological research in the AP. So

far, research attention has been mostly focused on the northern part of the AP with abundant ice-free areas. A number of studies have been specifically concerned with the environmental changes on the largest island of the north-eastern part of the AP, James Ross Island (JRI), and these include investigation of multi-proxy

[1]Department of Ecology, Faculty of Science, Charles University, Czech Republic
[2]Department of Geography, Faculty of Science, Masaryk University, Czech Republic
[3]Department of Physical Geography, Faculty of Science, Charles University, Czech Republic
[4]Scottish Universities Environmental Research Centre (SUERC), UK
[5]Instituto Antártico Argentino, Argentina
[6]Istituto per lo Studio degli Ecosistemi, Italy
[7]Botanic Garden Meise, Belgium

Corresponding author:
Anna Píšková, Department of Ecology, Faculty of Science, Charles University, Viničná 7, Prague 128 44, Czech Republic.
Email: anna@piska.net

palaeolimnological records (Björck et al., 1996), deglaciation chronologies (Glasser et al., 2014; Hjort et al., 1997; Johnson et al., 2011; Nývlt et al., 2014), ice core records (Abram et al., 2013; Mulvaney et al., 2012) and permafrost and active layer changes (Hrbáček et al., 2016a, 2016b, 2017). Other studies have examined the present hydrological systems (Kavan et al., 2016; Lecomte et al., 2016; Nedbalová et al., 2013) and the geochronology and geochemistry of alkaline lavas (Košler et al., 2009; Smellie et al., 2008). Besides JRI, there are potentially other locations in the vicinity that could serve as effective places to conduct studies on past climatic changes.

Vega Island is located north of JRI, and the Herbert Sound separates these two islands. The climate of Vega Island is influenced by its position at the transition between Continental and Maritime Antarctica, and is characterized by cold, arid barrier winds from the south and south-west, and by the presence of a precipitation shadow formed by the AP (Engel et al., 2012), with precipitation estimates of 300–500 mm/yr (Van Lipzig et al., 2004). However, most of the snow accumulation is transported away from land by wind, and effective accumulation is therefore reduced; dry air and high wind speeds also promote high evaporation rates (Nývlt et al., 2016). The mean annual air temperature at the nearby J.G. Mendel Station on the Ulu Peninsula, JRI, was −7.0°C over the period 2006–2015 (Hrbáček et al., 2017), and thus the James Ross Archipelago belongs to the continuous permafrost zone (Fukuda et al., 1992; Washburn, 1974).

More than 80% of Vega Island's 253 km² is covered by glaciers, leaving only small areas of the island presently ice-free. However, the timing of deglaciation of Cape Lamb is poorly constrained, and we must rely on recent studies from the nearby JRI, utilizing cosmogenic nuclide and ^{14}C dating of various archives, including granite erratic boulders (Glasser et al., 2014; Johnson et al., 2011; Nývlt et al., 2014), lake sediments (Björck et al., 1996), raised beaches (Hjort et al., 1997) and marine sediments (Minzoni et al., 2015). Acknowledging possible discrepancies caused by different dating methods and materials used, the overall pattern of deglaciation is still spatially and temporally highly variable. Whereas deglaciation of the Ulu Peninsula, JRI, began as early as ~13 ka BP (Nývlt et al., 2014) and was fully under way at the onset of the Holocene (Glasser et al., 2014; Johnson et al., 2011), the area around The Naze (~5 km south of Cape Lamb) started to deglaciate between 8 and 6 ka BP (Hjort et al., Davies B., unpublished data). In Croft Bay and Herbert Sound, the transition of the grounded ice into floating ice shelves occurred around 10 ka BP, and warm, open marine conditions prevailed after ~7.2 ka BP (Minzoni et al., 2015). Some areas deglaciated even later, around the Holocene Hypsithermal, and include the surroundings of Monolith Lake in the forefield of the Whiskey Glacier, inland part of the Ulu Peninsula (Björck et al., 1996) and elevated volcanic mesas (Johnson et al., 2011).

In the deglaciated areas of the northern part of AP, lake sediments were found to contain some of the best continuous climatic archives (Hodgson et al., 2004; Sterken et al., 2012) despite the highly challenging and problematic dating, including radiocarbon reservoir and contamination issues (Björck et al., 1991b; Heroy and Anderson, 2005). Although Vega Island hosts many lakes and ponds (Lecomte et al., 2016; Moreno et al., 2012), their potential as climatic and environmental archives has yet to be fully explored. One of the first studies from the Cape Lamb area was published by Moreno et al. (2012), providing a very thorough hydrological study of the area including Lake Esmeralda, and by Merino et al. (2012) who published work on the Cape Lamb soils. Lake Esmeralda sediments have been previously studied by Sinito et al. (2011) and Irurzun et al., 2013, 2017), who focused on the palaeomagnetic properties, especially relative magnetic palaeointensity used for establishing sediment chronology. However, a multi-proxy, high-resolution palaeoenvironmental study has not

yet been presented from Lake Esmeralda sediments, nor any other lake on Vega Island.

The aims of this study are to (1) explore the potential of Lake Esmeralda sediments for palaeoclimatic reconstructions, (2) improve the chronological control of Lake Esmeralda record and (3) provide preliminary analysis on the lamination, so far exceptional in the AP region.

Materials and methods

Catchment and lake description

Lake Esmeralda is situated on Cape Lamb, in the south-western part of Vega Island (63°50'S; 57°25'W, Figure 1) at an altitude of 68 m a.s.l. The bathymetry of the lake (Figure 1d) shows two sub-basins up to 6 m deep. Hydrology of the lake was studied by Moreno et al. (2012), who compared the geochemical composition of the ground and lake water, and concluded that the lake is presently endorheic. Streams and groundwater in the catchment are acidic, with pH values around 4. However, lakes in Cape Lamb generally reach pH values above 6, the only exception being Lake Esmeralda with a pH of 4.8 at the surface and decreasing with depth to 4.65 (Moreno et al., 2012). Our measurements of the surface water pH were 5.5 in 2014 and 2017.

The Lake Esmeralda catchment, delineated with ArcGIS Hydrology tools and REMA topography, covers an area of 0.2 km² (Figure 2b). The Cape Lamb Member (CLM) mudstones to sandstones of the Snow Hill Island Formation (Crame et al., 2004) form the basement of Lake Esmeralda and most of its catchment. Lake Esmeralda is located beneath the Neogene to Quaternary cliffs of the JRI Volcanic Group (JRIVG, Figure 2c; Smellie et al., 2013). Hyaloclastite breccia and basalt boulders are mantling the slopes above the present lake catchment. Above the upper reaches of the catchment there is probably a narrow band of Sandwich Bluff Member (SBM) strata of the López de Bertodano Formation sedimentary rocks (Marenssi et al., 2001). Several deep gullies, terminated by alluvial fans, occupy the eastern slopes of the catchment (during our visits the gullies were always dry). Numerous ephemeral streams (active during melt season or after rains) descend westward from the Leal Bluff slopes, but the direction of their flow is deflected towards north-west and south-west before they reach the catchment (Figure 2b). The flat, lowest-lying areas of the catchment surface are covered with efflorescent salt crusts, indicating that in the past, the higher lake level reached up to an altitude of a probable outflow to the north (Lirio et al., 2007). The lake is not currently fed by glacier meltwater, making precipitation and seasonal melting of the permafrost active layer the main sources of the lake water. We expect that the depth of the active layer is similar to JRI, where a thickness of 52–64 cm was documented (Hrbáček et al., 2016b) at the Abernethy Flats site with a similar lithology. The flora is composed mainly of bryophytes and lichens, but their distribution in the catchment is limited because of the deficiency of liquid water (Robinson et al., 2003).

Sediment coring and sample preparation

A total of 18 sediment cores were collected during the 2014 field season using a manual Russian chamber corer, which allows for obtaining semi-cylindrical cores of 7 cm in diameter and 1 m in length. All cores were photographed following their retrieval. The longer cores were sectioned at 1-cm intervals in the field whereas the shorter ones were kept in the tubes and transported frozen. In this study, the longest and most studied core, ESM3, was used (Figure 1e). Sedimentary core ESM3 was recovered from the sill in the central part of the lake separating two depocentres and is composed of two individual drives with a combined length of 177 cm (joined at 77 cm depth). However, the base of lacustrine
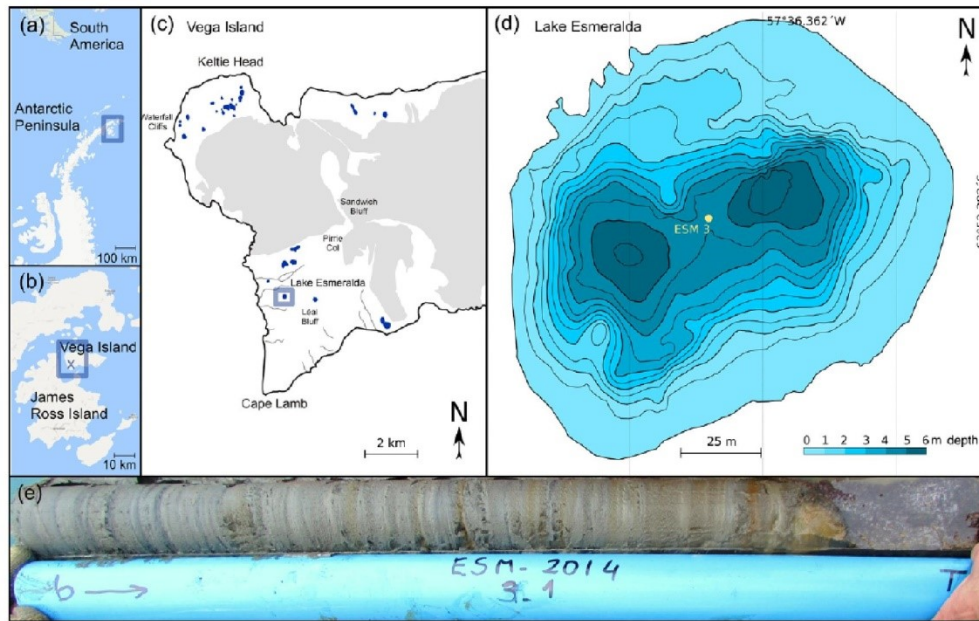
69

Figure 1. (a and b) Location of Vega Island. (c) Western part of Vega Island with highlighted ice-free areas (white), water bodies (blue) and present-day glacier extents (grey). (d) Bathymetry of Lake Esmeralda (Lirio et al., 2007 – modified). (e) Uppermost section of ESM3 core (0–77 cm).

sediments was not reached during the fieldwork, and the coring stopped at the depth of the permafrost table. This stands in contrast with the coring campaign in warmer summer of 2007, during which the whole lacustrine sequence was obtained using the same corer type, and when the coring terminated upon encountering a layer of coarse gravel, probably the underlying till, at variable depths of 190–240 cm (Irurzun et al., 2017). We perceive two main advantages of our sampling position between the two depocentres. First, it is located farther away from the 'deltaic' sedimentary environment with the possible disturbing effect of turbidites, and second, sedimentary particles from different inlets should be equally distributed because of the central position between the two depocentres. After core retrieval, the samples for optically stimulated luminescence (OSL) dating were taken at every 20 cm in conditions preventing zeroing the luminescence signal (in dark room at the Mendel Research Station). Afterwards the core was sectioned at 1-cm intervals, with the sections subsampled into halves: one-half was dried and used for inorganic analyses, while the other half was kept frozen in black Whirlpak® bags for biological analyses.

Geochronology

Three radiometric dating methods were applied to the ESM3 core including short-lived radioisotopes, radiocarbon and OSL dating:

1. The specific activity of ^{137}Cs, ^{210}Pb and ^{226}Ra was measured for the dried samples in the topmost 10 cm of the core using gamma spectroscopy in the Radiometric laboratory, Institute of Geochemistry, Mineralogy and Mineral Resources, Faculty of Science, Charles University in Prague.
2. AMS ^{14}C dating was performed in Poznań Radiocarbon Laboratory (Poland) on four samples of moss remains carefully selected and washed from the bulk sediment. Calibration of ^{14}C ages was carried out in OxCal v. 4.2.4 (Bronk Ramsey and Lee, 2013) using the SHCal13 atmospheric curve (Hogg et al., 2013) and Post-bomb atmospheric

curve of SH1-2 zone (Hua et al., 2013). Radiocarbon data are reported as conventional radiocarbon years BP (before present, i.e. CE 1950) with 1σ error, and calibrated years with 2σ (Table 1).
3. OSL dating was carried out on sediment sampled under light-protected conditions, from the interior of core samples, with a resolution of 20 cm (nine samples in total) at the Scottish Universities Environmental Research Centre (SUERC; Sanderson et al., 2017). Material was sampled and transported in dark cylindrical plastic boxes (photographic film boxes) and carefully packed in other light-protected plastic bags that were sealed up with thick silver tape. Luminescence profiling measurements were first conducted on bulk sediments using the SUERC Portable OSL instrument (Sanderson and Murphy, 2010), confirming that both IR and blue stimulation produce measurable signals. The intensities of both IR and blue (OSL) stimulated signals show local maxima at 40–60 cm and c. 140 cm depth, which may reflect changing luminescence sensitivities, dose rates or sedimentation rates with depth. Laboratory-based profiling was also conducted on separated 90–250 μm grains, with infrared stimulated luminescence (IRSL) and thermoluminescence (TL) measurements on paired poly-mineral aliquots, and OSL measurements on paired HF etched (nominally quartz) aliquots. These data were calibrated to account for sensitivity variations, and to produce equivalent dose (D_e) estimates. There were differences in sensitivity between the three readout methods, with OSL on the nominal quartz fraction showing the lowest sensitivity followed by IRSL and then TL on the poly-mineral fraction. The OSL showed some sensitivity changes across the measurement cycle, whereas IRSL and TL did not. The measurements showed dose estimates for OSL and IRSL that increase slightly with depth, with the IRSL estimates (1.5–17.0 Gy) approximately five times higher than the OSL estimates (0.5–3.4 Gy), and very large dose estimates for TL (>100 Gy) with no relationship with depth. This is consistent with experience from
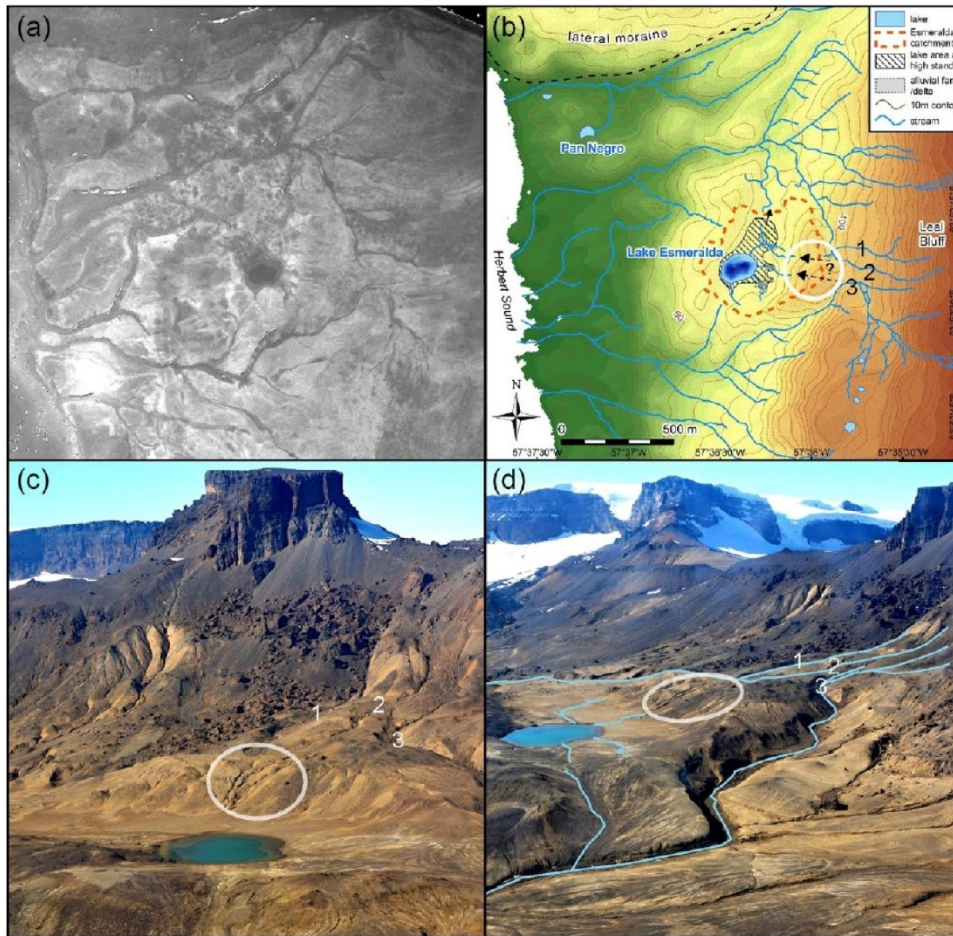
70

Figure 2. (a) Aerial orthophotograph from 1989 BAS survey showing the hydrographical network around the Lake Esmeralda area. (b) Delineated Esmeralda catchment with hatched area demonstrating our estimation of Lake Esmeralda high stand. Note the diversion of streams flowing from the Leal Bluff cliffs westwards. Contours are in 10-m intervals. REMA topographic model provided by the Byrd Polar and Climate Research Center and the Polar Geospatial Center. (c and d) Lake Esmeralda with highlighted area with main abandoned channels leading to the lake (white) and numbered possible past inlets (pictures taken during 2014 field trip).

Table 1. Results of AMS ^{14}C dating of aquatic mosses macroremains in core ESM3.

Sample	Laboratory number	Depth (cm)	mg C	Conventional ^{14}C age		Calibrated age (2σ range)	
				yr BP	± 1 σ	cal. yr BP	yr CE
ESM3/20–21	Poz-80420	20.5	0.4	101.61 pMC	0.33	–	1951–1959
ESM3/79–80	Poz-80421	79.5	0.17	1340	30	1118–1295	655–832
ESM3/122–123	Poz-80423	122.5	0.8	1445	30	1274–1354	596–676
ESM3/176–177	Poz-80424	176.5	>1	1020	30	798–934	1016–1152

other Antarctic lakes, where it is suggested that feldspars are not fully reset and carry residual IRSL and TL signals.

Based on the profiling measurements, OSL measurements on quartz were carried out for quantitative analysis of all nine samples. The samples were processed to extract 150–250 μm quartz grains, which were dispensed to 16 stainless steel discs. These were analysed using a single aliquot regenerative (SAR) approach to determine the stored dose for each aliquot, with the mean estimate most closely matching the centre of the major peak of dose distribution has been selected. Weighted or robust mean of all the aliquots that satisfied SAR quality checks combined with the dose rate used to determine the age of each sample. Measurements

were conducted using a Risø DA-15 automatic reader equipped with a 90Sr/90Y β-source for irradiation, blue LEDs emitting around 470 nm and infrared (laser) diodes emitting around 830 nm for optical stimulation, and a U340 detection filter pack to detect in the region 270–380 nm, while cutting out stimulating light (Bøtter -Jensen et al., 2000). Dose rates were measured using thick source beta counting (Sanderson, 1988) and high-resolution gamma spectrometry (HRGS), with the total dose rate determined from a combination of these measurements and a calculated cosmic dose rate. A Bayesian-based age-depth model using Markov Chain Monte Carlo techniques was constructed in the *Bacon* script for R (Blaauw and Christen, 2011; R Core Team, 2014).

Physical and chemical analyses

The following physical properties of the samples were analysed: grain size, magnetic susceptibility (MS), cation exchange capacity (CEC), elemental composition using x-ray fluorescence (XRF), mineral composition via x-ray diffraction (XRD) and geochemical composition: total organic carbon (TOC), total inorganic carbon (TIC) and total sulphur (TS). These methods were applied using 1-cm resolution (177 samples) unless otherwise stated in the methods description.

Measurement of magnetic properties of individual samples was performed on the multi-frequency Kappabridge MFK1-FA (AGICO Inc.) at the Department of Geography, Masaryk University, Brno. Mass-specific MS (χ) was measured at frequencies of 976, 3 904 and 15 616 Hz with induced magnetic field of 200 mA. Samples were measured in their original wet condition.

Grain size analysis was conducted using a CILAS 1064 laser granulometer at the Institute of Geology of the Czech Academy of Sciences in Prague. In all, 90 samples of air-dried sediments were disaggregated in water and underwent a chemical procedure consisting of three leaching steps: (1) 15 mL 10% KOH, (2) 15 mL 35% HCl and (3) removal of organic matter by H_2O_2 accompanied by gentle warming at 40°C until effervescence stopped. Each leaching step was followed by centrifugation and removing the supernatant. For grain-size parameter calculation, the Gradistat software (Blott and Pye, 2001) was used.

For determination of CEC, a Cu-trien method was used as described in Grygar et al. (2007, 2009). Before any treatment, all 90 samples were dried, homogenized and manually powdered. About 250 mg of sample was resuspended in 5 mL of water before the addition of 5 mL of 9 mM solution of Cu(trien)SO_4 (trien = 1,4,7,10-tetraazadecane). Cu^{2+} ions replace exchangeable cations in the expandable structures. Cu and Mg concentration was determined by atomic absorption spectroscopy and Ca by atomic emission spectroscopy using AAS3 spectrometer (Zeiss Jena, Germany).

XRF analyses were conducted at the Department of Geological Sciences, Masaryk University, Brno, using the Innov-X DELTA PREMIUM hand analyser. We acquired relative shares of the following elements: Al, Si, S, Cl, K, Ca, Ti, V, Cr, Mn, Fe, Ni, Cu, Zn, As, Rb, Sr, Zr, Pb, Th and light elements (LE) for all the ESM3 samples.

TOC, TIC and TS values were carried out at the Laboratories of the Czech Geological Survey in Brno on ELTRA Metalyt-CS-1000S analyser equipped with infrared detection. All laboratory measurements were conducted under the strict accredited procedure (SOP-HC). To achieve the highest accuracy and representativeness of the results, all samples were homogenized before measurement. They were dried, and mill- grounded, so only bulk (homogenized) material could be extracted. After calibration and a 'blank test', when steadiness of the analyser is examined, TC and TS content of all primary sample weights were measured, using thermal combustion (1350°C). The exact amount of material loss was measured via infrared detection. Secondary weight samples were measured to determine the amount of TIC using H_3PO_4 (1:1). Emitted CO_2, attributed to TIC was then detected by the detector, whereas TOC component was calculated by subtracting TIC from TC. TS and TIC values are in most of the ESM3 samples below the detection limit (<0.05%).

XRD analysis was undertaken at the Institute of Inorganic Chemistry of the Czech Academy of Sciences (CAS) in Řež, Czech Republic. Two types of samples were prepared – first, the powdered samples were used to produce general information about present mineral phases; second, oriented samples were prepared from suspension to describe the clay fraction in detail. Powdered samples were mounted to sample holders using the side-loading technique in order to minimize the preferred orientation of clay minerals. Diffraction patterns were collected with a PANalytical X'Pert PRO diffractometer equipped with a conventional x-ray tube (CoKα radiation, 40 kV, 30 mA, line focus) and a multichannel detector X'Celerator with an anti-scatter shield. X-ray patterns were measured in the range of 4–100° 2 Θ. Oriented specimens were prepared as air-dried layers of the upper part of water suspensions deposited on glass sample holders. Glycolated specimens were prepared by heating air-dried specimens at 70°C for 5 h in an atmosphere of ethylene glycol vapour. Samples were analysed immediately after drying or glycolation, respectively. X-ray patterns were measured in the range of 2.5–40° 2 Θ. In all, 10 samples were evaluated qualitatively while 2 of them were also evaluated quantitatively.

Biological analyses

Analysis of biological remains included sedimentary pigment analysis, diatom assemblages and characterization of faunal remains.

Photosynthetic pigments were extracted from the ESM3 core (the whole core at 10 cm resolution and the top 50 cm at 1 cm resolution). In total, 64 samples were analysed at ISE Instituto per lo Studio degli Ecosistemi, Verbania Pallanza, Italy. The samples were kept overnight under nitrogen, from about 1 g of fresh sediments using a solution of acetone (90%). Samples were then centrifuged at ca. 2700 g for 10 min and filtered through a 0.45 μm pore size filter. The total carotenoids (TCA), and chlorophyll derivatives (CD) were then quantified from the extract via spectrophotometry (as described by Guilizzoni et al. (2011) using a UV-VIS spectrophotometer (UV mc2, SAFAS). The acetone extract was used for determination of the specific algal pigment by high-pressure liquid chromatography (HPLC). The HPLC consisted in a quaternary pump, an autosampler and a DAD detector (Ultimate, Thermo Fisher) and the chromatography elution programme was the same as described in Lami et al. (2009). Individual pigments were identified and quantified using external standards, and sedimentary pigment concentrations were reported relative to the organic matter content of the sediment.

Samples for diatom analyses were oven-dried for 24 h at 50°C, and only 1 g of dry sediment was used for further sample preparation. Samples were later prepared following the method described in Van der Werff (1955). Small parts of the samples were cleaned by adding 37% H_2O_2 and heated to 80°C for about 1 h, followed by the addition of $KMnO_4$. After digestion and centrifugation (3 × 10 min at 3700 × g), the material was diluted with distilled water to avoid excessive concentrations of diatom valves and to unify sample volumes. From each sample, 50 μL was mixed with 50 μL of a sonicated (10 min) microsphere solution (6792.4 MS/μL) and 400 μL of distilled water and permanently mounted onto slides with Naphrax® medium. Samples and slides are stored at the Department of Ecology at Charles University, Prague, Czech Republic. In each sample, 400 valves were enumerated on random transects at 1000× magnification under oil immersion using an Olympus BX43 microscope, equipped with Nomarski Contrast and Olympus DP27 camera using the cellSens Entry Imaging Software. When necessary for detailed taxonomical analyses, scanning electron microscopy (SEM) was applied. Part of the suspension was filtered through polycarbonate membrane filters with a pore diameter of 1 μm, pieces of which were fixed on aluminium stubs after air-drying. The stubs were sputtered-coated with 20 nm of Pt–Pd and studied in SEM at 3 kV. Terminology is based mainly on Hendey (1964), Ross et al. (1979) and Round et al. (1990). Zidarová et al. (2016) was used as a main source of taxonomic identification. In each analysed layer, diatom productivity (number of valves per gram of sediment) was calculated as

$$\text{Productivity}\left(\frac{\text{diatom valves}}{[\text{g}]\,\text{dry material}}\right) = \frac{\dfrac{\text{counted diatom valves*}}{\dfrac{\text{added microspheres}}{\text{counted microspheres}}}}{[\text{g}]\,\text{dry material}}$$

Below 25 cm depth, the sediment core did not contain a sufficient amount of diatom valves for quantification, or no valves were present at all. Therefore, the ESM3 core was analysed for diatom assemblages only in the uppermost 25 cm, resulting in 24 continuous sample counts. Diatom species counts were transformed to relative abundances (% of total diatom valves per sample), and species richness, Shannon diversity (Shannon and Weaver, 1949) and evenness (Pielou, 1966) were calculated. Clusters were identified and divided using stratigraphically constrained cluster analysis (CONISS) on only those species present at >1% in any single sample or with more than two occurrences using the *rioja* package (Juggins, 2017) in the R software (R Core Team, 2014). Significant divisions were determined using a broken stick model, which compares a CONISS distance matrix with a random model (Bennett, 1996).

Six 1-cm layers of the ESM3 core were analysed (0–1, 5–6, 10–11, 15–16, 70–71 and 80–81 cm) to evaluate faunal remains in layers with and without diatoms. Preparation of samples for faunal analyses followed a protocol modified from Pražáková et al. (2006). Wet samples were oven-dried for 5 h at 95°C. Part of the sample (about 1 g dry weight) was then digested in hot 10% KOH on magnetic stirrer for 30 min. Digested samples were passed through a 40 μm phosphor bronze screen and washed with distilled water. Particles remaining on the screen were transferred into 50 mL of water and stained by safranin (Szeroczynska and Sarmaja-Korjonen, 2007). At least 5 mL of each sample was examined under Nikon Eclipse 300 microscope equipped with Canon EOS 650D camera. Faunal microfossils of tardigrades (eggs), rotifers (loricae) and crustaceans (spermatophores) were counted as a number of remains per gram of dry weight.

Results

Chronology

In total, four radiocarbon ages were obtained from carefully selected macroremains of aquatic mosses (Table 1). The lowermost sample exhibits an age reversal in respect to the two middle samples. The topmost ^{14}C sample exhibits modern carbon content, suggesting a very young age of the core top or contamination by modern organic material during coring. The specific activity of ^{137}Cs, ^{210}Pb and ^{226}Ra radioisotopes in the topmost 10 cm of ESM3 was below the limits of detection, and therefore not suitable for age-depth modelling.

The equivalent dose D_e values calculated from the SAR-OSL measurements of quartz grains are largely consistent with the estimates from the OSL profiling. On average, 60% of discs produced a usable OSL signal and passed the bleaching validity tests with recycling ratios 0.92–1. These D_e have been used with the measured dose rates (on average 3.44 ± 0.13 mGy yr^{-1} throughout the core) to calculate apparent ages (Table 2). These ages range from 0.1 to 0.5 ka, with mean age of ~0.3 ka, and show a general increase with depth. The samples SUTL 2959/3 and 2959/7 at 54.5 and 132.5 cm, respectively, deviate most substantially from the general linear trend of other OSL ages. The OSL ages are ~600–1000 years younger than radiocarbon ages except for the topmost post-bomb age, where the OSL age is about 200 years older than the corresponding depth.

Physical properties of sediment

The ESM3 sediment is a grey to greenish-grey silt with numerous dark, light and rusty laminae of different thicknesses (Figures 3 and 4)

Table 2. Summary results of dose rates and SAR-OSL equivalent dose (D_e) estimation.

SUTL Lab No.	Depth (cm)	Assumed saturated water content[a] (%)	Equivalent concentration[b]			Effective dose rate (mGy yr^{-1})			SAR-OSL			Apparent age[f]
			K/%	U/ppm	Th/ppm	Beta[c]	Gamma[d]	Total[e]	No. of discs	Recycle ratio	D_e (Gy)	
2959/1	15.5	17 ± 5	2.34 ± 0.24	2.97 ± 0.29	12.1 ± 0.8	2.32 ± 0.14	1.32 ± 0.07	3.81 ± 0.15	8	0.978 ± 0.081	0.97 ± 0.17	250 ± 50
2959/2	35.5	21 ± 5	2.37 ± 0.23	3.35 ± 0.29	12.7 ± 0.7	2.09 ± 0.12	1.23 ± 0.07	3.50 ± 0.14	11	0.924 ± 0.066	1.11 ± 0.25	320 ± 70
2959/3	54.5	21 ± 5	2.22 ± 0.24	2.47 ± 0.29	11.9 ± 0.7	1.96 ± 0.11	1.25 ± 0.07	3.37 ± 0.13	9	0.975 ± 0.049	0.42 ± 0.10	120 ± 30
2959/4	74.5	21 ± 5	2.51 ± 0.22	2.79 ± 0.29	12.7 ± 0.7	1.78 ± 0.11	1.28 ± 0.07	3.23 ± 0.13	7	0.989 ± 0.043	1.14 ± 0.12	350 ± 40
2959/5	92.5	25 ± 5	2.35 ± 0.27	3.60 ± 0.41	14.5 ± 1.1	1.99 ± 0.12	1.30 ± 0.07	3.46 ± 0.14	10	0.946 ± 0.033	1.17 ± 0.09	340 ± 30
2959/6	111.5	23 ± 5	2.78 ± 0.21	3.64 ± 0.34	11.5 ± 0.7	2.01 ± 0.11	1.34 ± 0.07	3.50 ± 0.13	14	0.934 ± 0.027	2.31 ± 0.11	370 ± 30
2959/7	132.5	26 ± 5	2.32 ± 0.23	3.75 ± 0.32	12.4 ± 0.8	1.90 ± 0.11	1.30 ± 0.07	3.36 ± 0.13	10	0.923 ± 0.030	1.70 ± 0.67	510 ± 200
2959/8	151.5	25 ± 5	2.22 ± 0.27	4.13 ± 0.41	14.0 ± 1.1	1.96 ± 0.12	1.32 ± 0.07	3.44 ± 0.14	9	0.972 ± 0.036	1.17 ± 0.15	340 ± 50
2959/9	171.5	31 ± 5	2.17 ± 0.27	4.01 ± 0.42	14.1 ± 1.1	1.83 ± 0.10	1.28 ± 0.06	3.27 ± 0.12	12	1.003 ± 0.034	1.17 ± 0.1	400 ± 30

[a] Water content measurement of the dated samples was considered unreliable because of prolonged sediment storage and possible drying. Splined water content measured on parallel samples of ESM3 was used instead.
[b] Determined by HRGS (conversion factors based on NEA (2000) decay constants); ^{40}K: 309.3 Bq kg^{-1} % K^{-1}, ^{238}U: 12.35 Bq kg^{-1} ppm U^{-1}, ^{232}Th: 4.057 Bq kg^{-1} ppm Th^{-1}.
[c] Effective beta dose rate combining water content corrections with inverse grain-size attenuation factors obtained by weighting the 150–250 μm attenuation factors of Mejdahl (1979) for K, U and Th by the relative beta dose contributions for each source determined by gamma spectrometry.
[d] Mean of sample and neighbouring samples from HRGS with water content corrections.
[e] Includes a cosmic dose contribution.
[f] Rounded to the nearest decade.
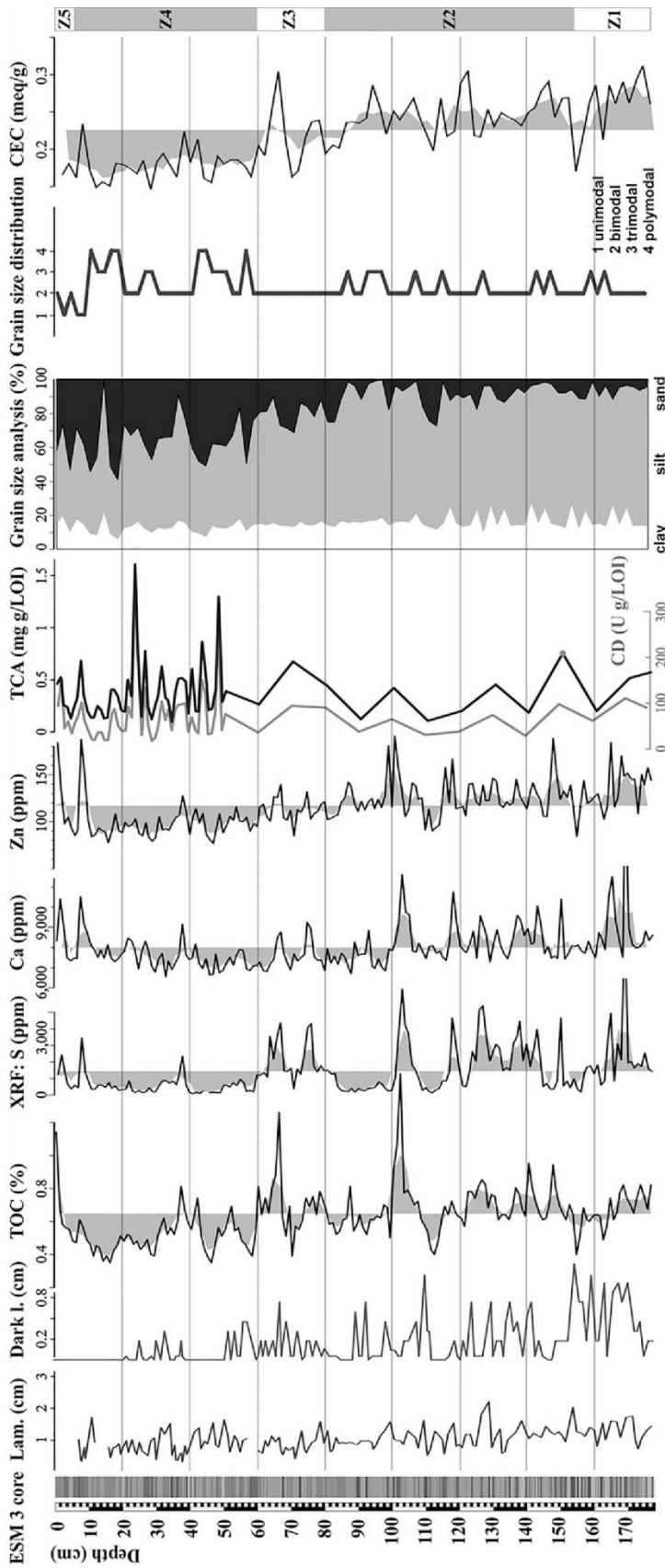
Figure 3. Lithology of ESM3 with lamination thickness (Lam.) and thickness of dark organic laminae (left); biological indicators: total organic carbon (TOC, %), shares of S, Ca and Z (ppm), chlorophyll derivatives (CD, U g/LOI), total carotenoids (TCA, mg g/LOI); relative content of grain-size fractions (%) – clay (white), silt (grey), sand (black), together with grain size distribution; cation exchange capacity (CEC, meq/g) (right). In the case of TOC, S, Ca, Zn and CEC grey areas represents the deviations from mean value and 5-spline of the measured values (black line). The last column shows zones of environmental changes.
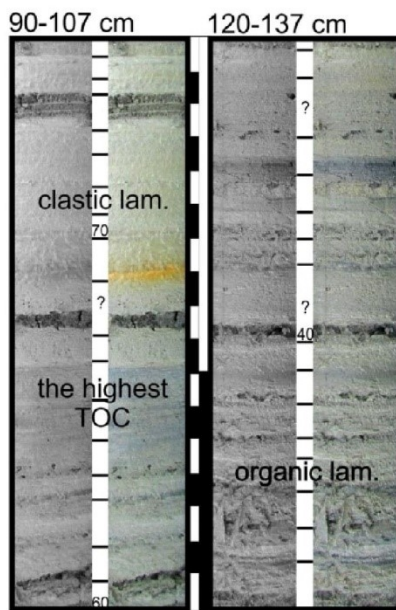
Figure 4. Details of different lamination patterns of two parts (both in greyscale and colour) of ESM3 core with emphasis to the highest TOC values, organic and clastic laminae. The boundaries of the varve-like laminae are marked with black lines in between the greyscale and colour image. Scale in the middle part of the figure is in centimetres.

most commonly with a sharp transition. Parts of the sediment are rich in moss macroremains. Regrettably, core ESM3 was not subjected to laminae counting before sub-sampling, therefore we performed macroscopic counting of laminae from field photographs of the whole core and estimated their thickness. Lamination (Figure 4) shows a rather complex pattern of transition between dark, presumably organic, and lighter, presumably minerogenic, layers, occasionally interspersed with a thin light layer, forming triplets. Often the lamination is manifested by grain-size changes only, with darker coarse-grained basal lamina grading to lighter fine-grained top lamina. The dark layers were often missing, and especially in the topmost 51 couplets, dark layers are scarce and indistinct. Therefore, we classify the lamination as a transitional type between clastic and organic varve-like laminae, following the definition of Birks et al. (2014). The thickness of the couplets is slightly decreasing towards the top of the core (Figure 3) and varies from 0.33 to 2.2 cm with median of 1 cm. We counted 175 couplets. However, we take this count as an estimation of the total number of laminae because the real number could be higher if more detailed photo-documentation were available, or the whole core preserved. Further research is needed on other cores to fully interpret the lamination pattern.

The MS values are displayed in Figure 5. MS does not show a significant correlation with Fe or other metal elements, except for Zr (R = 0.54; Table 3). Frequency-dependent MS (MS_{FD}) is highly variable throughout the profile. The splined MS_{FD} forms four cyclic intervals oscillating between 2% and 6% with interval frequency decreasing towards the top of the core.

TOC values in the ESM3 range between 0.35% and 1.49% with the average value 0.64%, exceeding 1% in only four samples. TIC (not displayed) were below the detection limit and therefore all measured carbon was classified as organic. The core section of higher TOC lies between 115 and 150 cm and the section far below the average values is from 5 to 60 cm with just a few samples reaching the average (Figure 3). Between these two

sections, values are generally around average with the exception of two major sharp peaks of the highest TOC values (98, 66 cm). TS results (not displayed) are in good agreement with sulphur concentrations from XRF, which are plotted in Figure 3. Its values vary from 0% to 0.5% and copy the trend of the TOC curve. The C/N ratio always has a value below 10, and only around 70 cm sediment depths is there a slight increase. CEC (Figure 3) ranges from 15 to 31 meq/100. The exchange complex was mostly occupied by Ca^{2+} and Mg^2.

Most of the ESM3 core is dominated by a silt fraction (Figure 3), ranging from 35% to 85% with a mean value of 65%, and linearly distributed among very fine to coarse silt. The clay fraction shows only minor variability within the core with an average of 9%, and ranging from 4% to 17% (Figure 3). The sand fraction has relatively low values from 178 cm up to 84 cm with 8% on average. However, at the topmost 84 cm of the core, the sand fraction is continuously increasing, and in some parts, exceeds 50%; the sand fraction's average share in this part is 32%. The higher volume of the sand fraction is accompanied by LE and Cl enrichment (Figure 3).

Elemental and mineral composition

The shares of main elements are displayed in Figures 3 and 5. Si, Fe, K, Cl, Al, Ca, Ti and S were the most common elements detected in ESM3, besides the unspecified LE. Correlation among elements for ESM3 (Table 3) shows the following elemental associations: Al + Si (R = 0.96), As + Fe (R = 0.89), Rb + Pb + Sr (R > 0.86). We also found significant positive correlation among K and Si as well as Al. No element was strongly positively correlated with Cl; the highest correlation coefficient was R = 0.37 for LE. However, 17 elements correlated negatively with Cl, some strongly (Table 3). All S peaks in the ESM3 core are accompanied with Ca. Principal component analysis (PCA; Figure 6) gave us three groups of elements: (1) Si, Al and K representing the main lithogenic allochthonous group. The period of the highest shares of these elements has an abrupt beginning at 153 cm and with minor changes lasts up to 88 cm. In the top 88 cm there are two other periods with high values, but not that high as in the previous case; the periods are centred at 53 and 30 cm, respectively, and lasts 12–14 cm. Minimum shares of lithogenic elements are at 20. 43, 79 and 169 cm; (2) S, Ca, and Zn together with TOC forming autochthonous group with at least 13 discrete peaks and (3) minor elements and metals, mainly Rb, Sr, Fe, As and Mn. As has only one peak at 100–94 cm, similar to Fe, which has the highest shares between 100 and 87 cm. Cl and Zr are isolated in the PCA (Figure 6) and enriched in the sand fraction. Si, Al and other lithogenic elements are inversely correlated with LE.

The ESM3 sediment consists of the following minerals: quartz and feldspars (microcline and albite), mica (illite), clinoptilolite, hornblende, smectite, and vermiculite or chlorite. The mineral composition shows little variability along the core, even the diffractograms of rusty laminae with high Fe shares detected by XRF contains the same mineral mixture (goethite or other Fe-weathering products were not detected). Smectites or interlayered illite/smectite represents the most important share of the minerogenic material (32–33%), second is quartz (26–30%), third is mainly composed of feldspars: albite (6–14%) and microcline (7–13%) and the rest is distributed among other minerals: illite (4–7%), chlorite (4–5%) and kaolinite (1–4%). The mineral analysis revealed that there are more possible sources of expandable material that can be responsible for the CEC. Apart from the expected and most common smectites, zeolites and vermiculite are also present. Although the CEC curve (Figure 3) represents changes in the total amount of all these minerals, the volume of smectite is so high that others can be neglected.
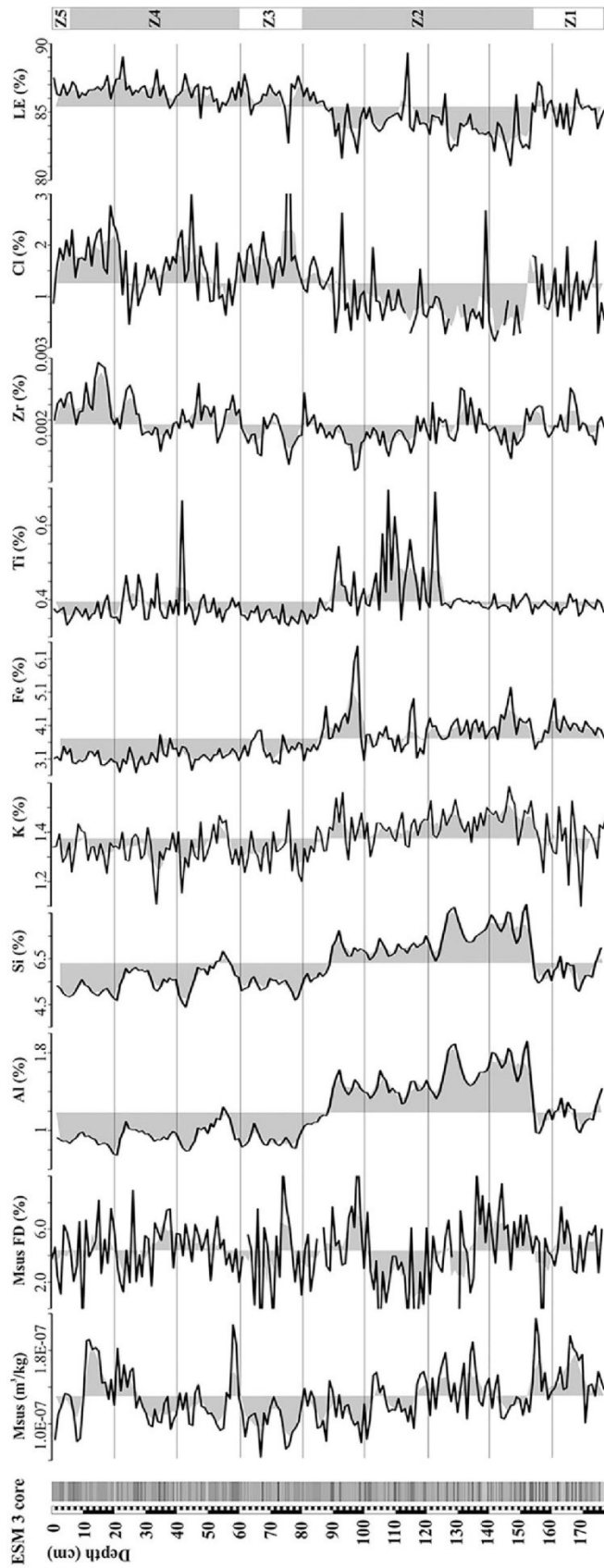
Figure 5. Lithology of ESM3 (left), magnetic susceptibility (Msus and Msus FD), shares of the following elements (%): Al, Si, K, Fe, Ti, Zr, Cl and light elements (LE). Grey areas represent deviations from mean value and 5-spline of the measured values (black line). The last column shows zones of environmental changes.

76

Table 3. Correlation coefficients for individual elements, total organic carbon (TOC), and magnetic susceptibility (MS).

	Si	S	Cl	K	Ca	Ti	V	Cr	Mn	Fe	Ni	Cu	Zn	As	Rb	Sr	Zr	Pb	Th	LE	TOC	MS FI
Al	**0.96**	0.20	−0.69	**0.75**	0.19	0.32	0.51	0.46	0.40	0.63	0.58	**0.66**	0.38	0.47	**0.68**	**0.70**	−0.29	**0.65**	−0.07	**−0.85**	0.31	0.05
Si	Si	0.13	−0.65	**0.82**	0.14	0.22	0.44	0.36	0.32	0.49	0.53	0.55	0.24	0.36	0.58	0.60	−0.22	0.52	−0.09	**−0.83**	0.19	0.06
S	x	S	−0.10	−0.02	**0.80**	−0.09	0.34	0.30	0.20	0.17	0.39	0.33	0.42	0.07	0.24	0.22	−0.20	0.33	0.07	−0.28	0.60	0.06
Cl	x	x	Cl	−0.31	−0.09	−0.27	−0.49	−0.33	−0.37	−0.44	−0.41	−0.56	−0.31	−0.34	**−0.66**	**−0.67**	0.12	−0.54	0.16	0.37	−0.21	−0.11
K	x	x	x	K	0.10	0.09	0.28	0.16	0.18	0.37	0.38	0.41	0.20	0.25	0.41	0.42	−0.18	0.38	0.08	**−0.76**	0.10	0.03
Ca	x	x	x	x	Ca	0.01	0.22	0.19	0.12	0.10	0.38	0.26	0.41	0.04	0.16	0.18	−0.05	0.22	0.12	−0.26	0.40	0.16
Ti	x	x	x	x	x	Ti	−0.09	0.27	0.17	0.19	0.10	0.18	0.11	0.14	0.23	0.22	−0.12	0.17	−0.04	−0.20	0.06	0.00
V	x	x	x	x	x	x	V	0.46	0.53	0.56	0.55	**0.73**	0.55	0.34	**0.73**	**0.70**	−0.26	**0.74**	−0.20	−0.50	0.45	0.04
Cr	x	x	x	x	x	x	x	Cr	0.43	0.33	0.57	0.55	0.30	0.16	0.44	0.44	−0.17	0.45	−0.33	−0.37	0.33	0.05
Mn	x	x	x	x	x	x	x	x	Mn	0.45	0.36	0.49	0.47	0.30	**0.65**	0.63	−0.18	0.53	−0.06	−0.39	0.34	0.00
Fe	x	x	x	x	x	x	x	x	x	Fe	0.39	**0.73**	0.47	**0.89**	**0.74**	**0.78**	−0.47	**0.80**	0.04	**−0.69**	0.38	0.00
Ni	x	x	x	x	x	x	x	x	x	x	Ni	0.56	0.38	0.24	0.44	0.48	−0.10	0.49	−0.26	−0.52	0.42	0.13
Cu	x	x	x	x	x	x	x	x	x	x	x	Cu	0.61	0.53	**0.78**	**0.80**	−0.36	**0.80**	−0.13	−0.63	0.48	0.04
Zn	x	x	x	x	x	x	x	x	x	x	x	x	Zn	0.38	**0.67**	**0.66**	−0.33	**0.68**	0.14	−0.39	**0.68**	−0.19
As	x	x	x	x	x	x	x	x	x	x	x	x	x	As	0.55	0.62	−0.36	0.57	0.17	−0.54	0.28	−0.05
Rb	x	x	x	x	x	x	x	x	x	x	x	x	x	x	Rb	**0.92**	−0.36	**0.87**	0.04	−0.62	0.46	−0.12
Sr	x	x	x	x	x	x	x	x	x	x	x	x	x	x	x	Sr	−0.34	**0.86**	0.03	−0.64	0.44	0.00
Zr	x	x	x	x	x	x	x	x	x	x	x	x	x	x	x	x	Zr	−0.47	0.05	0.36	−0.42	0.53
Pb	x	x	x	x	x	x	x	x	x	x	x	x	x	x	x	x	x	Pb	0.05	−0.65	0.57	−0.14
Th	x	x	x	x	x	x	x	x	x	x	x	x	x	x	x	x	x	x	Th	0.00	0.16	0.02
LE	x	x	x	x	x	x	x	x	x	x	x	x	x	x	x	x	x	x	x	LE	−0.35	0.01

Correlations > 0.65 are bold and negative correlations are in white.

Pigments. Plots of CD and carotenoid concentrations (TCA) (Figure 7) show a similar trend, suggesting that the whole oxygenic photoautotrophic community responded in a similar manner to changes in the environment. TCA and CD shows mean value around 80 U g/LOI and 0.5 mg g/LOI, respectively. The two proxies showed two abrupt peaks at 24 and 49 cm and other high values at 7.5, 26.5 and 43.5 cm. The ratio 430:410, an index of pigment preservation (Lami et al., 2009), shows a rather constant profile with a value around 0.8, suggesting good preservation. There are a few exceptions with values rather low (ca. 0.6) at 4.5, 35, 90, 110, and 160 cm depth, which might indicate a preservation problem. The ratio also shows rather high values at the same horizons, where high values for CD and TCA are observed (24 and 49 cm), suggesting better preservation because of the fact that the pigment originates from aquatic mosses with a thicker cell wall compared with algae.

Several common taxon-specific pigments have been identified in the ESM3 core, and they have been associated with their respective taxa according to Guilizzoni and Lami (2003). The most abundant carotenoids are those associated with green algae or mosses (lutein and chlorophyll *b*) and they show a profile similar to the total pigment, with rather stable values and some abrupt peaks at 24 and 49 cm. Specific pigments of diatoms (diatoxanthin and diadinoxanthin) as well as Dinophyta (dinoxanthin), and zeaxanthin associated with benthic cyanobacteria show the same kind of profile with high values at 7.5, 16, 24, 43 and 49 cm (Figure 7). This suggests that these taxa are dominated by epiphytic taxa associated with aquatic mosses. Echinenone (Cyanobacteria) and alloxanthin (Cryptophyta) do not show such evident increases, but the profile is more fluctuating around 40 and 83 nMol g LOI^{-1}, respectively. The ratio of alloxanthin to diatoxanthin shows rather constant values with a significant decrease at 80 cm and frequent oscillations in the top 50 cm of the core. The UV index based on the ratio between scytonemin and algal carotenoids shows the highest value at the top of the sediment core and sub-maxima at ca. 25 cm.

Diatom abundance and assemblage structure

For the Maritime Antarctic region, a diverse flora of 86 taxa was observed in the Lake Esmeralda sediment core. However, there were no distinct arrivals or disappearances in the section analysed, but changes in the relative abundances occurred (Figure 8). The number of species in the first 24 counted samples varied between 30 and 47 with an average of 42 species per sample, but with no significant distribution increases or decreases over the topmost 25 cm of the core. The most abundant species was *Microcostatus austroshetlandicus*, representing 21% of all valves counted, followed by *Nitzschia kleinteichiana* (10%), *Psammothidium papilio* (6%) and *Pinnularia magnifica* (5%). The most species-rich genera were *Luticola* with 12 species, followed by *Pinnularia* and *Psammothidium* with 9 species, *Navicula* with 8 species and *Humidophila* with 7 species. Species richness values were greatest at depths of 8–9, 16–17 and 19–20 cm, and were lowest at the depth of 7–8 cm. Shannon diversity values fluctuated between 2.39 and 3.26 with an average value of 2.97, and evenness values ranged from 0.64 to 0.88 with an average of 0.8.

Faunal microfossils

The remains of only three animal species were encountered; spermatophores of the calanoid copepod *Boeckella poppei*, eggs of the freshwater tardigrade *Dactylobiotus* cf. *ambiguus* and loricae
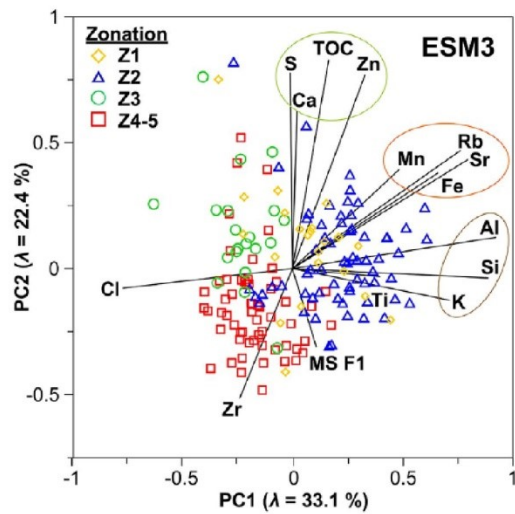
Figure 6. Principal component analysis for selected elements, TOC and MS. The first two principal components explain 33.1% and 22.4% of the total variability, respectively. PCA scores of individual samples are plotted according to their zonation using colour symbols. Three main element groups are circled.

of the rotifer *Notholca* sp. *Boeckella poppei* was present only in the uppermost part (i.e. 0–1 cm) of the core (30 spermatophores/g), where also a peak in abundance of *Notholca* sp. (80 loricae/g) was detected. In contrast *Dactylobiotus* cf. *ambiguus* was most abundant (35 eggs/g) at 70–71 cm depth, where no diatom remains were found.

Discussion

Geochronology

Radiocarbon dating of lake sediments in the AP region, and Antarctica in general, often yields ages that are too high (Hjort et al., 1997), as a result of a combination of different effects such as the input of ^{14}C-depleted carbon derived from glacial and permafrost meltwater or bedrock, contamination by marine reservoirs, restricted gaseous exchange because of prolonged periods of ice cover and disturbance of sediments by bottom-freezing or desiccation (Björck et al., 1991b). Furthermore, the apparent ages of the topmost sediments may be influenced by other factors, including the mixing of sediments because of bioturbation, resuspension of sediments by wind-driven circulation and waves, and possible loss of surface material during the core recovery (Moreton et al., 2004). Establishing a reliable chronology thus calls for application of multiple dating methods to cross-validate the results (Oliva et al., 2016; Roberts et al., 2009), and to obviate the inherent problems of these methods, including the reservoir effect of ^{14}C dating (Björck et al., 1991b) or incomplete bleaching in OSL dating (Berger et al., 2010; Roberts et al., 2009).

Irurzun et al. (2013, 2017) established a chronology of Lake Esmeralda sediments from core ESM6. It should be mentioned that their coring in a warmer austral summer (2007) allowed for the retrieval of a complete package of lacustrine deposits (Irurzun et al., 2017). The difference of the penetrating depth between the ESM3 core (this study) and ESM6 (Irurzun et al., 2017) is ~0.6 m. However, as could be seen on the photograph of the ESM6 core, it continues down with the same thickness as individual laminae. Their age-depth model, based on two ^{14}C ages from the bulk sediment (10,982 ± 129 cal. yr BP at 121 cm and 14,286 ± 279 cal. yr BP at 222.5 cm depth) and correlation of relative palaeomagnetic intensity curves, assumes the age of 10.2 k BP for the basal

sediment of their 2.4-m long record. Based on the ESM6 age-depth model (Irurzun et al., 2013, 2017), we expected that the ESM3 core would span at least the last 6 k or most of the Holocene, but our radiocarbon and OSL ages suggest otherwise. The coring site of Irurzun et al. (2017) was located in the lake depocentre and ~20 m east from ESM3 drilling site (located on a slightly elevated sill), we consider the depositional environments comparable and expect that the sedimentation covers approximately the same time period. Irurzun et al. (2017) also estimated a radiocarbon reservoir effect of ~5200 ± 300 years for Lake Esmeralda, and the authors state that their record captures the lake formation following the last deglaciation at the Pleistocene/Holocene transition.

In our study, radiocarbon ages of macroremains suggest the sediment is less than ~1.5 ka old, while OSL data yield apparent ages of 0.3–0.4 ka, which together implies a much younger age than the previous studies proposed by Irurzun et al. (2013, 2017) We acknowledge the discrepancy between the OSL and ^{14}C ages (~600–1000 years difference) and several reversals of the radiometric ages that complicate the age-depth modelling, yet we argue our results are more representative of the true/actual sediment age. The rationale behind relying on the ^{14}C ages from aquatic moss macroremains (the only reliably determined organic material in the sediment) rather than bulk material resides in minimizing the risks of contamination by 'old' bedrock and glacial/permafrost meltwater-derived carbon (Björck et al., 1991b). Nonetheless, the uptake of ^{14}C from the lakewater by aquatic plants does not preclude the problems posed by a possible reservoir effect, the magnitude of which can fluctuate in time depending on the environmental conditions. Despite this, several studies from the AP region successfully applied ^{14}C dating of single-species aquatic plant macroremains in carbon-poor sediments and bedrock settings (Björck et al., 1991b; Hodgson et al., 1998; Roberts et al., 2017). Given the well-preserved stratigraphic order of our core and insignificant contamination by 'old' carbon or modern vegetation (except for the topmost modern-carbon age), it seems probable that our ^{14}C ages suffer from an unspecified, very likely time-variable reservoir effect of ~600–1000 years, but which at the same time contradict the notion of the mid-Holocene age of the ESM3 core.

SAR-OSL dating, together with the single-grain OSL method, currently represents the most reliable approach for establishing the age of quartz grains (not only) in glacial sedimentary environments (Roberts et al., 2009). However, the incomplete bleaching or resetting of the luminescence signal during the transport of the mineral grains may result in preserving the residual signal from the previous depositional cycles, and yielding apparent ages that are too high (Berger et al., 2010; Hodgson et al., 2009; Roberts et al., 2009). On the other hand, stable luminescence centres of quartz minerals do not generally exhibit anomalous fading, the apparent SAR-OSL ages consisting of the heterogeneously bleached aliquots should thus be regarded as an approximation of the maximum rather than minimum ages (Roberts et al., 2009). The non-glaciated 'polar desert' environment of Cape Lamb then implies that the fluvial and aeolian activity likely represents the dominant transport pathways of quartz grains into Lake Esmeralda, offering relatively favourable conditions of zeroing the luminescence signal. Our confidence in the validity of OSL ages is further advanced by a simple linear increasing trend of sediment age with depth, as modelled in *Bacon* and covering approximately 180 years, which conspicuously corresponds to the 175–189 laminae counted in ESM3 and promotes thus the idea of annual varve formation.

Rather large standard deviations of OSL ages mean also a large 2σ confidence envelope of the Bayesian age-depth model based on the luminescence ages only (Figure 9). Bacon runs on unconstrained OSL ages, and consistently modelled a linear trend

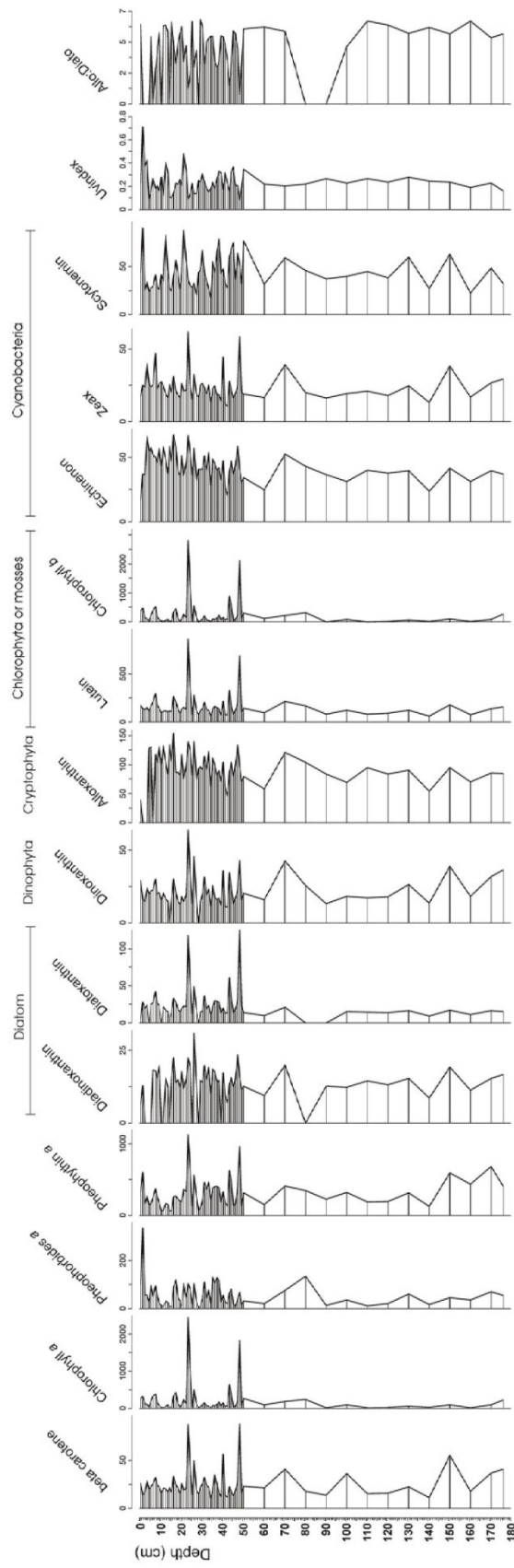**Figure 7.** Specific algal pigments from HPLC analysis; the association with taxa is based on Guilizzoni and Lami (2003), the units of x axes are nMol g/LOI.
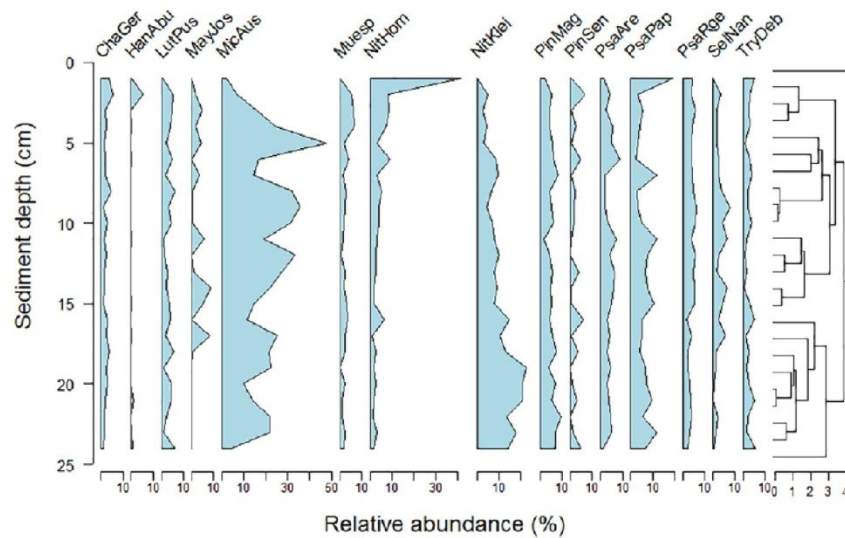
Figure 8. Relative abundance of diatom species (% of total diatom valves per sample) in the top 25 cm of the core ESM3. Clusters were identified and divided using stratigraphically constrained cluster analysis (CONISS) on only those species present at >1% in any single sample, or with more than two occurrences using the *rioja* package in R (Juggins, 2017).
ChaGer: Chamaepinnularia gerlachei; HanAbu: Hantzschia abundans; LutPus: Luticola pusilla; MayJos: Mayamaea josefelsteri; MicAus: Microcostatus austra-loshetlandicus; Muesp: Muelleria sp.1; NitHom: Nitzschia homburgiensis; NitKlei: Nitzschia kleinteichiana; PinMag: Pinnularia magnifica; PinSen: Pinnularia sensu lato; PsaAre: Psammothidium aretasii; PsaPap: Psammothidium papilio; PsaGre: Psammothidium rostrogermainii; SelNan: Sellaphora nana; TryDeb: Tryblionella debilis.

with accumulation rate of 1 cm yr⁻¹. The uncertainty, however, increases at the top of the core because of an OSL and ¹⁴C outlier, and an assumption of a modern lake bottom. Given the presumably young age of the sediment, this leaves us with a rather floating chronology, not accurately constrained on an absolute geochronological timescale. Furthermore, the extrapolation of the 'best-fit' linear model to the water-sediment interface is problematic, because this yields an age of 250 years for the core top, and suggests effectively the cessation of sediment accumulation after ~200 yr BP. On the contrary, we would have expected 'zero-age' of the modern lake bottom in concordance with the continuous sedimentation until present. We also do not consider likely more than a few centimetres of water-saturated sediment were lost from the ESM3 top during coring. Moreover, the post-bomb ¹⁴C age and the youngest OSL date at 54.5 cm depth are also in line with the lower age of the sediment. On the other hand, no specific activity of unsupported ²¹⁰Pb and ¹³⁷Cs was detected in ESM3 core top. Short-lived radioisotope chronologies were successfully constructed in the lacustrine sediments of the western AP, namely the South Shetland Islands (e.g. Roos et al., 1994; Toro et al., 2013). However, no example of this dating approach has been reported from the north-eastern AP so far, and we have also failed to detect any dateable ²¹⁰Pb and ¹³⁷Cs in Lake Esmeralda sediments. The absence of short-lived radioisotopes activity may be attributed to constricted pathways of the radioisotopes transport into the lake, either because of atmospheric circulation patterns (isolation of Antarctica and the blocking AP mountain range), or insufficient focusing effect of the small Lake Esmeralda catchment (Roos et al., 1994). Arguably, it may also mean that the water–sediment interface is not 'zero-age' and indeed is >200 years old, hence without any ²¹⁰Pb and ¹³⁷Cs activity. A mechanism explaining the old age of the top sediment might involve either a complete cessation of accumulation, or erosion by bottom-freezing (Björck et al., 1991b) or during periods of almost complete waterbody desiccation. It should be noted that the sill, where the ESM2 core was drilled, could be more vulnerable both to changes in sediment delivery as well as erosion than the neighbouring depocentres, even though these are only ~1 m deeper.
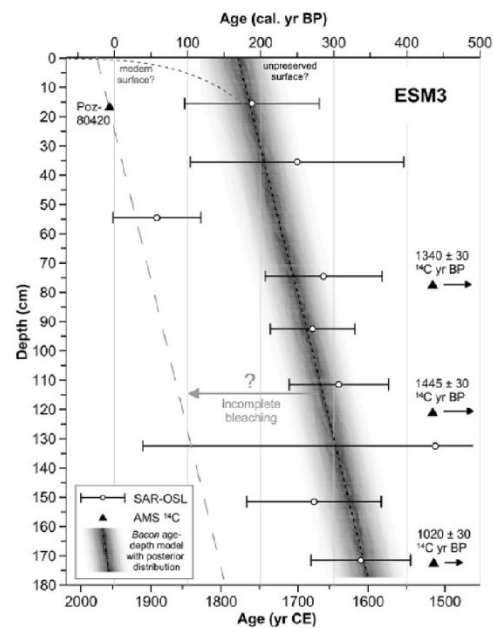
Figure 9. Age-depth model (middle line) with 2σ uncertainty envelope (95% confidence interval) based on OSL ages with plotted radiocarbon ages. Grey dashed line on left represents an alternative age model in the case of incomplete bleaching of the luminescence signal that may have occurred during relatively short transportation of sedimentary particles.

However, the bathymetry given in Figure 1d shows a rather wide shallow area in the north-eastern sector of the lake, which is connected with one of the two inflows, and we interpret it as a delta filling the northern part of the Lake Esmeralda. This stream was clearly most important for water and material input to the lake. The second inflow to the eastern coast of the lake is not connected

with any sub-aquatic sedimentary body, and was therefore less important for the material input to the lake basin.

With the newly available REMA topographic model, however, the hydrographic network in the wider catchment surroundings was analysed, which shows probable stream piracy by relatively fast headwater erosion of at least two streams (numbers 1 and 2 in Figure 2) flowing presently towards the north-west, and may be also a third (number 3 in Figure 2) heading to the south-west. On the oblique aerial images (Figure 2c and d), there are visible abandoned channels forming the connection between the lake and the upper streams supplying water and sediment to Lake Esmeralda. The lake level was much higher before the streams were captured and increased inflow water corresponded with continuous material input. The river piracy led to the cessation of the deposition in the Lake Esmeralda basin. Fluvial erosion processes are very active in the AP (Mink et al., 2014) as well as in Cape Lamb, where numerous slush flow tracks, rills and deep gullies were observed. According to the OSL dating, the capture by one, two or all the three streams may have occurred ~180 yr BP, thus decreasing sediment delivery towards the catchment and also causing a lake level drop.

The prospect of using our laminated sedimentary sequence as a basis for chronology depends on the precision of the (sometimes vaguely defined) laminae counting and on the assumption of annual formation of the lamination. Although we hypothesize that in the case of Lake Esmeralda the annual signal of permafrost active layer and snow melting/freezing exerts the strongest influence on the sediment accumulation (similar to analogical lakes in the Arctic; e.g. Cockburn and Lamoureux, 2008; Haltia-Hovi et al., 2007), we cannot provide any physical or geochemical proxy characterizing the lamination in ESM3 because of the 1-cm sampling step. Moreover, the annual formation of the laminae would be disrupted or obscured by multi-year periods of complete lake sealing by ice cover. Nevertheless, we do not intend to provide the definite varve chronology, but we rather regard the laminae count as a proxy for the minimal age of the sediment. However, we expect that further work on other cores from Lake Esmeralda can result in at least floating varve chronology.

If we accept the SAR-OSL ages as reliable and assume the annual mode of laminae formation and the 'non-zero' age of the ESM3 core top, then the mean accumulation rate of 1 cm in 1–3 years exceeds significantly that of Irurzun et al. (2017), that is, 1 cm in ~40 years. Mean sedimentation rates in lakes around the AP display large variability, with rates from ~20 years for 1 cm in Lake Boeckella (Zale, 1994), Hidden Lake and Lake Åsa (Björck et al., 1991a) to ~40 years for 1 cm in Monolith Lake (called Boulder Lake by Björck et al. (1991b). Our findings suggest the accumulation rates in Antarctic lakes can be 20–40 times higher than previously reported. We explain this extremely high accumulation rate by the position of Lake Esmeralda right under the unvegetated slopes formed by easily weathered rocks, which imply intensive geomorphological processes.

With the knowledge of the results presented here, the previously published lake chronologies (e.g. Björck et al., 1996; Hjort et al., 1997; Irurzun et al., 2017) based on radiocarbon dating may have produced significantly higher lake ages, as they were influenced by elevated radiocarbon reservoirs in their respective lake basins. The necessity to validate the radiocarbon ages by an independent dating method (such as the OSL dating) is crucial in the case of Antarctic lakes (Berger et al., 2010; Hodgson et al., 2009), for which local thawing of the ice sheet, individual glaciers and permafrost will produce a site-specific radiocarbon reservoir, which would change in time because of different mixing of older carbon from the cryosphere thawing with current precipitation. The radiocarbon reservoir has changed with respect to Holocene climate change (cf. Björck et al., 1991b; Irurzun et al., 2017). We suggest that the role of radiocarbon analyses in Antarctic lake

sediments undertaken on other material than terrestrial and in certain cases aquatic macrofossils should therefore aim to characterize the fractionation and recycling processes involving carbon containing materials and nutrients, rather than using these as a chronological method.

Changes within the lake waterbody

For formation of laminated sediment the lake must have fulfilled two conditions: (1) the water column was stratified and (2) the inflow was formed by a highly seasonal stream loaded with suspended sediment (Birks et al., 2014; Kemp et al., 1996). Two more conditions favour preservation of laminations: (3) sediment anoxia and/or (4) a high sedimentation rate (Kemp et al., 1996). Although the lamination of Lake Esmeralda resembles the lamination of higher altitude (glacier-fed) lakes, we find it quite exceptional in the AP region, mainly because of combination of factors that make the varve formation improbable in the other lakes of the area, such as the need for minimum water depth for stratification to occur or, more importantly, sufficiently high sedimentation rates. With respect to these findings, we consider the sediments of Lake Esmeralda quite unique in the AP region and worth further research.

The Lake Esmeralda sediment is a mixture from several sources of sedimentary material coming to the lake from its catchment. Biological activity and evaporation connected with salt precipitation are the leading autochthonous processes in the lake reflected in the sediment.

Biological activity. If we presume that TOC is the common proxy for bioproductivity, then the general trend is continually and slightly decreasing towards the top of the ESM3 core. The three highest TOC values (98, 67 and 2 cm) represent relatively short periods (a few years) of extremely high bioproductivity and possibly the warmest periods in the past centuries. Generally, the higher number of dark laminae correlates with higher TOC values, and therefore we take this as evidence that the dark laminae are organic. However, the highest TOC values do not correspond with the thick dark laminae, but rather with thick greyish layer with gradual transition (Figure 4), where the organic matter is probably dispersed. Below average TOC values associated with a minimum of visible dark laminae, lasting ~130 years at most (from 60 to 5 cm), are interpreted to reflect colder temperatures during this period. Björck et al. (1996) interpreted lake records from JRI differently. They related the peak in organic matter to climate cooling, explaining that more suitable conditions for algal growth are in the periods of decreased clastic inputs and enhanced stability of the substrate of water bodies. In our data, we see a positive correlation of TOC and increasing clastic input. We suggest that enhanced biological activity in the lake generally points to more ice-free days and therefore warmer periods.

The C/N ratios suggest that settling organic particles were mainly autochthonous in origin; only a slight increase of around 70 cm in sediment depth point to a possible increase in allochthonous inputs, and therefore enhanced biological productivity in the lake catchment. The pigment profile shows that the presence of aquatic mosses greatly influenced the composition of sediment, and their abundance fluctuates over the time. The aquatic mosses were inversely correlated with the alloxanthin: diatoxanthin ratio, indicating that when there are less mosses present, the primary producer has been planktonic biomass (i.e. more alloxanthin is present). The alloxanthin: diatoxanthin ratio shows a rather constant value with a significant decrease at 80 cm and frequent oscillations in the upper 50 cm of the core. A decrease in the alloxanthin: diatoxanthin ratio identifies periods with a lower

water level (Buchaca and Catalan, 2007) at 78 cm and repeatedly in the topmost 60 cm. The higher abundance of mosses is also associated with greater zeaxanthin (R = 0.81), and is often also associated with higher scytonemin (UV protective carotenoid). The UV index (Leavitt et al., 2003) indicates an increase in UV stress in recent years, with a primary producer community dominated by siliceous algae (diatoms) associated with aquatic mosses.

The absence of diatom remains in parts of the core deeper than 24 cm can be explained in two ways: either the diatoms were not present in the lake, or their valves were dissolved during the early sediment diagenesis. The presence of diatom pigments (diadinoxanthin and diatoxanthin) throughout the core contradicts the former explanation. Flower and Ryves (2009) explain differences in preservation in other lakes by different sedimentation rates and/or possible salinity and pH changes. However, we observed neither sedimentation rate nor salinity change, and pH changes cannot be demonstrably visible in our data.

The genus *Microcostatus*, mainly *M. australoshetlandicus*, dominates most of the core where diatoms are preserved, although it is rarely observed in recent material from the Maritime Antarctic Region. In a preliminary analysis of recent samples from Vega Island lakes, streams and seepages (Bulínová et al., in preparation), the species was only found in two samples from Lake Esmeralda. Relative abundances of *Microcostatus australoshetlandicus* in those samples never exceeded 2%. *Nitzschia kleinteichiana* and *Psammothidium papilio*, common species in circumneutral Maritime Antarctic lakes with low conductivity (Zidarová et al., 2016), were also common throughout the upper section of the core. Aerophilic genera, such as *Luticola, Muelleria, Humidophila*, usually very common in the Maritime Antarctic Region (Zidarová et al., 2016), represented only a small proportion of the total diatom flora, suggesting permanent aquatic conditions and less important reworking of aerophilic diatoms from the catchment by streams or sheet wash.

Faunal remains of species *Boeckella poppei, Dactylobiotus* cf. *ambi* and *Notholca* sp. are typical for lake sediments from Maritime Antarctica as they were found in several lakes across this region (Gibson et al., 2007; Gibson and Zale, 2006; Jones et al., 2000). Nonetheless, this is the first palaeolimnological evidence of these taxa from the James Ross Archipelago. Björck et al. (1996) reported (besides diatoms) only cysts of a fairy shrimp *Branchinecta gaini* in several lake cores from the nearby JRI. The absence of *B. gaini* in the ESM3 core is in accordance with its absence in the water column during field observations. This could be caused by low pH of Lake Esmeralda (Moreno et al., 2012) since in other lakes of the archipelago the pH is higher than 6 and most of them host populations of *B. gaini*. This is not the case of calanoid copepod *Boeckella poppei*, which was observed in the water column and found in the uppermost layer of the sediment. Its absence in older sedimentary material could be explained by recent colonization of this region by *B. poppei* or more probably by the breakdown of spermatophores in situ, as it was suggested by Gibson and Zale (2006). The peak in abundance of the tardigrade *Dactylobiotus* cf. *ambiguus* was at a depth of 70 cm before the onset of colder conditions revealed by other proxies.

Salinity. Although higher temperatures are connected with high evaporation rates, it may still result in a positive water balance of the lake because of increased inflow of water from the melting permafrost active layer and snow. The conductivity of lake water was studied by Moreno et al. (2012), who has measured a value of 1319 µS/cm, pointing to a low salinity level. Changes in salinity are linked with the presence/absence of precipitated salts (e.g. calcite, gypsum) that can be distinguished by Ca and S changes in elemental composition. The strong Ca, S and TOC association in the core sediments point either to gypsum precipitation or to the activity of cyanobacteria and algae. Although we observed the

presence of evaporites at many places in Vega Island as well as on the shores of Lake Esmeralda, XRD did not confirm gypsum presence even in the sample of the highest S values. Moreover, high S values are observed in periods interpreted as higher lake level. Therefore, we suggest that the salinity changes in the lake were insignificant. A strong correlation of Ca and TOC in ESM3 together with the acidity of the lake water (pH 4.65–5.5) and an undetectable level of inorganic carbon in sediments point to very low or no chemical influence of calcareous bedrock both on the sediment and lake water. Similar results were found by Čejka et al. (in review), who studied the sediments from Lake Anonima (north-eastern part of Vega Island; ~ 15 km to the north-east from Lake Esmeralda). The high correlation of Zn and TOC is not straightforward to explain. Liu et al. (2005) correlated high concentrations of Zn, Pb as well as S with seal excrements on King George Island. This is probably not the case for Lake Esmeralda sediments because of its high altitude and the substantial distance of the seashore. More likely, an enrichment of Zn and Pb, as well as other metal elements, is related to metal mobilization that was described by Merino et al. (2012) during periods of high evaporation (i.e. warm periods).

Environmental changes in the catchment

To interpret geochemical and mineralogical changes in the lake sedimentary record, it is crucial to have detailed knowledge of the composition of parent rocks. All the authors of geological maps and detailed studies of Cape Lamb (Del Valle et al., 1982; Marenssi et al., 2001; Pirrie, 1994; Smellie et al., 2013) ascribe the area around Lake Esmeralda to Cretaceous sediments of CLM which are overlain by volcanic rocks of JRIVG, but they fail to be consistent in their display of the Cretaceous sedimentary rocks of SBM. Volcanic rocks of JRIVG are mainly of basaltic composition with dominance of plagioclase, clinopyroxene and olivines (Marenssi et al., 2001). The mudstones to sandstone rocks of CLM contain mica, chlorite, kaolinite, quartz and calcite in addition to smectite. In contrast, the SBM sedimentary rocks typically have lower shares of mica, quartz, calcite and chlorite/kaolinite, and bear higher shares of smectite and zeolite mineral/s of the heulandite-clinoptilolite group (Pirrie, 1994). The presence of clinoptilolite in ESM3 indicates that Lake Esmeralda catchment includes SBM rocks and might therefore support the validity of the map by Marenssi et al. (2001), according to which SBM rocks form a narrow band between CLM and JRIVG rocks. SBM rocks also a contain higher proportion of heavy minerals (up to 13%) and therefore we can consider it as an important source of heavy metals that are mobilized during the summer melting period (Moreno et al., 2012). The main accessory minerals from parent rocks of Cape Lamb rocks are biotite, hornblende, glauconite, muscovite, pyrite, pyroxene, zircon, sphene and apatite (Pirrie, 1994). The mineral composition of ESM3 sediment is quite consistent with the results of the recent soil mineralogical studies from Cape Lamb (Merino et al., 2012) from both the qualitative and quantitative points of view, that is, we found 13–27% of feldspars, whereas Moreno et al. (2012) described the content at 10–15% and Merino et al. (2012) detected 30% of feldspars in soils of Cape Lamb. The main difference between minerogenic phases of ESM3 sediment and soils is the absence of jarosite that was found in soils as a typical weathering product of pyrite and probably dissolved during its transport. Pyrite presence in parent rocks (Pirrie, 1994) is probably the source of lake acidity as well as the source of detected sulphur in ESM3. All other lakes in lower altitudes with much higher pH (Moreno et al., 2012) are likely buffered by calcareous bedrock.

In the case of Lake Esmeralda, it is not straightforward to identify minerals, which are the weathering products because the parent rocks already contain minerals that are typically secondary (e.g. smectite and zeolite from SBM rocks or kaolinite and

chlorite in CLM rocks). This complicates the interpretation of environmental changes based on secondary mineral presence/absence. Therefore, it is also difficult to determine the rate and the role of chemical and mechanical weathering processes during the past few centuries.

Three main processes with different kinetics influence the volume of allochthonous material that is transported to the lake by water: (1) accumulated snow and active layer melting representing high rate processes occurring during summer, (2) mineral weathering, giving the long-term signature (Lecomte et al., 2016) and (3) rainfall. Our main indicators of weathering intensity are aluminosilicate and CEC changes. Shares of Si, Al and K could be regarded as appropriate proxies for siliciclastic detrital input (e.g. Davies et al., 2015). This elemental association is found in feldspars as the main primary minerals of Lake Esmeralda sediments and also in illite/smectite that is a secondary phase of feldspars chemical weathering. The period of the highest detrital input occurred from 154 to 87 cm, coinciding with most of the high lake bioproductivity periods, the last and the most pronounced of which ended at around 98 cm. The event around 100 cm is associated with the beginning of the most extreme Fe and As peaks and with the highest Fe/Mn ratio. The Fe/Mn indicates a substantial shift in lake bottom anoxic conditions after 100 cm, with the highest values suggesting more pronounced lake stratification possibly connected with the highest lake level, which is quite consistent with grain size analysis (low sand fraction) and pigment content (high alloxanthin: diatoxanthin ratio followed by a decrease), with a consistently positive water balance from 137 to 87 cm (period of ~50 years), when only minor lake level fluctuations may have occurred. Similar episodes, where TOC was correlated with Fe and As peaks, and also with high Fe/Mn ratio, were observed around 112, 87, 67 and 39 cm. However, intensities and durations were lower and shorter, respectively. However, not all the TOC maxima are connected with changes in redox conditions, such as 160–122 cm and 15 cm.

CEC indicates changes in detrital input connected mainly with smectite presence. CEC is half of the value measured in soil samples from Cape Lamb by Moreno et al. (2012), but the exchange ions are the same. If all the CEC would correspond to expandable clays, then its content would be about 10% of smectite that can correspond to 20–30% of interlayered illite/smectite in the sediment. XRD quantitative analysis also shows ~30% of smectites, or interlayered illite/smectites, respectively. This amount is unexpectedly high for the region with arid and cold climate and low intensity of chemical weathering; however, the value can be explained by the primary presence of smectite in parent rocks (Pirrie, 1994). CEC minima correspond with periods of low bioproductivity, which is because low TOC periods coincide with low minerogenic input carrying the CEC signal.

Aeolian activity. Aeolian material entering the lake can be divided depending on its provenance into two main groups: (1) terrigenic and (2) sea spray derived. The source was differentiated via chlorine concentration changes. Periods rich in Cl are taken as indicators of more intensive storms and winds.

Even in periods with higher shares of sandy particles the chemical composition of sediment was alike, particularly the Al and Si concentration trends in the core are almost identical. Therefore, we assume that the composition of the terregenic aeolian material is similar to the particles derived by flowing water (rich in aluminosilicates and quartz). The periods of high influence of aeolian activity can be distinguished from the higher amount of coarse fraction from grain size analyses.

We interpret the sand fraction increase at the topmost 84 cm of the core, similar to Björck et al. (1996), as an increase of aeolian material income because the sand fraction is positively correlated with LE, Cl enrichment and higher modality of sediment grains

(polymodal distribution), but can also indicate lake level decrease and changes in the lake current system (Weinrich et al., 2014). However, lake level decrease can also relate to periods with increased aeolian input. Assuming that Cl is derived from the sea and Ti from weathering of catchment rocks, we use the Cl/Ti ratio as a proxy of aeolian transport connected with sea spray – therefore indicating higher wind strength, or more frequent storm conditions. Cl/Ti is high from 177 to 159 cm (~20 years) and then from the 92 cm in three periods lasting ~25 years with minima in the following depths: 72–65 and 44–31 cm. Similarly, aeolian transport has been found to be one of the most important processes for the input of suspended and bedload material in proglacial streams of northern JRI (Kavan et al., 2016; Kavan and Nývlt, 2018).

Sinito et al. (2011) claim that the main magnetic carrier of the remnant magnetization in the Lake Esmeralda sediments is (titano)magnetite. We cannot confirm whether (titano)magnetite is present in the ESM3 core. If yes, its concentrations must be very low (i.e. below XRD detection limit). This is consistent with Irurzun et al. (2013), who claim that the concentration of (ferro) magnetic grains is between 0.003% and 0.03%. The only element that shows a positive correlation with MS is zirconium, which points to the linkage of magnetic carrier with the coarse fraction pointing to possible Aeolian-derived material.

Zonation of environmental record

Based on the best-fit OSL age-depth model and environmental changes discussed above, we identified the following zones (Figure 10):

Z1: 177–154 cm (~25 years). This is characterized by average aeolian input, a lower level of weathering intensity and lake bioproductivity being variable but relatively high. The end of the zone is connected with a shift towards higher weathering intensity.

Z2: 154–80 cm (~75 years). Several high bioproductivity periods occur during this time interval. The highest weathering intensity (shares of Si and Al increase twofold in comparison with zone Z4) together with well-preserved lamination with most of the dark layers, indicate that both the lake itself and its surroundings experienced conditions that were more favourable for moss, bryophyte and lichen growth than in the other zones, possibly as a result of a milder summer climate. Lake level was possibly at its highest point during Z2. Depths at 100–80 cm represent the end of the lake level high stand characterized by still fairly high input of minerogenic material, high Fe content and the longest period of lake bottom anoxia connected with changes in the lake stratification. Moreno et al. (2012) pointed out that morphology of the lake surroundings suggests the past existence of a hydrological connection with the lower basin during lake overflows. We suggest that in this period, conditions might have been favourable for such a state, probably connected with a higher number of inflowing streams than today as discussed before (Figure 2).

Z3: 80–60 cm (~20 years). Still a highly productive period, but with attenuating detrital input (only slightly recovering during the peaks of bioproductivity, and both stay below average), which leads to the interpretation that at 78 cm, changes in the hydrological conditions of the catchment took place. It is likely that one of the catchment inflows was captured by an adjacent stream because of headwater erosion. This would mean that the Si/Al proxy is driven by a combination of climatic forces, and erosional changes, in the catchment.

Z4: 60–5 cm (130 years or ~55 years in the case of incomplete OSL signal bleaching age depth model – Figure 9). In con-
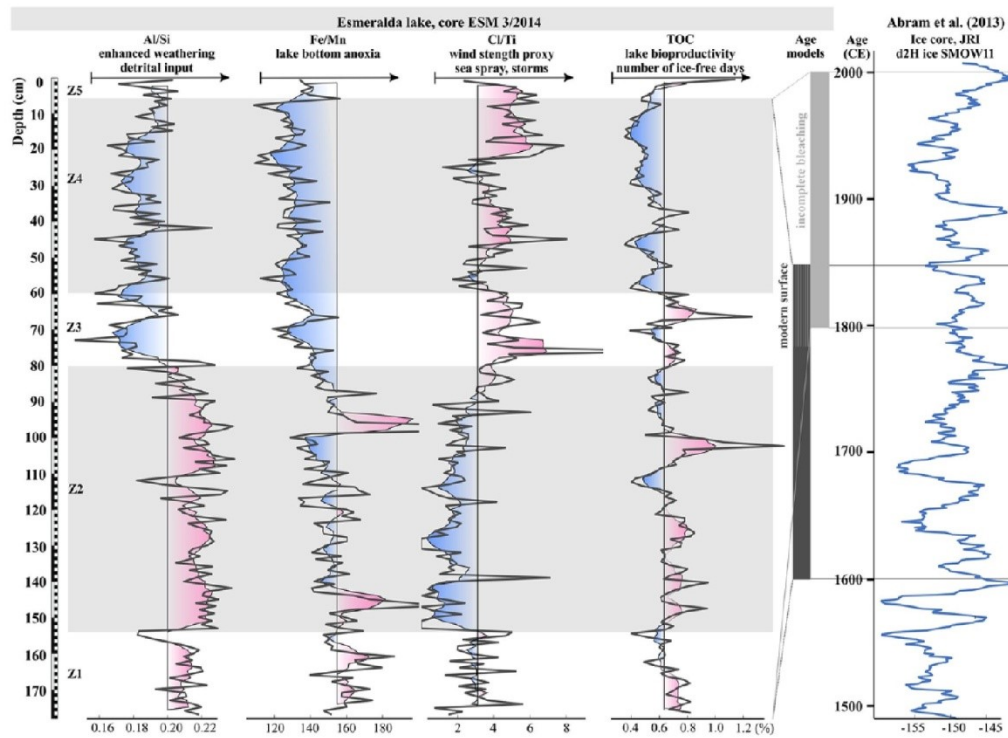
Figure 10. ESM3 proxies: TOC, Cl/Ti, Al/Si and Fe/Mn alongside deuterium isotope record (Abram et al., 2013). Proxy curves are displayed together with a colour-shaded 5-point spline and average value (vertical line). On the right-hand side, deuterium isotope record from JRI ice core (Abram et al., 2013) is tentatively correlated with ESM3/2014 in both alternative age-depth chronologies (grey rectangles).

trast to the quite dynamic and productive zone Z2, the period between 60 and 5 cm seems to be characterized by the opposite conditions: low weathering intensity, low bioproductivity, lamination without organic laminae, high aeolian input and polymodal grain-size distribution together with an increase in the sand fraction. This indicates relatively colder and possibly drier conditions, perhaps interrupted by only few warmer seasons. Colder/drier conditions could lead to a negative water balance and therefore lake level decreases. At the end of the Z4 (12 cm), a weathering intensity increase started, but the values of Al/Si still remain below the whole sequence average.

Z5: 5–0 cm (~160 years or ~5 years in the case of incomplete OSL signal bleaching age depth model). Z5 is characterized by lack of lamination, unimodal grain-size distribution and significant bioproductivity rise. Provided we rely on our OSL ages, this entire zone may possibly represent more than 160 years of very slow sedimentation with accumulation rate closer to the more common values in the AP region. We suggest the possibility that the accumulation rate changes occurred after the final lake inflow was captured by an adjacent stream, which stopped the sediment influx. Subsequently, the lake may have been fed only by sub-surface flow from the active layer and snow melting, and the aeolian material represented the major sediment input. From that point the sediment should be mostly aeolic, which is not supported by Cl/Ti ratio nor coarser fraction increase. However, the particle size distribution show higher sorting and point to reduction of sedimentary sources.

The climate of north-eastern AP over the past millennium. In order to place our sedimentary record into the context of other studies, it is appropriate to have similar parameters (age, resolution, region). Suggesting that OSL results represent maximal ages

rather than the true age of deposition, and that laminae counting represents the minimal number of years, then the lake sediment sequence approximately covers the time period CE 1600–present. We assume that Lake Esmeralda sediments may have been deposited during the past 200–400 years. In terms of age and resolution, none of the close lake records are comparable fit, but there are ice cores. Applying the regional condition of the north-eastern AP, the only comparable record left is from the Mt Haddington ice core from JRI (Abram et al., 2013; Mulvaney et al., 2012).

Their record documents pronounced cooling to temperatures that were on average 0.7 ± 0.3°C lower than the present-day between 800 and 400 yr BP (1150–1550 CE), and on a decadal timescale temperature may have at times been $>1.8 \pm 0.3$°C lower. Sterken et al. (2012) also inferred a cooler period from lake sediments on Beak Island, ~32 km north-east of Lake Esmeralda, indicated by a nutrient-depleted, low-productivity environment that ended ~540 cal. yr BP. This marks the beginning of sustained warming that began approximately 600 years ago in the James Ross Archipelago (Mulvaney et al., 2012; Sterken et al., 2012). Together, these records demonstrate an early culmination of the Neoglacial period and the absence of a widespread 'Little Ice Age' signal in the north-eastern AP that would be comparable with the Northern Hemisphere climatic variability (Mulvaney et al., 2012). On the other hand, Bentley et al. (2009) summarized the evidence for colder conditions from ~700 to ~150 cal. yr BP, fingerprinted in marine sedimentary records (Domack et al., 2001; Monien et al., 2011) and glacier advances primarily in western AP, which are related to the 'Little Ice Age'. These authors, however, also note that the 'Little Ice Age' has not been sufficiently well demonstrated in lake sediments.

The Mt Haddington ice core record suggests that the periods of marked warming, with rates exceeding 1.5°C per century, occurred

at JRI during the intervals spanning 1518–1621 CE and 1671–1777 CE (Mulvaney et al., 2012). The period ~1600–1800 CE may have experienced similarly high temperatures from those in the 20th century. According to our age-depth model, this was the period covered by the ESM3 core, and probably reflects enhanced melting of snow and the active layer, thus delivering sediment to the lake. The increased fluvial activity, however, also caused stream capture by the neighbouring streams, which ended the accumulation at ~1800 CE. The warming of Mulvaney et al. (2012) might correspond to the detected warmer period of Zones 1–3 in the ESM3 record. This is followed by the colder Zone 4 until the return to warm conditions in Zone 5, possibly connected either with a short-lived warming at the beginning of the 19th century, or with the 20th-century warming. Abram et al. (2013) stated that the recent warming trend at JRI began around the 1920s and has been statistically significant since the 1940s, although its rate is not unprecedented in the Holocene record (Mulvaney et al., 2012).

Conclusion

We provide a high-resolution, multi-proxy record from a laminated sediment core taken from Lake Esmeralda, Vega Island, north-eastern Antarctic Peninsula. Our age-depth model based on OSL data suggests a younger age of the lake sediment sequence than previously reported by radiocarbon dating. Achieved temporal resolution is thus subdecadal, and the record most probably covers a time window between 1600 and 1800 CE. Subsequently, the inflowing streams were captured by head-water erosion of neighbouring streams, which reduced or effectively stopped the accumulation in the lake.

Geochemical data were used to explore changes in detrital input (shares of minerogenic elements), to identify periods of anoxic conditions (Fe/Mn), intensification of aeolian transport (Cl/Ti) and to study relationships between individual elements with emphasis on their provenance. We identified a lake level high stand in the 17th century and colder climatic conditions from ca. 1700 to at least 1760 CE. Biological data such as diatoms, fossil pigments and crustacean remains analyses were used to provide a more complex picture of the microbial activity in the study area. Finally, geomorphological evidence indicates that river capture isolated the lake catchment from upslope sediment delivery, effectively terminating accumulation ~230 years ago. The results of this study lead us to reconsider our knowledge, not only of the history of Lake Esmeralda and its environmental setting, but also to recommend that radiocarbon dating of Antarctic lake sediments should be supplemented by data from independent methods when developing sedimentary chronologies.

The usage of Lake Esmeralda sediments for palaeoclimatic reconstructions is limited with the unexpected young age of the sediments as well as possible significant hydrological changes in the lake catchment. However, as lamination in the AP region is very rare, connected in this case with extraordinary high sedimentation rates, we consider the sediments of Lake Esmeralda quite unique in the AP region. We recommend further research, especially on the lamination pattern of Lake Esmeralda sediments, to test our assumption of annual lamination. Detailed understanding of the lamination pattern over the lake could be used not only to determine lake chronology, but also the calculation of rates of sediment influx and of rates of erosion from the Lake Esmeralda catchment.

ORCID iDs

Anna Píšková https://orcid.org/0000-0001-8371-7215
Matěj Pokorný https://orcid.org/0000-0003-0169-3737
Andrea Lami https://orcid.org/0000-0003-3627-0363
Simona Musazzi https://orcid.org/0000-0001-5549-0084

References

Abram NJ, Mulvaney R, Wolff EW et al. (2013) Acceleration of snow melt in an Antarctic Peninsula ice core during the twentieth century. *Nature Geoscience* 6: 404–411.

Bennett KD (1996) Determination of the number of zones in a biostratigraphical sequence. *New Phytologist* 132: 155–170.

Bentley MJ, Hodgson DA, Smith JA et al. (2009) Mechanisms of Holocene palaeoenvironmental change in the Antarctic Peninsula region. *The Holocene* 19: 51–69.

Berger GW, Doran PT and Thomsen KJ (2010) Single-grain and multigrain luminescence dating of on-ice and lake-bottom deposits at Lake Hoare, Taylor Valley, Antarctica. *Quaternary Geochronology* 5: 679–690.

Birks J, Battarbee R, Mackay A et al. (2014) *Global Change in the Holocene*. New York: Routledge.

Björck S, Håkansson H, Zale R et al. (1991a) A Late-Holocene lake sediment sequence from Livingston Island, South Shetland Islands, with paleoclimatic implications. *Antarctic Science* 3: 61–72.

Björck S, Hjort C, Ingólfsson Ó et al (1991b) Radiocarbon dates from the Antarctic Peninsula region – Problems and potential. *Quaternary Proceedings* 1: 55–65.

Björck S, Olsson S, Ellis-Evans C et al. (1996) Late-Holocene palaeoclimatic records from lake sediments on James Ross Island, Antarctica. *Palaeogeography Palaeoclimatology Palaeoecology* 121: 195–220.

Blaauw M and Christen JA (2011) Flexible paleoclimate age-depth models using an autoregressive gamma process. *Bayes Anal* 6: 457–474.

Blott SJ and Pye K (2001) GRADISTAT: A grain size distribution and statistics package for the analysis of unconsolidated sediments. *Earth Surface Processes and Landforms* 26: 1237–1248.

Bøtter-Jensen L, Bulur E, Duller GAT et al. (2000) Advances in luminescence instrument systems. *Radiation Measurements* 32: 523–528.

Bracegirdle TJ, Covvolley WM and Turner J (2008) Antarctic climate change over the twenty first century. *Journal of Geophysical Research* 113: D03103.

Bronk Ramsey C and Lee S (2013) Recent and planned developments of the program OxCal. *Radiocarbon* 55: 720–730.

Buchaca T and Catalan J (2007) Factors influencing the variability of pigments in the surface sediments of mountain lakes. *Freshwater Biology* 52: 1365–1379.

Bulínová et al. (in preparation). On the track of limno-terrestrial diatoms from Vega Island (NW of James Ross Island, NE Antarctic Peninsula): Diversity and ecology revealed. *Plant Ecology and Evolution*.

Čejka T, Nývlt D, Kopalová K et al. (in review) Timing of the Neoglacial onset on the north-eastern Antarctic Peninsula based on lacustrine archive from Lake Anónima, Vega Island. *Global and Planetary Change*.

Cockburn JMH and Lamoureux SF (2008) Inflow and lake controls on short-term mass accumulation and sedimentary particle size in a High Arctic lake: Implications for interpreting varved lacustrine sedimentary records. *Journal of Paleolimnology* 40: 923–942.

Crame JA, Francis JE, Cantrill DJ et al. (2004) Maastrichtian stratigraphy of Antarctica. *Cretaceous Research* 25: 411–423.

Davies SJ, Lamb HF and Roberts SJ (2015) Micro-XRF core scanning in palaeolimnology: Recent developments. In: Croudace IW and Rothwell RG (eds) *Micro-XRF Studies of Sediment Cores: Applications of a Non-destructive Tool for Environmental Sciences. Developments in Paleoenvironmental Research*. Dordrecht: Springer, pp. 189–226.

Del Valle RA, Fourcade NH and Medina FA (1982) The stratigraphy of Cape Lamb and the Naze, Vega and James Ross islands, Antarctica. In: Craddock C (ed.) *Antarctic Geoscience*. Madison, WI: University of Wisconsin Press, pp. 275–280.

Domack E, Leventer A, Dunbar R et al. (2001) Chronology of the Palmer Deep site, Antarctic Peninsula: A Holocene palaeoenvironmental reference for the circum-Antarctic. *The Holocene* 11: 1–9.

Engel Z, Nývlt D and Láska K (2012) Ice thickness, areal and volumetric changes of Davies Dome and Whisky Glacier in 1979–2006 (James Ross Island, Antarctic Peninsula). *Journal of Glaciology* 58: 904–914.

Flower RJ and Ryves DB (2009) Diatom preservation: Differential preservation of sedimentary diatoms in two saline lakes. *Acta Botanica Croatia* 68: 381–399.

Fukuda M, Strelin J, Shimokava K et al. (1992) Permafrost occurrence of Seymour Island and James Ross Island, Antarctic Peninsula Region. In: Yoshida Y, Kaminuma K and Shiraishi K (eds) *Recent Progress in Antarctic Earth Science*. Tokyo, Japan: Terra Scientific Publishing Company, pp. 745–750.

Gibson JAE and Zale R (2006) Holocene development of the fauna of Lake Boeckella, northern Antarctic Peninsula. *The Holocene* 16: 825–634.

Gibson JAE, Cromer L, Agius JT et al. (2007) Tardigrade eggs and exuviae in Antarctic lake sediments: Insights into Holocene dynamics and origins of the fauna. *Journal of Limnology* 66: 65–71.

Glasser NF, Davies BJ, Carrivick JL et al. (2014) Ice-stream initiation, duration and thinning on James Ross Island, northern Antarctic Peninsula. *Quaternary Science Reviews* 86: 78–88.

Grygar T, Bláhová A, Hradil D et al. (2007) Lake Baikal climatic record between 310 and 50 ky BP: Interplay between diatoms, watershed weathering and orbital forcing. *Palaeogeography, Palaeoclimatology, Palaeoecology* 250: 50–67.

Grygar T, Kadlec J, Žigová A et al. (2009) Chemostratigraphic correlation of sediments containing expandable clay minerals based on ion exchange with Cu (II) complex with triethylenetetramine. *Clays and Clay Minerals* 57: 168–182.

Guilizzoni P and Lami A (2003) Paleolimnology: Use of algal pigments as indicators. In: Bitton G (ed.) *Encyclopedia of Environmental Microbiology*. Chichester: John Wiley & Sons, pp. 2306–2317.

Guilizzoni P, Marchetto A and Lami A (2011) Use of sedimentary pigments to infer past phosphorus concentration in lakes. *Journal of Paleolimnology* 45: 433–445.

Haltia-Hovi E, Saarinen T and Kukkonen M (2007) A 2000-year record of solar forcing on varved lake sediment in eastern Finland. *Quaternary Science Reviews* 26: 678–689.

Hendey NI (1964) *An Introductory Account of the Smaller Algae of British Coastal Waters. Part V Bacillariophyceae (Diatoms)*. London: Her Majesty's Stationery Office.

Heroy DC and Anderson JB (2005) Ice-sheet extent of the Antarctic Peninsula region during the Last Glacial Maximum (LGM) – Insights from glacial geomorphology. *Geological Society of America Bulletin* 117(11–12): 1492–1512.

Hjort C, Ingólfsson Ó, Möller P et al. (1997) Holocene glacial history and sea-level changes on James Ross Island, Antarctic Peninsula. *Journal of Quaternary Science* 12: 259–273.

Hodgson DA, Doran PT, Roberts D et al. (2004) Paleolimnological studies from the Antarctic and Subarctics Islands. In: Pienitz R, Douglas MSV and Smol JP (eds) *Long-term Environmental Change in Arctic and Antarctic Lakes*. Dordrecht: Springer, pp. 419–474.

Hodgson DA, Dyson CL, Jones VJ et al. (1998) Tephra analysis of sediments from Midge Lake (South Shetland Islands) and Sombre Lake (South Orkney Islands), Antarctica. *Antarctic Science* 10: 13–20.

Hodgson DA, Roberts SJ, Bentley MJ et al. (2009) Exploring former subglacial Hodgson Lake, Antarctica. Paper II: Palaeolimnology. *Quaternary Science Reviews* 28: 2310–2325.

Hogg AG, Hua Q, Blackwell PG et al. (2013) SHCal13 Southern Hemisphere calibration, 0–50,000 Years cal BP. *Radiocarbon* 55: 1889–1903.

Hrbáček F, Láska K and Engel Z (2016a) Effect of snow cover on active-layer thermal regime – a case study from James Ross Island, Antarctic Peninsula. *Permafrost and Periglacial Processes* 27: 307–315.

Hrbáček F, Nývlt D and Láska K (2017) Active layer thermal dynamics at two lithologically different sites on James Ross Island, Eastern Antarctic Peninsula. *Catena* 149: 592–602.

Hrbáček F, Oliva M, Láska K et al. (2016b) Active layer thermal regime in two climatically contrasted sites of the Antarctic Peninsula region. *Cuadernos de Investigatión Geográfica* 42: 457–474.

Hua Q, Barbetii M and Rakowski AZ (2013) Atmospheric radiocarbon for the period 1950–2010. *Radiocarbon* 55: 2059–2072.

Irurzun MA, Chaparro MAE, Sinito AM et al. (2013) Preliminary relative paleointensity record and chronology on sedimentary cores from Lake Esmeralda (Vega Island, Antarctica). *Latinmag Letters* 3: 1–7.

Irurzun MA, Chaparro MAE, Sinito AM et al. (2017) Relative palaeointensity and reservoir effect om Lake Esmeralda, Antarctica. *Antarctic Science* 29: 356–368.

Johnson JS, Bentley MJ, Roberts SJ et al. (2011) Holocene deglacial history of the north east Antarctic Peninsula – a review and new chronological constraints. *Quaternary Science Reviews* 30: 3791–3802.

Jones VJ, Hodgson DA and Chepstow -Lusty A (2000) Palaeolimnological evidence for marked Holocene environmental changes on Signy Island, Antarctica. *The Holocene* 10: 43–60.

Juggins S (2017) Rioja: Analysis of quaternary science data. *R Package Version 0.9-15.1*. Available at: https://cran.r-project.org/web/packages/rioja/index.html.

Kavan J and Nývlt D (2018) Blowing in the wind – Where does the Antarctic fluvial suspended load come from? In: *Proceedings*

of the Polar 2018 – SCAR & IASC Conference, 19–23 June 2018, Davos.

Kavan J, Ondruch J, Nývlt D et al. (2016) Seasonal hydrological and suspended sediment transport dynamics in proglacial streams, James Ross Island, Antarctica. *Geografiska Annaler: Series A, Physical Geography* 99(1): 38–55.

Kemp AES (ed.) (1996) Laminated sediments as palaeo-indicators. In: Kemp AES and Kemp AE (eds) *Palaeoclimatology and Palaeoceanography from Laminated Sediments*. London: Geological Society of London (Geological Society Special Publication no. 116), pp. vii–xii.

Košler J, Magna T, Mlčoch B et al. (2009) Combined Sr, Nd, Pb and Li isotope geochemistry of alkaline lavas from northern James Ross Island (Antarctic Peninsula) and implications for back-arc magma formation. *Chemical Geology* 258: 207–218.

Lami A, Guilizzoni P, Ruggio D et al. (1992) Role of pigments on algal communities and photosynthesis. *Aquatic Science* 54: 321–330.

Lami A, Musazzi S, Marchetto A et al. (2009) Sedimentary pigments in 308 alpine lakes and their relation to environmental gradients. *Advances in Limnology* 62: 217–238.

Leavitt PR, Reasoner M, Pienitz R et al. (2003) Climatic control of ultraviolet radiation effects on lakes. *Limnology and Oceanography* 48: 2062–2069.

Lecomte KL, Vignon PA, Córdoba FE et al. (2016) Hydrological systems from the Antarctic Peninsula under climate change: James Ross archipelago as study case. *Environmental Earth Sciences* 75(623): 4–20.

Lirio JM, Chaparro A, Yermolin E et al. (2007) Carecterísticas batimétricas de las Lagunas Esmeralda y Pan Negro, Cabo Lamb, Isla Vega, Antártida. In: *VI Simposio Argentino y III Latinoamericano Sobre Investigaciones Antᴗrticas*, Buenos Aires, Argentina, 10–14 September.

Liu X, Sun L, Yin X et al. (2005) A preliminary study of elemental geochemistry and its potential application in Antarctic Seal palaeoecology. *Geochemical Journal* 39: 47–59.

Marenssi S, Salani S and Santillana S (2001) Geología de cabo Lamb, isla Vega, Antártida. *Contribuciones Cientᴗficas Instituto Antᴗrtico Argentino* 530: 1–43.

Mejdahl V (1979) Thermoluminescence dating: beta-dose attenuation in quartz grains. *Archaeometry* 21: 61–72.

Merino LM, Silva- Buso A, Ermolin E et al. (2012) Caracterización de solutos inorgánicos lixiviables en los Gelisoles del Cabo Lamb, Isla Vega (Península Antártica). *Geogaceta* 51: 47–50.

Mink S, López-Martínez J, Maestro A et al. (2014) Insights into deglaciation of the largest ice-free area in the South Shetland Islands (Antarctica) from quantitative analysis of the drainage system. *Geomorphology* 225: 4–24.

Minzoni R, John A, Rodrigo F et al. (2015) Marine record of Holocene climate, ocean, and cryosphere interactions: Herbert Sound, James Ross Island, Antarctica. *Quaternary Science Reviews* 129: 239–259.

Monien P, Schnetger B, Brumsack H-J et al. (2011) A geochemical record of Late-Holocene palaeoenvironmental changes at King George Island (maritime Antarctica). *Antarctic Science* 23: 255–267.

Moreno L, Silva-Buso A, López-Martínez J et al. (2012) Hydrogeochemical characteristics at Cape Lamb, Vega Island, Antarctic Peninsula. *Antarctic Science* 24: 591–607.

Moreton SG, Rosqvist G, Davies SJ et al. (2004) Radiocarbon reservoir ages from freshwater lakes, South Georgia, sub-Antarctic: Modern analogues from particulate organic matter and surface sediments. *Radiocarbon* 46(2): 621–626.

Morris EM and Vaughan DG (1994) Snow surface temperatures in West Antarctica. *Antarctic Science* 6: 529–535.

Mulvaney R, Abram NJ, Hindmarsh RCA et al. (2012) Recent Antarctic Peninsula warming relative to Holocene climate and ice-shelf history. *Nature* 489: 141–144.

NEA (2000) The JEF-2.2 Nuclear Data Library: Nuclear Energy Agency. *Organisation for Economic Co-operation and Development*. JEFF Report, v. 17.

Nedbalová L, Nývlt D, Kopáček J et al. (2013) Freshwater lakes of Ulu Peninsula (James Ross Island, NE Antarctic Peninsula): Origin, geomorphology and physical and chemical limnology. *Antarctic Science* 25: 358–372.

Nývlt D, Braucher R, Engel Z et al. (2014) Timing of the Northern Prince Gustav Ice Stream retreat and the deglaciation of northern James Ross Island, Antarctic Peninsula during the last glacial-interglacial transition. *Quaternary Research* 82: 441–449.

Nývlt D, Nývltová Fišáková M, Barták M et al. (2016) Death age, seasonality, taphonomy and colonization of seal carcasses from Ulu Peninsula, James Ross Island, Antarctic Peninsula. *Antarctic Science*: 28: 3–16.

Oliva M, Antoniades D, Giralt S et al. (2016) The Holocene deglaciation of the Byers Peninsula (Livingston Island, Antarctica) based on the dating of lake sedimentary records. *Geomorphology* 261: 89–102.

Oliva M, Navarro F, Hrbáček F et al. (2017) Recent regional climate cooling on the Antarctic Peninsula and associated impacts on the cryosphere. *Science of the Total Environment* 580: 210–223.

Pielou E (1966) The measurement of diversity in different types of biological collections. *Journal of Theoretical Biology* 13: 31–144.

Pirrie D (1994) Petrography and provenance of the Marambio Group, Vega Island, Antarctica. *Antarctic Science* 6: 517–527.

Pražáková M, Veselý J and Fott J (2006) The long-term succession of cladoceran fauna and palaeoclimate forcing: A 14,600 – Year record from Plešné Lake, the Bohemian forest. *Biologia* 61: S387–S399.

R Core Team (2014) R: A language and environment for statistical computing. *R Foundation for Statistical Computing, Vienna, Austria*. Available at: http://www.R-project.org/.

Reynolds JM (1981) The distribution of mean annual temperatures in the Antarctic Peninsula. *British Antarctic Survey Bulletin* 80: 21–49.

Roberts SJ, Hodgson DA, Bentley MJ et al. (2009) Holocene relative sea-level change and deglaciation on Alexander Island, Antarctic Peninsula, from elevated lake deltas. *Geomorphology* 112: 122–134.

Roberts SJ, Monien P, Foster LC et al. (2017) Past penguin colony responses to explosive volcanism on the Antarctic Peninsula. *Nature Communications* 8: 14914.

Robinson SA, Wasley J and Tobin AK (2003) Living on the edge-plants and global change in continental and maritime Antartica. *Global Change Biology* 9: 1681–1717.

Roos P, Holm E, Persson RBR et al. (1994) Deposition of 210Pb, 137Cs, 239+240Pu, 238Pu, and 241Am in the Antarctic Peninsula area. *Journal of Environmental Radioactivity* 24: 235–251.

Ross R, Cox EJ, Karayeva NI et al. (1979) An amended terminology for the siliceous components of the diatom cell. *Nova Hedwigia* 64: 513–533.

Round FE, Crawford RM and Mann DG (1990) *The Diatoms: Biology and Morphology of the Genera*. Cambridge: Cambridge University Press.

Sanderson DCW (1988) Thick source beta counting (TSBC): A rapid method for measuring beta dose-rates. *Nuclear Tracks and Radiation Measurements* 14: 203–207.

Sanderson DCW and Murphy S (2010) Using simple portable OSL measurements and laboratory characterisation to help

understand complex and heterogenous sediment sequences for luminescence dating. *Quaternary Geochronology* 5: 299–305.

Sanderson DCW, Cresswell AJ, Roman M et al. (2017) Luminescence Measurements of Sediment Cores from Lake Esmerelda and Monolith Lake. James Ross Island Archipelago, SUERC Report, Glasgow, University of Glasgow.

Schwerdtfeger W (1984) *Weather and Climate of the Antarctic.* Amsterdam: Elsevier.

Shannon CE and Weaver W (1949) *The Mathematical Theory of Communication.* Urbana, IL: Urbana University Press.

Sinito AM, Chaparro MAE, Irurzun MA et al. (2011) Preliminary palaeomagnetic and rock-magnetic studies on sediments from lake Esmeralda (Vegy Island). *Antarctica, Conference paper 2ª Reuni□n Bienal de la Asociaci□n Latinoamericana de Paleomagnetismo y Geomagnetismo.* 23–26 November 2011, Buenos Aires.

Smellie JL, Johnson JS and Nelson AE (2013) *Geological map of James Ross Island. I. James Ross Island Volcanic Group (1:125 000* Scale). Bas Geomap 2 Series, Sheet 5. Cambridge: British Antarctic Survey.

Smellie JL, Johnson JS, McIntosh WC et al. (2008) Six million years of glacial history recorded in the James Ross Island Volcanic Group, Antarctic Peninsula. *Palaeogeography, Palaeoclimatology, Palaeoecology* 260: 122–148.

Sterken M, Roberts SJ, Hodgson DA et al. (2012) Holocene glacial and climate history of Prince Gustav Channel, northeastern Antarctic Peninsula. *Quaternary Science Reviews* 31: 93–111.

Szeroczyńska K and Sarmaja-Korjonen K (2007) *Atlas of Subfossil Cladocera from central and northern Europe.* Świecie: Friends of the Lower Vistula Society.

Toro M, Granados I, Pla S et al. (2013) Chronostratigraphy of the sedimentary record of Limnopolar Lake, Byers Peninsula, Livingston Island, Antarctica. *Antarctic Science* 25(2): 198–212.

Turner J, Colwell SR, Marshall GJ et al. (2005) Antarctic climate change during the last 50 years. *International Journal of Climatology* 25: 279–294.

Turner J, Lu H, White I et al. (2016) Absence of 21st century warming on Antarctic Peninsula consistent with natural variability. *Nature* 535: 411–415.

Van der Werff A (1955) A new method of concentrating and cleaning diatoms and other organisms. *Verhandlungen Internationalen Vereinigung für Theoretische und Angewandte Limnologie* 2: 276–277.

Van Lipzig NPM, King JC, Lachlan-Cope TA et al. (2004) Precipitation, sublimation, and snow drift in the Antarctic Peninsula region from a regional atmospheric model. *Journal of Geophysical Reasearch* 109: D24106.

Vaughan DG, Marshall GJ, Connelly WM et al. (2003) Recent rapid regional climate warming on the Antarctic Peninsula. *Climate Change* 60: 243–274.

Washburn AL (1974) Periglacial Processes and Environments. London: Arnold, 320pp.

Weinrich V, Minyuk PS, Borkhodoev V et al. (2014) Pliocene to Pleistocene climate and environmental history of Lake El'gygytgyn, Far East Russian Arctic, based on high-resolution inorganic geochemistry data. *Climate of the Past* 10: 1381–1399.

Zale R (1994) 14C age corrections in antarctic lake sediments inferred from geochemistry. *Radiocarbon* 36: 173–185.

Zidarová R, Kopalová K and Van de Vijver B (2016) *Diatoms from the Antarctic Region. I: Maritime Antarctica.* Iconographia Diatomologica, vol. 24. 509pp. Available at: https://www.nhbs.com/iconographia-diatomologica-volume-24-diatoms-from-the-antarctic-region-maritime-antarctica-book.

CHAPTER 5

Timing of the Neoglacial onset on the north-eastern Antarctic Peninsula based on lacustrine archive from

Lake Anónima, Vega Island

Global and Planetary Change; in review
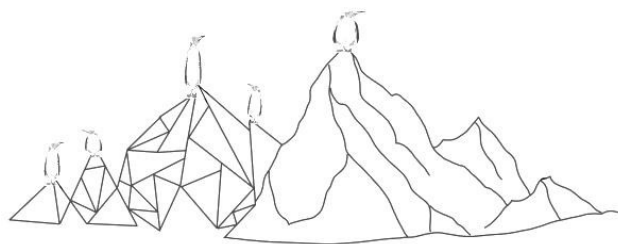
TIMING OF THE NEOGLACIAL ONSET ON THE NORTH-EASTERN ANTARCTIC PENINSULA BASED ON LACUSTRINE ARCHIVE FROM LAKE ANÓNIMA, VEGA ISLAND.

TOMÁŠ ČEJKA[a,b], DANIEL NÝVLT[a], KATEŘINA KOPALOVÁ[c,d], MARIE BULÍNOVÁ[c], JAN KAVAN[a], JUAN M. LIRIO[e], SILVIA H. CORIA[e], BART VAN DE VIJVER[f,g]

[a] Department of Geography, Faculty of Science, Masaryk University, Kotlářská 2, 602 00 Brno, Czechia

[b] Global Change Research Institute, Czech Academy of Sciences, Bělidla 4a, 603 00 Brno, Czechia

[c] Department of Ecology, Faculty of Science, Charles University, Viničná 7, 12844 Prague, Czechia

[d] Academy of Sciences of the Czech Republic, Institute of Botany, Section of Plant Ecology, Dukelská 135, CZ-37982 Třeboň, Czechia

[e] Instituto Antártico Argentino, Av. 25 de Mayo 1143, San Martín B1650HMK, Buenos Aires, Argentina

[f] ECOBE, Department of Biology, University of Antwerp, Universiteitsplein 1, B-2610 Wilrijk, Belgium

[g] Botanic Garden Meise, Research Department, Nieuwelaan 38, B-1860 Meise, Belgium

Abstract

To understand the complexity of the climate patterns in the Holocene, it is necessary

to build detailed chronologies that provide a holistic picture of the individual climate periods occurring in the Polar Regions. In this regard, here we present a completely new, ^{14}C-dated and synchronised multi-proxy chronology from the Lake Anónima (Vega Island, north-eastern Antarctic Peninsula) that provides a unique insight into the Late Holocene environment. In particular, we aim to interpret the substantial environmental and climatic change between the mid-late Holocene Hypsithermal and Neoglacial periods using various geochemical (total organic carbon, X-ray fluorescence spectroscopy), petrophysical (magnetic susceptibility, laser granulometry) and biological (diatom biostratigraphy) proxies. The termination of the mid-late Holocene Hypsithermal, characterised by overall warmer climate with favourable conditions for biogenic productivity, is followed by the regional-scale Neoglacial period, distinctive by the onset of climate deterioration, decreased siliciclastic input, suppressed biogenic (diatom) productivity and low organic content. Based on a principal component analysis, a multi-proxy record provides the precise timing of the Neoglacial onset in the Lake Anónima record at 2100 (2σ: 2040–2180) cal. yrs b2k. Applying an adjacent and correlative ice-core (James Ross Island ice cap, r = 0.42), as well as a composite lake sediment (Beak Island, r = 0.49) chronologies, our research provides a refined timing of the Neoglacial onset for the north-eastern Antarctic Peninsula, which is determined to be 2120 ± 50 yrs. b2k. Moreover, the Neoglacial onset was compared with other studies from respective parts of the Antarctic Peninsula.

Keywords: Antarctic Peninsula, James Ross Archipelago, multi-proxy, lake record, mid-late Holocene hypsithermal, Neoglacial

Introduction

As the largest ice-free area (~20 %) of the Antarctic Peninsula (AP; Pritchard & Vaughan 2007) together with numerous lakes that were created in the James Ross Archipelago (JRA) as a result of the Late Glacial and Holocene deglaciation (Johnson et al. 2011; Nývlt et al. 2014), the region of the north-eastern AP represents an excellent area for palaeolimnological research. Numerous have focused on recent changes in the AP climate, such as the disintegration of ice shelves (e.g., Cook et al. 2005; Scambos et al. 2009),the retreat of local glaciers (e.g., Engel et al. 2012), a rapid increase in air surface temperature in the AP over the past 40 years (e.g. Smith 2002; Vaughan et al. 2003), an acceleration in the duration of the summer season (Vaughan 2006; Hrbáček et al. *in press*) and recent changes in the biodiversity of polar lakes (e.g., Quayle et al. 2002; Smol & Douglas et al. 2007). Such a variety of topics is a result of the AP's uniqueness in the context of its geological and glaciological history, diversity in ecosystem types and biogeographical conditions (Øvstedal & Lewis-Smith 2001) as well as climate variability. With respect to the latter, the climate in the AP region was generally unstable over the entire Holocene, as evidenced by the presence of the mid-late Holocene hypsithermal and the following Neoglaciation (e.g. Ingólfsson et al. 1998; Jones et al. 2000; Bentley et al. 2009; Hall 2009). These observations relied on palaeolimnological methods, indicating that the Polar lakes represent sensitive and useful indicators of climatic changes, although the causes and impacts on ecosystems, especially under diverse physical-geographical setting, remain poorly understood.

Using a multi-proxy approach, we focus in this paper on an examination and description of the last significant environmental change of the Late Holocene that was recorded in Lake Anónima (LA) and that frequently occurs in the AP records as reported by several authors from ice-core (Mulvaney et al. 2012), lacustrine (e.g. Björck et al. 1996a, Jones et al. 2000; Sterken et al. 2012; Hodgson et al. 2013) and marine (e.g. Brachfeld et al. 2003; Michalchuk et al. 2009; Milliken et al. 2009; Barnard et al. 2014; Christ et al. 2015; Minzoni et al. 2015; Kyrmanidou et al. 2018) records.

Site location and regional setting

Lake Anónima (63°49'20"S, 57°19'30"W; 24 m a.s.l.) is located in the northern part of Vega Island (Figure 5.1B), ~28 km east of the Czech Mendel Polar Station and ~17 km north-east of the Terrapin Hill on JRI. The lake is almost circular, ~60 m long and ~40 m wide with a total surface area of ~2000 m². Bathymetry that was performed by Argentinian colleagues (see further info in Chaparro et al. 2017) during the Argentinian-Czech expedition 2012/13 indicated that it is a shallow lake with two subbasins with a maximum depths of 4.1 m (NE) and 4.6 m (SW) respectively, separated by a shallow ridge. Depth at core retrieval locality was 3.8 m with a lake floor being slightly sloped.
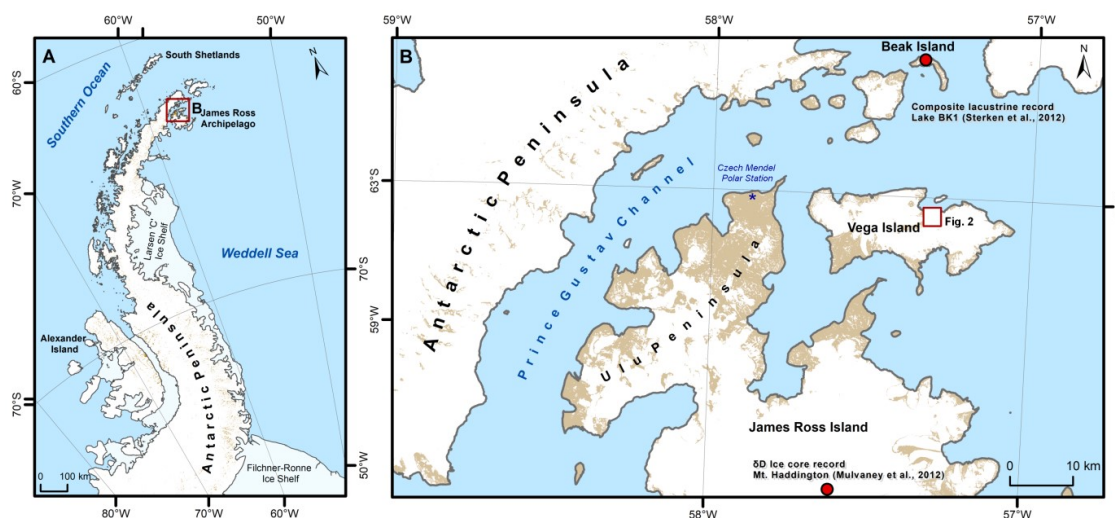
Figure 5.1 (A) Antarctic Peninsula. (B) James Ross Archipelago and locations of data (red dot) used in the synthesis – Mount Haddington's δD ice-core record (Mulvaney et al. 2012), BK1 lake's composite record (Sterken et al. 2012).

The LA (Figure 5.2) is situated in a till plain (proglacial zone) of the local glacier Bahía del Diablo (Figure 5.2; Marinsek & Ermolin 2015). Local bedrock is composed of Cretaceous sediments of the Marambio Group, whereas the surrounding area is composed of elevated volcanic mesas formed by Neogene back-arc volcanic rocks (basalt, hyaloclastite breccia) of the James Ross Island Volcanic Group (JRIVG; Smellie et al. 2008, 2013). The Cretaceous strata of Vega Island consists of fossiliferous marine mudstones, sandstones and conglomerates of the Santa Marta, Snow Hill Island and López de Bertodano formations (Roberts et al. 2014). The proglacial valley floor is filled mainly with Holocene till with predominant local volcanic rocks and in a smaller proportion with Cretaceous sediments (Zale & Karlén 1989). Along the northern coast of Bahía del Diablo, deltaic and marine deposits produced by marine transgressions after the early Holocene deglaciation are interbedded with till. However, marine processes failed to reach the area of LA (Figure 5.2) and had no direct effect on its origin and subsequent development. On the contrary, in the southern part of the valley, tills were partially reworked and are covered by glaciofluvial sediment (Ermolin et al. 2002), which directly underlain the lake.
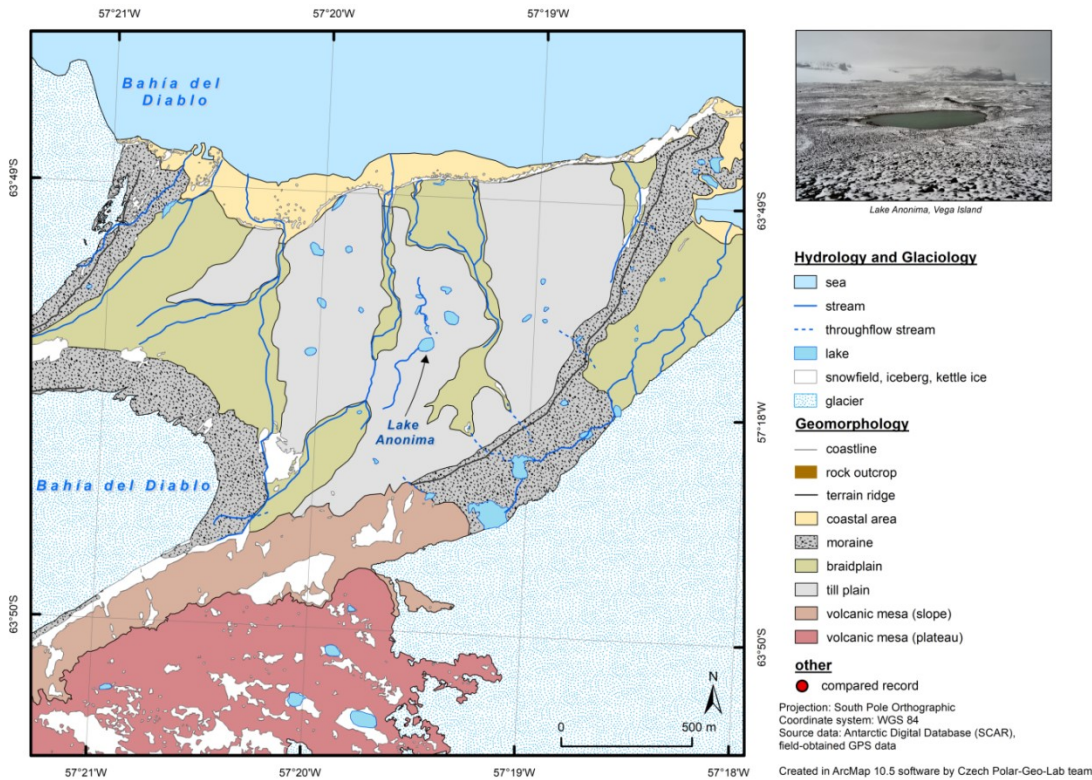
Figure 5.2 The geomorphological setting in the proglacial zone of the glacier Bahía del Diablo, Vega Island.

The climate in the JRA is semi-arid, Polar-continental, influenced by an orographic barrier of the Trinity Peninsula Mountains (Davies et al. 2013). The mean annual air temperature at the Czech Mendel Polar Station (see Figure 5.1 for location) was −7.0 °C (period 2006–2015; Hrbáček et al. 2017) with annual snowfall 300–500 mm.yr^{-1} w.e. (Van Lipzig et al. 2004). The lake collects surface runoff and is simultaneously connected to a water input from streams and snowmelt with a sediment load that has formed a small delta on the south-western coast of the lake (Chaparro et al. 2017). Despite this, the lake basin is considered to be endorheic (Chaparro et al. 2017), the ice in the till plain damming the lake melts seasonally causing fluctuations in the water level (~1 m), as well as an underground drainage into surface streams and the nearby lake systems. Thus, the lake could be regarded as through-flow. Winter (June – August) season snow accumulation onto the lake's surface results in its melting and active permafrost layer thawing during the summer (December – February) season (Chaparro et al. 2017).

The flora of the area is composed mainly of bryophytes and lichens, and their distribution is limited due to the deficiency in liquid water (Robinson et al. 2003), which results in flora coverage near the lakes or along the (seasonally active) streams only. In contrast, the micro-flora, mostly composed of cyanobacteria, green algae and diatoms, is well developed in freshwater ecosystems such as seepages, lakes, and streams, which are usually supplied by meltwater from thawing glaciers and snowfields (Engel et al. 2012). Even though the invertebrate

fauna has been poorly studied, both *Boeckella poppei* (Mrazek) and *Branchinecta gainii* (Daday) are present in the lakes of the area (Nedbalová et al. 2017). The nearest penguin colony is located on nearby Devil's Island. Additionally, flying seabirds frequently visit the island. The human influence is limited to only occasional summer campaigns.

Methods

Coring and sub-sampling

The coring was undertaken during the Antarctic summer season 2012/13 (11 February 2013) by an Argentinian-Czech expedition. The 69-cm long sediment core was extracted from LA (referred to as AN13) using a manual Russian chamber corer, which allows for obtaining semi-cylindrical cores of 7 cm in diameter and 1 m in length. The core was wrapped (potential moisture contamination and microbial overgrowth) in a plastic tube and stored after transport at standard room temperature for two and half years. Before analysis, the sediment was photographed at high-resolution, sliced in 1-cm intervals and stored at room temperature. The destructiveness of a method determined the order of the implemented analyses. Since the Russian Corer is considered capable of collecting sediment without vertical compaction, the compaction effect uncertainty was not considered.

Geochronology

Radiocarbon (^{14}C) dating of five selected samples (Table 5.1; terrestrial macrofossils or, in the absence thereof, bulk sample) was performed at Poznań Radiocarbon Laboratory by means of AMS. Calibrated ages (SHCal13; Hogg et al. 2013) are presented on the b2k time-scale, and the negative ^{14}C ages are being calibrated by the post-bomb curve (SH Zone 1–2; Hua et al. 2013). The age-depth modeling was processed in the R-code package Clam ver. 2.2 (Blaauw et al. 2010) within 95% confidence ranges, using a linear interpolation method with 10,000 iterations. Calibrated best-age was determined using a weighted average of the age-depth model derived ages. Mid-point calculation for the best-age as well as 95% confidence ranges was processed directly in R code. Sedimentation rate for each centimetre (yr.cm^{-1}) and year (mm.yr^{-1}) was calculated, and, due to linear time-scale usage, some depth values of corresponding ages were recalculated to obtain more realistic simulation.

Physical proxies

Determination of magnetic susceptibility (κ) was performed using AGICO MFK1-FB in three measuring frequencies (976, 3904 and 15616 Hz) with 200 mA.m^{-1} magnetic field. Predefined sample volume (10 cm^3) was used for mass κ (χ) calculation according to Evans & Heller (2003), with H_2O diamagnetism and paramagnetism neglection due to comparatively stable water content throughout a core (samples measured in original conditions). Frequency-dependent susceptibility (χ$_{FD}$) was estimated according to Dearing et al. (1996). Grain-size measures were obtained via CILAS Particle Size Analyser 1190L after sample homogenization in 10% KOH (biogenic silica) and 30% H_2O_2 (organic matter; Vaasma, 2008). Volumetric grain-size parametres (mean grain-size – MGS, clay, silt and sand content, sorting, skewness) were calculated from the raw grain-size data (range 0.04–2500 μm) in the GRADISTAT software, v 8.0 (Blott & Pye 2001), and are presented in graphical method (μm) of Folk & Ward (1957).

Geochemistry

The elemental analysis was conducted using the Innov-X DELTA PREMIUM hand analyser with H_2O affect as well as plastic batch composition neglection. Averaged data of the three measurements in Soil Geochem/Vanad mode are presented in parts per million (ppm) ratios. Total carbon (TC), total in-/organic carbon (TIC, TOC) and total sulphur (TS) determination was performed using ELTRA Metalyt-CS-1000S analyser. TC and TS contents of homogenised samples were measured using thermal combustion (1350 °C) and infrared detection. TOC was calculated by subtracting TIC (CO_2 released after H_3PO_4 combustion) from TC.

Diatoms

Diatom samples were oven-dried (24 h, 50 °C) and only sub-sampled 1 g of dry sediment was later used for further homogenization according to van der Werff (1955). Samples were cleaned by adding 37% H_2O_2 (80 °C heating for one hour), followed by $KMnO_4$ addition. After digestion and centrifugation (3 × 10 minutes at 3700 × g^{-1}), the material was diluted with distilled water (volume unification and avoiding valve's excessive concentrations). Then 50 μl of each sample was mixed with 50 μl of sonicated (10 min) microsphere solution (6792.4 MS/μl) and 400 μl distilled water and mounted in Naphrax$^{®}$. In each second sampled layer exactly 400 valves (due to low abundance only 50 valves in layers 33–51) were enumerated on random transects at 1,000 × magnification under oil immersion using an Olympus BX43 microscope, equipped with Nomarski Differential Interference Contrast (Nomarski) optics and the Olympus DP27 camera using the cellSence Entry Imaging Software. Terminology is based mainly on Hendey (1964), Ross et al. (1979) and Round et al. (1990). For taxonomical identification Iconographia Diatomologica vol. 24 (Zidarova et al. 2016) was used. For several species, identification up to species level was not possible due to their unclear taxonomic situation.

Data analyses

The suitability of the correlation matrix was tested using the Kaiser-Meyer-Olkin test. Forcing patterns in the data were analysed by applying principal component analysis (PCA). Minimum data contribution in each variable was designated to 80 % except all diatom data (contribution ~50 %). Due to time-consuming diatom biostratigraphy analysis, only every 2nd, or 3rd sample, respectively, was pre-treated and subsequently analysed. These have been further taken into consideration throughout the PCA interpretation. Via biostratigraphy, a number of valves per gram of sediment − relative abundance (% of total diatom valves per sample), species richness, Shannon diversity (Shannon & Weaver 1949) and evenness (Pielou 1966) were calculated. Significant clusters were identified and divided using stratigraphically constrained cluster analysis (*CONISS*) with the significant division based on comparing a *CONISS* distance matrix with a random model based on broken stick model (Bennett 1996) using the *rioja* package in R (Juggins 2009). Delivered correlations (*r*) were calculated from measured data and were significant at the 0.01 level (*p*) unless stated otherwise. Compared variables (10-yr (°C) anomalies from Mt. Haddington ice-core (Mulvaney et al. 2012) – interval value equals to mid-interval; Loss on ignition 550 °C (LOI, %) and χ (10^{-5} $kg^{-1}.m^3$) from the Lake BK1 (Sterken et al. 2012) located on Beak Island) were first interpolated to equal age of the proxies and splined (5-step simple moving average – SMA) to a smooth high-frequency signal. Spline data were further used for statistics, and all presented graphs were produced in *Grapher* v. 11.

Results

Lithology and age-depth model

The lithological profile (Figure 5.3) lacks annual lamination or visible stratification. For an age-depth model of deposition in LA, five radiocarbon ages were obtained from the core (Table 5.1), although the fifth and concurrently nethermost sample (66–67 cm) revealed a significantly underestimated radiocarbon age. Due to the reversal age of the lowermost sample, only the first four radiocarbon ages, revealing a proper chronostratigraphic sequence (goodness-of-fit 4.96), were included into the calculation of age-depth model (Figure 3) with a base onset at 2440 cal. yrs b2k. Besides, the lowermost sample contains the lowest carbon amount and we thus consider it as less reliable than the other above-lying samples. Table 1 shows, that the topmost part (5.5–0 cm) accumulated after AD 1950 hence post-bomb ^{14}C age, where the amount of nuclide is conventionally expressed as pMC entailing "percentage of modern carbon" – normalised to 100 % (Reimer et al. 2004). Short-lived isotopes (^{137}Cs, ^{210}Pb) dating proved shallow specific activities (Bq/g) in the samples. Thus relationship purification between age and depth within recent decades was not possible.

Sample	Lab code	Depth (cm)	Material	mg C[a]	[14]C years BP	Min.–Max. cal. yrs b2k (±2σ)
AN13_5-6	Poz-85803	5 – 6	lacustrine moss	0.09	100.99 ± 0.39 pMC	43 – 44
AN13_16-17	Poz-89401	16 – 17	lacustrine mud	–	555 ± 30	554 – 604
AN13_28-29	Poz-89403	28 – 29	lacustrine mud	–	1650 ± 30	1468 – 1615
AN13_54-55	Poz-89402	54 – 55	lacustrine mud	–	2130 ± 30	1991 – 2204
AN13_66-67	Poz-89404	66 – 67	lacustrine mud	0.06	1260 ± 80	–

Table 5.1 Radiocarbon ages of dated samples from the Lake Anónima. [a] milligrams of C in the analysed sample, where the amount of C was < 0.1 mg
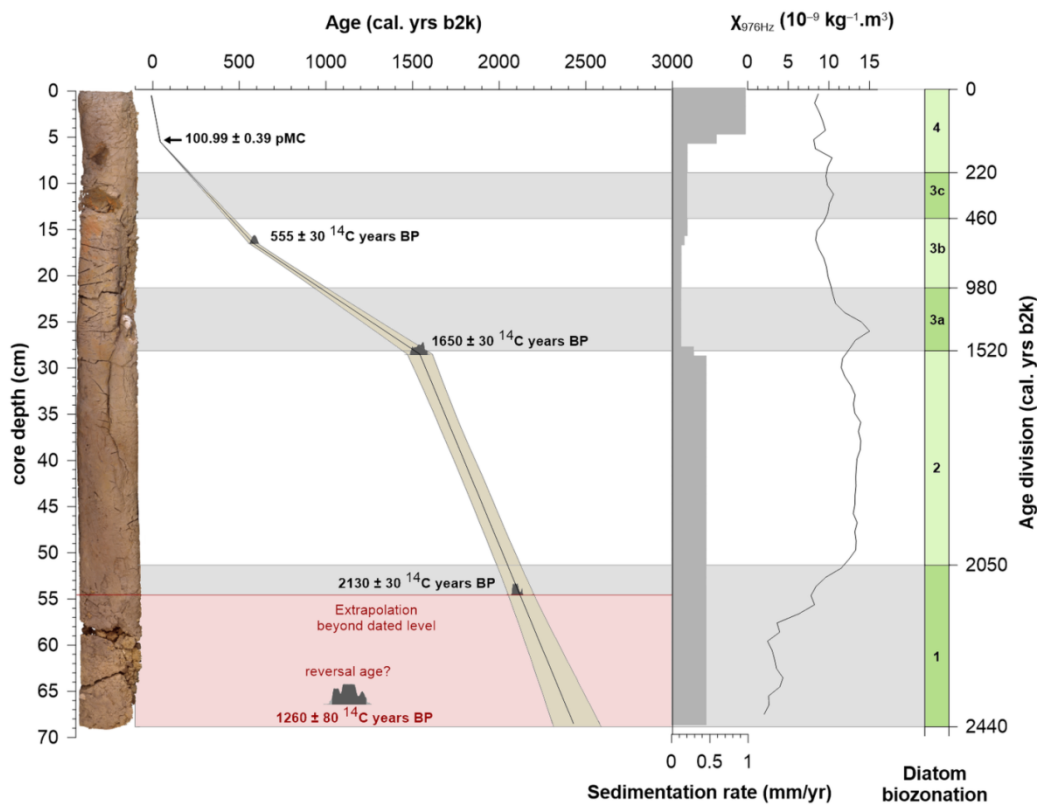
Figure 5.3 Best estimate age-depth model (blackish middle line) with 2σ uncertainty envelope (95 % confidence interval) based on four ^{14}C ages derived from the core. The lowermost reversal ^{14}C age is not included in the age-depth model calculation. Supplemented by probability distribution curves of calibrated ages, sedimentation rate (mm.yr^{−1}), low-field χ (976 Hz) and diatom biozonation (model of Bennett 1966).

Physical proxies

Figure 5.4 depicts the χ values that are rather low throughout the core (Figure 5.4; within range of 10^{-9} m^3.kg^{-1}) showing a limited influence of ferri- and ferromagnetic particles and a dominance of diamagnetic and paramagnetic matter. A comparatively variable sedimentation rate (0.13–0.97 mm.yr^{-1}) is result of variable clastic input.

The lowest section (2440–2100 cal. yrs b2k), characterized by a low χ (varying around ~3.10^{-9} m^3.kg^{-1}), increased χ$_{FD}$ (~5 %), and enhanced MGS (~12.8 μm) correlating (r = 0.93) with higher sand (increase up to 13 %) and lower clay fraction (decrease down to 12 %), is typical by reversed values in comparison to the middle section, whose maximum age is 2100 cal. yrs b2k. The pre-2100 cal. yrs b2k period is also characterized by sediments that are poorly sorted and indicate a relatively higher sedimentation rate (0.45 mm.yr^{-1}). The 2100 cal. yrs b2k onset demonstrates a rapid increase of χ (~13.10^{-9} m^3.kg^{-1}) with subsequent continual decrease starting at 1400 cal. yrs b2k and ceasing at 550 cal. yrs b2k (~8.10^{-9} m^3.kg^{-1}). Significant change is marked as well by χ$_{FD}$, MGS and sand content decrease (to ~3.5 %, 5.5 μm, 0.03 %), and transition to changes in sorting in each 5–7 cm interval from moderately sorted to poorly sorted and conversely, respectively. Sedimentation rate decreased within the middle section (since 1560 cal. yrs b2k) down to ~0.17 mm.yr^{-1}. During the last 2000 cal. yrs b2k, the χ$_{FD}$ continually increases up to 5 %, which is supplemented by χ variation (~8–10.10^{-9} m^3.kg^{-1}) in the last 550 cal. yrs b2k. In the recent 50 cal. yrs b2k there is an increase in sand content (~5 %), as well as in MGS (~10 %), and the sedimentation rate rises to 0.97 mm.yr^{-1}, which might correspond with smaller compaction of the uppermost part of the core.

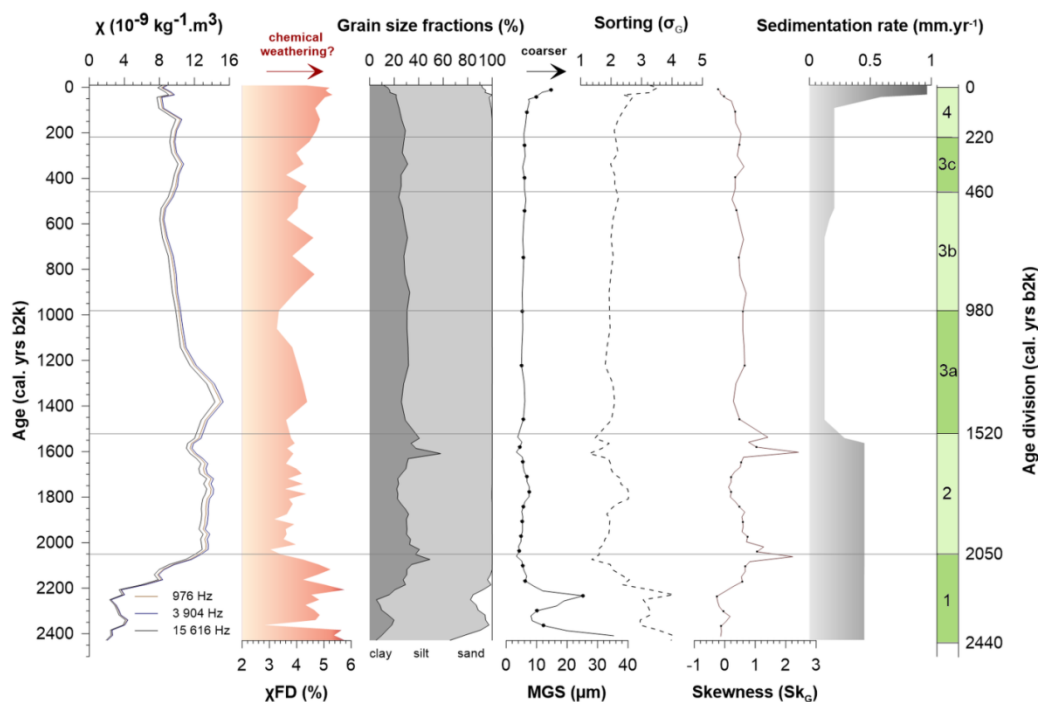**Figure 5.4** Physical proxies (left to right): mass magnetic susceptibility χ (10^{-9} kg^{-1}.m^3), frequency-dependent magnetic susceptibility χ$_{FD}$ (%), grain-size fractions (%), mean grain size MGS (μm), sorting degree, skewness and sedimentation rate (mm.yr^{-1}) plotted against b2k time-scale.

Geochemistry

While no inorganic carbon was detected in the entire core, TOC and TS values correlate (Figure 5.5), with their highest relative values (maximum TOC 5.1 % and TS 0.2 %) in the pre-2100 cal. yrs b2k period. Fe/Mn, Si/Ti and Zr/Ti show the higher values (~90.73, ~11.27, ~0.03) within this time interval as well, while Al/Si, Fe, Ca and Mn yielded – in comparison to post-2100 cal. yrs b2k – low (0.17; 21,234 ppm; 15,468 ppm; 248 ppm) values. Concerning distinguishing the primary processes, material sources in the catchment area and heterogeneity and variable water influence in the core, we rely on ratios over ppm content of individual elements. The subsequent period since 2100 cal. yrs b2k is the complete opposite, meaning almost completely reduced TOC and TS. The organic matter increases in the 1250–250 cal. yrs b2k period, where TOC oscillates roughly around ~1%. Fe/Mn, Si/Ti and Zr/Ti reveal shift to low values (~60.72, ~6.36, ~0.02), whereas Al/Si, Fe, Ca and Mn show increased values (0.27; 44,632 ppm; 37,798 ppm; 741 ppm). Fluctuations linkage with subsequent inorganic proxies is best expressed with light elements (LE) content (r = 0.90) and Rb/Sr (r = 0.87) plus Fe/Mn (r = 0.86) ratios. The direct relationship between the latter two is also apparent (r = 0.89), whereas biogenic silica (BSi) presence, expressed circuitously by Si/Ti ratio, corresponds with TOC (r = 0.81) as well. Grain-size Zr/Ti and Al/Si proxies also bear coherence (r = −0.86) establishing these two ratios as a stable proxy for grain-size distribution.
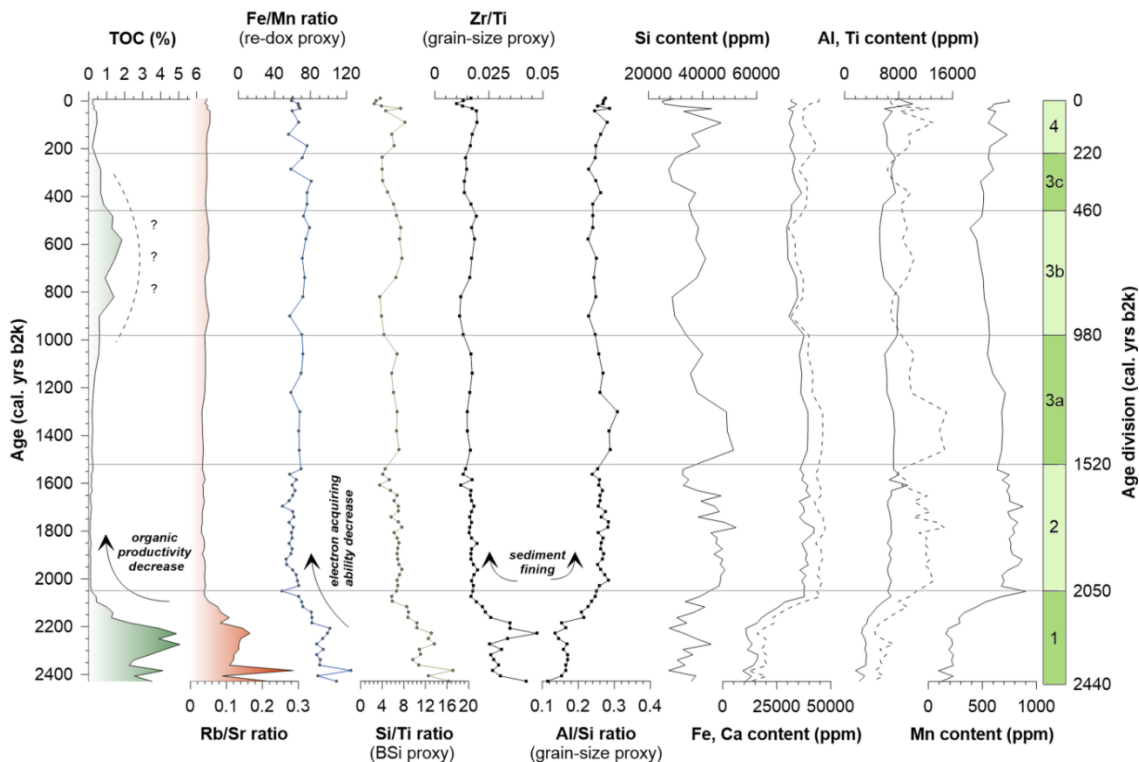

Figure 5.5 Geochemical proxies (left to right): total organic carbon TOC (%), Rb/Sr, Fe/Mn, Si/Ti, Zr/Ti and Al/Si ratios, Si, Fe, Ca, Al, Ti and Mn contents (ppm).

Diatom biostratigraphy

The complete diatom flora includes a total of 80 species belonging to 26 genera (Figure 5.6a). CONISS clustering splits the core into six diatom zones (from now on a "biozone"), four of which (biozones 1–4) are statistically significant based on the broken stick model (Bennett 1996). Subdivisions within biozone 3 are not statistically significant, but they are retained due to their correspondence with changeable TOC within biozone 3.

Richness (Figure 5.6b) increases overall from biozone 1 and 2 to the peak in biozone 4. Shannon diversity (Figure 5.6b) is more stable with the lowest values in biozone 1 (1.36–2.49) and the highest in biozone 4 (maximum 2.89). Evenness (Figure 5.6b) reveals a more fluctuating pattern with the highest value in biozone 2, where it reaches its maximum of 0.93. The diatom community is dominated by the genus *Nitzschia* (average share ~41 %), and the abundances are relatively uniform. The next most abundant taxon is *Planothidium rostrolanceolatum*, which occurs in share up to ~41 % in zone 3. All other taxa contribute by smaller proportions and are more variable.

The genus *Nitzschia* dominates biozone 1 (2440–2050 cal. yrs b2k) (46–67 %), followed by *Achnanthidium australexiguum* (4–22 %), *Sellaphora antarctica* (4–16 %), *Stauroneis delicata* (0.2–10 %, being mostly present only in biozone 1 and subzone 3c), and *Gomphonema maritimo-antarcticum* (0.7–11 %). *Brachysira minor*, the most abundant species in the biozone 2, is almost lacking from biozone 1. TOC reaches its peak together with the diatom highest abundance (Figure 5.6b; 604×10^4 valves.g^{-1} of dry sediment) in biozone 1.

Biozone 2 (2050–1520 cal. yrs b2k) is scarce (10×10^4), meaning limited specimens were counted (up to 50 instead of 400) and subsequently there may be artificial reduction of the calculated richness or/and increase of Evenness. The diatom communities mainly present (semi-)terrestrial diatom species such as *Hantzschia amphioxys*, showing abundance within a range of 0.5–10 %, *Luticola muticopsis* (0.5–18 % appearing only in the biozone 2), the genus *Humidophila*. *Sellaphora gracillima* is absent in most of biozone 2. The genus *Nitzschia* still dominates the community, but within this genus *N. homburgiensis* comprises up to 18 % of the community, in contrast to the rest of the core where it is present in very low abundances.

Biozone 3 (1520–220 cal. yrs b2k), subdivided into three sub-zones (3a: 1520–980 cal. yrs b2k, 3b: 980–460 cal. yrs b2k and 3c: 460–220 cal. yrs b2k), is characterised by co-dominance of *Planothidium rostrolanceolatum* and the genus *Nitzschia*, with *Planothidium rostrolanceolatum* showing the highest abundance in sub-zone 3c (14–32 %). *Achnanthidium australeexiguum*, present in sizable amounts throughout the core is almost absent in zone 3a. The characteristic feature of biozone 4 (220 cal. yrs b2k – recent) is the decrease in abundance of *Planothidium rostrolanceolatum* and the increase of *Sellaphora gracillima*. *Humidophila keiliorum* re-appears after its near absence in biozone 3. In biozones 3 and 4, productivity is intermediate and variable ranging 20×10^4 – 210×10^4 valves.g^{-1}.
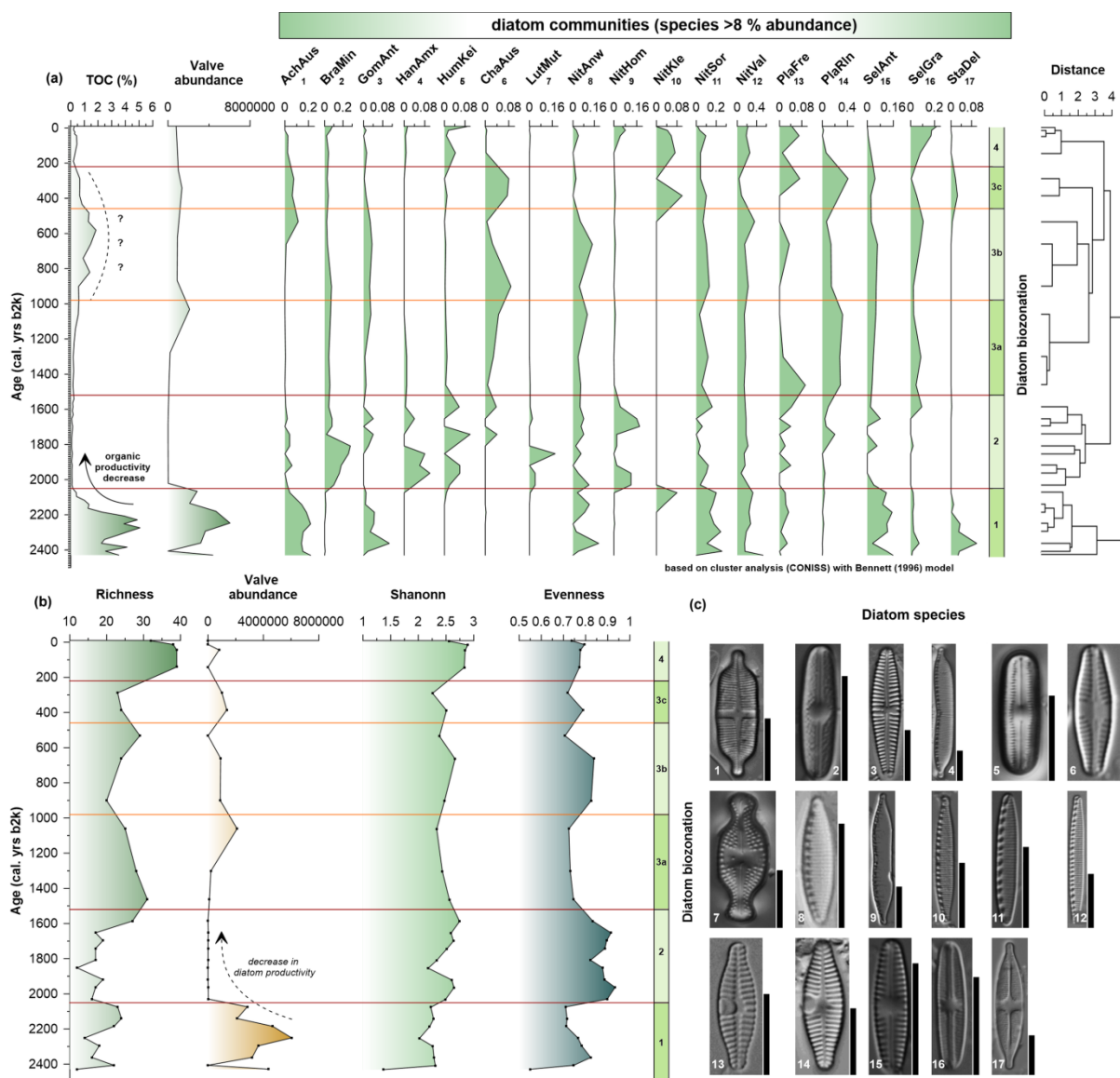
Figure 5.6 (a) Diatom stratigraphy of the Lake Anónima plotted against b2k time-scale supplemented by TOC (to the left). Zonation of the core is based on a CONISS analysis of the diatom species composition and significant (p = 0.05) group divisions are marked with red lines. Depicted are only diatom species with a relative abundance >8 %. (b) Diatom's indices – Species richness (number of taxa in the sample), Valve abundance (diatom valves per 1 gram of dry sediment), Shannon diversity (diversity of a population in which each member belongs to a unique group/species), Evenness (homogeneity of the species). (c) List of stated taxa and abbreviations (LM micrographs taken from Zidarova et al. 2016): [1] *Achnanthidium australexiguum* (*AchAus*), [2] *Brachysira minor* (*BraMin*), [3] *Gomphonema maritimo-antarcticum* (*GomAnt*), [4] *Hantzschia amphioxys f. muelleri* (*HanAmx*), [5] *Humidophila keiliorum* (*HumKei*), [6] *Chamaepinnularia australomediocris* (*ChaAus*), [7] *Luticola muticopsis* (*LutMut*), [8] *Nitzschia annewillemsiana* (*NitAnw*), [9] *Nitzschia homburgiensis* (*NitHom*), [10] *Nitzschia kleinteichiana* (*NitKle*), [11] *Nitzschia soratensis* (*NitSor*), [12] *Nitzschia velazqueziana* (*NitVal*), [13] *Planothidium frequentissimum* (*PlaFre*), [14] *Planothidium lanceolatum* (*PlaRln*), [15] *Sellaphora antarctica* (*SelAnt*), [16] *Sellaphora gracillima* (*SelGra*), [17] *Stauroneis delicata* (*StaDel*). Black scale bar above LM's represents 10 μm.

PCA

The principal component analysis (Figure 5.7) yields 72.42 % of the total explained variability (KMO value 0.79 – "middling" sample adequacy) and shows that variability throughout the core is driven primarily by PC1, with 53.28 % of explained variance. It bears a strong positive correlation with organic matter constituted by LE (*r* 0.97) and TOC (*r* 0.93). As well Rb/Sr (*r* = 0.91), Fe/Mn (*r* = 0.90), Zr/Ti (*r* = 0.84) and Si/Ti (BSi *r* = 0.80) elemental ratios have a substantial positive relationship, while binding between petrophysical proxies and PC1 is still important, but less intense (sand *r* = 0.79, χ_{FD} *r* = 0.58). An indirect link of PC1 is visible with a few elements (Fe, Ca, Sr, Zn *r* = −0.97; Ti *r* = −0.86; Al *r* = −0.79), as well as with elemental ratios Al/Si (*r* = −0.94) and petrophysical proxies (clay *r* = −0.65, χ_{976Hz} *r* = −0.95). Unlike the PC1, subsequent PC2 explains less (12.64 %) of the variability. It associates mainly with diatom assemblages (*Sellaphora antarctica r* = 0.63, *Sellaphora gracillima r* = 0.56, *Brachysira minor r* = 0.54), and diatom indices (Shannon, Evenness *r* = 0.95; richness *r* = 0.89), however, productivity has a smaller correlation coefficient with both components (PC1 *r* = 0.54, PC2 *r* = 0.49).
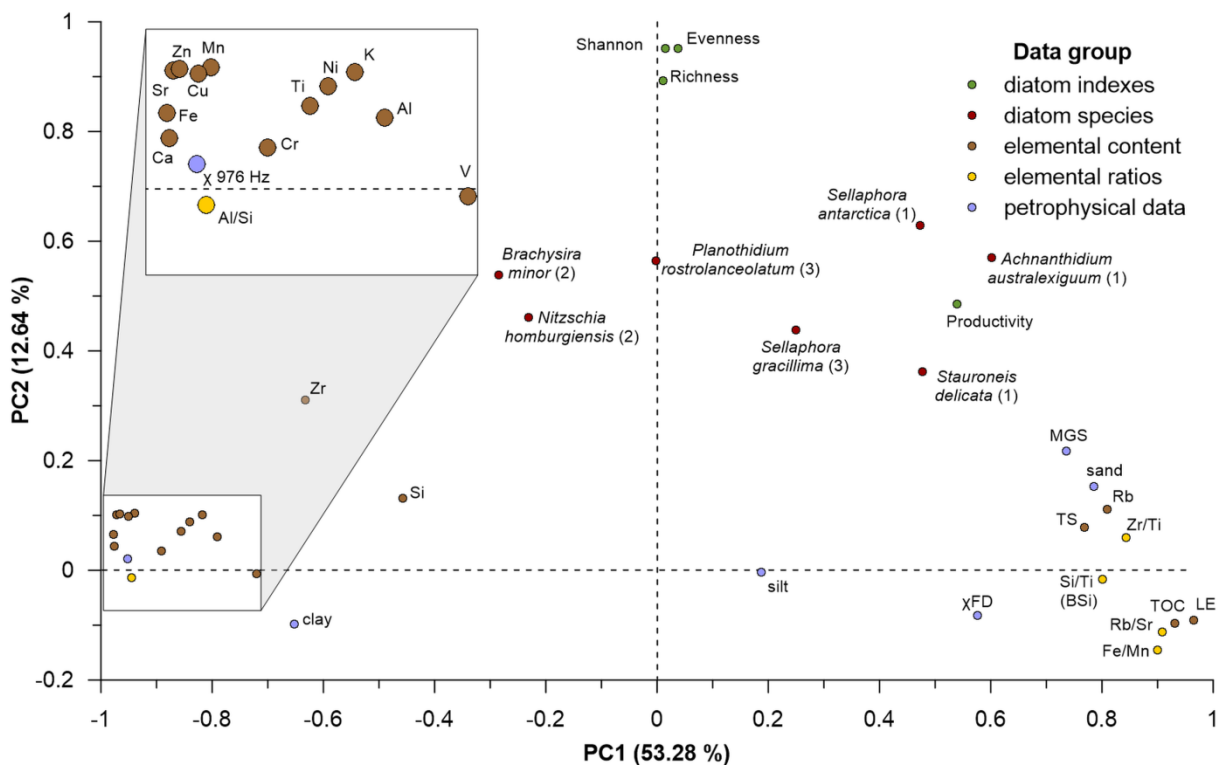

Figure 5.7 Two-dimensional biplot diagramming PC1 (53.28 %) against PC2 (12.64 %) along with all abiotic and selected biotic variables being colourised by data group. The number in brackets for the diatom name constitutes for which biozone the diatom species is ecologically representative. Note space distortion due to PC2 axis adjusted range.

Discussion

According to our age-depth model, the LA record extends over the last ~2450 years (sediment base 2440 cal. yrs b2k), thus spanning the environmental and climatic history of a significant part of the Late Holocene. Although the lowermost sample (66–67) yielded a very young age (1260 ± 80 ^{14}C yrs BP) that has been excluded out of the age-depth model, authors decided to do so because (a) sample has a very low concentration of carbon isotope, (b) sample is out of the chronostratigraphic sequence relative to the remaining ages, and (c) mutual correlation of LA proxies with the ice core (Mulvaney et al. 2012) and lacustrine (Sterken et al. 2012) archives using a presented age-depth model supports the timely consistent environmental change (Figure 5.8). The change revealed by multi-proxy records has been assumed to mark the onset of the Neoglacial phase associated with pronounced cooling (Mulvaney et al. 2012) and possible advances of local glaciers (e.g. Carrivick et al. 2012; Davies et al. 2014). Therefore, the correlation with other records brings a more robust timing for the onset of the Neoglacial period and a better record of associated environmental changes in the north-eastern AP region.

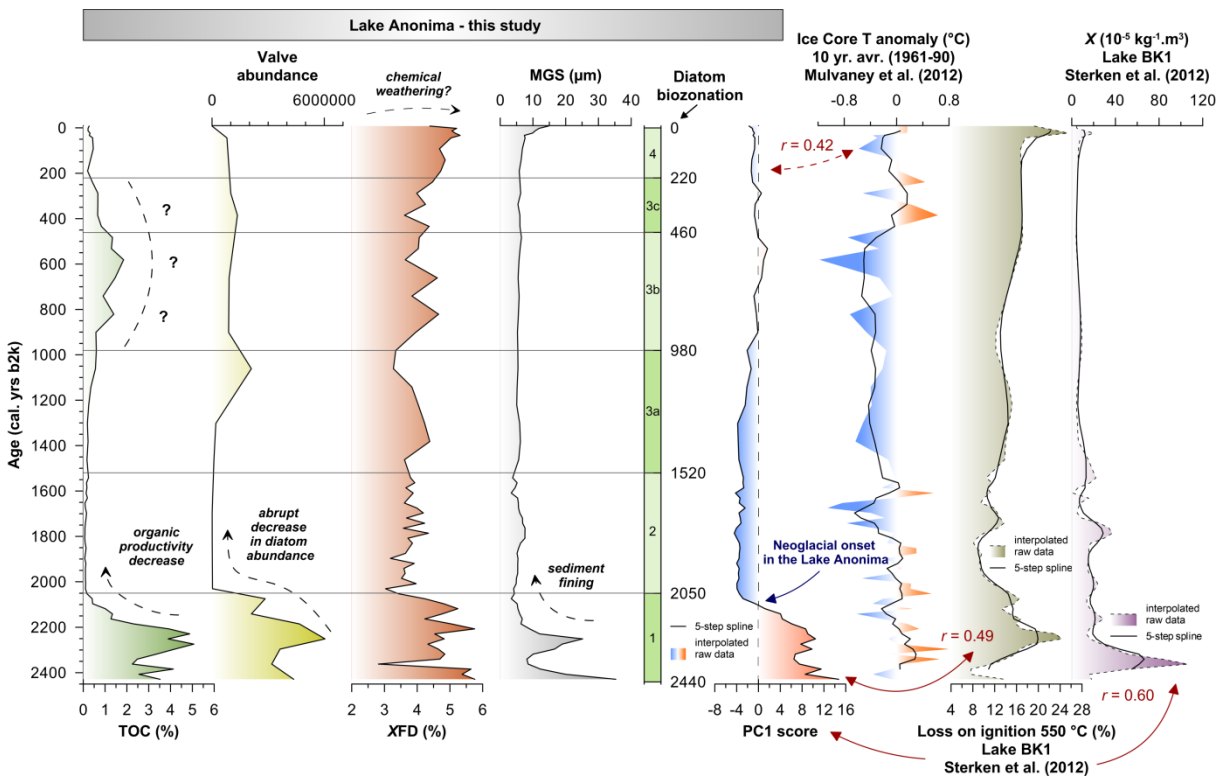**Figure 5.8** Regional comparison – the most explanatory proxies from Lake Anónima (TOC, valve abundance, χ_{FD}, MGS, PC1 score), 10-year averaged temperature anomalies from the Mt. Haddington ice-core (James Ross Island; Mulvaney et al. 2012) and loss on ignition with χ from composite lake sediment record (Beak Island; Sterken et al. 2012) related to interpolated (Lake Anónima) timescale.

Pre-2100 cal. b2k: Termination of the Late Holocene Hypsithermal

The pre-2100 cal. yrs b2k (Figure 5.8) period is distinguished by low χ (~3 × 10^{-9} $m^3.kg^{-1}$) caused by a low content of iron-bearing minerals (Evans & Heller 2003), suggesting generally warmer climatic conditions (Maher & Thompson 1999). A higher sand fraction (~13 %) and coarser MGS (~11.8 μm) associates with intensified siliciclastic input into the lake basin, presumably induced by increased thawing of local glaciers and the permafrost active layer and increased meltwater runoff. Increased material input coincides with a higher sedimentation rate (~0.45 $mm.yr^{-1}$), Zr/Ti, Al/Si ratios (Lopez et al. 2006; Taboada et al. 2006; Kylander et al. 2013) and change in chemical proxies (e.g., Rb/Sr values; Xu et al. 2010). Considering the previous 10% KOH sample's homogenization (removal of biogenic silica) for the grain-size analysis, together with enhanced material input and increased MGS, it is apparent that accumulated diatom frustules (biogenic silica productivity) in the lake bottom do not significantly influence the sedimentation rate, nor does their concentration enhance increased siliciclastic input in this period. This is supported by the opposite position of Si and BSi on the PC1 axis, as it proves that sediment, in general, contains both organic and lithogenic variation of silica.

The pre-2100 cal. yrs b2k period almost precisely corresponds with biozone 1 dominated by aquatic species, lasting until 2050 cal. yrs b2k. The higher abundance of *Achnanthidium australexiguum* (4–22 %) and *Stauroneis delicata* (0.2–10 %) suggests the presence of a large water-body with a circumneutral to weakly alkaline pH (7.2–7.7), low nutrient content and moderate (110–190 $μS.cm^{-1}$ *A. australexiguum*), or low (<100 $μS.cm^{-1}$ *S. delicata*) conductivity environment (Zidarova et al. 2016). *Sellaphora antarctica* is distinctive for large, stable lakes with silt drapes and algal mats on the lake floor and links to decreased conductivity level (<100 $μS.cm^{-1}$), circumneutral pH (7.3) and generally suggests enhanced vegetation growth around the lakes. All three species have the strongest relationship with productivity (*A. australexiguum* r = 0.83; *S. delicata* r = 0.58; *S. antarctica* r = 0.81). Since some species are not yet described in full detail, resulting from the remoteness of the studied area, its absolute ecological and physiological preferences are not known either. However, a stable and productive environment (O'Sullivan & Reynolds, 2008) is supported by the highest productivity (~299 × 10^4), TOC (max. 5.07 %), TS (max. 0.91 %) and Fe/Mn. Rather a non-diversified habitat is supported by Shannon (~2.2) and Evenness (~0.74) indices and low richness (~19). PC1 has the strongest influence (7.79) and explains the increase in organic matter (TOC r = 0.93, LE r = 0.97, TS r = 0.70, Fe/Mn r = 0.90) and BSi proxy (Si/Ti r = 0.80). Productivity relationship to PC1 is on the same level as to PC2, meaning complicated coherence with organic matter as well as with other indices. Proxies' outcomes suggest that positive PC1 very likely indicates for warmer climate conditions.

High $χ_{FD}$ (~4.72 %) is associated generally with a higher amount of superparamagnetic (SP) grains (diameter <0.3 μm; Dearing et al. 1996) and suggests intensified chemical weathering. However, since necessary conditions, e.g. mild precipitation, adequate aeration, nearly-neutral pH and comparatively warmer climate conditioning pedogenesis are not representative of Polar

environments (Worm 1998), the absolute origin of SP particles in the lake, located in a dry-maritime climate, remains ambiguous. Results from a previous study of a few sampling sites on Livingston Island in the humid-maritime climate of South Shetlands (Jordanova et al. 2016) indicate conditions favourable for pedogenesis (χ_{FD} >5 %). Based on the outcomes of the elemental and chemical composition of soils, Navas et al. (2008) conclude that the outcropping bedrock geology has the most substantial influence, thus physical weathering is the main driving force of pedogenesis in Antarctica. However, Haus et al. (2016) demonstrated that the driving element of chemical weathering within the studied region are enhanced by tephra deposits from Deception Island. Despite this, the χ_{FD} proxy in the context of extreme (Polar) environment requires further examination as some authors support a chemical weathering origin and generally "warmer climate" trigger since χ_{FD} substantially contributes to PC1 (r 0.58) and highly correlates with a sand fraction ($r = 0.71$). Rb/Sr connection with PC1 ($r = 0.91$) establishes proxy rather for chemical weathering than chemical changes (Xu et al. 2010) induced by various lithology.

The most substantial reconstructed 10-yr and 100-yr average anomalies (°C; AD 1961–1990 average) based on δD chronology from Mt. Haddington ice-core (Mulvaney et al. 2012) located near the summit of JRI, span 14,000 years of warmer climate (mid-late Holocene hypsithermal) terminating around 2550 yrs b2k (mean anomaly of 0.2 ± 0.2 °C). The record reveals that positive temperature anomalies at 10-yr averages mostly persist until 2000 yrs b2k and start to interchange with negative temperature anomalies at 10-yr averages at 2380 yrs b2k. Therefore, the period 2550–2000 yrs b2k regards as a transition from mid-late Holocene Hypsithermal to late Holocene Neoglacial phase with the most significant change at circa 2100 cal. yrs b2k (Figure 5.8).

Although the LA record slightly pre-dates the JRI ice-core record (proxy PC1 score − 5.2), both signals significantly correlate ($r = 0.42$), establishing LA as a regional low-frequency record of climate variability. The composite lake record from Beak Island (~20 km north of LA; Sterken et al. 2012) shows, although in comparison to LA pre-dated and persisting until 2170 cal. yrs b2k, the mid-late Holocene hypsithermal as well. Increased LOI$_{550}$ (loss-on-ignition at 550 °C – equivalent to TOC in LA record), total pigment concentration and higher sedimentation rate identify coherence with the LA record, which is supplemented by a significant correlation between PC1 score and LOI$_{550}$ ($r = 0.49$). Unlike in LA, Sterken et al. (2012) associate higher χ (tephra-removed) with a coarser fraction (coarse gravel – silt). Since Beak Island is, in general, consisted of volcanic rocks (porphyritic basalt, hyaloclastites) and therefore iron(-titanium) oxide-rich material, increased χ together with sedimentation rate during this period might be explained by seasonally active meltwater streams transporting heavier magnetic particles into the lake. Unlike in LA, the increased diversity is apparent and caused by the dominance of (yellow-)green algae and cyanobacteria supporting the development of a microbial mud community.

At nearby JRI, the mid-late Holocene hypsithermal is very likely recorded in the lake sediments as having occurred between 4250 and 3050 ^{14}C yrs b2k (Björck et al. 1996a), although chronologic resolution is limited to two to three ^{14}C dates per core and possible effect of kerogene from underlying Cretaceous strata may lead to higher ages. Of the three lakes (Terrapin, Boulder = Monolith, Keyhole lakes) being dated, only the latter could be considered as a reliable sequence. According to the authors, the Lake Terrapin record lacks several hundred years, while in Monolith Lake only the upper organic-rich horizon was dated (Björck et al. 1996a). It is important to mention that dated material (*Branchinecta* eggs) refers to the 10-cm core part of the profile, which implies substantial uncertainty.

Zale & Karlén (1989) set the climate deterioration at around 5050 ^{14}C yrs b2k with the subsequent phase of warming culminating around 1250–550 [14]C b2k. Non-corresponding data with the LA observations are probably caused by several factors, including LOI_{550}, used as only, thus overestimated climate variable, and non-absolutely dated lichen diameters originally supplementing absolute (^{14}C), though not calibrated, chronology.

Grid-styled collection of the bottom lake sediment samples (Chaparro et al. 2017) was intended to investigate present day sedimentary dynamic in the LA and not throughout the Late Holocene. Apart from hydrochemical results, a cluster analysis (CA) identifies two main depositional environments (coarse-fine sand facies and coarse-fine silt facies) within a lake. Depending on grain-size, further four groups (areas) are established, one of which – profundal – contains a sampling point for our study. Its characteristics agree with the data presented here and proves that the central area experiences rather stable and prolonged sedimentary changes (higher χ and TOC, silt and clay content), in comparison to the littoral area, which is highly influenced by short-term discharge changes transporting sand fraction to the coastal zone of the lake. Therefore, careful selection of coring position is supported by an enhanced risk of erosion and perturbation in the littoral zone, meaning that our record valuably neglects high-frequency signal, and oppositely records the low-frequency and more important regional variations.

Underestimating sufficiency quantity of dated samples (only two) for ^{14}C chronology is also introduced by Irurzun et al. (2017) studying the sediment core from Lake Esmeralda, southern Vega Island. Despite various magnetic properties being provided, it lacks ample level of detail in absolute chronology, supplementing relative paleointensity dating (RPI; five global modelled curves), which is necessary to correctly understand material deposition throughout a time. Taking into consideration circa 222.5-cm long core with three obtained ^{14}C ages in total, one of which (core's top sample) being extremely overaged (24,710 ± 170 ^{14}C BP) and second of which dated at 121 cm, it is double-sided to presume, with vast space for various re-deposition processes between the intervals, a valid chronostratigraphic sequence. The uncertainty of the Lake Esmeralda dating is also supplemented by establishing reservoir age to 5200 years based on a comparison of RPI (as non-absolute method) and ^{14}C dating. However, the chronology of Irurzun et al. (2017) is not confirmed by the optically-stimulated luminescence (OSL) dating supplemented by varve-like laminae counting from Lake Esmeralda as applied by Píšková et al. (*in press*).

Demonstrated controversy depicts that radiocarbon ages from north-eastern AP should be used with caution or had better be supplemented by following available dating techniques, e.g. OSL dating, or correlated with established chronologies as in this study. Apart from uncertainties resulting in incorrect placement on a timescale, the whole age-depth sequences must be produced in mathematical-statistical software, e.g., Clam (Blaauw et al. 2010) or Bacon (Blaauw & Christen 2011).

Timing of the Neoglacial onset in the north-eastern Antarctic Peninsula

Since PC1 of the LA multi-proxy record profoundly explains natural climate variability, negative scores correspond with climate deterioration conditions, while oppositely, positive values correlate with climatically optimal conditions. Together with the obtained age-depth sequence, the PC1 score is used for a specification of the precise timing of the Neoglacial onset in this area (Figure 5.8); the presence of it as such is indicated and proved by individual proxies and by the correlation with other lacustrine (Sterken et al. 2012) and ice-core (Mulvaney et al. 2012) records from north-eastern AP area. Hence, the adequate calibrated age of a zero score refers to the transition between the Late Holocene hypsithermal and Neoglacial phases, and it is achieved by interpolating age (b2k) of adjoining PC1's (−0.57 = 2096 cal. yrs b2k; 1.19 = 2118 cal. yrs b2k). The established age of the Neoglacial onset in LA is at 2103 (2σ: 2038–2184) cal. yrs b2k, or rounded 2100 (2σ: 2040–2180) cal. yrs b2k, respectively. To specify regional Neoglaciation onset, a significantly correlating 10-yr average temperature (°C) anomalies (1961–90) from the JRI ice-core (Mulvaney et al. 2012; *r* = 0.42) and LOI_{550} proxy from the Lake BK1 (Sterken et al. 2012; *r* = 0.49) on Beak Island are included. For correlation purposes, interpolated (LA timescale) comparative data were applied, while for further statistical procedures, an original dataset is used. The exact age of abrupt decrease in frequency of positive 10-yr temperature (°C) anomalies (2050 ± 200 yrs b2k) is used here as a marker for the beginning of the Neoglacial period in JRI ice-core, while in the Lake BK1 (Beak Island) an age of terminating peak in LOI_{550} proxy (2241 (2σ: 2078–2380) or rounded 2240 cal. yrs b2k) suggesting initiation of decrease in organic matter content (LOI_{550} 26.65 → 8.01 %) is applied as a marker in this record. Here, the originally published 2170 cal. yrs b2k is used for the Neoglaciation onset, while for the precise timing a new calibrated chronology (2240 ± 140 cal. yrs b2k; as shown in supplementary Figure 17g in Roberts et al. 2017) is used. To compare different ages of individual records, the method proposed by Ward & Wilson (1978) based on the Chi-square (χ^2) analysis is applied. Since the calculated value at *p* < 0.05 level confirmed data suitability, the calculated weighted mean denoted reference age for the Neoglacial onset in the north-eastern AP at 2120 ± 50 yrs. b2k.

Post-2100 cal. b2k: Neoglacial phase

The post-2100 cal. yrs b2k (Figure 5.8) phase is overall distinguished by opposite trends in several proxies within the LA record. It concerns an increase of χ (~13.07 × 10^{-9} $m^3.kg^{-1}$) suggesting higher content of para- and ferromagnetic matter (Evans & Heller 2003), as well as of clay content

(~31.3 %), which with respect to decreased MGS (~5.5 μm) indicates reduction of siliciclastic input. Tight link of χ with clay fraction (r = 0.65) suggests that susceptibility signal is associated with clay content variation, thus magnetic signal of the sedimentary infill is very likely carried by fine-grained minerals, e.g., magnetite and maghemite as it is supported by Chaparro et al. (2017). Considering (in comparison to the pre-2100 cal. yrs b2k period) a corresponding Al/Si (~0.26), Zr/Ti (~0.02; Lopez et al. 2006; Taboada et al. 2006; Kylander et al. 2013) and Rb/Sr (~0.04) values together with decreased χ_{FD} (~3.74 %) – latter two supposedly indicating chemical weathering (see *Pre-2100 cal. b2k: Termination of the Late Holocene Hypsithermal*) – the petrophysical proxies themselves presumably indicate climate deterioration conditions. The assumption is supported by low Fe/Mn (~59.31), TOC (~0.12 %) and TS below the limit of detection, together with overall PC1 negative scores (~ −3.38) inducing influence of colder climate conditions associated with limited meltwater, or precipitation input into the lake basin, which might have possibly afterwards resulted in lake level drop. Conditions are supported by BSi (~6.37) decrease and the presence of several (mainly aerophilic) diatom species (*Hantzschia amphyoxis*, *Luticola muticopsis*, *Humidophila keiliorum*) being clustered within a biozone 2 (2050–1520 cal. yrs b2k), which corresponds with a succession of climate deterioration in our record. Since (seasonal) drying of shallow lakes (Váczi et al. 2011) was described also in present time, occurrence of *Brachysira minor* referring to more barren (unproductive) conditions and *Nitzschia homburgiensis* being found besides in the littoral muddy drying area of JRI (unpublished data by Bart Van de Vijver), conclusively evidences, with respect to productivity decrease (~2.63 × 10^4) and higher Evenness (~0.87) a prolonged period of colder and drier conditions in the LA record.

Ambiguous PC2 suggests that indices (except productivity) together with the most representative non-biozone 1 species (biozone 2: *Brachysira minor*, *Nitzschia homburgiensis*; biozone 3: *Planothidium rostrolanceolatum, Sellaphora gracillima*) are to a substantial extent driven by other not yet known factor contributing to the primary climate dependent behaviour. Considering uncertainty associated with the absence of knowledge of the diatom assemblages occurring in non-analysed depths, authors believe that PC2 might represent chemically-induced changes conditioned by a different lithology. With respect to supposedly "chemical weathering proxy" Rb/Sr (see *Pre-2100 cal. b2k: Termination of the Late Holocene Hypsithermal*), PC2's variations are supported by Rb/Sr's position close to PC1 rather than PC2. The "chemical" hypothesis would imply that diatom assemblages in the biozones 2 and 3 as well as Richness (diversity), Shannon and Evenness are not primarily climate-dependent, although such assumption needs to be taken into consideration with caution and verified by further analyses. Since biotic (organic) proxies point out 50 years of difference, the response might represent a useful contribution to the understanding of how sensitively an aquatic diatom ecosystem reacts to changes in the non-catchment area.

The overall climate deterioration in the north-eastern AP was particularly reported by Mulvaney et al. (2012) and Sterken et al. (2012). Front mentioned depicts a high frequency of negative 10-yr

temperature (°C) anomalies initiating around 2050 yrs b2k, although precise timing gets more problematic as the pronounced cooling trend distinctive by frequent interchanging of positive and negative temperatures initiates already at around 2550 yrs b2k (see *Pre-2100 cal. b2k: Termination of the Late Holocene Hypsithermal*). Starting at 850 yrs b2k and terminating at 450 yrs b2k temperatures were on average 0.7 ± 0.3 °C and 1.8 ± 0.3 °C cooler than present on the annual and decadal timescale. Climate deterioration recorded on the Beak Island starting at 2170 cal. yrs b2k (Sterken et al. 2012) is evidenced by a decrease of total pigment concentration and LOI_{550}; in addition, supplemented by the presence of *Brachysira minor* and *Psammothidium abundans*. Simultaneous occurrence of *B. minor* in Lake BK1 as well as in LA enhances concurrent environmental signal consisting of low nutrients, low carbonate content and reduced productivity (the latter two are supported by low TOC content and diatom productivity). Despite 7.5–9.0 pH and 110–217 $\mu S.cm^{-1}$ conductivity (Zidarova et al. 2016), *B. minor* might have been according to Wetzel (2001) additionally associated with the acidic conditions originating in benthic mosses established on the lake floor. Importance of this species is evidenced by its use as a bioindicator for presented specifics also in subsequent lakes of the AP region (Gibson & Zale 2006). Published data from these two best correlating records correspond with a decreased PC1 score of LA supporting the Neoglaciation signal within this period in the north-eastern AP.

The manifestation of the Neoglacial period in Herbert Sound at 2550 cal. yrs b2k (Minzoni et al. 2015; see Figure 5.9) is mainly based on suppressed productivity (decrease in TOC), sediment fining and distinct diatom PCA component (presence of *Navicula* spp.) that cumulatively indicate water stratification, sea-ice and cold-water conditions. Increase in ice-rafted debris is supportive for higher glacial influence, and is relatively consistent with interpretations of both, the LA signal that indicates dry and cold environment, and adjacent studies, which suggest only partial advances of local glaciers (Carrivick et al. 2012) and increased sea-ice cover (Leventer et al. 1996; Pudsey & Evans 2001; Yoon et al. 2003; Heroy et al. 2008). Even though the diatom taxa in LA record refer to the Neoglacial cooling, the biostratigraphy with Minzoni et al. (2015) cannot be compared since freshwater and marine habitats reveal completely different physical-chemical characteristics. Together with a more optimal time resolution of lake records, this fact has been also a limitation when calculating the timing of the Neoglacial onset in the north-eastern AP.

Even though Björck et al. (1996a) is the most complex palaeolimnological study on JRI published so far, the data do not agree with the LA record. It is because Björck et al. (1996a) characterise a period 4250–3050 ^{14}C yrs b2k (MHH) by increased humidity and glacial advances, while a subsequent phase 3050–1200 ^{14}C yrs b2k is described in Björck et al. (1996a) by a cold and arid climate with ongoing glacier recession (see Figure 5.9). The period before 4250 ^{14}C yrs b2k is by Björck et al. (1996a) oppositely described by glacier retreat and precipitation starvation. However, all of this is in contrary to the Hjort et al. (1997), which present glacial and relative sea-level history based on the lithostratigraphy appended by radiocarbon dating and suggest that the northern part

of the James Ross Island experienced major glacial advance that culminated at circa 4750 cal. yrs b2k as a result of increased precipitation caused by enhanced cyclonic systems from the west. Although Hjort et al. (1997) describe the post-4750 cal. yrs b2k period as typical by a glacier retreat, out of which is, according to the study, a drier and colder climate onset deductible, it does not offer any further information on glacier-climate development in the Late Holocene that might be comparable with the LA record.

Björck et al. (1996a) also do not correspond with the re-modelled timing of Whisky Glacier (IJR-45) advances (after 1550 cal. yrs b2k; Carrivick et al. 2012; Davies et al. 2014) as well as with the overall climate cooling after 2050 cal. yrs b2k as recorded in our study and analysed by Davies et al. 2014. On top of that and with respect to LA record, the Davies et al. (2014) attributes a glacial expansion in the northern part of James Ross Island to temperature rather than precipitation changes (as proposed by Hjort et al. 1997) and shows that temperature decrease is essential for glacial growth. Based on various proxies we propose (see *Pre-2100 cal. b2k: Termination of the Late Holocene Hypsithermal*) a glacier recession and melting during the mid-late Holocene hypsithermal as this trend is highly correlated with the record from Mt. Haddington ice core (Mulvaney et al. 2012).

In light of glacier growth, Strelin et al. (2006) identify a six Holocene glacial advances on JRI, three of which are allegedly to occur after the mid-late Holocene hypsithermal (3950–3050 ^{14}C yrs b2k) and before LIA (~350 ^{14}C yrs b2k). Even though these relatively young post-hypsithermal moraines are undated (Johnson et al. 2011), some of them might be synchronous with the early stages of the LIA (Carrivick et al. 2012). Unfortunately, the past several hundred years of the LA development are reduced to a short-term proxy changes with decadal resolution implying lower informative ability for Little Ice Age (LIA), or other phenomena such as Medieval Climate Anomaly known rather from the northern hemisphere (Mann et al. 2008). To address changes for the most recent period, it is necessitated to obtain a high-resolution sequence supplemented by firm ^{210}Pb and [137]Cs (or other type of) dating, such as that from the Esmeralda Lake, Vega Island recently analysed in Pišková et al. (*in press*).

Neoglacial trend from the LA is also coherent with the reformation of Prince Gustav Ice Shelf at 1950 ^{14}C yrs b2k, which was preceded by a warm and seasonally open water in Prince Gustav Channel (Pudsey & Evans 2001; Pudsey et al. 2006; see Figure 5.9), while comparable to the south the Larsen-A Ice Shelf reformed at 1450 cal. yrs b2k (Brachfeld et al. 2003). Neoglacial appears to have occurred earlier in the area south of Joinville Island (Firth of Tay) as it experienced climatic cooling and variable sea-ice cover from 3550 cal. yrs b2k (Michalchuk et al. 2009), while the adjacent area north of Joinville Island (Perseverance Drift) shows a delayed initiation of the Neoglacial to the 1850 cal. yrs b2k (Kyrmanidou et al. 2018; see Figure 5.9).

Neoglacial in adjacent regions of the AP

Western AP

There is not much of evidence for the Neoglacial in the southwestern AP since this period is in George VI Ice Shelf within the Late Holocene poorly recognized (Clapperton & Sugden 1982; Smith et al. 2007). Even though Smith et al. (2007) declare that the ice shelf remained present throughout a middle and late Holocene (since 7780 cal. yrs b2k), evident variations in C/N and magnetic susceptibility in upper part of the profile are linked to certain, although not yet understood, environmental changes that might suggest manifestation of the Neoglacial as suggested by Smith et al. (2007).

Lake records from Marguerite Bay evidence the onset of Neoglacial conditions at 2680 (Narrows Lake, Pourquoi-Pas Island) and 2080 (Col Lake 1, Horseshoe Island) cal. yrs b2k based on a decline in TOC and sedimentation rate (Hodgson et al. 2013; see Figure 5.9), which is relatively consistent with the results reported in Neny Fjord after 2850 cal. yrs b2k (Allen et al. 2010), and in Lallemand Fjord at 2750 ^{14}C yrs b2k (increased sea-ice; Shevenell et al. 1996) and at 2930 cal. yrs b2k (Taylor et al. 2001). Further north in Barilari Bay, the Neoglacial have been suggested to occur within a 2865–780 cal. yrs b2k with a subsequent culmination of glacial expansion of fjord-wide ice shelf during the LIA at 780–132 cal. yrs b2k (Christ et al. 2015), while on Anvers Island this period initiated at 2650 ^{14}C yrs b2k (Leventer et al. 1996; see Figure 5.9).

The area of high interest, the Palmer Deep, contains a strong and resilient Late Holocene signal of the Neoglacial period that is based on records from several cores (Kirby et al. 1998; Domack et al. 2001, 2002; Ishman & Sperling 2002; Shevenell & Kennett 2002; Sjunneskog & Taylor 2002; Taylor & Sjunneskog 2002). The longest magnetic susceptibility record shows an earlier onset of the Neoglacial pattern at 3410 cal. yrs b2k, which is based on a decrease in accumulation rate and an increase of coarse fraction in ice-rafted debris (Domack et al. 2001, 2002; see Figure 5.9). This is accompanied by diatom abundance and assemblages that are consistent with alternating periods of more sea-ice and open water and surface water that were never warm long enough for subpolar species to become established (Sjunneskog & Taylor 2002; Taylor & Sjunneskog 2002). The neoglacial pattern in Palmer Deep, supplemented by a discussion on forcing mechanisms, is also evidenced from benthic foraminiferal isotope (Ishman & Sperling 2002; Shevenell & Kennett 2002) and petrophysical (Kirby et al. 1998) records.

The Bransfield Basin reveals a strong Neoglacial signal between the 2650 and 1650 cal. yrs b2k (Barnard et al. 2014), yet another record by Heroy et al. (2008) provides

the same timing (2650 cal. yrs b2k), but rather a subtle transition from the mid-late Holocene hypsithermal towards the Neoglacial (see Figure 5.9). Subsequently, Khim et al. (2002) provide an insight into Late Holocene climate oscillations including LIA.

South Shetland Islands, South Orkneys and South Georgia

Different temporal occurrence of the 'cold climate' period has been evidenced further north on the South Shetland Islands (John & Sugden 1971; Sugden & John 1973; Curl et al. 1980; Björck et al. 1991a, 1991b, 1993; Yoon et al. 2004; Hodgson & Convey, 2005; Hall 2007; Yoo et al. 2009; Milliken et al. 2009; Chu et al. 2017), South Orkneys (Jones et al. 2000) and South Georgia (Strother et al. 2015). However, only few provide a description of the Neoglacial phase distinctive by an abrupt change in various proxies that might be comparable with the LA record.

Lake sequence from Livingston Island shows a period of cold and arid climate between 1550 and 550 ^{14}C yrs. b2k (Björck et al. 1991a), which is characterised by a low accumulation rate for pollen and spores, low organic content and slow sedimentation rate. Another lake study from the same island unravels a similar trend as the climate deterioration onset is expressively suggested to ~2550 ^{14}C yrs b2k (Björck et al. 1993) with reference to the last 1450 years that are described as fairly arid and cold. Supportive to the LA record is that the Fe/Mn ratio during the last 2550 ^{14}C yrs b2k depicts a gradual decrease, the epiphytic flora data indicate relatively lower water levels, allochthonous/erosional variables suggest a fair decrease and the conditions are described as generally stable. Oppositely, moss bank archive from Elephant Island does not show any significant cooling in the Late Holocene, but instead rather short-term pulses at 5550–4350, ~3550 and 2550–2450 ^{14}C yrs. b2k that might be descriptive with the cold and arid characteristics (Björck et al. 1991b; see Figure 5.9).

Valuable, although not effectively comparable, tephrochronology from Livingston and Elephant Island (Björck et al. 1991c) is based on high induced isothermal remanent magnetization (HIRM) parameter, indicating various scale eruptions mainly originating from Deception Island within a period 4750–300 [14]C b2k. Unfortunately, more-detailed magnetic analyses were not performed in case of LA sediments, thus a reliable comparison is not possible. In so doing, it is not possible to establish a relationship between χ_{FD} and HIRM as well since SP grains do not have any remanent magnetization (Smirnov & Tarduno 2001). Therefore, it is not feasible to establish the merits of using χ_{FD} in the Polar environment.

Marine record from King George Island sets the Neoglacial period at 2750 cal. yrs b2k based on the distinct reduction of $LOI_{550°C}$ and TOC (Chu et al. 2017; see Figure 5.9), while another archive from Maxwell Bay indicates that Neoglacial phase started at 2650 cal. yrs b2k, although already

since 5650 cal. yrs b2k a continual decrease in sea-surface temperatures and the sea-ice cover increase was in progress (Milliken et al. 2009). The absence of LIA and presence of only subtle glacier variations on King George Island (Milliken et al. 2009) is not consistent with the glacial advance at 1500–1800 ^{14}C yrs b2k, allegedly caused by increased precipitation and warmer climate. Relative disagreement with Milliken et al. (2009) and Chu et al. (2017) is also represented by Yoo et al. (2009), which on a ~1500 ^{14}C yrs-old continental shelf record show the general absence of cold conditions with exception of LIA at 380 ^{14}C yrs b2k. The manifestation of LIA is supported by an advance of Collins Ice Cap (King George Island) at ~700 cal. yrs b2k (Hall 2007) and moraine-evidenced movement of local glaciers on the South Shetland Islands (John & Sugden 1971; Sugden & John 1973; Curl 1980). The LIA presence at 300–500 cal. yrs b2k is also very well constrained by Simms et al. (2012). Björck et al. (1996b) found evidence for neoglacial expansion within the last 800 ^{14}C years (roughly LIA) on the Livingston Island in a form of moraines transgressing earlier Holocene raised beaches.

Even though research in the sub-Antarctic zone (South Georgia, South Orkney Islands) illustrates a presence of the mid-late Holocene hypsithermal, there is generally a lack of explicit Neoglacial signal in the lake records (Jones et al. 2000; Hodgson & Convey 2005; Strother et al. 2015). Pollen sequence from South Georgia shows cooling at 2800 cal. yrs b2k, however at 1720 cal. yrs b2k a termed Medieval Warm Period had effect as it transferred warm and moist air from the west (Strother et al. 2015). The South Orkney Islands reveal overall the same trend since the cooling onset is recorded at 1350 ^{14}C yrs. b2k (Jones et al. 2000) and 1450 cal. yrs b2k (Hodgson & Convey 2005; see Figure 5.9).

There is, without any doubt, an evident but inconsistent Neoglacial signal in the AP region and sub-Antarctic zone, though the spatiotemporal occurrence is highly variable. Even though such a trend has been present, its character, timing, periodicity and manifestation in various regions on both, geosystems and ecosystems, substantially differ. Therefore, it is critical not only to create chronologies for as many localities as possible but also to establish a synchronised Neoglacial onset for each region that has comparable physical-geographic settings. Such an approach would generate a robust signal that might be reflected against possible driving factors for the climate patterns.
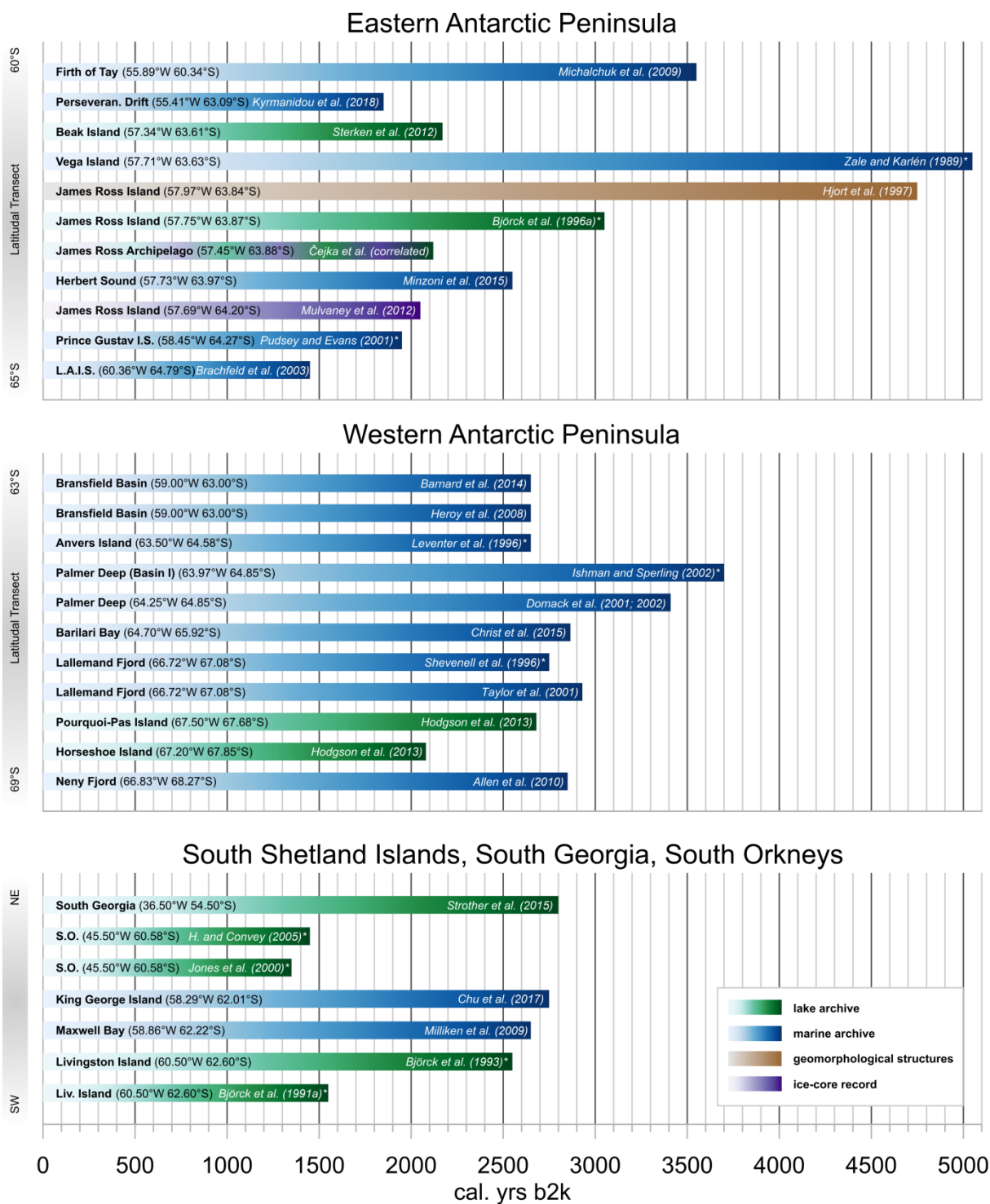
Figure 5.9 Overview of the Neoglacial onset in the Antarctic Peninsula region and adjacent sub-Antarctic zone. Included are only publications that (a) thoroughly link the terms as "cooling", "deterioration", "colder period" and/or "neoglacial" to the Neoglacial period following, or intersecting the mid-late Holocene Hypsithermal (~6000–2000 cal. yrs b2k), (b) concurrently and clearly suggest such a shift by majority of available (including stratigraphic) proxies, which are supplemented by absolute and original ages, (c) indicate Neoglacial depending on the ice shelf reformation (out of which a large-scale cooling pattern is deductible), (d) do not describe Neoglacial towards the glacial advances during the last millennium (LIA). Radiocarbon (non-calibrated) ages are marked with an asterisk.

Conclusions

The sediment core from LA is amongst the first records from the James Ross Archipelago (Zale & Karlén 1989; Björck et al. 1991a, 1996a; Sterken et al. 2012; Píšková et al. *in press*) to show a lacustrine response to the most recent environmental change of the Late Holocene in this area.

(1) The multi-proxy record from LA covers the last ~2450 years and captures the low-frequency regional-scale climate variability including the Late Holocene Hypsithermal and Neoglacial periods of the north-eastern AP.

(2) The climate deterioration phase in LA initiates at 2100 (2σ: 2040–2180) cal. yrs b2k reflecting climate deterioration, decreased siliciclastic input and suppressed biogenic productivity in the sedimentary archive.

(3) The correlation of three high-quality lacustrine and ice-core records depicts the Neoglacial period onset in the north-eastern AP at 2120 ± 50 yrs b2k.

(4) Calibration and proper verification of radiocarbon ages are absolutely crucial when considering high spatiotemporal climate variability and the overall lack of datable sample material in the AP region.

Data Availability

Datasets related to this article can be found

at http://dx.doi.org/10.17632/kbrxvfmhf6.1, an open-source online data repository hosted at Mendeley Data (Čejka et al. 2018)

[dataset] Čejka, Tomáš; Nývlt, Daniel; Kopalová, Kateřina; Bulínová, Marie (2018), "Timing of the Neoglacial onset on the north-eastern Antarctic Peninsula based on lacustrine archive: Dataset from Lake Anónima, Vega Island", Mendeley Data, v1, http://dx.doi.org/10.17632/kbrxvfmhf6.1.

REFERENCES

Allen, C.S., Oakes-Fretwell, L., Anderson, J.B., Hodgson, D.A. (2010). A record of Holocene glacial and oceanographic variability in Neny Fjord, Antarctic Peninsula. The Holocene, 20, 551-564.

Barnard, A., Wellner, J.S., Anderson, J.B. (2014). Late Holocene climate change recorded in proxy records from a Bransfield Basin sediment core, Antarctic Peninsula. Polar Research, 33, 1-13.

Bennett, K.D. (1996). Determination of the number of zones in a biostratigraphical sequence. New Phytologist, 132, 155-170.

Bentley, M.J., Hodgson, D.A., Smith, J.A., Ó Cofaigh, C., Domack, E.W., Larter, R.D., Roberts, S.J., Brachfeld, S., Leventer, A., Hjort, C., Hillenbrand, C-D., Evans, J. (2009). Mechanisms of Holocene palaeoenvironmental change in Antarctic Peninsula region. The Holocene, 19, 51-69.

Björck, S., Håkansson, H., Zale, R., Karlén, W., Jönssen, B. L. (1991a). A late Holocene lake sediment sequence from Livingston Island, south Shetland islands, with palaeoclimatic implications. Antarctic Science, 3, 61-72.

Björck, S., Malmer, N., Hjort, Ch., Sandgren, P., Ingólfsson, Ó., Wallén, B., Smith, R.I.L., Jónsson, B.L. (1991b). Stratigraphic and Paleoclimatic Studies of a 5500-Year-Old Moss Bank on Elephant Island, Antarctica. Arctic and Alpine Research, 23, 361-374.

Björck, S., Sandgren, P., Zale, R. (1991c). Late Holocene tephrochronology of the northern Antarctic Peninsula. Quaternary Research 36, 322-328.Björck, S., Håkansson, H, Olssen, S., Banekow, L., Janssens, J., 1993. Paleoclimatic studies in south Shetland islands, Antarctica, based on numerous stratigraphic variables in lake sediments. Journal of Paleolimnology, 8, 233-272.

Björck, S., Olsson, S., Ellis-Evans, C., Håkansson, H., Humlum, O., de Lirio, J.M. (1996a). Late Holocene palaeoclimatic records from lake sediments on James Ross island, Antarctica. Palaeogeography, Palaeoclimatology, Palaeoecology, 121, 195-220.

Björck, S.C.G., Hjort, C., Ingólfsson, O., Zale, R., Ising, J. (1996b). Holocene deglaciation chronology from lake sediments. In: Geomorphological Map of Byers Peninsula, Livingston Island. British Antarctic Survey, Bas Geomap Series Sheet 5-a, Cambridge, pp. 49-51.

Blaauw, M., Christen, J.A. (2011). Flexible paleoclimate age-depth models using an autoregressive gamma process. Bayesian Analysis, 6, 457-474.

Blaauw, M. (2010). Methods and code for 'classical' age-depth modeling of radiocarbon sequences. Quaternary Geochronology, 5, 512-518.

Blott, S.J., Pye, K. (2001). GRADISTAT: a grain size distribution and statistics package for the analysis of unconsolidated sediments. Earth Surface Processes and Landforms, 26, 1237-1248.

Brachfeld, S., Domack, E., Kissel, C., Laj, C., Leventer, A., Ishman, S.E., Gilbert, R., Camerlenghi, A., Eglinton, L.B. (2003). Holocene history of the Larsen-A Ice Shelf constrained by geomagnetic paleointensity daing. Geology, 31, 749-752.

Carrivick, J.L., Davies, B.J., Glasser, N.F., Nývlt, D., Hambrey, M.J. (2012). Late-Holocene changes in character and behaviour of land-terminating glaciers on James Ross Island, Antarctica. Journal of Glaciology, 58, 1176-1190.

Chaparro, M.A.E., Chaparro, M.A.E., Córdoba, F.E., LeComte, K.L., Gargiulo, J.D., Barrios, A.M., Urán, G.M., Manograsso Czalbowski, N.T., Lavat, A., Böhnel, H.N. (2017). Sedimentary analysis and magnetic properties of Lake Anonima, Vega Island. Antarctic Science, 29, 1-16.

Christ, A.J., Talaia-Murray, M., Elking, N., Domack, E.W., Leventer, A., Lavoie, C., Brachfeld, S., Yoo, K-C, Gilbert, R., Jeong, S-M., Petrushak, S., Wellner, J., LARISSA Group (2015). Late Holocene glacial advance and ice shelf growth in Barilari Bay, Graham Land, west Antarctic Peninsula. GSA Bulletin, 127, 297-315.

Chu, Z., Sun, L., Wang, Y., Huang, T., Zhou, X. (2017). Depositional environment and climate changes during the Holocene in Grande Valley, Fildes Peninsula, King George Island, Antarctica. Antarctic Science, 29, 545-554.

Clapperton, C.M., Sugden, D.E., 1982. Late Quaternary Glacial History of George VI Sound Area, West Antarctica. Quaternary Research 18, 243-267.Cook, J.L., Fox, A.J., Vaughan, D.G., Ferrigno, J.G. (2005). Retreating Glacier Fronts on the Antarctic Peninsula over the Past Half-Century. Science, 308, 541-544.

Curl, J.E. (1980). A glacial history of the South Shetland Islands, Antarctica. Institute of Polar Studies Report, 63, 1-129.

Davies, B.J., Glasser, N.F., Carrivick, J.L., Hambrey, M.J., Smellie, J.L., Nývlt, D. (2013). Landscape evolution and ice-sheet behaviour in a semi-arid polar environment: James Ross Island, NE Antarctic Peninsula. In: Hambrey, M.J., Barker, P.F., Barrett, P.J., Bowman, V., Davies, B., Smellie, J.L., Tranter, M. (Eds.), Antarctic Palaeoenvironments and Earth-Surface Processes. Geological Society, London, pp. 353-395.

Davies, B.J., Golledge, N.R., Glasser, N.F., Carrivick, J.L., Ligtenberg, S.R.M., Barrand, N.E., Van der Broeke, M.R., Hambrey, M.J., Smellie, J.L. (2014). Modelled glacier response to centennial temperature and precipitation trends on the Antarctic Peninsula. Nature Climate Change, 4, 993-998.

Dearing, J.A., Dann, R.J.L., Hay, K., Lees, J.A., Loveland, P.J. Maher, B.A. O'Grady, K. (1996). Frequency-dependent susceptibility measurements of environmental materials. Geophysical Journal International, 124, 228-240.

Domack, E.W., Leventer, A., Dunbar, R., Taylor, F., Brachfeld, S., Sjunneskog, C., ODP Leg 178 Scientific Party (2001). Chronology of the Palmer Deep site, Antarctic Peninsula: a Holocene palaeoenvironmental reference for the circum-Antarctic. The Holocene, 11, 1-9.

Domack, E.W., Duran, D., McMullen, K., Gilbert, R., Leventer, A. (2002). Sediment lithofacies from beneath the Larsen B Ice Shelf: Can we detect ice shelf fluctuation? Eos (Transactions, American Geophysical Union), 83, F301.

Engel Z., Nývlt D., Láska K. (2012). Ice thickness, areal and volumetric changes of Davies Dome and Whisky Glacier in 1979–2006 (James Ross Island, Antarctic Peninsula). Journal of Glaciology, 58, 904-914.

Ermolin, E., De Angelis, H., Skvarca, P. (2002). Mapping of permafrost on Vega Island, Antarctic Peninsula, using aerial photography and satellite image. Annals of Glaciology, 34, 184-188.

Evans, M., Heller, F. (2003). Environmental Magnetism: Principles and applications of enviromagnetics. Academic press, New York.

Folk, R.L., Ward, W.C. (1957). Brazos River bar [Texas]; a study in the significance of grain size parameters. Journal of Sedimentary Research, 27, 3-26.

Gibson, J.A.E., Zale, R. (2006). Holocene development of the fauna of Lake Boeckella, northern Antarctic Peninsula. The Holocene, 16, 625-634.

Hall, B.L. (2007). Late-Holocene advance of the Collins Ice Cap, King George Island, South Shetland Islands. The Holocene, 17, 1253-1258.

Hall, B.L. (2009). Holocene glacial history of Antarctica and the sub-Antarctic islands. Quaternary Science Reviews, 28, 2213-2230.

Haus, N., Wilhelma, K., Bockheim, J., Fournelle, J., Miller, M. (2016). A case for chemical weathering in soils of Hurd Peninsula, Livingston Island, South Shetland Islands, Antarctica. Geoderma, 263, 185-194.

Hendey, N.I. (1964). An introductory account of the smaller algae of British coastal waters. Part V. Bacillariophyceae (Diatoms). Her Majesty's Stationery Office, London.

Heroy, D.C., Sjunneskog, C., Anderson, J.B. (2008). Holocene climate change in the Bransfield Basin, Antarctic Peninsula: evidence from sediment and diatom analysis. Antarctic Science, 20, 69-87.

Hjort, C., Ingólfsson, Ó., Möller, P., Lirio, J.M. (1997). Holocene glacial history and sea-level changes on James Ross Island, Antarctic Peninsula. Journal of Quaternary Science, 12, 259-273.

Hodgson, D.A., Convey, P. (2005). A 7000-year Record of Oribatid Mite Communities on a Maritime-Antarctic Island: Responses to Climate Change. Arctic, Antarctic, and Alpine Research, 37, 239-245.

Hodgson, D.A., Roberts, S.J., Smith, J.A., Verleyen, E., Sterken, M., Labarque, M., Sabbe, K., Vyverman, W., Allen, C.S., Leng, M.J., Bryant, C. (2013). Late Quaternary environmental changes in Marguerite Bay, Antarctic Peninsula, inferred from lake sediments and raised beaches. Quaternary Science Reviews, 68, 216-236.

Hogg, A.G., Hua, Q., Blackwell, P.G., Niu, M., Buck, C.E., Guilderson, T.P., Heaton, T.J., Palmer, J.G., Reimer, P.J., Reimer, R.W., Turney, C.S.M., Zimmerman, S.R.J. (2013). SHCal13 southern hemisphere calibration, 0–50,000 cal. BP. Radiocarbon 55, 1889-1903.

Hrbáček, F., Nývlt, D., Láska, K. (2017). Active layer thermal dynamics at two lithologically different sites on James Ross Island, Eastern Antarctic Peninsula. Catena, 149, 592-602.

Hrbáček, F., Vieira, G., Oliva, M., Balks, M., Guglielmin, M., de Pablo, M.Á., Molina, A., Ramos, M., Goyanes, G., Meiklejohn, I., Abramov, A., Demidov, N., Fedorov-Davidov, D., Lupachev, A., Rivkina, E., Láska, K., Kňažková, M., Nývlt, D., Raffi, R., Strelin, J., Sone, T., Fukui, K., Dolgikh, A., Zazovskaya, E., Mergelov, N., Osokin, N., Miamin, V. (in press). Active layer monitoring in Antarctica: an overview of results from 2006 to 2015. Polar Geography, 1-16.

Hua, Q., Barbetti, M., Rakowski, A.Z. (2013). Atmospheric radiocarbon for the period 1950–2010. Radiocarbon, 55, 2059-2072.

Ingólfsson, Ó., Hjort, Ch., Berkman, P.A., Björck, S., Colhoun, E., Goodwin, I.D., Hall, B., Hirakawa, K., Melles, M., Möller, P., Prentice, M.L. (1998). Antarctic Glacial History Since the Last Glacial Maximum: An Overview of the Record on Land. Antarctic Science, 10, 326-344.

Irurzun, M.A., Chaparro, M.A.E., Sinito, A.M., Gogorza, C.S.G., Nuñez, H., Nowaczyk, N.R., Böhnel, H.N. (2017). Relative palaeointensity and reservoir effect on Lake Esmeralda, Antarctica. Antarctic Science 29, 356-368.

Ishman, S.E, Sperling, M.R. (2002). Benthic foraminiferal record of Holocene deep-water evolution in the Palmer Deep, western Antarctic Peninsula. Geology, 30, 435-438.

John, B.S., Sugden, D.E. (1971). Raised marine features and phases of glaciation in the South Shetland Islands. British Antarctic Survey Bulletin, 24, 45-111.

Johnson, J.S., Bentley, M.J., Roberts, S.J., Binnie, S.A., Freeman, S.P.H.T. (2011). Holocene deglacial history of the northeast Antarctic Peninsula – A review and new chronological constraints. Quaternary Science Reviews, 30, 3791-3802.

Jones, V.J., Hodgson, D.A., Chepstow-Lusty, A. (2000). Palaeolimnological evidence for marked Holocene environmental changes on Signy Island, Antarctica. The Holocene, 10, 43-60.

Jordanova, N. (2016). Soil Magnetism: Applications in Pedology, Environmental Science and Agriculture. Academic Press, San Diego.

Juggins, S. (2017). rioja: Analysis of Quaternary Science Data, R package version, (0.9-15.1).

Khim, B-K. (2002). Unstable Climate Oscillations during the Late Holocene in the Eastern Bransfield Basin, Antarctic Peninsula. Quaternary Research, 58, 234-245.

Kirby, M.E., Domack, E.W., McClennen, C.E. (1998). Magnetic stratigraphy and sedimentology of Holocene glacial marine deposits in the Palmer Deep, Bellingshausen Sea, Antarctica: implications for climate change? Marine Geology, 152, 247-259.

Kylander, M.E., Klaminder, J., Wohlfarth, B., Löwemark, L. (2013): Geochemical responses to paleoclimatic changes in southern Sweden since the late glacial: the Hässeldata Port lake sediment record. Journal of Paleolimnology, 50, 57-70.

Kyrmanidou, A., Vadman, K.J., Ishman, S.E., Leventer, A., Brachfeld, S., Domack, E.W., Wellner, J.S. (2018). Marine Micropaleontology, 141, 10-22.

Leventer, A., Domack, E.W., Ishman, S.E., Brachfeld, S., McClennen, C.E., Manley, P. (1996). Productivity cycles of 200–300 years in the Antarctic Peninsula region: understanding linkages among the sun, atmosphere, oceans, sea ice, and biota. Geological Society of America Bulletin 108, 1626-1644.Lopez, P., Navarro, E., Marce, R., Ordoñez, J., Caputo, L., Armengol, J., 2006. Elemental ratios in sediments as indicators of ecological processes in Spanish reservoirs. Limnetica, 25, 499-512.

Maher, B.A., Thompson, R. (1999). Quaternary climates, environments and magnetism. Cambridge University Press, Cambridge.

Mann, M., Zhang, Z., Hughes, M.K., Bradley, R.S., Miller, S.K., Rutherford, S., Ni, F. (2008). Proxy-based reconstructions of hemispheric and global surface temperature variations over the past two millennia. Proceedings of the National Academy of Sciences, 105, 252-257.

Marinsek, S., Ermolin, E. (2015). 10-year mass balance by glaciological and geodetic methods of Glaciar Bahía del Diablo, Vega Island, Antarctic Peninsula. Annals of Glaciology, 56, 141-146.

Michalchuk, B.R., Anderson, J.B., Wellner, J.S., Manley, P.L., Majewski, W., Bohaty, S. (2009). Holocene climate and glacial history of the northeastern Antarctic Peninsula: the marine sedimentary record from a long SHALDRIL core. Quaternary Science Reviews, 28, 3049-3065.

Milliken, K.T., Anderson, J.B., Wellner, J.S., Bohaty, S.M., Manley, P.L. (2009). High-resolution Holocene climate record from Maxwell Bay, South Shetland Islands, Antarctica. GSA Bulletin, 121, 1711-1725.

Minzoni, R.T., Anderson, J.B., Fernandez, R., Wellner, J.S. (2015). Marine record of Holocene climate, ocean, and cryosphere interactions: Herbert Sound, James Ross Island, Antarctica. Quaternary Science Reviews, 129, 239-259.

Mulvaney, R., Abram, N.J., Hindmarsh, R.C.A., Arrowsmith, C., Fleet, L., Triest, J., Sime, L. C., Alemany, O., Foord, S. (2012). Recent Antarctic Peninsula warming relative to Holocene climate and ice-shelf history. Nature, 489, 141-144.

Navas, A., López-Martínez, J., Casas, J., Machín, J., Durán, J., Serrano, E., Cuchi, J.-A., Mink, S. (2008). Soil characteristics on varying lithological substrates in the South Shetland Islands, maritime Antarctica. Geoderma, 144, 123-139.

Nedbalová, L., Nývlt, D., Lirio, J. M., Kavan, J., Elster, J. (2017). Current distribution of Branchinecta gaini on James Ross Island and Vega Island. Antarctic Science, 29, 341-342.

Nývlt, D., Braucher, R., Engel, Z., Mlčoch, B., ASTER Team (2014). Timing of the Northern Prince Gustav Ice Stream retreat and the deglaciation of northern James Ross Island, Antarctic Peninsula during the last glacial–interglacial transition. Quaternary Research, 82, 441-449.

O'Sullivan, P., Reynolds, C.S. (2008). The lakes handbook: lake restoration and rehabilitation. John Wiley & Sons. Hoboken.

Øvstedal, D.O., Lewis-Smith, R.I. (2001). Lichens of Antarctica and South Georgia: a guide to their identification and ecology. Cambridge University Press, Cambridge.

Pielou, E.C. (1966). The measurement of diversity in different types of biological collections. Journal of Theroretical Biology, 13, 131-144.

Píšková, A., Roman, M., Bulínová, M., Pokorný, M., Sanderson, D., Cresswell, A., Lirio, J.M., Coria, S.H., Nedbalová, L., Lami, A., Musazzi, S., Van de Vijver, B., Nývlt, D., Kopalová, K. (in press). Late-Holocene palaeonvironmental changes at Lake Esmeralda (Vega Island, Antarctic Peninsula) based on a multi-proxy analysis of laminated lake sediment. The Holocene, https://doi.org/10.1177/0959683619838033

Pritchard, H.D., Vaughan, D.G. (2007). Widespread acceleration of tidewater glaciers on the Antarctic Peninsula. Journal of Geophysical Research: Earth Surface, 112, 1-10.

Pudsey, C.J., Evans, J. (2001). First survey of Antarctic sub-ice shelf sediments reveals Mid-Holocene ice shelf retreat. Geology, 29, 787-790.

Pudsey, C.J., Murray, J.W., Appleby, P., Evans, J. (2006). Ice shelf history from petrographic and foraminiferal evidence, Northeast Antarctic Peninsula. Quaternary Science Reviews, 25, 2357-2379.

Quayle, W.C., Peck, L.S., Peat, H., Ellis-Evans, J.C., Harrigan, P.R. (2002). Extreme responses to climate change in Antarctic lakes. Science, 295, 645-645.

Reimer, P.J., Brown, T.A., Reimer, R.W. (2004). Discussion: reporting and calibration of post-bomb 14C data. Radiocarbon 46, 1299-1304.

Roberts, E.M., Lamanna, M.C., Clarke, J.A., Meng, J., Gorscak, E., Sertich, J.J.W., O'Connor, P.M., Claeson, K.M., MacPhee, R.D.E. (2014). Stratigraphy and vertebrate paleoecology of Upper Cretaceous–? lowest Paleogene strata on Vega Island, Antarctica. Palaeogeography, Palaeoclimatology, Palaeoecology, 402, 55-72.

Roberts, S.J., Monien, P., Foster, L.C., Loftfield, J., Hocking, E.P., Schnetger, B., Pearson, E.J., Juggins, S., Fretwell, P., Ireland, L., Ochyra, R., Haworth, A.R., Allen, C.S., Moreton, S.G., Davies, S.J., Brumsack, H-J., Bentley, M.J., Hodgson, D.A. (2017). Past Penguin colony responses to explosive volcanism on the Antarctic Peninsula. Nature Communications, 8, 14914.

Robinson, S.A., Wasley, J., Tobin, A.K. (2003). Living on the edge-plants and global change in continental and maritime Antarctica. Global Change Biology, 9, 1681-1717.

Ross, R., Cox, E.J., Karayeva, N.I., Mann, D.G., Paddock, T.B.B., Simonsen, R., Sims, P.A. (1979). An amended terminology for the siliceous components of the diatom cell. Nova Hedwigia, 64, 513-533.

Round, F.E., Crawford, R.M., Mann, D.G. (1990). The diatoms: biology and morphology of the genera. Cambridge, Cambridge University Press.

Scambos, T., Fricker, H.A., Liu, C.C., Bohlander, J., Fastook, J., Sargent, A., Massom, R., Wu, A.M. (2009). Ice shelf disintegration by plate bending and hydro-fracture: Satellite observations and model results of the 2008 Wilkins ice shelf break-ups. Earth and Planetary Science Letters, 280, 51-60.

Shannon, C.E., Weaver, W. (1949). The mathematical theory of communication. Urbana University Press, Illinois.

Shevenell, A.E., Domack, E.W., Kernan, G.M. (1996). Record of Holocene palaeoclimate change along the Antarctic Peninsula: evidence from glacial marine sediments, Lallemand Fjord. Papers and Proceedings of the Royal Society of Tasmania, 130, 55-64.

Shevenell, A.E., Kennett, J.P. (2002). Antarctic Holocene climate change: A benthic foraminiferal stable isotope record from Palmer Deep. Paleoceanography 17, 1-12.Simms, A.R., Ivins, E.R., DeWitt, R., Kouremenos, P., Simkins, L.M., 2012. Timing of the most recent Neoglacial advance and retreat in the South Shetland Islands, Antarctic Peninsula: insights from raised beaches and Holocene uplift rates. Quaternary Science Reviews, 47, 41-55.

Sjunneskog, C., Taylor, F. (2002). Postglacial marine diatom record of the Palmer Deep, Antarctic Peninsula (ODP Leg 178, Site 1098) 1. Total diatom abundance. Paleoceanography, 17, 1-8.

Smellie, J.L., Johnson, J.S., McIntosh, W.C., Esser, R., Gudmundsson, M.T., Hambrey, M.J., van Wyk de Vries, B. (2008). Six million years of glacial history recorded in volcanic lithofacies of the James Ross Island Volcanic Group, Antarctic Peninsula. Palaeogeography, Palaeoclimatology, Palaeoecology, 260, 122-148.

Smellie, J.L., Johnson, J.S., Nelson, A.E. (2013). Geological map of James Ross Island. 1. James Ross Island Volcanic Group (1:125 000 scale). BAS GEOMAP 2 Series, Sheet 5. British Antarctic Survey, Cambridge.

Smirnov, A.V., Tarduno, J.A. (2001). Estimating superparamagnetism in marine sediments with the time dependency of coercivity of remanence. Journal of Geophysical Research. Solid Earth, 106, 135-143.

Smith, J.A., Bentley, M.J., Hodgson, D.A., Roberts, S.J., Leng, M.J., Lloyd, J.M., Barrett, M.S., Bryant, C., Sugden, D.E. (2007). Oceanic and atmospheric forcing of early Holocene ice shelf retreat, George VI Ice Shelf, Antarctica Peninsula. Quaternary Science Reviews, 26, 500-516.

Smith, D.A., Klinck, J.M. (2002). Water properties on the west Antarctic Peninsula continental shelf: a model study of effects of surface fluxes and sea ice. Deep Sea Research Part II: Topical Studies in Oceanography, 49, 4863-4886.

Smol, J.P., Douglas, M.S. (2007). From controversy to consensus: making the case for recent climate change in the Arctic using lake sediments. Frontiers in Ecology and the Environment, 5, 466-474.

Sterken, M., Roberts, S.J., Hodgson, D.A., Vyverman, W., Balbo, A.L., Sabbe, K., Moreton, S.G., Verleyen, E. (2012). Holocene glacial and climate history of Prince Gustav Channel, northeastern Antarctic Peninsula. Quaternary Science Reviews, 31, 93-111.

Strelin, J.A., Sone, T., Mori, J., Torielli, C.A., Nakamura, T. (2006). New Data Related to Holocene Landform Development and Climatic Change from James Ross Island, Antarctic Peninsula. In: Fütterer, D.K., Damaske, D., Kleinschmidt, G., Miller, H., Tessensohn, F. (Eds.), Antarctica: Contributions to global earth sciences, Springer-Verlag, Berlin, pp. 477.

Strother, S.L., Salzmann, U., Roberts, S.J., Hodgson, D.A., Woodward, J., Nieuwenhuyze, W.V., Verleyen, E., Vyverman, W., Moreton, S.G. (2015). Changes in Holocene climate and the intensity of Southern Hemisphere Westerly Winds based on a high-resolution palynological record from sub-Antarctic South Georgia. The Holocene, 25, 263-279.

Sugden, D.E., John, B.S. (1973). The ages of glacier fluctuations in the South Shetland Islands, Antarctica. In: van Zinderen Bakker, E.M. (Eds), Palaeoecology of Africa, the surrounding islands and Antarctica. Balkema, Cape Town, pp. 254.

Taboada, T., Cortizas, A.M., García, C., García-Rodeja, E. (2006). Particle-size fractionation of titanium and zirconium during weathering and pedogenesis of granitic rocks in NW Spain. Geoderma, 131, 218-236.

Taylor, F., Sjunneskog, C. (2002). Postglacial marine diatom record of the Palmer Deep, Antarctic Peninsula (ODP Leg 178, Site 1098) 2. Diatom assemblages. Paleoceanography, 17, 1-12.

Taylor, F., Whitehead, J., Domack, E.W. (2001). Holocene paleoclimate change in the Antarctic Peninsula: evidence from the diatom, sedimentary and geochemical record. Marine Micropaleontology, 41, 25-43.

Vaasma, T. (2008). Grain-size analysis of lacustrine sediments: a comparison of pre-treatment methods. Estonian Journal of Ecology, 57, 231-243.

Váczi, P., Barták, M., Nedbalová, L., Elster, J. (2011). Comparative analysis of temperature courses in Antarctic lakes of different morphology: Study from James Ross Island, Antarctica. Czech Polar Reports, 1, 78-87.

van der Werff A. (1955). A new method of concentrating and cleaning diatoms and other organisms. Verhandlungen Internationalen Vereinigung für Theoretische und Angewandte Limnologie, 2, 276-277.

Van Lipzig, N.P.M., King, J.C., Lachlan-Cope, T.A., van der Broeke, M.R. (2004). Precipitation, sublimation and snow drift in the Antarctic Peninsula region from a regional atmospheric model. Journal of Geophysical Research, 109, 1-16.

Vaughan, D.G., Marshall, G., Connolley, W.M., Parkinson, C., Mulvaney, R., Hodgson, D.A., King, J.C., Pudsey, C.J., Turner, J., Wolff, E. (2003). Recent rapid regional climate warming on the Antarctic Peninsula. Climatic Change, 60, 243-274.

Vaughan, D.G. (2006). Recent trends in melting conditions on the Antarctic Peninsula and their implications for ice-sheet mass balance and sea level. Arctic, Antarctic, and Alpine Research, 38, 147-152.

Ward, G.K., Wilson, S.R. (1978). Procedures for comparing and combining radiocarbon age determinations: a critique. Archaeometry, 20, 19-31.

Wetzel, R.G. (2001). Limnology: Lake and River ecosystems. Academic Press, San Diego.

Worm, H.-U. (1998). On the superparamagnetic - stable single domain transition for magnetite, and frequency dependence of susceptibility. Geophysical Journal International, 133, 201-206.

Xu, H., Liu, B., Wu, F. (2010). Spatial and temporal variations of Rb/Sr ratios of the bulk surface sediments in Lake Qinghai. Geochemical Transactions, 11, 1-8.

Yoo, K.C., Yoon, H.I., Kim, J.K., Khim, B.L. (2009). Sedimentological, geochemical and palaeontological evidence for a neoglacial cold event during the late Holocene in the continental shelf of the northern South Shetland Islands, West Antarctica. Polar Research, 28, 177-192.

Yoon, H.I., Park, P.K., Kim, Y., Kang, Yun, Cheon, Kang, S.H. (2003). Origins and paleoceanographic significance of the layered diatom ooze interval from the Bransfield Straight in the northern Antarctic Peninsula around 2500 years BP. In: Domack, E.W., Leventer, A., Burnett, A., Bindschadler, R., Convey, P., Kirby, M. (Eds.), Antarctic Peninsula Climate Variability: Historical and Paleoenvironmental Perspectives. American Geophysical Union, Washington, D.C., pp. 225-238.

Yoon, H.I., Yoo, K.C., Park, B-K., Kim, Y., Khim, B-K., Kang, C-Y. (2004). The origin of massive diamicton in Marian and Potter coves, King George Island, West Antarctica. Geosciences Journal, 8, 1-10.

Zale, R., Karlén, W. (1989). Lake sediment cores from the Antarctic Peninsula and surrounding island. Geografiska Annaler: Series A, Physical Geography, 71, 211-220.

Zidarova, R., Kopalová, K., van de Vijver, B. (2016). Diatoms from the Antarctic Region, Maritime Antarctica. Koeltz Botanical Books, Oberreifenberg.

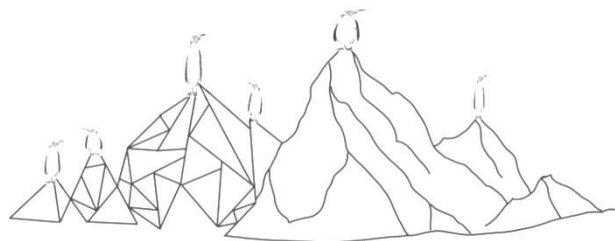# CHAPTER 6

PALEOLIMNOLOGICAL ANALYSIS - COMPARISON OF LAKE ESMERALDA CORE

WITH LAKE ANONIMA CORE

General diatom descriptions of the Lake Esmeralda and Lake Anonima cores

Species composition

Comparison of communities

Paleolimnological analysis - comparison of Lake EsmEralda core WITH lake anonima core

While the investigation of modern diatom communities provides a snapshot in the spatial and environmental controls governing diatom community structure and assembly, paleo-records can provide these data at much greater temporal intervals, thus providing important comparisons. Here, were compare the diatom assemblages recovered from two sediment cores, one from the NE side (Lake Anonima), and the other from the SW side (Lake Esmeralda) of Vega Island to provide complementary data on observations from the modern communities discussed in the previous chapter. In addition, results from the previous chapter can help interpret the data reported below.

General diatom description of the Esmeralda core

A total of 9600 diatom valves were counted in the 24 topmost samples of the Lake Esmeralda sediment core (see Chapter 4). This resulted in the identification of 86 different taxa representing 31 genera (Appendix 3). The number of species varied between 30 and 47 (average = 42), but no significant changes in distribution or structure occurred in the topmost 25 cm of the core, as neither distinct arrivals nor disappearances were observed.

General diatom composition of Anonima core

A total of 11 600 diatom valves were counted in 29 samples (see Chapter 5). This resulted in the identification of 80 different taxa representing 26 genera (Appendix 4). The number of species varied between 12 and 39 (average = 22.9), and changes in their distribution were observed in the core and followed trends of other proxies. Biozone 1 was dominated by the genus *Nitzschia* (46–67 %). Following biozone 2 is productively scarce and the diatom communities mainly present (semi-)terrestrial diatom species such as *Hantzschia amphioxys*, *Luticola muticopsis* and the genus *Humidophila*. Biozone 3 is characterised by co-dominance of *Planothidium rostrolanceolatum* and the genus *Nitzschia* and main character of biozone 4 is decrease in abundance of *Planothidium rostrolanceolatum* and the increase of *Sellaphora gracillima* (see Chapter 5)*.

SPECIES COMPOSITION

For both Esmeralda and Anonima sediment cores, the most species rich genus was *Luticola,* followed by *Pinnularia* and *Psammothidium* (and *Planothidium* in case of Anonima) (Figure 6.1).
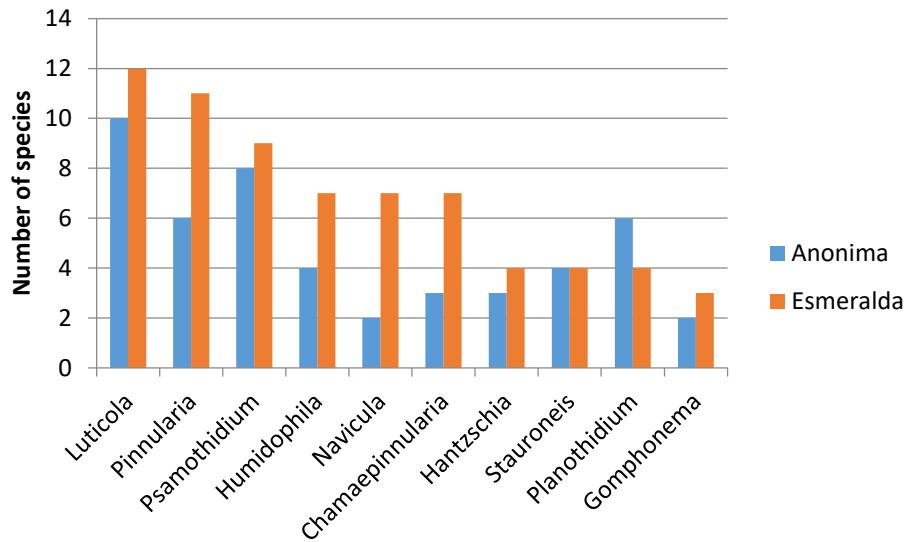

Figure 6.1 number of species in genera

The most abundant genus in Lake Esmeralda sediment core was *Microcostatus* (22 %), followed by *Psammothidium* (16 %), *Nitzschia* (14 %), and *Pinnularia* (11 %). For the Anonima sediment core, counts were dominated by representatives from the genus *Nitzschia* (41 %), followed by *Planothidium* (15 %), *Sellaphora* (140 %), and *Achnanthes* (6 %) (Table 6.1).

	Anonima		Esmeralda	
	total number of diatoms counted	**total relative abundance**	**total number of diatoms counted**	**total relative abundance**
Achnanthes	**724**	**6.2%**	2	0.0%
Brachisira	**723**	**6.2%**	23	0.3%
Fragilaria	**255**	**2.2%**	4	0.0%
Gomphonema	**217**	**1.9%**	34	0.4%
Humidophila	**297**	**2.6%**	**300**	**3.3%**
Chamaepinnularia	203	1.8%	**469**	**5.1%**
Luticola	**298**	**2.6%**	670	7.3%
Mayamaea	41	0.4%	**310**	**3.4%**
Microcostatus	82	0.7%	**2043**	**22.2%**
Nitzschia	**4750**	**40.9%**	**1313**	**14.3%**
Pinnularia	101	0.9%	**976**	**10.6%**
Planothidium	**1736**	**15.0%**	**285**	**3.1%**
Psamothidium	**218**	**1.9%**	**1441**	**15.7%**
Sellaphora	**1162**	**10.0%**	**268**	**2.9%**

Table 6.1 Overview of the 10 most valve abundant diatom genera based on Anonima and Esmeralda sediment core.

The most abundant species in the Anonima core was *Nitzschia velazqueziana,* representing 20 % of all counted valves (Table 6.2). It was followed by *Nitzschia soratensis* (9 %), *Planothidium lanceolatum* (9 %), and *Brachisira minor* (6 %). All other taxa contributed smaller proportions and were more variable. The Esmeralda core was dominated by *Microcostatus austroshetlandicus,* and represented 21 % of all counted valves. The species dominated the entire analyzed section of the core. It was followed by *Nitzschia kleinteichiana* (10 %), *Psammothidium papilio* (6 %), and *Pinnularia magnifica* (6 %).

	Anonima		Esmeralda	
	total number of diatoms counted	total relative abundance	total number of diatoms counted	total relative abundance
Achnanthidium australoexiguum	**700**	**6.0%**	0	0.0%
Brachisira minor	**723**	**6.2%**	23	0.3%
Luticola pusilla	0	0.0%	**316**	**3.4%**
Microcostatus australoshetlandicus	0	0.0%	**1974**	**21.5%**
Muelleria sp	3	0.0%	**240**	**2.6%**
Nitzschia annewillemsiana	**620**	**5.3%**	0	0.0%
Nitzschia homburgiensis	**368**	**3.2%**	350	3.8%
Nitzschia kleinteichiana	153	1.3%	**963**	**10.5%**
Nitzschia soratensis	**1065**	**9.2%**	0	0.0%
Nitzschia velazqueziana	**2331**	**20.1%**	0	0.0%
Pinnularia magnifica	0	0.0%	**510**	**5.5%**
Planothidium frequentissimum	**265**	**2.3%**	65	0.7%
Planothidium lanceolatum	**1051**	**9.1%**	0	0.0%
Psammothidium aretasii	0	0.0%	**387**	**4.2%**
Psammothidium papilio	119	1.0%	**589**	**6.4%**
Psammothidium rostrogermainii	2	0.0%	**367**	**4.0%**
Sellaphora antarctica	**593**	**5.1%**	0	0.0%
Sellaphora gracillima	**549**	**4.7%**	0	0.0%
Sellaphora nana	0	0.0%	**268**	**2.9%**

Table 6.2 Overview of the 10 most abundant diatom taxa based on Anonima and Esmeralda sediment core.

COMPARISON OF COMMUNITIES

Raw relative abundance data were visualized with a dot plot diagram organized by different sediment cores (Figure 6.2). From this, it is clear that diatom communities from each core are unique and do not resemble each other.

Figure 6.2 Dot plot representation of relative abundance counts averaged by sample. Sample codes are on the x-axis, and species names are on the y-axis. The size of a dot is proportional to the average relative abundance of a particular species in a given sample. Anonima core samples are shown on the right side as filled brown circles, and Esmeralda core samples are shown on the left side as un-filled brown circles. Diatoms with relative abundances greater than 1 % are plotted. The key for species abbreviations are shown in Appendices 3 and 4.

Only a few species were observed in both sediment cores. Among them, it was typically lacustrine species common for the region such as *Psammothidium papilio*, *Planothidium frequentissimum* and *Planothidium australe* (Zidarova et al. 2016).
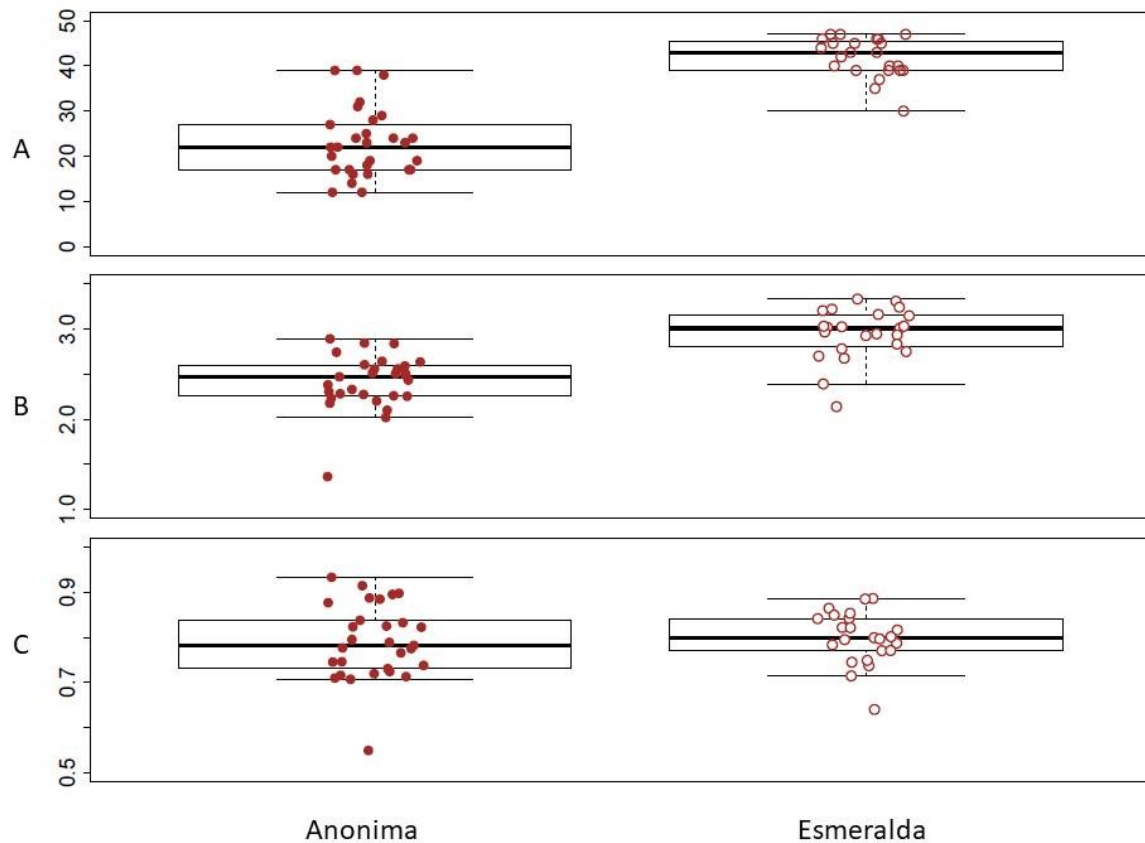
Figure 6.3 Boxplots of species richness (A), Shannon diversity (B), and evenness (C) calculated for Lake Anonima and Lake Esmeralda sediment core samples. Box bottoms and tops represent first and third quartiles, and the thick black lines represent median values.

The Esmeralda sediment core exceeded Anonima in richness and diversity indices (Figure 6.3). Shannon diversity values fluctuated between 2.39 and 3.26 (average = 2.97) in the Esmeralda core and ranged from 0.55–0.93 (average = 0.79) in the Anonima core. Differences in evenness were less pronounced, with Esmeralda dominating again (0.64–0.88; average = 0.8), and with Anonima evenness values ranging from 0.55–0.93 (average = 0.79). These findings correspond to the distribution of richness, diversity, and evenness on each side of the island reported in the previous section, where Cape Lamb exhibited greater values than Devil's Bay.
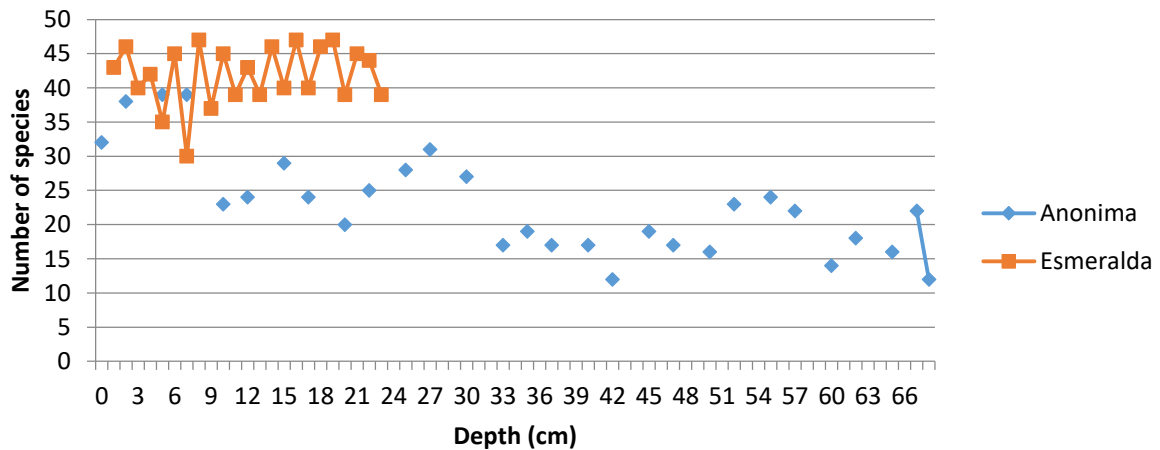
Figure 6.4 Diatom species richness plotted by depth in Lake Esmeralda and Lake Anonima sediment cores.

Species richness values in Lake Esmeralda core were greatest at depths of 8–9, 16–17 and 19–20 cm, and were lowest at the depth of 7 –8 cm. No significant changes occurred in species richness over the topmost 25 cm of the sediment core (Figure 6.4).

For Anonima, species richness values were greatest at depths of 2-3, 5-6 and 7-8 cm, and were lowest at the depth of 42-43 and 68-69 cm. Species richness significantly decreased with depth (Figure 6.4). Even though that richness or diversity is not considerate to be primarily climate-dependent, it needs to be taken into consideration since they decrease with becoming period of colder and drier conditions in the LA record.

PCA

A PCA generated for the Esmeralda core samples alone explained 33.2 % and 22.6 % of the species variation on the first and second axis respectively and an additional 29.5 % was explained by the third and fourth axes together.

Figure 6.5 The Principal component analysis (PCA) of Lake Esmeralda core samples. Diatoms with relative abundances greater than 8 % are plotted. Numbers indicate a layer of the sediment core in cm.

Even though the community is stable over the time, some differences can be seen as the topmost 10 samples (1th -10th cm) are influenced by *Nitzschia homburgensis*, following samples (except 15th- 16th cm) are influenced by *Mayamaea josefelsteri* in combination with *Psammothidium aretasi*i, whereas the lowermost samples are influenced by *Pinnularia magnifica (*Figure 6.5).

The Lake Anonima core PCA explained 30.2 % and 15.1 % of the variation on the first and second axis, respectively, and an additional 20.1 % was explained by the third and fourth axes together.
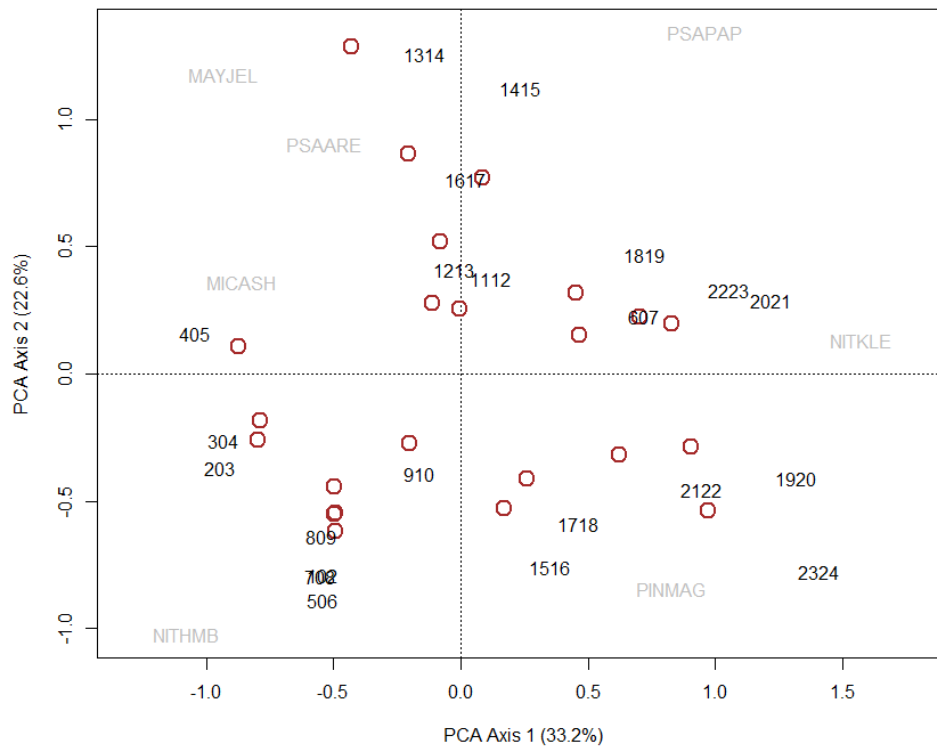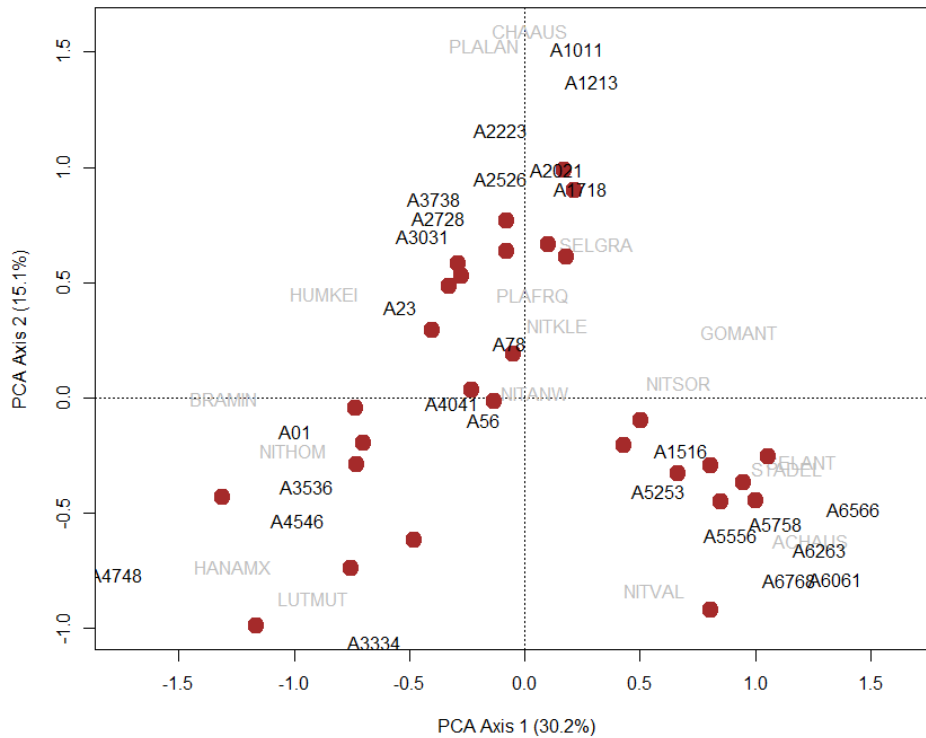
Figure 6.6 The Principal component analysis (PCA) of Anonima core samples. Diatoms with relative abundances greater than 8 % are plotted. Numbers indicate a layer of the sediment core in cm.

Clear, distinct differences within the diatom stratigraphy were found on the PCA biplot (Figure 6.6). The layer 15-16 and the lowermost samples (from 52-53 cm) are distinct by their abundances of *Nitzschia velazqueziana, Achnanthidium australexiguum, Stauroneis delicate,* and *Sellaphora antarctica*, and are representatives of biozone 1. The topmost samples are influenced by *Nitzschia annewillemsiana, Brachysira minor,* and *Nitzschia homburgiensis,* and are representative of biozone 2. The middle part of the core, 10-31 cm, is influenced by *Chamaepinnularia australomediocris, Planothidium rostrolanceolatum,* and *Sellaphora gracillima*, ecological representatives of biozone 3.

CONCLUSIONS

This chapter focused on the ecological comparison of two lake sediment cores from Vega Island (Lake Esmeralda and Lake Anonima) located to the southwest (Cape Lamb) and northeast (Devil's Bay), respectively.

Main results:

- In total, 52 samples were analyzed and 134 diatom species were identified for both cores.
- Different diatom assemblages were found in each core suggesting different histories for each lake.
- Species richness and diversity is higher in the Lake Esmeralda sediment core, which corresponds to patterns between the modern diatom communities analyzed from Cape Lamb versus Devil's Bay.
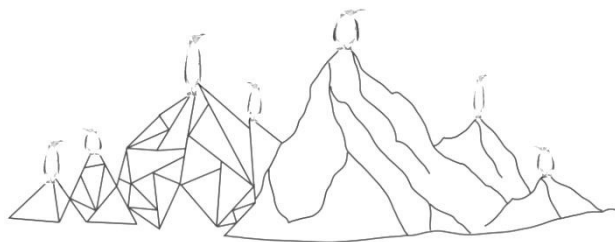
CHAPTER 7

GENERAL DISCUSSION

General discussion on the influence of habitat type and island aspect

Comparison with Clearwater Mesa, JRI

Comparison of lake sediment cores with recent material

Overall conclusions

Four different habitat types (ponds, streams, seepages, and mosses) were sampled on Vega Island from two different localities (Cape Lamb located on the SW of the island and Devil's Bay to the NE). A total of 136 diatom taxa (including species, varieties, and forms) belonging to 31 genera were observed, and a complete list of taxa is presented in Appendix 2. In addition, a lake sediment core was recovered from each locality to study the paleo-record of diatom assemblages in order to infer local environmental changes. A complete list of observed taxa is in Appendices 3 and 4. Habitat type was found to be a crucial factor in determining diatom community structure, stronger than the aspect of island. The lake sediment cores differed substantially from each other and reflected the differences in richness and diversity observed in recent communities (even though the diatom communities differed from the recent ones), suggesting that similar drivers of diversity are operating over both modern and distant timescales.

Influence of habitat type

In Antarctica, different habitat types exert strong selective controls on diatom community structure and assembly due to the environmental conditions they promote and are exposed to (Spaulding et al. 2010). For example, the extent and duration of ice cover for lakes and ponds functions as the main control over life in these Antarctic habitats (Smol & Cumming 2000; Douglas et al. 2004; Foreman et al. 2004; Hodgson & Smol 2008). Similarly, Antarctic stream communities are limited by the melting of water at their source, and life here is limited by annual periods of desiccation and freezing (Esposito et al. 2006). As for mosses, moisture availability and content is the main control for resident communities (Chipev & Temniskova Topalova 1999; Van de Vijver et al. 2004; Vinocur & Maidana 2010), with dry mosses routinely reporting fewer species than wet ones (e.g. Van de Vijver and Beyens 1999). Previous work has further found that the distance to an aquatic source (either freshwater of marine) is more influential than the water's physical-chemical composition (Vinocur & Maidana 2010). Vinocur & Maidana (2010) suggest that moss habitats may not be directly influenced by nutrient concetrations because of a sheltered microenvironment that is created within moss layer. Seepages are, on the other hand, often exhibit orders of magnitude greater conductivity and nutrient concentrations than other nearby waterbodies (Jones 1993; McKnight et al. 2004; Spaulding et al. 2010; Kopalová & Van de Vijver 2013b; Kopalová et al. 2013c). While also ephemeral like Antarctic streams, seeps may provide a more ‚stable' hydrologic environment given their lower flow rates and thus reduced shear stress and scour. In any case, the amount of exposure, availability of liquid water, and the availibility of nutrients and light play a fundamental role in forming diatom communities across all Antarctic habitat types.

The data suggests that Vega Island moss and pond habitats are more diverse than streams and seepages. This may suggest that these former habitat types have greater stability in contrast to the ephemerally-fed streams and seepages that can potentially exhibit more abrupt changes in aquatic regime.

The submerged aquatic habitats of Vega Island were dominated by the genus *Nitzschia*, which contrasts with ponds from the sub-Antarctic Islands, where *Nitzschia* species are less abundant (Van de Vijver et al. 2008). Additionally, Sakaeva et al. (2016) reported only two *Nitzschia* species from ponds in McMurdo Sound Region near McMurdo Station, none which were dominant.

From stream and pond habitats, three *Nitzschia* species were common: *Nitzschia kleinteichiana*, *Nitzschia paleacea* and *Nitzschia homburgiensis*. The first, *Nitzschia kleinteichiana,* is one of the most common *Nitzschia* species in the Maritime Antarctic Region (Zidarova et al. 2016). It exhibits a broad ecological niche, being found in every habitat investigated (Hamsher et al. 2016). Another *Nitzschia* species, *Nitzschia homburgiensis,* was also observed at high abundances, and has previously been reported from streams in the Maritime Antarctic region (Kellogg & Kellogg 2002; Hamsher et al. 2016). Aside from *Nitzschia* spp., the diatom *Fistulifera pelliculosa* was also common in studied streams. This genus, in general, tolerates unstable flow conditions in streams, including high velocities (Stabell 1985; Denys 1990). This rather small, lightly-silicified species is commonly observed in other Antarctic streams and is in fact hypothesized to be an important indicator of change in the McMurdo Dry Valleys (Stanish 2011). For example, this species might preferentially colonize high-nutrient areas, such as hyporheic up-welling zones (Kohler et al. 2016), and is probably easily mobilized and transported in the water column from sediments before being deposited to other habitats such as microbial mats (Stanish 2011; Kohler et al. 2015).

Diatom communities from moss habitats were characterized by species typically reported from Antarctic Peninsula moss samples, such as *Chamaepinnularia krookiformis*, *Nitzschia kleinteichiana,* and *Humidophila vojtajarosikii* (Kopalová et al. 2014; Zidarova et al. 2016). *Humidophila vojtajarosikii* is a common species on both JRI and the South Shetland Islands: it has been reported from all of Livingston Island (reported as *Diadesmis* sp2 in Kopalová et al. 2014), King George Island, Nelson Island, and Deception Island (Zidarova, pers. obs.), although rarely exceeding 10% of the total diatom count. The largest populations were found in moist terrestrial to submerged aquatic moss vegetation close to larger lakes (Kopalová et al. 2015). In limited datasets from seepages, diatom communities are dominated by *Nitzschia kleinteichiana,* the species common in every habitat in the Maritime Antarctic, *Chamaepinnularia krookiformis* (most abundant among wet and moist mosses on the shore of small ponds with elevated salinity and nutrients), and *Luticola muticopsis.* The latter species is usually the most abundant in terrestrial habitats influenced by sea birds and sea sprays (Zidarova et al. 2016).

EFFECT OF ASPECT

The Maritime Antarctic region is experiencing a temperature increase, which is predicted to increase average precipitation in the future (King 1994; Vaughan et al. 2001, 2003; Turner et al. 2005). Therefore, I compared two slightly climatically different sites on Vega Island (Kopalová *pers. obs*.). One of them, Cape Lamb, is assumed to be more influenced by nearby the JRI, reporting a warmer climate with more precipitation than the other side, represented here by Devil's Bay, which is located more in the precipitation shadow of the Antarctic Peninsula with colder weather (Engel et al. 2012).

I found that of the 118 species identified from Cape Lamb, 34 of them unique for that side. The unique species were predominately from *Luticola, Planothidium, Psamothidium* and *Stauroneis* genera, which probably reflects the differences in sampled habitat types between sites. Also, some of these unique species were only represented by one or two valves. In contrast, of the 101 species identified in Devil's Bay, 18 of them were found to be unique for this side of the island (Appendix 2).

Given the unequal diversity in the frequency of habitat types between the two sides, I focused quantitative comparisons in the diatom communities on pond habitats, since these were the best represented habitats on both sides. Cape Lamb pond communities were largely composed of *Nitzschia paleacea*, *Gomphonema maritimo-antarcticum* (common mostly in alkaline ponds), *Nitzschia kleinteichiana*, the rather common Antarctic species *Psammothidium papilio,* and *Nitzschia annewillemsiana,* a species also known from wet mosses (Hamsher et al. 2016). Devil's Bay ponds were similarly dominated by *Nitzschia kleinteichiana and Nitzschia paleacea,* as well as *Nitzschia homburgiensis*. The differences in diversity may be a result of wind currents coming in the south-west direction from JRI and by the presence of a precipitation shadow formed by the AP, bearing greater influence on Devil's Bay (Engel et al. 2012).

The overall similarities between these two sides of the island despite their different position and possible different climatic influence may be due to the relatively small spatial scale under investigated and the large potential for diatoms to disperse themselves, which may homogenize communities across sites. Therefore, it was not possible to suggest a community trend that might be possible to anticipate with ongoing climate changes across the island. However, the strong patterns by habitat shown in this work can bring a new perspective on evaluation of pond sediment paleorecords, as warm periods of deglaciation are connected with an increased input of nutrient supply by glacial melt, but also with changes in the size and number of aquatic and semi-aquatic habitats. In any case, the study of these differences now is necessary, due to irreversible changes that are to come with clime change.

COMPARISON WITH CLEARWATER MESA

The biogeographical distribution analysis (Figure 2.1) confirmed that Vega Island belongs to the transition zone between Maritime and Continental Antarctic regions. Those results show a close similarity to the results from JRI and several others (Kopalová 2013a). However, since a newly revised and established fine-grained taxonomy was applied, comparison with most studies from this region is difficult. On exception is Clearwater Mesa from nearby JRI (Kopalová et al. *in review*), on which a dataset has been recently generated using the same fine-grained taxonomy. Clearwater Mesa (CWM; 64°1´ S, 57°43´ W), located in north-central JRI, is a lava-fed delta composed of JRI Volcanic Group rocks (Smellie et al. 2013), found in an altitudinal range of ~200–275 m a. s. l. The mesa covers an area of ~8 km^2 and has a levelled surface (e.g. Johnson et al. 2009). To the east, the wider CWM area consists of lower-lying promontory connecting the mesa and the ice cap (Roman et al. *in press*). Also, due to large gradients of chemical characteristics found in lakes, and its position in transition zone between Maritime Antarctic region and continental Antarctica (Terauds & Lee 2016), CWM potentially represents a biodiversity hotspot (Roman et al. *in press*). Therefore, we compared the diatom communities between these two nearby localities in order to put the Vega Island diatom flora into regional context (Figure 7.1). In total, 35 epipelon, 33 epilithon, 24 moss, and 21 seepage samples were analyzed from CWM by Kopalová (*in review*).

Figure 7.1 Principle components analysis (PCA) of dataset from Vega Island and Clearwater Mesa from JRI. Diatoms with relative abundances greater than 8 % are plotted. Symbol shapes indicate different habitat type. Pond habitats are indicated by circles, moss habitats by diamonds, seepages by squares, and streams by triangles.

Interestingly, the results of the PCA (Figure 7.1) showed that the samples farther from JRI (Devil's Bay) clustered more closely with CWM than ponds from the opposite side of Vega Island (Cape Lamb). This is the opposite of what would be expected given geographical proximity, which might be a proxy for dispersal potential and suggest more similar climate conditions. However, clear differences are seen between the two islands.

In general, species richness on Vega Island is higher than on CWM. For instance, CWM moss samples had an average richness value of 7.2, and some samples revealed only 1 species. In CWM pond samples, the average number was 12.3 for epilithon and 10.8 for epipelon. In contrast, Vega Island diatom species richness reached an average of 19.20 for ponds and 17.5 for moss samples. This could imply more extreme and dry conditions experienced by CWM mosses, low variability of moss habitats (e.g. their altitude, nutrients content, etc.), or a combination of both.

In general, the diatom diversity of limno-terrestrial Antarctic habitats is much lower than in temperate (Jones 1996) and Arctic regions (Douglas et al. 2004; Vyverman et al. 2007) due largely from the physical isolation of the Antarctic continent, since it is surrounded by a circumpolar ocean (Heywood 1977). For the continent itself, the most diverse region is the Antarctic Peninsula (Kopalová 2013a), since it is typically warmer and closer to another continent, specifically South America.

Within Vega Island, the southwest side is both more species rich and diverse than the northeast side (Figure 2.7). According to its proximity with JRI, there should be better dispersal probability. The same pattern is observed from the lake sediment records. The southwest (Esmeralda) sediment record shows higher diversity and species richness than the northeast Lake Anonima sediment core. Thus, the results of this study suggest that the same controls operating at relatively small timescales also operate over longer temporal scales. Even though this pattern is strong (see Figure 6.3 and 6.4) attention should be given to the differences in core ages.

LAKE ESMERALDA CORE

A total of 86 taxa belonging to 31 genera were found in the topmost 24 cm of the Esmeralda sediment core. No significant changes in species distribution were observed; however, under the 25th cm, valve abundance rapidly decreased, and in the lower half of the core no valves were found at all. This can potentially be explained by dissolution of valves during the early sediment diagenesis. However, no physical changes (sedimentation rate, salinity, pH as Flower & Ryves (2009) suggest) were observed in the lower part of the sediment core to confirm these hypotheses.

One of the most striking characteristics of this core is that the topmost 25 cm of the core are dominated by *Microcostatus australoshetlandicus*. *M. australoshetlandicus* was described from a soil sample (pH = 6.95) from Deception Island, though the species is only rarely observed in the Maritime Antarctic region. For example, on Livingston Island, only very small populations were found in small pools and almost dry mosses (Zidarova et al. 2016). The analyzed modern material from Vega Island did not contain this species aside from one exception- recent samples from Lake Esmeralda (see Chapter 2), though the relative abundances of

M. australoshetlandicus in those samples never exceeded 2 %. The occurrence of *M. australoshetlandicus* only in Lake Esmeralda could be explained by its hydrologic isolation, since the lake is not fed by any streams, and it could be a remnant of a past diatom community in this region.
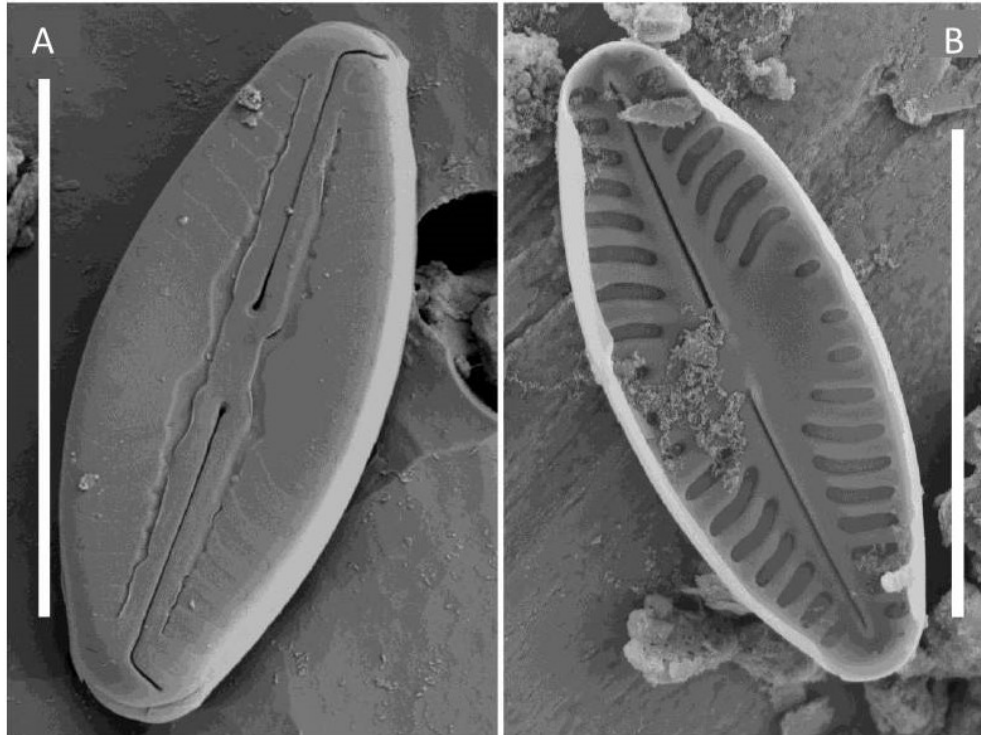

Figure 7.2 SEM photo of *Microcostatus australoshetlandicus* from Zidarova et al. 2016, p. 145, Figures 18,19, scale bar = 5 µm

Other species common in the Esmeralda core were *Nitzschia kleinteichiana* and *Psammothidium papilio*. Those are commonly found in lakes from Maritime Antarctic region, though usually at lower conductivity (Zidarová et al. 2016).

From the observations of the environmental preferences of the diatom composition we can assume that Lake Esmeralda was permanently watered and never developed intense moss cover because not many aerophilic genera, such as *Luticola*, *Humidophila,* or *Muelleria,* were found, and no species from these genera dominated the core.

Comparison of Esmeralda core with the recent samples from Cape Lamb

PCA results (Figure 7.3) of the combined dataset of the recent material and the Esmeralda sediment core shows that the entire sediment core can be considered an outlier relative to the recent samples, indicating that the diatom assemblages in the sediment core never closely resembled any of the recent samples throughout the history of the core, with an exception being the recent samples from Lake Esmeralda.
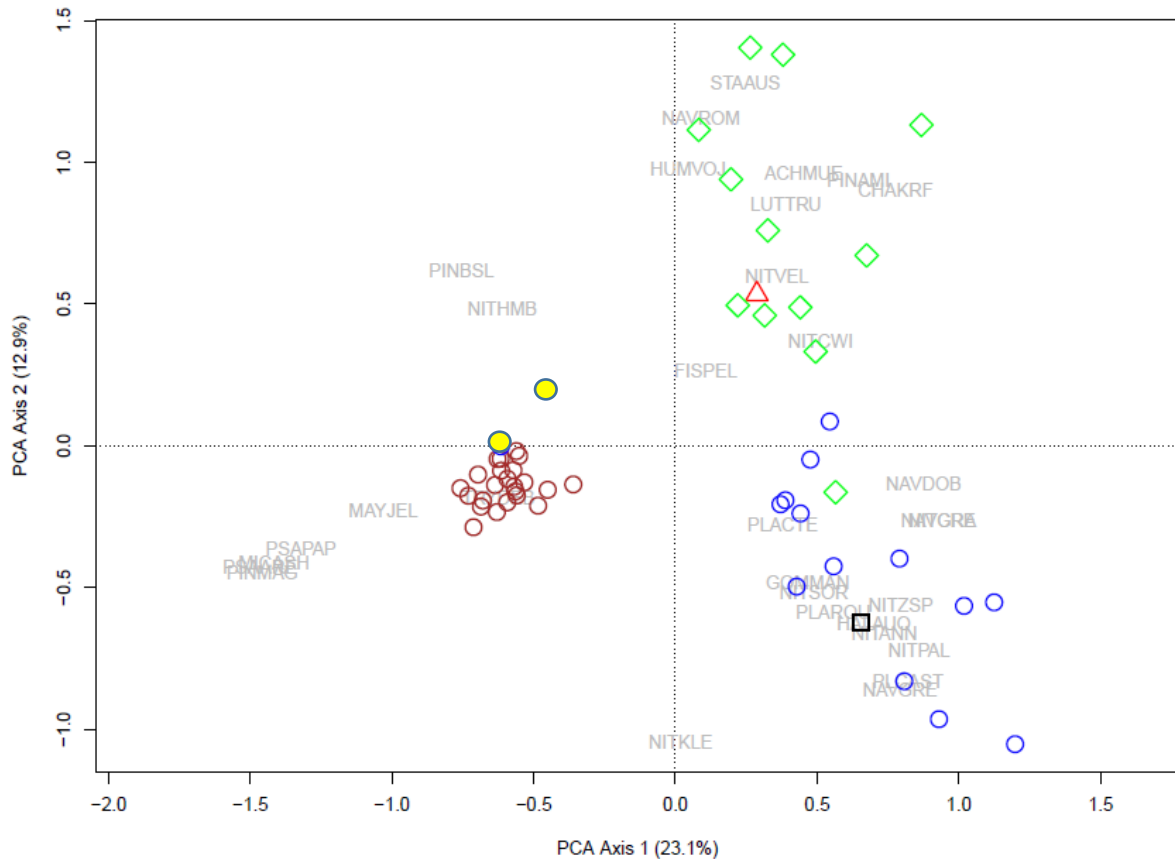

Figure 7.3 Principle components analysis (PCA) of Esmeralda core samples and recent samples from Cape Lamb. Diatoms with relative abundances greater than 8 % are plotted. Recent pond habitats are indicated by blue circles, sediment core samples by brown circles, moss habitats by green diamonds, seepages by black squares, and streams by red triangles. Yellow circles with thick outlines indicate the recent samples from Lake Esmeralda. Diatom codes are superimposed onto Figure (key for species abbreviations are available in Appendix 2).

While this could be caused by differences in sampled pond habitats, since the sediment core was taken in the center of Esmeralda lake thus represents a benthic (and possibly epipelic) diatom community, the recent samples of epilithic diatom communities from Esmeralda also cluster with the core samples. Another reason for these differences may be the already stated fact that Lake Esmeralda does not have any inflow. Therefore, the diatom flora within the lake may relatively isolated from other waterbodies.

LAKE ANONIMA CORE

In total, 29 sediment samples were analyzed from Lake Anonima sediment core. 80 species were observed belonging to 26 different genera. Changes in richness and diversity throughout the sediment core were observed with more fluctuating values in biozones 1 and 2 and with richness and diversity peak in biozone 4 (see Chapter 5). Evenness showed the highest values in biozone 2 (Čejka et al. *in review*). The core was dominated by *Nitzschia* genera, especially *Nitzschia velazqueziana,* which is a species known from lakes and pools with a slightly alkaline pH (7.3-7.7) and low to moderately high conductivity (50–600 µS/cm). Large populations of this diatom were also observed on wet mosses on JRI and South Shetland Islands (Zidarova et al. 2016).
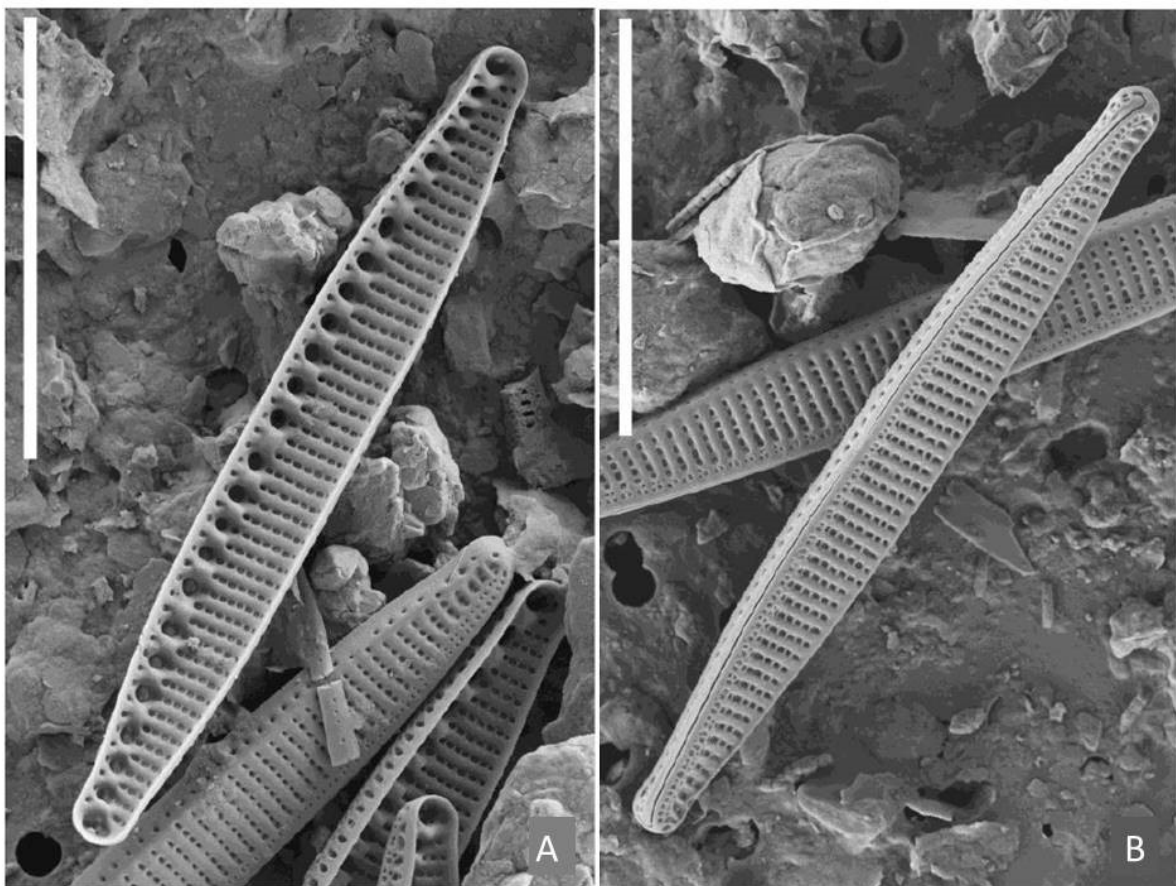

Figure 7.4 SEM photo of *Nitzschia velazqueziana* from Hamsher et al. 2016, p. 96, Figures 198, 199, scale bar = 10 µm

In general biozone 1 of the core is dominated by species common from lakes with neutral to alkaline pH and rather low conductivity level. Biozone 2 is largely dominated with species known from mosses and cyanobacterial mats. Biozones 3 and 4 are again dominated mainly by aquatic species (see Chapter 5).

Comparison of Anonima core with the recent samples from Devil's Bay

PCA results (Figure 7.5) showed differences between the entire sediment core and recent Devil's Bay material on axis 1. Interestingly, there was no clear association with Anonima core samples and modern material from different habitats, as communities from recent samples showed greater resemblance to each other than with paleo-assemblages. While the differences between these assemblages may again be caused by differences in pond habitat of core samples, one other possibility is that Lake Anonima is connected to a stream system, unlike Lake Esmeralda, which facilitate species transport. In addition, Lake Anonima exhibits underground drainage into surface streams and the nearby lake systems (Čejka et al. *in review*).
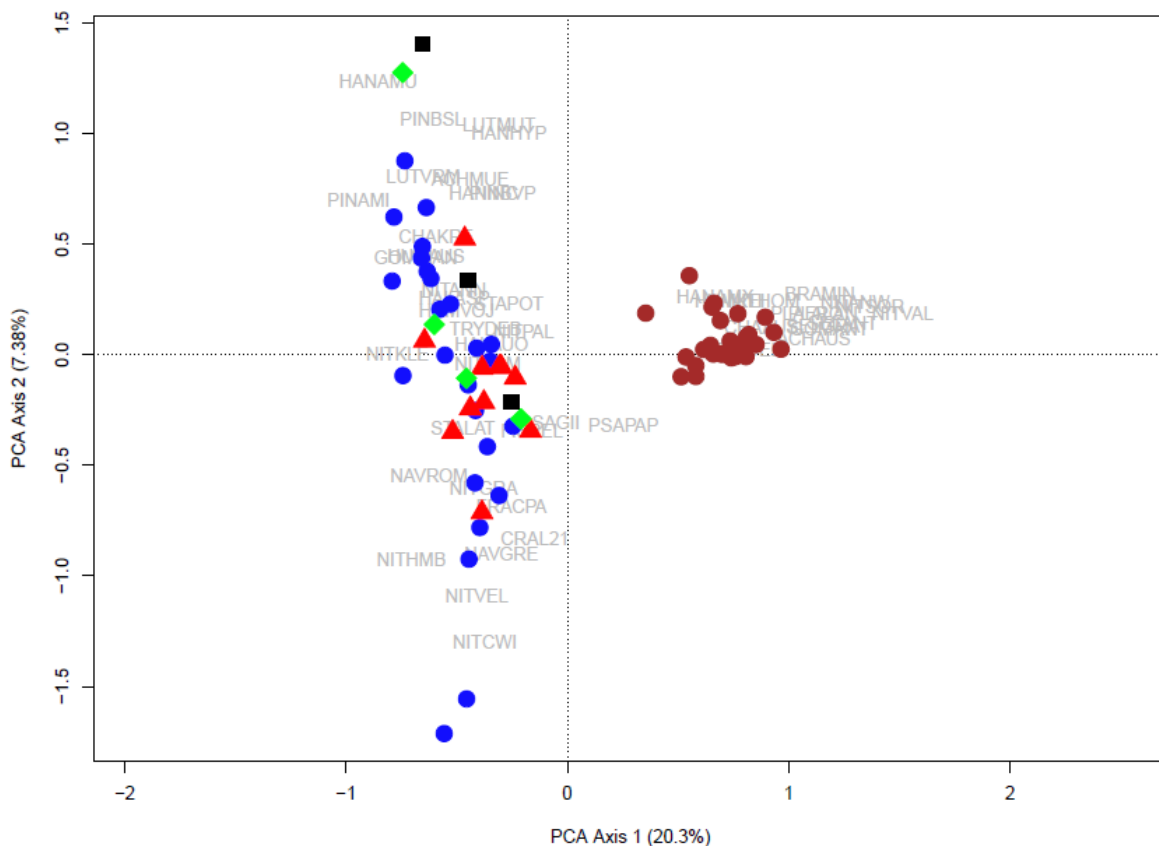

Figure 7.5 Principle components analysis (PCA) of Anonima sediment core and Devil's Bay recent samples. Diatoms with relative abundances greater than 8 % are plotted. Recent pond habitats are indicated by blue circles, sediment core samples by brown circles, moss habitats by green diamonds, seepages by black squares, and streams by red triangles. Diatom codes are superimposed onto Figure (key for species abbreviations are available in Appendix 2).

While there were differences in the core that were associated with other factors allowing for the differentiation of biozones, these differences were overall trivial in the context of the overall variability observed in diatom communities on the northeast side of Vega Island, thus the core diatoms cluster apart from the recent material.

Summary comparison of the entire Vega dataset

Finally, a PCA was generated for the entire dataset from Vega Island (Figure 7.6). Lake Esmeralda core together with the two samples of modern material were distinct from the rest of the dataset, emphasizing their uniqueness on Vega Island and the region. Furthermore, and supported our notions above, Lake Anonima samples clustered most closely with streams, suggesting that these assemblages are at least partially constructed with inputs from stream water.

Figure 7.6 The principal component analysis (PCA) of the entire Vega dataset. Pond habitats are indicated by blue circles (core samples by brown circles), moss habitats by green diamonds, seepages by black squares, and streams by red triangles. Symbols for north sites are filled, and south sites are represented by outlines only.

REFERENCES

Chipev, N. & Temniskova-Topalova, D. (1999). Diversity, dynamics and distribution of diatom assemblages in land habitats on the Livingston Island (the Antarctic). Bulgarian Antarctic Research Life Sciences, 2, 32-42.

Denys, L. (1990). Fragilaria blooms in the Holocene of the western coastal plain of Belgia. In Proceedings of the 10th International Diatom Symposium. Koeltz Science, Koenigstein (Vol. 397406).

Douglas, M. S. V., Hamilton, P. B., Pienitz, R., & Smol, J. P. (2004). Algal indicators ofenvironmental change in Arctic and Antarctic lakes and ponds. In Long-term Environmental Change in Arctic and Antarctic Lakes, ed. R. Pienitz, M. Douglas, & J. Smol, Dordrecht: Springer, pp. 117-58.

Esposito, R. M. M., Horn, S. L., McKnight, D. M., Cox, M. J., Grant, M. C., Spaulding, S. A., Doran, P. T. & Cozzetto, K. D. (2006). Antarctic climate cooling and response of diatoms in glacial meltwater streams. Geophysical Research Letters, 33(7).

Engel, Z., Nývlt, D., & Láska, K. (2012). Ice thickness, areal and volumetric changes of Davies dome and whisky glacier (James Ross Island, Antarctic peninsula) in 1979–2006. Journal of Glaciology, 58(211), 904-914.

Flower, R. J., & Ryves, D. B. (2009). Diatom preservation: differential preservation of sedimentary diatoms in two saline lakes. Acta Botanica Croatica, 68(2), 381-399.

Foreman, C. M., Wolf, C. F., & Priscu, J. C. (2004). Impact of episodic warming events. Aquatic Geochemistry, 10(3-4), 239-268.

Hamsher, S., Kopalova, K., Kociolek, J. P., Zidarova, R., & Van De Vijver, B. (2016). The genus Nitzschia on the South Shetland Islands and James Ross Island. Fottea/Czech Phycological Society.-Praha, Czech Republic, 2007, currens, 16(1), 79-102.

Heywood, R. B. (1977). Antarctic freshwater ecosystems: review and synthesis. Adaptation within Antarctic ecosystems. Smithsonian Institution, Washington, DC, 801-828.

Hodgson, D. A., & Smol, J. P. (2008). High latitude paleolimnology. In Polar Lakes and Rivers - Limnology of Arctic and Antarctic Aquatic Ecosystems, ed. W. F. Vincent & J. Laybourn-Parry, Oxford: Oxford University Press, pp. 43-64.

Johnson, J. S., Smellie, J. L., Nelson, A. E., & Stuart, F. M. (2009). History of the Antarctic Peninsula Ice Sheet since the early Pliocene—evidence from cosmogenic dating of Pliocene lavas on James Ross Island, Antarctica. Global and Planetary Change, 69(4), 205-213.

Jones, V. J., Juggins, S., & Ellis-Evans, J. C. (1993). The relationship between water chemistry and surface sediment diatom assemblages in maritime Antarctic lakes. Antarctic Science, 5(4), 339-348.

Jones, V. J. (1996). The diversity, distribution and ecology of diatoms from Antarctic inland water. Biodiversity and Conservation 5: 1433-1449.

Kellogg, T. B., & Kellogg D. E. (2002). Non-marine and littoral diatoms from Antarctic and Sub-Antarctic regions. Distribution and up- dated taxonomy. Diatom monographs 1: 1-795.

King, J. C. (1994). Recent climate variability in the vicinity of the Antarctic Peninsula. International journal of climatology, 14(4), 357-369.

Kohler, T. J., Stanish, L. F., Crisp, S. W., Koch, J. C., Liptzin, D., Baeseman, J. L., & McKnight, D. M. (2015). Life in the main channel: long-term hydrologic control of microbial mat abundance in McMurdo Dry Valley streams, Antarctica. Ecosystems, 18(2), 310-327.

Kohler, T. J., Van Horn, D. J., Darling, J. P., Takacs-Vesbach, C. D., & McKnight, D. M. (2016). Nutrient treatments alter microbial mat colonization in two glacial meltwater streams from the McMurdo Dry Valleys, Antarctica. FEMS Microbiology ecology, 92(4)

Kopalová, K. (2013a). Taxonomy, ecology and biogeography of aquatic and limno-terrestrial diatoms (Bacillariophyta) in the Maritime Antarctic Region. (Ph.D. Thesis). Charles Univesity and Universiteit Antwerpen. Prague. Czech Republic.

Kopalová, K., & Van de Vijver, B. (2013b). Structure and ecology of freshwater benthic diatom communities from Byers Peninsula, Livingston Island, South Shetland Islands. Antarctic Science, 25(2), 239-253.

Kopalová, K., Nedbalová, L., Nývlt, D., Elster, J., & Van de Vijver, B. (2013c). Diversity, ecology and biogeography of the freshwater diatom communities from Ulu Peninsula (James Ross Island, NE Antarctic Peninsula). Polar Biology, 36(7), 933-948.

Kopalová, K., Ochyra, R., Nedbalová, L., & Van de Vijver, B. (2014). Moss-inhabiting diatoms from two contrasting Maritime Antarctic islands. Plant Ecology and Evolution, 147(1), 67-84.

Kopalová, K., Kociolek, J. P., Lowe, R. L., Zidarova, R., & Van de Vijver, B. (2015). Five new species of the genus Humidophila (Bacillariophyta) from the Maritime Antarctic Region. Diatom Research, 30(2), 117-131.

Kopalová, K., Soukup, J., Kohler, T. J., Roman, M., Coria, S. H., Vignoni, P. A., Lecomte, K. L., Nedbalová, L., Nývlt, D. & Lirio, J. M. (*in review*). Habitat controls on limno-terrestrial diatom communities of Clearwater Mesa, James Ross Island, Maritime Antarctica. Polar Biology.

McKnight, D. M., Runkel, R. L., Tate, C. M., Duff, J. H., & Moorhead, D. L. (2004). Inorganic N and P dynamics of Antarctic glacial meltwater streams as controlled by hyporheic exchange and benthic autotrophic communities. Journal of the North American Benthological Society, 23(2), 171-188.

Roman, M., Nedbalová, L., Kohler, T. J., Lirio, J. M., Coria, S. H., Kopáček, J., Vignoni, P. A., Kopalová, K., Lecomte, K. L., Elster, J. & Nývlt, D. (*in press*). Lacustrine systems of Clearwater Mesa (James Ross Island, northeastern Antarctic Peninsula): geomorphological settings and limnological characterization. Antarctic Science.

Smellie, J. L., Johnson, J. S., & Nelson, A. E. (2013). Geological map of James Ross Island. I. James Ross Island volcanic group.

Smol, J. P., & Cumming, B. F. (2000). Tracking long-term changes in climate using algal indicators in lake sediments. Journal of Phycology, 36(6), 986-1011.

Spaulding, S. A., Van de Vijver, B., Hodgson, D. A., McKnight, D. M., Verleyen, E., & Stanish, L. (2010). Diatoms as indicators of environmental change in Antarctic and subantarctic freshwaters. The diatoms: applications for the environmental and earth sciences, 267-283.

Stabell, B. (1985). The development and succession of taxa within the diatom genus Fragilaria Lyngbye as a response to basin isolation from the sea. Boreas, 14(4), 273-286.

Stanish, L. (2011). Ecological controls on stream diatom communities in the McMurdo Dry Valleys, Antarctica. Dissertation thesis, University of Colorado, Boulder.

Turner, J., Colwell, S. R., Marshall, G. J., Lachlan-Cope, T. A., Carleton, A. M., Jones, P. D., Labun, V., Reid, P. A. & Iagovkina, S. (2005). Antarctic climate change during the last 50 years. International journal of Climatology, 25(3), 279-294.

Van de Vijver, B., & Beyens, L. (1999). Moss diatom communities from Ile de la Possession (Crozet, Subantarctica) and their relationship with moisture. Polar biology, 22(4), 219-231.

Van de Vijver, B., Beyens, L., Vincke, S., & Gremmen, N. J. (2004). Moss-inhabiting diatom communities from Heard Island, sub-Antarctic. Polar biology, 27(9), 532-543.

Van de Vijver, B., Gremmen, N., & Smith, V. (2008). Diatom communities from the sub-Antarctic Prince Edward Islands: diversity and distribution patterns. Polar biology, 31(7), 795-808.

Vaughan, D. G., Marshall, G. J., Connolley, W. M., King, J. C., & Mulvaney, R. (2001). Devil in the detail. Science, 293(5536), 1777-1779.

Vaughan, D. G., Marshall, G. J., Connolley, W. M., Parkinson, C., Mulvaney, R., Hodgson, D. A., ... & Turner, J. (2003). Recent rapid regional climate warming on the Antarctic Peninsula. Climatic change, 60(3), 243-274.

Vinocur, A., & Maidana, N. I. (2010). Spatial and temporal variations in moss-inhabiting summer diatom communities from Potter Peninsula (King George Island, Antarctica). Polar biology, 33(4), 443-455.

Vyverman, W., Verleyen, E., Sabbe, K., Vanhoutte, K., Sterken, M., Hodgson, D. A., Mann, D. G., Juggins, S., Van de Vijver, B., Jones, V., Flower, R.,Roberts, D., Chepurnov, V. A., Kilroy, C.,Vanormelingen, P. & De Wever, A. (2007). Historical processes constrain patterns in global diatom diversity. Ecology, 88(8), 1924-1931.

Zidarova, R., Kopalová, K., Van de Vijver, B., & Lange-Bertalot, H. (2016). Diatoms from the Antarctic Region, Maritime Antarctica. Iconographia Diatomologica, 24, 1-509

OVERALL CONCLUSIONS

Unique diatom communities were found among the different habitat types investigated on Vega Island. Altogether, 136 taxa were identified belonging to 31 genera, and their known distributions support the notion that Vega Island is a transitional zone between the Maritime Antarctic and Continental bioregions. Habitat type was found to be a crucial factor in determining diatom community structure, with moss habitats characterized by their relatively high abundances of *Chamaepinnularia krookiformis,* and together with ponds showed the greatest richness and diversity of the different habitat types. Stream habitats were separated by their abundances of the small diatom *Fistulifera pelliculosa,* while pond habitats were separated from the others by their abundances of *Nitzschia paleacea.* Overall, the diatom flora on the southwest side was more diverse and species rich than northeast side. 34 unique species have been identified on southwest side, whereas only 18 species were found to be unique on northeast side. Also, a new species was described during the analyses belonging to the genus *Hantzschia*.

The modern diatom communities were then compared with paleo-assemblages characterized from sediment cores extracted from prominent lakes on both sides of the island. For the sediment cores together, 134 diatom species were identified. Those cores differed substantially from each other in their species richness and diversity, suggesting different histories for each lake. However, diatom assemblages were relatively uniform throughout both, and reflected the differences in richness and diversity observed in modern communities (even though the diatom communities differed substantially from the present ones), suggesting that similar drivers of diversity are operating over both modern and distant timescales.

Collectively, this survey expands ongoing research of diatom diversity and distributions on Maritime Antarctic islands, and improves our knowledge of factors structuring past and modern diatom communities in this region, revealing that both habitat and spatial controls are prominent.

APPENDIX 1

List of recent samples and its environmental characteristics
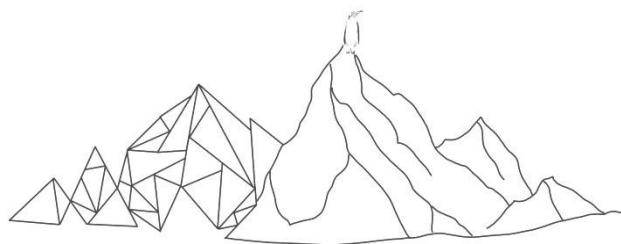
Appendix 1 List of recent samples and its environmental characteristics.

Sample code	Sample name	Sampling location	Sampling date	Altitude (m)	Coordinates (GPS)		pH	Conductivity	Pielou	Richness	Shannon	Habitat type
L_NE_1	L1-F1	Devil's Bay	16.1.2013	14	63.82123333	57.32266667	9.22	370	0.656	22	2.029	lake
L_NE_2	L2-F1	Devil's Bay	16.1.2013	16	63.82216667	57.32553333	8.9	156	0.788	45	3.000	lake
L_NE_3	L3-F1	Devil's Bay	16.1.2013	16	63.82151667	57.32506667	8.7	235	0.698	23	2.189	lake
L_NE_4	L4- F1	Devil's Bay	16.1.2013	16	63.82141667	57.32508333	9.75	320	0.856	37	3.091	lake
L_NE_5	L5-F1	Devil's Bay	16.1.2013	13	63.82141667	57.3252	9.7	220	0.646	16	1.790	lake
L_NE_6	L6-F1	Devil's Bay	16.1.2013	4	63.8185	57.33111667	9.4	560	0.555	16	1.538	lake
L_NE_7	L8-F1	Devil's Bay	17.1.2013	12	63.82105	57.33008333	9.3	240	0.556	6	0.996	lake
L_NE_8	L12-F1	Devil's Bay	17.1.2013	2	63.81612	57.32415	9.6	580	0.721	14	1.904	lake
L_NE_9	L13-F1	Devil's Bay	18.1.2013	19	63.82502	57.33007	9	180	0.763	11	1.830	lake
L_NE_10	L14-F1	Devil's Bay	18.1.2013	13	63.82241667	57.33383333	9.3	435	0.751	17	2.127	lake
L_NE_11	L18-F1	Devil's Bay	18.1.2013	47	63.82633333	57.31726667	9.1	130	0.438	20	1.312	lake
L_NE_12	L19-F1	Devil's Bay	19.1.2013	23	63.81968333	57.3164	9.6	235	0.473	16	1.312	lake
L_NE_13	L20-F1	Devil's Bay	19.1.2013	9	63.81535	57.30463333	9.1	320	0.638	8	1.327	lake
L_NE_14	L21-F1	Devil's Bay	19.1.2013	8	63.81565	57.30466667	9.3	320	0.668	15	1.808	lake
L_NE_15	L23-F1	Devil's Bay	20.1.2013	28	63.82101667	57.3173	9.1	140	0.661	29	2.226	lake
L_NE_16	L28-F1	Devil's Bay	20.1.2013	24	63.82186667	57.30888333	9.3	110	0.553	17	1.567	lake
L_NE_17	L29-F1	Devil's Bay	20.1.2013	24	63.8214	57.3088	10	160	0.634	23	1.987	lake
L_NE_18	L31-F1	Devil's Bay	21.1.2013	9	63.81953333	57.32791667	8.65	157	0.375	11	0.900	lake
L_NE_19	L33-F1	Devil's Bay	23.1.2013	23	63.8201	57.31	10.4	260	0.421	9	0.926	lake
L_NE_20	L37-F1	Devil's Bay	30.1.2013	28	63.82005	57.32403333	8.5	229	0.650	18	1.878	lake
L_NE_21	L38-F1	Devil's Bay	30.1.2013	31	63.82036667	57.32555	9.25	202	0.719	15	1.947	lake
L_NE_22	L40-F1	Devil's Bay	1.2.2013	56	63.82676667	57.32838333	8.8	130	0.306	11	0.734	lake
L_NE_23	L43-E	Devil's Bay	11.2.2013	247	63.79433333	57.36275	9.5	54	0.267	7	0.520	lake
L_NE_24	L45-E	Devil's Bay	11.2.2013	218	63.79055	57.36131667	9	92	0.473	17	1.341	lake

Sample code	Sample name	Sampling location	Sampling date	Altitude (m)	Coordinates (GPS)		pH	Conductivity	Pielou	Richness	Shannon	Habitat type
L_NE_25	R1	Devil's Bay							0.551	11	1.322	lake

Appendix 1 continued

| Sample code	Sample name	Sampling location	Sampling date	Altitude (m)	Coordinates (GPS)		pH	Conductivity	Pielou	Richness	Shannon	Habitat type
L_SW_26	L1E	Cape Lamb	8.2.2014		63.86745	57.61853	8	301	0.266	9	0.584	lake
L_SW_27	L2 ESM	Cape Lamb	9.2.2014	68	63.87375	57.60696	5.5	420	0.619	38	2.252	lake
L_SW_28	L3 EPP	Cape Lamb	10.2.2014	43	63.87535	57.61427	8.77	664	0.596	24	1.894	lake
L_SW_29	L4 EPP	Cape Lamb	11.2.2014	23	63.86724	57.62341	10.4	455	0.640	15	1.733	lake
L_SW_30	EPL ESM	Cape Lamb							0.597	34	2.107	lake
L_SW_31	LMR1EPP	Cape Lamb	11.2.2014		63.86281	57.62299	9.92		0.699	23	2.192	lake
L_SW_32	LMR4EPPC	Cape Lamb	11.2.2014	61	63.86272	57.62029	10.2	401	0.702	22	2.170	lake
L_SW_33	pool154	Cape Lamb							0.696	27	2.295	lake
L_SW_34	pool163	Cape Lamb							0.802	28	2.671	lake
L_SW_35	pool165	Cape Lamb							0.816	24	2.592	lake
L_SW_36	pool167E	Cape Lamb							0.784	27	2.583	lake
L_SW_37	LMR2E	Cape Lamb	11.2.2014		63.86262	57.62169	9.93	458	0.605	17	1.713	lake
L_SW_38	LMR3	Cape Lamb	11.2.2014		63.86251	57.62156	9.83	349	0.574	5	0.924	lake
L_SW_39	LMR5E	Cape Lamb	11.2.2014		63.8617	57.62787	9.25	209	0.317	5	0.510	lake
L_SW_40	pool 164E	Cape Lamb			63.87194	57.53972	9.89	729	0.616	9	1.353	lake
ST_NE_41	S1A	Devil's Bay	7.2.2013				10.1	184	0.324	6	0.581	stream
ST_NE_42	S2A	Devil's Bay	17.1.2013				8.65	285	0.600	18	1.735	stream
ST_NE_43	S3A	Devil's Bay	17.1.2013				9	180	0.562	10	1.295	stream
ST_NE_44	S5-A	Devil's Bay	17.1.2013				9	86	0.241	7	0.469	stream
ST_SW_46	STRE168	Cape Lamb	25.1.2013				9.92	237	0.366	9	0.804	stream
ST_NE_45	X1-E	Devil's Bay							0.659	26	2.030	stream
ST_NE_47	X2-E	Devil's Bay					8.9	190	0.623	11	0.774	stream
ST_NE_48	X5-E	Devil's Bay					9.29	120	0.323	5	0.631	stream
ST_NE_49	X6-E	Devil's Bay					9.12	120	0.392	10	0.503	stream

Sample code	Sample name	Sampling location	Sampling date	Altitude (m)	Coordinates (GPS)		pH	Conductivity	Pielou	Richness	Shannon	Habitat type
ST_NE_50	X7E	Devil's Bay					8.87	118	0.219	8	0.264	stream

Appendix 1 Continued

Sample code	Sample name	Sampling location	Sampling date	Altitude (m)	Coordinates (GPS)		pH	Conductivity	Pielou	Richness	Shannon	Habitat type
ST_NE_51	X9E	Devil's Bay	26.1.2013				9.15	184	0.127	15	1.671	stream
M_NE_54	M4	Devil's Bay	18.1.2013		63.82162	57.32407	8.8	210	0.646	17	1.830	moss
M_NE_55	M6	Devil's Bay							0.164	4	0.228	moss
M_NE_56	M7	Devil's Bay	20.1.2013				9.5	80	0.582	11	1.396	moss
M_SW_57	M1	Cape Lamb							0.463	17	1.311	moss
M_SW_58	M161	Cape Lamb							0.518	18	1.496	moss
M_SW_59	ML4	Cape Lamb							0.641	15	1.735	moss
M_SW_60	ML3	Cape Lamb							0.603	17	1.709	moss
M_SW_61	M2	Cape Lamb							0.699	19	2.059	moss
M_SW_62	M151	Cape Lamb							0.653	17	1.850	moss
M_SW_63	m163	Cape Lamb							0.687	19	2.022	moss
M_SW_64	m152	Cape Lamb							0.632	20	1.894	moss
M_SW_65	m165	Cape Lamb							0.742	16	2.057	moss
M_SW_66	m160	Cape Lamb							0.813	23	2.550	moss
M_SW_67	pool167 epp m	Cape Lamb							0.772	27	2.543	moss
M_SW_68	m stream168	Cape Lamb							0.775	21	2.360	moss
SE_NE_69	S11-A	Devil's Bay	1.2.2013				8.9	94	0.590	17	1.671	seepage
SE_NE_70	S4-A	Devil's Bay	17.1.2013				9	260	0.430	9	0.945	seepage
SE_SW_71	SP1	Cape Lamb	8.2.2014		63.86434	57.61686	9.59	263	0.115	17	1.432	seepage
SE_NE_72	S7-A	Devil's Bay	20.1.2013				9.4	140	0.505	6	0.205	seepage

158

Sample code	Acid neutralization	Na	K	Ca^2	SO$_4$^{2}	Cl	TN	DN	TP	DOC	F	NH$_4$_N	NO$_3$_N	NO$_2$_N
L_NE_1	0.83	40.8	2.11	9.8	3.3	80.7	2.16	1.64	0.0945	20.6	0.0392	0.057	0.0186	0.004
L_NE_2	0.571	15.1	0.86	5.13	4.6	24.3	0.32		0.0162	1.65	0.028	0.037	0.0107	0.001
L_NE_3	0.83	19.2	0.787	2.99	7.5	26.7	0.37		0.0226	0.77	0.0201	0.074	0.146	0.001
L_NE_6	0.726	76.9	4.16	43.8	83.1	394	1.13	1.7	0.0101	6.78	0.0509	0.045	0.0099	0.001
L_NE_8	0.861	87	5.29	3.3	26.5	270	1.43	1.32	0.115	1.78	0.0975	0.049	3.6	0.047
L_NE_11	0.156	7.29	0.359	0.847	1.21	10.4	0.29		0.0314	1.26	0.0279	0.017	0.0476	0
L_NE_12	0.965	32.2	0.851	3.69	4.75	28.6	0.41		0.0886	1.56	0.0283	0.059	0.298	0.001
L_NE_14	0.342	14.7	1.1	1.49	31	8.75	0.28		0.148	1.59	0.0777	0.045	0.0339	0.016
L_NE_15	0.674	23.3	0.651	3.37	5.34	34	0.45		0.0489	2.33	0.0289	0.083	0.0248	0.001
L_NE_16	1.66	26.7	0.841	1.54	6.33	20.8	0.33		0.144	1.22	0.0548	0.005	0.406	0.002
L_NE_21	0.747	24.8	1.13	8.31	8.4	35.5	0.51		0.0439	0.63	0.042	0.002	1.11	0.001
L_NE_22	0.467	16.9	0.771	3.8	2.56	24.2	0.26		0.0429	0.87	0.0446	0.004	0.128	0.001
L_SW_28	0.969	96.7	2.15	29.1	37.3	129	1	0.91	0.015	6.31	0.0714	0.0204138	0.0046	0.028
L_SW_29	0.51	73.6	1.41	7.3	17.5	91.2	0.8	0.75	0.015	2.72	0.0293	0.072	0.005	0.008
L_SW_32	0.582	58.5	1.12	4.45	27.4	65.9	0.46		0.015	1.73	0.0403	0.0262069	0.0076	0.006
ST_NE_41	0.571	24.5	0.841	3.37	5.94	29.3	0.49		0.0761	0.75	0.0454	0.003	1.9	0.001

APPENDIX 2

List of all observed species in the investigated recent samples
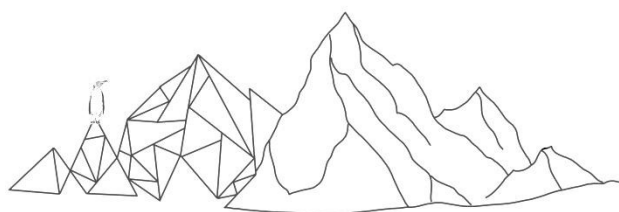
APPENDIX 2 – List of all observed species in the investigated recent samples from Vega Island. Distribution: MA= Maritime Antarctic Region, MA/CA = Maritime and Continental Antarctic Region, MA/SA = Maritime and Sub- Antarctic Region, MA/AM= Maritime Antarctic and South America, SH=Southern Hemisphere, CA/MA/AM= Continental and Maritime Antarctic and South America, MA/CA/SA = entire Antarctic Region, C = Cosmopolitan, U= Unknown.

code	Taxon name	Distribution				
					Vega Island	
		Region	Livingston Island	James Ross Island	Cape Lamb	Devil's Bay
ACHCOA	*Achnanthes coarctata* (Brébisson) Grunow	C	x	x	x	x
ACHMUE	*Achnanthes muelleri* Carlson	MA/SA	x	x	x	x
ACHTAY	*Achnanthes taylorensis* D.E.Kellogg Stuiver T.B.Kellogg & G.H.D.Denton	MA/CA		x	x	
ACHAUS	*Achnanthidium australexiguum* Van de Vijver	MA			x	x
AMPMAR	*Amphora* sp.	U				x
CALAUS	*Caloneis australis Zidarova,* Kopalová & Van de Vijver	MA			x	x
CRAANT	*Craticula antarctica* Van de Vijver & Sabbe	MA/CA	x	x	x	x
CRAOBA	*Craticula obaesa* Van de Vijver, Kopalová &Zidarová	MA			x	x
CRARSP	*Craticula* sp.	U			x	
CRAL21	*Craticula* sp. L21	U				x
DENJAM	*Denticula jamesrossensis* Van de Vijver, Kopalová, Kociolek & Ector	MA			x	x
FISPEL	*Fistulifera pelliculosa* (Brébisson) Lange-Bertalot	C				x
FRACPA	*Fragilaria cf. Parva* Tuji & D.M.Williams	C				x
GEIGAB	*Geissleria gabrielae* Van de Vijver & Zidarova	MA	x	x		x
GOMJAM	*Gomphonema jamesrossense* Van de Vijver, Kopalová, Zidarova &Kociolek	MA			x	x
GOMMAN	*Gomphonema maritimo-antarcticum* Van de Vijver, Kopalová, Zidarova &Kociolek	MA			x	x
GOMPSP	*Gomphonema* sp.	U			x	
HALAUO	*Halamphora cf. ausloosiana*	U			x	x
HALASP	*Halamphora* sp.	U			x	x
HALGHO	*Halamphora* sp. ghost	U			x	x

code	Taxon name	Distribution			Vega Island	
		Region	Livingston Island	James Ross Island	Cape Lamb	Devil's Bay
HALVEN	*Halamphora veneta (Kützing) Levkov*	C				x
HANABU	*Hantzschia abundans* Lange-Bertalot	C	x	x	x	x
HANAMU	*Hantzschia amphioxys f. muelleri* Ts.Ko-Bayashi	CA/MA/AM			x	x
HANCAB	*Hantzschia cf. abundans* Lange-Bertalot	C			x	x
HANHYP	*Hantzschia hyperaustralis* Van de Vijver & Zidarova	MA/CA	x	x	x	x
HANINC	*Hantzschia incognita* Zidarova & Van de Vijver	MA	x		x	x
HANTSP	*Hantzschia* sp.	U			x	x
HANSPH	*Hantzschia* sp. 1	U			x	
HANSPM	*Hantzschia* sp. M2	U				x
HUMAUS	*Humidophila australis* (Van de Vijver & Sabbe) R.L.Lowe et al.	MA/CA			x	x
HUMASH	*Humidophila australoshetlandica* Kopalová, Zidarova & Van de Vijver	MA				x
HUMINC	*Humidophila incounspicua (Kopalová&Van de Vijver) R.L.Lowe et al.*	MA			x	x
HUMKEI	*Humidophila keiliorum Kopalová*	MA			x	x
HUMNIE	*Humidophila nienta (Carter) R.L.Lowe et al.*	SH			x	
HUMSCE	*Humidophila sceppacuerciae Kopalová*	MA			x	x
HUMISP	*Humidophila* sp.	U			x	x
HUMVOJ	*Humidophila vojtajarosikii Kopalová, Zidarova & Van de Vijver*	MA			x	x
CHAAME	*Chamaepinnularia australomediocris* (Lange-Bertalot & R.Schmidt) Van de Vijver	MA/SA	x	x	x	x
CHACKR	*Chamaepinnularia cf. krookiiformis* (Krammer) Lange-Bertalot & Krammer	C			x	
CHAGER	*Chamaepinnularia gerlachei* Van de Vijver & Sterken	MA	x	x	x	x
CHAKRO	*Chamaepinnularia krookii* (Grunow) Lange-Bertalot & Krammer	C	x			x
CHAKRF	*Chamaepinnularia krookiiformis* (Krammer) Lange-Bertalot & Krammer	C	x	x	x	x

| code | Taxon name | Distribution | | | Vega Island | |
		Region	Livingston Island	James Ross Island	Cape Lamb	Devil's Bay
CHAMSP	*Chamaepinnularia* sp.	U			x	x
LUTADE	*Luticola adelae Van de Vijver & Zidarova*	MA			x	x
LUTAND	*Luticola andina Levkov, Metzeltin & Pavlov*	MA/AM			x	
LUTAMU	*Luticola australomutica* Van de Vijver	MA	x	x	x	x
LUTATL	*Luticola austroatlantica* Van de Vijver. Kopalová. S.A.Spaulding & Esposito	MA/CA	x	x	x	x
LUTCON	*Luticola contii Zidarova, Levkov & Van de Vijver*	MA			x	
LUTDEL	*Luticola delicatula Van de Vijver, Kopalová, Zidarova & Levkov*	MA				x
LUTDES	*Luticola desmetii Kopalova & Van de Vijver*	MA		x	x	
LUTDOL	*Luticola doliiformis Kopalová & Van de Vijver*	MA		x	x	x
LUTGIG	*Luticola gigamuticopsis* Van de Vijver	MA	x	x	x	x
LUTHIG	*Luticola higleri* Van de Vijver. Van Dam & Beyens	MA	x	x	x	x
LUTMUT	*Luticola muticopsis* (Van Heurck) D.G.Mann	MA/CA/SA	x	x	x	x
LUTNEG	*Luticola neglecta Zidarova, Levkov & Van de Vijver*	MA			x	x
LUTOLG	*Luticola olegsakharovii Zidarova, Levkov & Van de Vijver*	MA			x	
LUTPMU	*Luticola permuticopsis Kopalová & Van de Vijver*	MA	x	x	x	x
LUTPUS	*Luticola pusilla* Van de Vijver. Kopalová. Zidarova & Levkov	MA	x	x	x	x
LUTRAY	*Luticola raynae Zidarova & Van de Vijver*	MA			x	x
LUTISP	*Luticola* sp.	U			x	x
LUTSP1	*Luticola* sp. *1*	U			x	x
LUTKUM	*Luticola* sp. *2*	U			x	
LUTSPP	*Luticola* sp. *518*	U			x	
LUTSPM	*Luticola* sp. *M163*	U			x	
LUTSCR	*Luticola subcrozetensis* Van de Vijver, Kopalová, Zidarova & Levkov	SH			x	x

code	Taxon name	Distribution			Vega Island	
		Region	Livingston Island	James Ross Island	Cape Lamb	Devil's Bay
LUTTOM	*Luticola tomsui* Kopalová	MA		x		x
LUTTRU	*Luticola truncata* Kopalová & Van de Vijver	MA	x	x	x	x
LUTVDV	*Luticola vandevijveri* Kopalová. Zidarova & Levkov	MA	x	x	x	x
LUTVRM	*Luticola vermeulenii* Van de Vijver	MA	x	x	x	x
MAYCAT	*Mayamaea cf. atomus* (Kützing) Lange-Bertalot	C			x	x
MAYEXC	*Mayamaea excelsa* (Krasske) Lange-Bertalot	C		x	x	x
MAYJEL	*Mayamaea josefelsterii* Kopalová Nedbalová & Van de Vijver	MA	x	x	x	x
MAYPER	*Mayamaea permitis* (Hustedt) Bruder & Medlin	C	x	x	x	x
MAYASP	*Mayamaea sp.*	U			x	x
MAYSWE	*Mayamaea sweetloveana* Zidarova, Kopalová & Van de Vijver	MA				x
MICASH	*Microcostatus australoshetlandicus* Van de Vijver. Kopalová. Zidarova & Cox	MA	x		x	
MICNAU	*Microcostatus naumannii* (Hustedt) Lange-Bertalot	C	x	x	x	x
MUECRG	*Muelleria regigeorgiensis* Van de Vijver & S.A.Spaulding	MA	x	x		x
MUELSP	*Muelleria sp.*	U			x	x
MUESSB	*Muelleria subsabbei* Van de Vijver, Zidarova & Kopalová	MA			x	
NAVASH	*Navicula australoshetlandica* Van de Vijver	MA	x		x	x
NAVCPM	*Navicula cf. perminuta*	U			x	
NAVCRE	*Navicula cremeri* Van de Vijver & Zidarova	MA	x	x	x	x
NAVDOB	*Navicula dobrinatemniskovae* Zidarova & Van de Vijver	MA	x		x	
NAVGRE	*Navicula gregaria* Donkin	C	x	x	x	x
NAVMAR	*Navicula marine*	U			x	x
NAVROM	*Navicula romanedwardii* Zidarova, Kopalová & Van de Vijver	MA			x	x
NAVISP	*Navicula sp.*	U			x	x

| code	Taxon name	Distribution				
		Region	Livingston Island	James Ross Island	Vega Island	
					Cape Lamb	Devil's Bay
NITGRA	*Nitzchia gracilis* Hantzsch	C	x	x	x	x
NITANN	*Nitzschia annewillemsiana* Hamsher, Kopalová, Kociolek, Zidarova & Van de Vijver	MA			x	x
NITACM	*Nitzschia australocommutata* Hamsher, Kopalová, Kociolek, Zidarova & Van de Vijver	MA/CA			x	x
NITCST	*Nitzschia cf. stelmachpessiana*	MA			x	
NITCWI	*Nitzschia cf. wilmotteana*	MA			x	x
NITHMB	*Nitzschia homburgiensis* Lange-Bertalot	C	x	x	x	x
NITKLE	*Nitzschia kleinteichiana* Hamsher, Kopalová, Kociolek, Zidarova & Van de Vijver	MA			x	x
NITPAL	*Nitzschia paleacea* Grunow	C	x	x	x	x
NITSOR	*Nitzschia soratensis* E.Morales & Vis	C			x	x
NITZSP	*Nitzschia* sp.	U			x	x
NITVEL	*Nitzschia velazqueziana* Hamsher, Kopalová, Kociolek, Zidarova & Van de Vijver	MA			x	x
ORTCRO	*Orthoseira cf. roeseana*	C				x
PINAMI	*Pinnularia australomicrostauron* Zidarova. Kopalová & Van de Vijver	MA	x	x	x	x
PINASC	*Pinnularia australoschoenfelderi* Zidarova Kopalová & Van de Vijver	MA	x	x	x	
PINBSL	*Pinnularia borealis s. l.*	C			x	x
PINBVP	*Pinnularia borealis* var. *pseudolanceolata* Van de Vijver & Zidarova	MA	x	x	x	x
PINMAG	*Pinnularia magnifica* Zidarova Kopalová & Van de Vijver	MA	x		x	
PINNSP	*Pinnularia* sp.	U			x	
PLAAUS	*Placoneis australis* Van de Vijver & Zidarova	MA			x	x
PLAAST	*Planothidium australe* (Manguin) R. Le Cohu	MA/SA	x	x	x	x
PLACAP	*Planothidium capitatum* (O.Müller) Van de Vijver, Kopalová, C.E.Wetzel & Ector	MA/AM			x	x
PLACTE	*Planothidium cf. capitatum* (O.Müller) Van de Vijver, Kopalová, C.E.Wetzel & Ector	MA/AM			x	

code	Taxon name	Region	Livingston Island	James Ross Island	Vega Island Cape Lamb	Devil's Bay
PLAFTE	*Planothidium cf. frequentissimum* (Lange-Bertalot) Round & Bukhtiyarova	C			x	
PLARQU	*Planothidium cf. renei*	U			x	
PLAFRQ	*Planothidium frequentissimum* (Lange-Bertalot) Round & Bukhtiyarova	C	x	x	x	x
PLARLA	*Planothidium rostrolanceolatum* Van de Vijver, Kopalová & Zidarova	MA				x
PLANSP	*Planothidium* sp.	U			x	x
PLACPS	*Planothidium* sp.1	U			x	
PSAARE	*Psammothidium aretasii* (Manguin) Le Cohu	C	x		x	
PSACON	*Psammothidium confusoneglectum* Kopalová, Zidarova & Van de Vijver	MA			x	
PSAGII	*Psammothidium germainii* (Manguin) Sabbe	MA/SA	x	x		x
PSAGES	*Psammothidium germainioides* Van de Vijver, Kopalová & Zidarova	MA			x	
PSAICG	*Psammothidium incognitum* (Krasske) Van de Vijver	C	x		x	
PSAPAP	*Psammothidium papilio* (Kellogg et al.) Kopalová & Van de Vijver	MA/CA	x	x	x	x
PSARGI	*Psammothidium rostrogermainii* Van de Vijver, Kopalová & Zidarova	MA/CA			x	x
PSASAT	*Psammothidium subatomoides* (Hustedt) Bukhtiyarova & Round	C	x	x	x	
SELANT	*Sellaphora antarctica* Kopalová, Zidarova & Van de Vijver	MA			x	x
SELGRA	*Sellaphora gracillima* Kopalová, Zidarova & Van de Vijver	MA			x	
SELJRO	*Sellaphora jamesrossensis* (Kopalová & Van de Vijver) Van de Vijver & C.E.Wetzel	MA			x	x
STAINE	*Stauroforma inermis* Flower, Jones & Round	SH			x	x
STAAUS	*Stauroneis australobtusa*	MA			x	
STADEL	*Stauroneis delicata* Zidarova, Kopalová & Van de Vijver	MA			x	
STALAT	*Stauroneis latistauros* Van de Vijver & Lange-Bertalot	MA/CA	x	x	x	x
STAPMU	*Stauroneis pseudomuriella* Van de Vijver & Lange-Bertalot	MA/SA	x	x	x	x
STAPOT	*Staurosira pottiezii* Van de Vijver	MA				x

APPENDIX 2 – (continued)

code	Taxon name	Distribution				
					Vega Island	
		Region	Livingston Island	James Ross Island	Cape Lamb	Devil's Bay
STAURO	*Staurosirella sp.*	U			x	
TRYDEB	*Tryblionella debilis* Arnott	C			x	x

APPENDIX 3

List of diatom taxa observed within the Lake Esmeralda sediment core
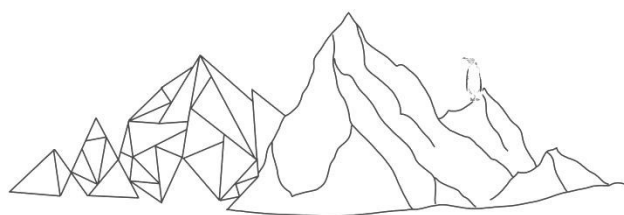
Appendix 3 List of diatom taxa observed within the Lake Esmeralda sediment core.

TAXON NAME	CODE	TAXON NAME	CODE
Achnanthes taylorensis	AchTay	*Microcostatus naumanii*	MicNau
Brachysira minor	BraMin	*Muelleria kratka*	MueKra
Caloneis australis	CalAus	*Muelleria sp*	Muesp
Caloneis short	Calshor	*Navicula australoshetlandica*	NavAus
Chama sp suspicious	ChaSuspi	*Navicula cf. perminuta-marine*	Navmar
Chamaepinnularia australomediocris	ChaAus	*Navicula cf. shackletoni*	NavSha
Chamaepinnularia antarctica	ChaAnt	*Navicula cf. glaciei*	NavGla
Chamaepinnularia elliptica	ChaEli	*Navicula dobrinatemniskovae*	NavDob
Chamaepinnularia gerlachei	ChaGer	*Navicula gregaria*	NavGre
Chamaepinnularia krookiformis	ChaKro	*Navicula romanedwardii*	NavRom
Chamaepinnularia s. l.	Chasen	*Navicula s. l.*	Navsen
Denticula jamesrossensi	DenJam	*Nitzschia homburgiensis*	NitHom
Fragilaria cf. parva	FraPar	*Nitzschia paleacea*	NitPal
Fragilariopsis cylindrus	FraCyl	*Nitzschia sp*	Nitsp
Gomphonema cf. parvulum	GomPar	*Nitzschia kleinteichiana*	NitKlei
Gomphonema maritimo-antarcticum	GomAnt	*Pinnularia australomicrostauron*	PinAmi
Gomphonema s. l.	Gomsen	*Pinnularia australoschoenfelderi*	PinAsf
Hantzschia abundans	HanAbu	*Pinnularia borealis s. l.*	PinBor
Hantzschia amphyoxis	HanAmp	*Pinnularia borealis var. pseudolanceolata*	PinPla
Hantzschia confusa	HanCon	*Pinnularia cf. divergens*	PinDiv
Hantzschia sp	Hansp	*Pinnularia livingstonensis*	PinLiv
Humidophila australoshetlandica	HumAus	*Pinnularia magnifica*	PinMag
Humidophila inconspicua	HumInc	*Pinnularia s. l.*	PinSen
Humidophila keiliorum	HumKei	*Pinnularia strictissima*	PinStr
Humidophila nienta	HumNie	*Placoneis australis*	PlaAust
Humidophila sceppaceurciae	HumSce	*Planothidium australe*	PlaAus
Humidophila sensu	Humsen	*Planothidium capitatum*	PlaCap
Humidophila vojtajarosikii	HumVoj	*Planothidium cf. frequentissimum*	PlaFre
Luticola australomutica	LutAus	*Planothidium s. l.*	Plasen
Luticola doliiformis	LutDol	*Psammothidium cf. abundans*	PsaAbu
Luticola higleri	LutHig	*Psammothidium aretasii*	PsaAre
Luticola katkae	LutKat	*Psammothidium germainioides*	PsaGer
Luticola sp minipusilla	LutPum	*Psammothidium incognitum*	PsaInc
Luticola neglecta	LutNeg	*Psammothidium manguinii asi*	PsaMan
Luticola olegsakharovii	LutOle	*Psammothidium papilio*	PsaPap
Luticola permuticopsis	LutPer	*Psammothidium subatomoides*	PsaSub
Luticola pusilla	LutPus	*Psammothidium rostrogermainii*	PsaRge
Luticola raynae	LutRay	*Psammothidium s. l.*	Psasen
Luticola s. l.	Lutsen	*Psammothidium superpapilio*	PsaSpa
Luticola vermueleni	LutVer	*Sellaphora antarctica*	SelAnt
Luticola subcrozetensis	LutSub	*Sellaphora nana*	SelNan
Mayamaea josefelsteri	MayJos	*Stauroneis latistauros*	StaLat
Mayamaea permitis	MayPer	*Stauroneis minutula*	StaMin
Mayamaea s. l.	Maysen	*Stauroneis pseudomuriella*	StaPse
Microcostatus australoshetlandicus	MicAus	*Stauroneis s. l.*	StaSen
		Tryblionella debilis	TryDeb

APPENDIX 4

List of diatom taxa observed within the Lake Anonima sediment core

Appendix 4 List of diatom taxa observed within the Lake Anonima sediment core.

TAXON NAME	CODE	TAXON NAME	CODE
Adlafia submuscora	AdlSub	*Navicula gregaria*	NavGre
Achnanthes coarctata	AchCoa	*Neidium antarcticum*	NeiAnt
Achnanthes muelleri	AchMue	*Nitzschia annewillemsiana*	NitAnw
Achnanthidium australexiguum	AchAus	*Nitzschia gracilis*	NitGra
Brachysira minor	BraMin	*Nitzschia homburgiensis*	NitHom
Caloneis australis	CalAus	*Nitzschia kleinteichiana*	NitKle
Craspedostauros laevissiumus	CraLae	*Nitzschia paleacea*	NitPal
Craticula antarctica	CraAnt	*Nitzschia soratensis*	NitSor
Craticula cf. obaesa	CraOba	*Nitzschia valazqueziana*	NitVal
Craticula subpampeana	CraSub	*Orthoseira roeseana*	OrtRoe
Fragilaria cf. Parva	FraPar	*Pinnularia australoglobiceps*	PinAug
Gomphonema jamesrossense	GomJam	*Pinnularia australomicrostauron*	PinAus
Gomphonema maritimo-antarcticum	GomAnt	*Pinnularia australoschoenfelderi*	PinAum
Hallamphora oligotraphenta	HalOli	*Pinnularia borealis*	PinBor
Hantzschia abundans	HanAbu	*Pinnularia microstauroides*	PinMic
Hantzschia amphioxys	HanAmx	*Pinnularia splendida*	PinSpl
Hantzschia hyperaustralis	HanHyp	*Placoneis australis*	PlcAus
Humidophila arcuata	HumArc	*Planothidium australe*	PlaAus
Humidophila australis	HumAus	*Planothidium capitatum*	PlaCap
Humidophila keiliorum	HumKei	*Planothidium frequentissimum*	PlaFre
Humidophila sceppacuerciae	HumSce	*Planothidium renei*	PlaRen
Chamaepinnularia australomediocris	ChaAus	*Planothidium rostrolanceolatum*	PlaLan
Chamaepinnularia krookiformis	ChaKrf	*Planothisium wetzelectorianum*	PlaWet
Chamaepinnularia krookii	ChaKro	*Psammothidium germanii*	PsaGer
Luticola austroatlantica	LutAus	*Psamothidium abundans*	PsaAbu
Luticola cf. cohni	LutCoh	*Psamothidium atomus*	PsaAto
Luticola desmetii	LutDes	*Psamothidium germanoides*	PsaGos
Luticola doliiformis	LutDol	*Psamothidium incognitum*	PsaInc
Luticola higleri	LutHig	*Psamothidium papilio*	PsaPap
Luticola muticopsis	LutMut	*Psamothidium rostrogermanii*	PsaRos
Luticola permuticopsis	LutPer	*Psamothidium sp. 1(small)*	Psasp1
Luticola raynae	LutRay	*Psamothidium superpapilio*	PsaSup
Luticola sp. 2	Lutsp2	*Sellaphora antarctica*	SelAnt
Luticola truncata	LutTru	*Sellaphora gracillima*	SelGra
Luticola vandevijveri	LutVan	*Sellaphora jamesrossensis*	SelJam
Mayamaea excelsa	MayExc	*Stauroforma inermis*	StaIne
Mayamaea sweetloveana	MaySwe	*Stauroneis delicata*	StaDel
Microcostatus naumannii	MicNau	*Stauroneis huskvikensis*	StaHus
Muelleria aequistriata	MueAeq	*Stauroneis latistauros*	StaLat
Navicula cremerii	NavCre	*Stauroneis pottiezii*	StaPot